Author:
Chavez Lara, Claudia

Title:
Ecosystem changes and paleoclimatic implications from the Chihuahua Desert (Mexico) during the late Pleistocene and Holocene

Ecosystem changes and paleoclimatic implications from the Chihuahua Desert (Mexico) during the late Pleistocene and Holocene

by

Claudia Magali Chávez Lara

School of Chemistry

September 2018

A thesis submitted to the University of Bristol in accordance with the requirements for award of the degree of Doctor of Philosophy in the Faculty of Science

Word count: 39616

Abstract

Climate change is affecting the subtropical northern Mexico by reducing the amounts of rainfall and increasing the severity of droughts. The rainfall system of this area is governed by the North American Monsoon which mechanism and dynamics regarding past global temperature change are still unclear. Hydroclimate variation of the northwest Mexico, specifically during the late Pleistocene and Holocene is an active area of debate, with uncertainty in the nature and sources of precipitation. Previous research has inferred the influences of winter storms, summer monsoonal rain and autumn tropical cyclones. Moreover, the impacts on regional and local ecosystems are not well constrained.

In this thesis, I employ organic and inorganic geochemical methods, studying a variety of lipid biomarkers from aquatic and terrestrial sources, as well as the isotopic composition of endogenic carbonates to investigate two basins in central northern Mexico: the Satiaguillo and El Potosi basins at the western and eastern limits of the Chihuahua Desert. I investigate the response of lacustrine and terrestrial habitats of these basins to hydrological changes occurring since the late last glacial. Biomarkers from both sedimentary records reflect variable input of organic matter from algal and bacterial biomass, aquatic microfauna and surrounding vegetation. Changes in these inputs reveal distinct stages of ecosystem development and correlate with endogenic carbonate isotopic changes over the last 27,000 years on the Santiaguillo area and 20,000 years on the El Potosi area. Overall, the areas presented opposite environmental conditions during the last glacial maximum and deglaciation period. However, over the early- and mid-Holocene, both records reveal increasing aridity and a shrinking water body, while the late Holocene was characterized by less dry environment with higher proportions of C_4 grasses. Finally, this thesis illustrates the great potential of biomarker applications for paleoenvironmental reconstructions of dry settings areas with poor pollen preservation and other fossil particulate matter.

To Lucía and Román

Acknowledgments

First of all, I would like to thank my supervisors Richard D. Pancost, Jens Holtvoeth and Priyadarsi D. Roy for their support and guidance throughout my PhD.

Very special thanks to CONACyT for funding me on this adventure.

Thank you very much to all my friends and family who have always believed in me.

Author’s declaration

I declare that the work in this dissertation was carried out in accordance with the requirements of the University's Regulations and Code of Practice for Research Degree Programmes and that it has not been submitted for any other academic award. Except where indicated by specific reference in the text, the work is the candidate's own work. Work done in collaboration with, or with the assistance of, others, is indicated as such. Any views expressed in the dissertation are those of the author.

SIGNED…….. DATE……...

Table of contents

List of figures

List of tables

List of equations

Abbreviations

°C	degrees Celsius
‰	permil
ACL	Average Chain Length
AD	anno Domini
AMS	Accelerator Mass Spectrometry
B/A	Bølling-Allerød
BIT	Branched Isoprenoid Tetraether
BP	Before present
brGDGT	branched GDGT
BSTFA	N,O Bis(trimethylsilyl)-trifluoroacetamide
cal	calendar
CBT	degree cyclisation ratio of branched GDGT
CESM	Community Earth System Model
CO_2	carbon dioxide
CONAGUA	Comisión Nacional del Agua
CPI	carbon preference index
FA	fatty acids
FIDESUR	Fideicomiso para el Desarrollo del Sur del Estado de Nuevo León
FIS	Fennoscandian ice sheet
GC/C/IRMS	gas chromatography / combustion / isotope ratio mass spectrometry
GC/MS	gas chromatography / mass spectrometry
GDGT	glycerol dialkyl glycerol tetraether
GDGTs	glycerol dialkyl glycerol tetraether
GoC	Gulf of California
GoM	Gulf of Mexico
H1	Heinrich event 1
HPLC/MS	high performance liquid chromatography / mass spectrometry
HTM	Holocene thermal maximum
iGDGT	isoprenoidal GDGT
INEGI	Instituto Nacional de Estadística y Geografía
ITCZ	Inter Tropical Convergence Zone
ka	thousand years
l	long-chain
LGM	last glacial maximum
LIS	Laurentide ice sheet
m	mid-chain
MAAT	mean annual air temperature
MUFA	monounsaturated fatty acid
N	north
NAM	North American Monsoon

NH	Northern hemisphere
OH	alcohol
OH-FAs	Hydroxy fatty acids
PUFA	Poliunsaturated fatty acid
Ri/b	total iGDGTs to total brGDGTs ratio
s	short-chain
SAGARPA	Secretaría de Agricultura, Ganadería, Desarrollo Rural, Pesca y Alimentación
SEGOB	Secretaria de Gobernacion
SMN	Servicio Meteorologico Nacional
sp	species
SST	sea surface temperature
SW	south west
TEX_{86}	TetraEther indeX of tetraethers consisting of 86 carbon atoms
Ti	titanium
TIC	total ion count
TLE	total lipid extract
TN	total nitrogen
TOC	total organic carbon
UNAM	National Autonomous University of Mexico
USA	United States of America
v/v	volume/volume
VPDB	Vienna PeeDee Belemnite
YD	Younger Dryas
$\delta^{13}C$	carbon isotopic composition
$\delta^{18}O$	oxygen isotopic composition

CHAPTER I
Introduction

Photo by C.M. Chávez-Lara

Climate change can be described as a physical phenomenon that can be observed, quantified and measured (Solomon *et al*., 2007). Over the last few decades, this subject has become of high interest to the scientific community as it poses a threat to the human society (UNFCCC, 2015). The effects of anthropogenic global warming are now manifested globally, including the northern part of Mexico. Climate change is affecting this region by reducing the amounts of rainfall and increasing the severity of droughts. It is the main cause of water scarcity and reduction in the agricultural products that feed both animals and humans. Because the economy of this region is largely based on agriculture, water scarcity has additional impacts on Mexican society, including falling income and employment for farmers. Around 40% of the Mexican livestock population is located in the states of Coahuila, Chihuahua, Durango, San Luis Potosi, Nuevo Leon and Zacatecas (SAGARPA, 2015), where the rainfall is governed by the North American Monsoon (NAM) system (Reyes *et al*., 2009).

Currently, our knowledge of this meteorological mechanism and its dynamics with respect to global temperature change are still unclear (Metcalfe *et al*., 2015). One way to understand it is by documenting the changes occurred in the geological past (i.e. paleoclimate) and detecting which factors triggered such changes. Aside from the social dimensions, there is an active debate about the relative role of winter rainfall through storm tracks vs. summer rainfall through the NAM for the last glacial maximum (LGM) hydrology in this region (e.g. Roy *et al*., 2015; Bhattacharya *et al*., 2017). Understanding the past climate systems (previews to the instrumental and historical records) is crucial for understanding past climate change as well as developing models for future environmental conditions.

Lacustrine sediments represent an excellent geological archive of continental environmental conditions. Commonly, archives of vegetation change are based on fossil pollen analysis. This biological proxy not only is indicative of vegetation type, but is also influenced by amounts of precipitation, migration patterns of humidity and CO_2 concentration (Rhode, 2002; Caballero *et al*., 2005; Ortega-Rosas *et al*., 2008). All of these factors make fossil pollen a powerful tool for paleoclimate reconstructions. Unfortunately, the preservation of fossil pollen is poor in arid and desert areas such as the central-northern and northern Mexico. In this research project, I am applying, for the very first time, organic geochemistry techniques – such as lipid biomarkers and compound specific isotopes in sediments collected

from two different ephemeral lacustrine basins located in the arid central-northern Mexico. I use those to reconstruct past environmental changes, from the late last glacial to present. One of the principal aims is to demonstrate that organic geochemical proxies have great potential to decipher paleoenvironmental conditions in the challenging dry ecosystems. This project also includes the analysis of carbon and oxygen isotope compositions ($\delta^{13}C$, $\delta^{18}O$) of endogenic carbonates; both the organic and inorganic results are compared with other paleoclimate records for a better understanding of regional and global climatic system. This Ph.D. project is a research collaboration between the University of Bristol (UK) and the National Autonomous University of Mexico (UNAM).

1.1 Thesis aims and objectives

My overall aim is to explore and understand the responses of lacustrine ecosystems (and their surrounding catchments) of the central-northern Mexico to the major climate perturbations that occurred over the late Pleistocene and Holocene. In order to achieve this, I have analysed 31 sediment samples from the Santiaguillo lacustrine basin (state of Durango) and another 31 samples from the El Potosi lacustrine basin (state of Nuevo Leon), with each record extending back to the last glacial maximum. These provide a context for understanding the major controls on this climatically sensitive region – and in particular controls on moisture delivery – and how they might vary in the future.

Specific aims include:

- Characterisation of organic matter assemblages in these lacustrine basins, including an assessment of sources of the organic matter.
- Reconstruction of past ecosystems (lacustrine vs. terrestrial vegetation and C_3 vs C_4 terrestrial vegetation) in and around the lacustrine basins using compound specific isotope values ($\delta^{13}C$). This allows me to identify the vegetation type and ecology of the surrounding areas.
- Reconstruction of water column temperature in the lacustrine basins using the oxygen isotopic composition ($\delta^{18}O_{calcite}$) of bulk carbonates. This allows me to test climatic models and compare results with other sea surface temperature reconstruction trends, in order to identify possible forcings on rainfall variability.

- Infer the biological and environmental responses (temperature, sources of moisture and vegetation change) to global climatic events such as the LGM, Heinrich event 1 (H1), Bølling-Allerød (B/A), Younger Dryas (YD) and the early Holocene thermal maximum at southern part of the Chihuahua Desert of Mexico.
- Crucially, these records are compared with other previously published regional paleoclimate records in order to document spatio-temporal climatic variations in the region and determine possible forces that govern NAM variability.

1.2 Thesis structure

This chapter (**Chapter I**) contains a brief explanation of climate change and how it affects the North of Mexico. Also, it presents an overview of why we need paleoclimate reconstructions and describes the challenges that most arid areas present regarding paleoenvironmental reconstruction. This chapter includes the general and particular aims of this thesis. **Chapter II** (Scientific Background) contains general information on the North American Monsoon (NAM), presenting the known facts and identifying gaps in the knowledge of past NAM variability. This chapter also introduces some of the global climatic events occurred during the late Pleistocene-Holocene transition. Existing information about the paleoclimatic and paleoenvironmental reconstructions from the north of Mexico are presented in this chapter. Subsequently, previous work carried out in the study areas of this project is described. Also, this chapter includes a brief review of the organic and inorganic geochemical proxies which are used in this work. This is followed by **Chapter III** (Materials and methodology), which describes the general sample processing as well as the methodologies followed for each organic and inorganic analysis. Also, the data processing techniques are explained.

Chapter IV focuses on the Santiaguillo lacustrine basin. It provides a general description of the area and presents all of the identified lipid compounds found in 31 sediment samples, spanning the last 27,000 years, such as fatty acids (FA), hydroxy FA, branched FA, unsaturated FA, alcohols, *n*-alkanes, methyl ketones, sterols, and those that are less common and episodic in their occurrence. This chapter then explores the possible sources of those lipids and mechanisms behind observed temporal vegetation changes, placing such

interpretations in the context of regional climatic development since the last glacial. This chapter has been published as a paper in Quaternary Science Reviews.

Chapter V is analogous to the previous chapter but focuses on the El Potosi lacustrine basin and includes a description of all the identified lipid compounds found in 31 sediment samples spanning the last 20,000 years; due to more abundant biomarkers, the distributions of glycerol dialkyl glycerol tetraether lipids (GDGTs) and carbon isotopic compositions of fatty acids are also included. This chapter also explores possible sources of organic matter and uses those findings to reconstruct past ecosystem changes (lacustrine vs. terrestrial vegetation and C_3 vs. C_4 terrestrial vegetation). This chapter provides a panorama of the regional climatic development over the last 20,000 years.

Chapter VI presents a comparison between the Santiaguillo and El Potosi basins, but also presents and explores, the stable isotopic composition of endogenic carbonates from both sedimentary records. Temperature and source of dissolved carbonates from both records will be compared. The vegetation responses to global climate events such as last glacial maximum, Heinrich 1, Younger Dryas and the early Holocene thermal maximum in the Chihuahua Desert of Mexico will also be presented. Based on this integrated data, as well as other records, chapter VI explores the climatic forces linked to the NAM development in northern Mexico and south-western USA since the late last glacial.

General and particular conclusions are presented in **Chapter VII**; most of them will be a compilation of conclusions of the previous chapters. However, this chapter also integrates new and published data, providing the opportunity to assess how lacustrine records can deepen our understanding of past climate development.

CHAPTER II
Scientific Background

2.1 The Chihuahua Deseret

The Chihuahua Desert is one of the deserts that form the North American Desert system, which includes the Great Basin, the Mojave and the Sonoran Desert (Figure 2.1). Located between 22-32º N and 100-109º W, to form the southern and eastern borders of one of the biggest deserts in the world. Its area extends through the northern Mexican states of Chihuahua, Coahuila, Nuevo Leon, Durango, Zacatecas and San Luis Potosi and the southern USA states of New Mexico, Texas and Arizona (Palacios-Fest *et al*., 2002).

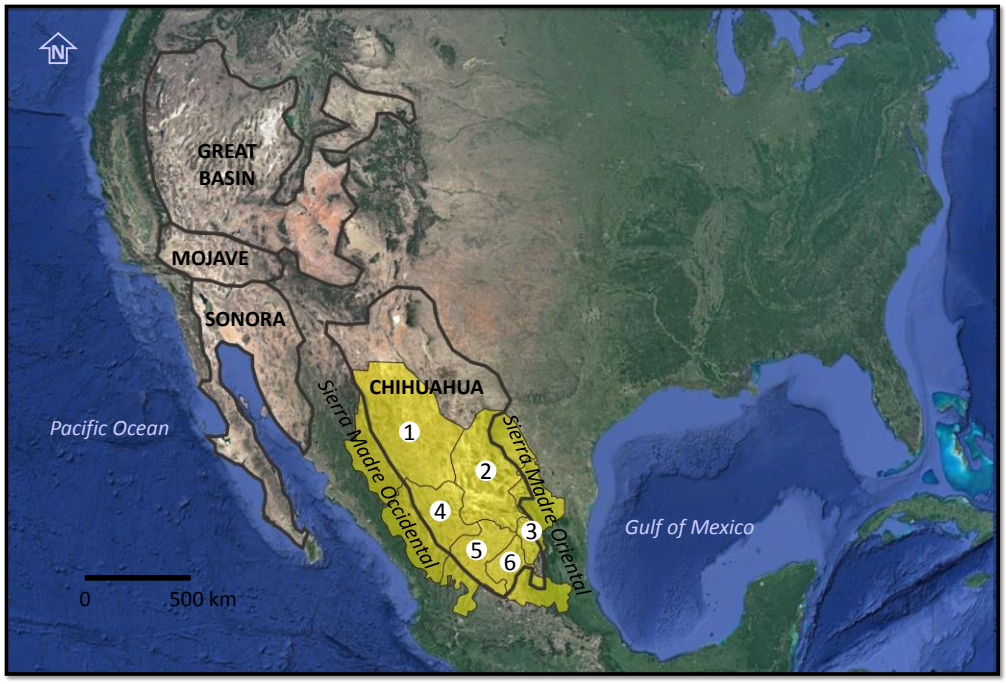

Figure 2.1 Location of the North American Desert system. The Chihuahua Desert forms the southern part of this desert system. (1) Chihuahua, (2) Coahuila, (3) Nuevo Leon, (4) Durango, (5) Zacatecas and (6) San Luis Potosi are the Mexican states that are part of the Chihuahua Desert.

The Chihuahua Desert has an extension of 362,000 km^2 and contains extensive plains bounded by mountains. The climate is dry, with temperatures reaching up to 40ºC in the summer and dropping below 0ºC in the winter, and a mean annual precipitation of 235 mm (Schmidt, 1979). The Mexican states in the Chihuahuan Desert are characterized by a regime of summer and autumn rainfall, where most of the precipitation occurs between June and September (Figure 2.2). Durango is the state that receives the least moisture (precipitation of 501 mm/year), whereas San Luis Potosi State has the highest precipitation ever recorded (923 mm/year; see also Figure 2.2; Source: SMN-CONAGUA).

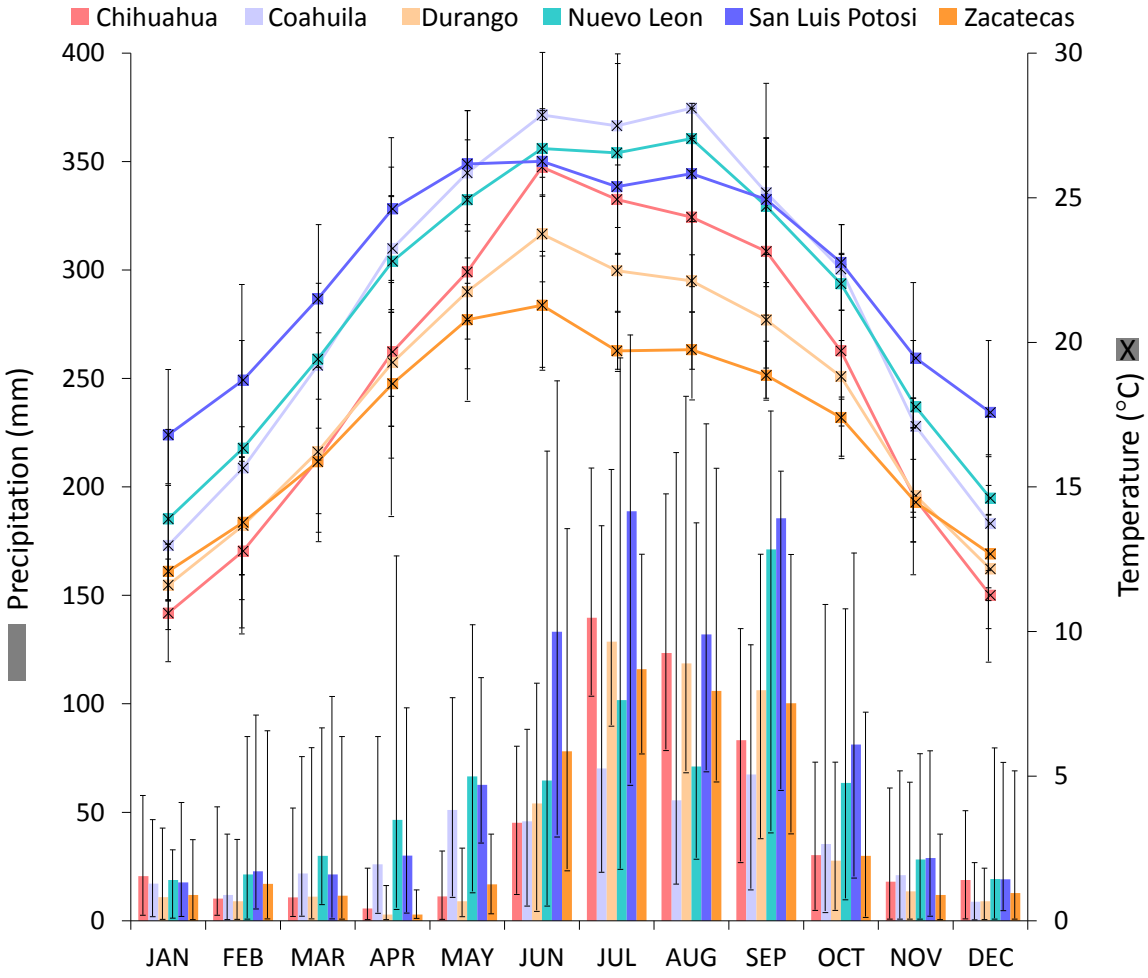

Figure 2.2 Distribution of mean monthly precipitation (bars) and temperature (curves) of the Mexican states that are part of the Chihuahuan Desert from AD 2004 to 2017 (Source: SMN-CONAGUA).

The report from Nacional Institute of Statistics and Geography (INEGI, 2015) divided the vegetation of the Chihuahua Desert into three different types: steppe, halophyte vegetation and a combination of deserts and xeric shrublands. This means that the Chihuahua Desert is dominated by distinctive arid and semi-arid shrubs. Endemism is high in the region. Crop agriculture is carried out on a low scale due to the scarcity of water, shallow soil with poor nutrients and the exclusion from locations with insufficient economic resources for irrigation infrastructure. On the other hand, livestock is widespread, which has caused overgrazing in some xeric areas. Steppe vegetation is mostly present at the downhills of the Sierra Madre Occidental mountains dominated by graminoid. These areas are often used for livestock production. The halophyte vegetation mostly develops in soils of closed basins with high contents of salts and gypsum, where the dominant species are from *Poaceae* and *Chenopodiaceae* families.

2.2 The North America Monsoon

The term "monsoon" has its origin from an Arabic word meaning season. Sailors used this term several centuries ago, to describe the south-westerly wind during the summer, and north-easterly wind during the winter over the Arabian Sea (Oliver, 2005). Now, the term monsoon broadly refers to an atmospheric phenomenon where the mean surface wind reverses its direction from summer to winter - although the term is popularly used to denote the rains without reference to the winds. In monsoon regions, wind blows inland from the cooler oceans toward the warm continents in the summer and from the cold continents toward the warm oceans during the winter. The North America Monsoon (NAM), also known as the Mexican Monsoon, is responsible for summer rainfall in the northwestern part of Mexico and the southwestern USA (Reyes *et al*., 2009). Therefore, it is responsible for most of the humidity in the Chihuahuan Desert, the working area of this project. The NAM has a particularly strong influence over the mountains of the Sierra Madre Occidental and is very important for the agriculture and livestock contributing to approximately 70-80% of annual precipitation in northwest Mexico. Approximately 40-50% of annual precipitation in Arizona and New Mexico of the USA also comes through the NAM (Douglas *et al*., 1993; Stensrud *et al*., 1995).

Under the current climatic regime, the NAM is largely governed by seasonal insolation controlling the Inter Tropical Convergence Zone (ITCZ). The ITCZ influences the direction of dominant winds in North America and, therefore, the sources of humidity for northwestern Mexico, southwestern USA and the Caribbean and Gulf of Mexico regions (Metcalfe *et al*., 2000). During the Northern Hemisphere (NH) summer, the ITCZ shifts north due to warming. This shift induces moisture transport from the Gulf of Mexico and the Caribbean to the eastern regions of Mexico through trade winds, as well as moisture from the Pacific and the Gulf of California to northwest Mexico and southwest USA through southeast Pacific winds (Douglas *et al*., 1993; Stensrud *et al*., 1995).

Annual evolution of the NAM is characterized in three different stages:

1) The development stage occurs during the months of May and June. The main characteristic is the transition from a cold seasonal regime to a warm one in the NH. These conditions induce the northward shift of the polar front and ITCZ at the end of June (Parker *et al*., 1989). Climate conditions in the northern part of Mexico are not fully humid at this stage and gradual warming of the ocean surface allows the formation of clouds.

2) The maturity stage occurs during the months of July and August, beginning with heavy rainfall in southern Mexico, expanding to the north, and finally along the Sierra Madre Occidental Mountains to reach Arizona and New Mexico (Douglas *et al*., 1993; Stensrud *et al*., 1995; Higgins *et al*., 1997). This increase of rainfall in North America matches the increase of east Pacific surface temperature (Carleton *et al*., 1990), the increase of humidity transported vertically through convection (Douglas *et al*., 1993) and the increase of southerly winds in the Gulf of California (Badan-Dangon *et al*., 1991).

3) The decay stage occurs during September and October and is characterised by a reversal of the trends described for the maturity stage (Higgins *et al*., 1997). The climatic system starts to slowly shift to the south, the NAM becomes weaker and rainfall decreases in northern Mexico (Higgins *et al*., 1997) until the monsoon rains in North America finally end.

Although our understanding of NAM has improved, aspects of its behaviour remain controversial. For example, the source of summer rainfall in northwest Mexico and southwest USA is heavily disputed because of the topography of Mexico (Metcalfe *et al*., 2015). Reyes

et al. (2009) showed that rainfall variation in the Chihuahua State is similar to the dynamics of tropical cyclone frequency from the east Atlantic, suggesting that precipitation in this area comes from the Gulf of Mexico and the Atlantic Ocean. On the other hand, Higgins *et al*. (1997) point out that for the same region, the source of moisture is the eastern tropical Pacific and the Gulf of California. Using the information from the past, it will be easier to understand the mechanisms and main forces that might explain severe drought and possible relationships between climatic and cultural changes (Mendez and Magaña, 2010; Stahle *et al*., 2012). In a recent review of paleoclimate registers from the region, Metcalfe *et al*. (2015) demarcated the limitations and suggested the necessity to use methods that discriminate seasonality when reconstructing climate in NAM regions, as the seasonality is only inferred in most of the existing records. In addition, more research using organic geochemical methods should be used to better understand precipitation and evapotranspiration during the transition from LGM to the Holocene, and fully coupled high resolution models would be useful to explore past NAM variations (Metcalfe *et al*., 2015).

2.3 Climatic conditions during the Late Pleistocene-Holocene

The Quaternary represents the past 2.6 million years (Ma) and is divided into two different epochs, the Pleistocene from 2.6 Ma to 11,500 years and the Holocene from 11,500 years until present day. It is a period of high climatic instability divided into glacial-interglacial (G-IG) cycles (Gornitz, 2008) and the abrupt high-amplitude environmental changes were observed across the entire planet (Bradley, 1999). The northern hemisphere was covered by two large ice sheets for extended periods and they are known as the Laurentide (LIS) and Fennoscandian ice sheets (FIS). Variations in their sizes directly affected the North American climatic system and, therefore, the NAM (Barron *et al*., 2012; Kirby *et al*., 2012).

Marine sediment and ice core records indicate that climate conditions in the North Atlantic region were characterized by cold intervals (stadials) alternating with warmer ones (interstadials). Each warm period began with a rapid increase of temperature (in the order of decades) followed by gradual cooling. These oscillations between stadials and interstadials are known as D-O events (Dansgaard *et al*., 1993; Benson *et al*., 2003). The high resolution of the Greenland ice core records ($\delta^{18}O$) has enabled the identification of 24 D-O events during the last glacial (Dansgaard *et al*., 1993) with a mean periodicity of 1,500 years,

although this is still debated (Gornitz, 2008). Causes of these oscillations are still not clear because they are not easily observable or are absent in southern hemisphere records (Gornitz, 2008). They do, however, appear to respond to an increase in solar insolation or to freshening of the northern Atlantic Ocean during Heinrich events, which often occurred at the end of D-O events (Heinrich, 1988; Bond *et al*., 1993).

The Heinrich millennial-scale events are global climatic fluctuations during the Last Glacial that apparently co-occurred with Laurentide iceberg release events, and specifically from northern latitudes between 45º and 60º (Heinrich, 1988). The trigger of these events is not yet well established (Gornitz, 2008). The injection of ice and their subsequent melting has been invoked as the cause for decreased temperature and salinity in the North Atlantic, which affected the oceanic thermohaline circulation and the global climate (Maslin and Shackleton, 1995; Vidal *et al*., 1997). The six Heinrich events were denoted as H1-H6, although some authors claim the Younger Dryas (YD; Figure 2.3) anomaly as the H0 event (Bond and Lotti, 1995).

During the Late Pleistocene, the earth experienced the peak of the last glacial period. This event is known as the Last Glacial Maximum (LGM) and occurred between 24,000 to 19,000 cal. years BP (Clark and Mix, 2002). Both the LIS and FIS achieved their greatest extent of the last G-IG cycle and the sea level was 130-120 m lower compared to today. Both modified the atmospheric and thermohaline circulations (Bowen, 2009). Both the LGM and subsequent deglaciation, but also the other millennial-scale global climatic events affected the hydroclimate of the northwest Mexico and southwest USA (Van Devender, 1987; Ortega Ramirez, 1998; Metcalfe *et al*., 1997).

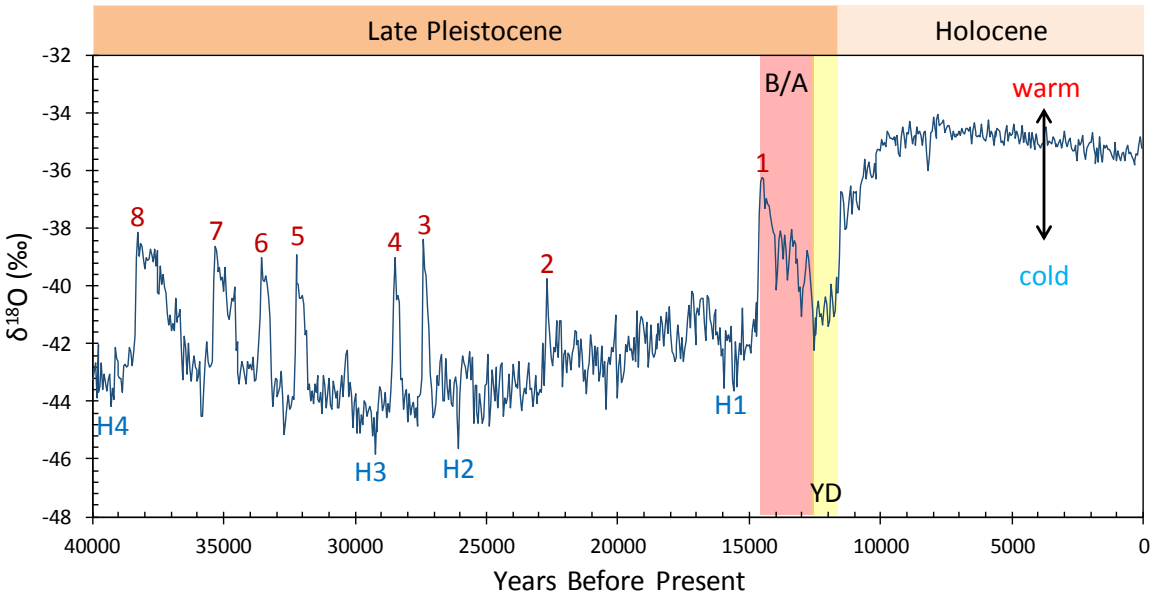

Figure 2.3 Proxy based ($\delta^{18}O$) North Greenland temperature over the last 40,000 years (modified after North Greenland Ice Core Project members, 2004). This graphic shows 8 D-O Events (in red), 4 Heinrich Events (in blue), the Bølling-Allerød (B/A) and the Younger Dryas (YD).

The Bølling-Allerød (B/A) is a warm phase during the glacial-interglacial transition (ca. 14.6-12.5 cal ka BP) named after the type localities Bølling and Allerød in Denmark (Gornitz, 2008). The B/A was followed by the cold YD or H0 event (Figure 2.3), named after the occurrence of the characteristic arctic-alpine plant species Dryas octopetala. The glacial-interglacial transition was a period of rapid climate change.

2.4 Hydroclimate of northwest Mexico and southwest USA during the Late Pleistocene and Holocene

The environmental evolution of northwest Mexico and southwest USA during the Pleistocene-Holocene transition has been examined by numerous workers, with records developed using a range of archives, including lacustrine sediments, marine sediments, speleothems and packrat middens. During the last glacial period, the decrease in solar insolation and expansion of the LIS were the dominant influences on the North America climate. The polar jet stream, subtropical jet stream and polar and Ferrel cells expanded to lower latitudes, affecting the atmospheric circulation that delivers moisture into northern Mexico (Zic *et al*., 2002; Benson, *et al*., 2003; Cheshire, 2005). The path of the westerlies was shifted southward (COHMAP members, 1988; Bartlein *et al*., 1998; Negrini, 2002) to

29º N (Metcalfe *et al*., 2002), resulting in 9 ºC lower temperatures and 700 mm higher precipitation than the modern annual means (Barbour, 1988; Heusser, 1998).

Higher lake levels in North America were related to higher precipitation and low evaporation rate (e.g. Enzel *et al*., 2003, Kirby *et al*., 2006). Moreover, paleovegetation records reveal the presence of cold climate species at sites where nowadays desert shrublands exist (Van Devender, 1990; McAuliffe *et al*., 1998; Holmgren *et al*., 2003, 2006). One hypothesis suggests that the latitudinal shift of the climatic system responded to variation of seasonal insolation during the late Pleistocene (Holmgren *et al*., 2003; Kirby *et al*., 2006). This caused heavy winter rains brought by the westerly winds and proportionally less summer rain by the southerly and southeasterly winds (e.g. Badan-Dangon *et al*., 1991; Roy *et al*., 2010).

Furthermore, the high albedo of the ice sheet cooled the land surface and caused anomalous northwesterly winds, reducing the NAM circulation during the LGM and imported cold-dry air into the northwest of Mexico (Bhattacharya *et al*., 2017). However, wetter conditions in the central-northern Mexico during the late last glacial appear to be related to formation of tropical cyclones in the eastern North Pacific during the autumn with restricted rainfall swaths (Roy *et al*., 2015).

The Pleistocene-Holocene transition in the southwest USA and northwest Mexico was characterized by mesic to xeric conditions (Holmgren *et al*., 2006). Conditions were dry and warm from ~15 to 13 ka BP, whereas the YD and Heinrich events were manifested as cooler and more humid climates (Polyak *et al*., 2004; Holmgreen *et al*., 2006; Kirby *et al*., 2006; Wagner *et al*., 2010; Roy *et al*., 2012). None of the authors have explored the response of NAM to the D-O events due to the resolution of the records.

For the early Holocene (11.7-8.2 ka BP), cold weather vegetation migrated to higher latitudes and elevations over 2,000 m a.s.l. as it was replaced by shrub and desert species, leading to the establishment of the North American deserts (Sears and Clisby, 1956; Van Devender, 1990; Holmgreen *et al*., 2003; Figure 2.1). Simultaneously, wetter conditions have been inferred from proxy records – most clearly in California and Nevada – and associated with the establishment of the modern NAM, although it was still not fully developed (Metcalfe *et al*., 2015). Ortega-Rosas *et al*. (2008), on the other hand, point out that greater winter

precipitation persisted during ~9 ka BP in the Sierra Madre Occidental mountains (Figure 2.1). All these illustrate the complexity of the climatic system among the area during this period.

The middle Holocene was characterised by slightly warmer SSTs across the Gulf of California (Barron *et al*., 2005; McClymont *et al*., 2012), and the NAM reached its Holocene peak, extending its influence north of its current area (Harrison *et al*., 2003; Barron *et al*., 2012). Consequently, precipitation increased relatively to the early Holocene and temperatures became warmer by ca. 2 °C than modern at the Sierra Madre Oriental mountains (Ortega-Rosas *et al*., 2008). However, there is a wide area across North America with high runoff variability, i.e. severe drought followed by more humid periods. Lake level fluctuations were susceptible to changes in intensities of the El Niño and La Niña conditions. Winter precipitation increased in southwest USA during the dominant El Niño intervals, whereas summer precipitation increased in northwestern Mexico during the dominant La Niña intervals, according to proxies and isotopic analyses of modern precipitation and groundwater (Menking and Anderson, 2003).

During the late Holocene, proxy records indicate that warmer Pacific temperatures and changes in the El Niño-Southern Oscillation (ENSO) resulted in more protracted El Niño-like conditions (Barron *et al*., 2004; Pérez-Cruz, 2006; Conroy *et al*., 2008), causing a decrease in the amount of summer precipitation in northwestern Mexico. However, in modern era, warmer Pacific temperatures also enhance the activity of tropical cyclones and frontal systems (Horel and Wallace, 1981; Ropelewski and Halpert, 1987; Magaña *et al*., 2003).

2.5 Lacustrine deposits and previous research on Santiaguillo and the El Potosi basins

Endorheic lakes are water bodies in basins within the continent and have no direct connection to the sea. They can be classified based on the basin source or physiochemical properties (Eugster and Hardie, 1978). The paleolakes studied here are lacustrine systems located in an endorheic basin within a dry or semidry area, such that the water is ephemeral and maintained only during the rainy season. Such lakes suffer from a high evaporation rate during the rest of the year and ultimately dry out (Hardie *et al*., 1978; Cohen, 2003). Similar lacustrine basins

are generally located close to 30º latitude, occurring near the Earth's large deserts and usually are the economic support of local populations as they are a source of water or evaporitic minerals with economical potential (i.e. halite, sylvite, etc.). The sedimentological and stratigraphic characteristics of lacustrine systems can provide insight into the climatic change (Cohen, 2003), with lacustrine deposits falling into three categories: allogenic, authigenic and biogenic.

Allogenic sediments have an external source. They are derived from geomorphologic processes occurring in the basin surroundings and transported through fluvial, pluvial or aeolian ways. Authigenic sediments or evaporites are formed in situ and precipitate from a concentrated brine after mineral saturation. Meanwhile, the biogenic fraction of sediments represents materials from a biological source such as planktonic organisms, e.g., ostracodes, diatoms, etc. (Bradley, 1999). Previous studies of both the Santiaguillo and the El Potosi lacustrine deposits have relied on all three sedimentary archives.

Sedimentation of detrital material depends on transport energy, erosion level and ground cover that can be a barrier during transportation (Nichols, 2009). Commonly, the deposited sediments are of fine grain size, from clay to fine sand, although it is not rare to find coarse or medium-sized textures. The texture depends on transport energy but, generally, the larger grains are deposited along borders of the basin or close to the inflow, whereas the finer grain sizes are deposited in the depocenter.

Sedimentation of evaporite minerals is the result of gradual chemical concentration of brine responding to a negative water balance, where the loss of water through evaporation is higher than the inflow. These physicochemical characteristics enable the deposition of authigenic minerals in a predictable sequence in response to increased salinity and physicochemical characteristics of the water body. Carbonate minerals are precipitated first, followed by sulphates and, finally the chlorides and mixed-salts at highest salinity (Eugster and Hardie, 1978). In this work, we analyse isotopes ($\delta^{13}C_{calcite}$ and $\delta^{18}O_{calcite}$) in bulk carbonates from the two sedimentary basins.

Organic or biogenic material supply to a lacustrine sediment sequence depends on ground cover in the surrounding areas, lake organic productivity and water physicochemical

characteristics. Therefore, the organic material can be allogenic and authigenic. Organic matter preservation can therefore indicate conditions such as aeration of the water body, transport energy, water depth, ground cover density, seasonality, water temperature, source of water, etc. (Katz, 1990; Beuning *et al*., 1997). In this work, we focus on the analysis of organic material preserved in lake sediments. Sediments accumulated in the lakes basins can provide paleoclimatic records as their physical, chemical and biological characteristics respond to the surrounding climatic variability relatively quickly. Generally, the accumulation level in lakes is high and the lake sediments offer great potential for reconstructing high resolution (properly dated) past continental climatic variability (Bradley, 1999).

2.5.1. The Santiaguillo Basin

The first study at the Santiaguillo Basin was carried out by Nieto-Samaniego *et al.* (2012). They propose eight lithostratigraphic units – from Eocene to Quaternary – as the basement rocks and catchment geology. The bottom of the sequence is composed of andesite followed by an ignimbrite sequence, rhyolite, and basalts. Alluvium and lake sediments represent the top of the sequence. Six deformation stages are proposed and the big faults have main orientation of NW-SE. This fault system is still active.

Subsequently, Roy *et al*. (2014a) presented a multiproxy paleoclimate reconstruction over the last 14 cal ka. They determine that higher runoff during ca. 12.5-9 cal ka BP, was contemporary to the south migration of ITCZ and a warmer Gulf of California. Dry conditions with high aeolian activity were reported during 14-12.5 cal ka BP, 5.5-4.5 cal ka BP and last thousand years. During the last 3.5 cal ka, less runoff was linked to higher ENSO frequency and reduced precipitation.

Paleoecology reconstruction during the las 27 cal ka BP, based on ostracods and carbon to nitrogen ratios, was carried out by Chávez-Lara *et al*. (2015). Perennial and oligohaline lake with high productivity was present during the late glacial (27-19 cal ka BP). A shift in the lake conditions with decreased lacustrine productivity and increased salinity is registered around 19 cal ka BP. The lake became mesohaline during 9.5-4 cal ka BP and absence of ostracod valves suggest periodic desiccation over the last 3.5 cal ka.

Roy *et al*. (2015) presented a paleoclimate reconstruction during the las 27 cal ka BP, based on multiproxy records. They suggest wetter conditions during ~27-18 ka associated with enhanced tropical cyclones from the Pacific Ocean, as well as deposition of authigenic carbonates was due to dryer conditions during 18-4 ka.

Subsequently, Quiroz-Jiménez *et al*. (2017) determined the paleoclimate conditions during the six Heinrich events (H1-H6), based on multiproxy records. Lower precipitation is registered during H6, H4, H2 and H1, whereas precipitation above the average during H5 and H3. A possible hemispheric hydroclimate link between hydroclimates of central-northern Mexico and East Asia Monsoon is suggested.

The most recent study of the Santiaguillo Basin was by Quiroz-Jiménez *et al*. (2018). Here, the authors reconstruct the orbital-scale dynamics of droughts over the late Quaternary, based on multiproxy records. Dry conditions at 13.5 ka and 7 ka are associated to higher spring insolation, fluctuating global temperature and strong ENSO activity.

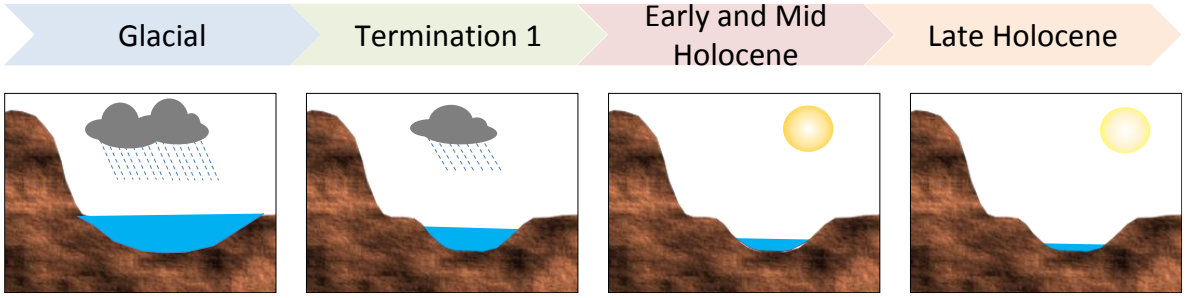

Figure 2.4 Cartoon representing the evolution of the Santiaguillo Lake, based on previous studies. During the last glacial and Termination, conditions were relatively wetter than during the Holocene.

2.5.2. The El Potosi Basin

Compared to the Santiaguillo Basin, fewer studies have been carried out from the El Potosi Basin. The first one focuses on subsidence and subsurface fire over the last 3 decades. Roy *et al*. (2014b) conclude that the occurrence of peat in the subsurface, drought and unregulated ground water extraction caused subsurface fire and subsidence.

More recent research documents the paleoclimate conditions over the last 20 cal ka BP, based on multiproxy records (Roy *et al.*, 2016). Conditions during the LGM were dryer compared

to the deglaciation (19-12 ka). Wetter climate during the B/A is linked to a warmer Gulf of Mexico. The Holocene was drier compared to the deglaciation.

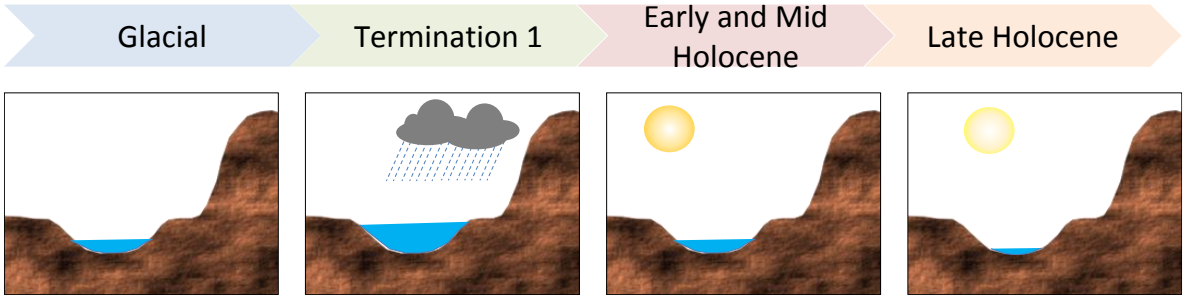

Figure 2.5 Cartoon representing the evolution of the El Potosi Lake, based on previous studies. During Termination 1, conditions were relatively wetter than during the last glacial and the Holocene.

This previous work illustrates the potential of these sedimentary archives for reconstructions of past climate. However, there have been no investigations of these lakes using lipid biomarkers; moreover, there have been no biomarker investigations of any lakes in the Chihuahua Desert, and such analyses can potentially generate new insights for this region.

2.6 Organic Geochemistry

2.6.1 Lipid biomarkers

The particulate detritus of plants that once lived in the water column or surrounding areas of the lake basin is the main source of organic matter (OM) in lake sediments. Sedimentary OM can provide information about changing source inputs, algal productivity and/or vegetation changes due to climate. A great variety of lipids can be found in lacustrine sediments, and their composition is the result of biological material influx and its utilization by microorganisms or direct contributions from microorganisms to the sediment biomass (Perry *et al*., 1979). Many of these lipid compounds have specific biological origins, and all reflect enzymatic control on their molecular structures. Because of the retention of their biological heritage, they earn the name "biological marker" or most commonly abbreviated as "biomarker". All these characteristics make the lipid fraction important to paleoenvironment reconstruction (Meyers and Benson, 1988).

The specific provenance of an individual lipids can be difficult to determine as many biomarkers can be present in a range of organisms (e.g. Holtvoeth *et al*., 2016). Evaluation

of the compound in context with other lipids, however, allows us to narrow down the possible source in a particular depositional context, for example, by considering it as part of a more source-specific distribution of compounds (geochemical fingerprinting).

The *n*-alkyl compounds (*n*-alkanoic acids or *n*-fatty acids, *n*-alkanols or *n*-alcohols and *n*-alkanes) are common in lake sediments, including those investigated here, and are frequently used to examine changes in organic matter source. The short-chain fatty acids (*n*-FAs) such as C_{16} and C_{18} *n*-FA are near-ubiquitous compounds in the environment and they are derived from membrane lipids of all eukaryotes and most bacteria (Matsuda and Koyama, 1977), also forming part of biopolyesters such as cutin and suberin (Kolattukudy, 1981). In contrast, the long-chain *n*-FAs are derived nearly exclusively from leaf waxes of terrestrial plants (Eglinton and Hamilton, 1967). Similarly, hydroxy acids are also found in a wide range of sources but typically in lower proportions than the *n*-FAs (e.g., Eglinton *et al*., 1968; Yano *et al*., 1971; Cranwell, 1982), while the unsaturated FAs have a range of bacterial and eukaryotic sources (e.g. Bobbie and White, 1980; Kattner *et al*., 1983; Ahlgren *et al*., 1992).

The short chain *n*-alcohols (*n*-OHs) – primarily the C_{16} and C_{18} homologues – are mainly derived from phytoplankton and bacteria (Meyers and Ishiwatari, 1993), whereas the long chain *n*-OHs predominantly occur in terrestrial plant wax esters (Eglinton and Hamilton, 1967; Řezanka and Sigler, 2009).

Similarly, the *n*-Alkanes can originate from different biological sources, but they have been studied more extensively, sometimes allowing more nuanced interpretations than the corresponding fatty acids and alcohols. For example, C_{17} and C_{19} *n*-alkanes are generally thought to derive from algae and photosynthetic bacteria (Han *et al*., 1968; Han and Calvin, 1969; Cranwell *et al*., 1987; Meyers, 2003), whereas the C_{27}, C_{29} and C_{31} *n*-alkane are constituents of land plants (leaf waxes), with the C_{31} *n*-alkane frequently being the most abundant *n*-alkane in grasses (Maffei, 1996; Ficken *et al*., 2002). *n*-Alkanes typically have an odd carbon-number predominance (Debyser *et al*., 1975; Dastillung and Corbet, 1978). In some settings, the even-numbered *n*-alkanes, especially the C_{14}-C_{22} homologues, occur in elevated proportions and are attributed to a bacterial source (Grimalt *et al*., 1986; Grimalt and Albaigés, 1987). Although *n*-alkanes are derived from a wide range of sources, some mid-chain *n*-alkanes can indicate input from more specific sources if present in greater

proportion. For example, the *n*-C_{23} and *n*-C_{25} *n*-alkanes are abundant and frequently the dominant *n*-alkane in many *Sphagnum* species (Baas *et al*., 2000; Nott *et al*., 2000), and *n*-C_{21} can be dominant in some aquatic plants (Cranwell, 1984).

Sterols are ubiquitous in eukaryotes, such that they are widespread in diverse organisms, but their distributions can provide some organic matter source insights (Volkman, 1986). They are derived from both algal and aquatic and higher plant inputs, with the latter typically associated with a dominance of C_{29} and sometimes C_{28} components, i.e. sitosterol (24-ethylcholesta-5-en-3β-ol), stigmasterol (24-ethylcholesta-5,22-dien-3β-ol) and campesterol (24-methylcholesta-5-en-3β-ol) (Goad and Goodwin, 1972). Pentacyclic triterpenoids, including the amyrins (α and β) occur in terrestrial plants (Volkman *et al*., 2005), commonly occurring in barks and resins. Specifically, higher amounts of α-amyrin are found in resins of the *Bursera* and *Protium* species from the *Burseraceae* family (Hernández-Vázquez *et al*., 2012).

2.6.2 GDGTs

2.6.2.1 Isoprenoidal GDGTs

Isoprenoid glycerol dialkyl glycerol tetraethers (GDGTs) are membrane lipids synthesised by Thaumarchaeota and they occur ubiquitously in a wide range of environments such as oceans, lakes, (sub)surface sediments and soils (Schouten *et al*., 2013). This type of lipid consists of an isoprenoid carbon skeleton ether bonded to a glycerol-moiety containing cyclopentane rings (GDGT 1-3 and crenarchaeol; Figure 2.6). They can be used as proxies for reconstructing marine and lake surface temperatures, as well as examining inputs of the soil organic matter into the marine or lacustrine environments.

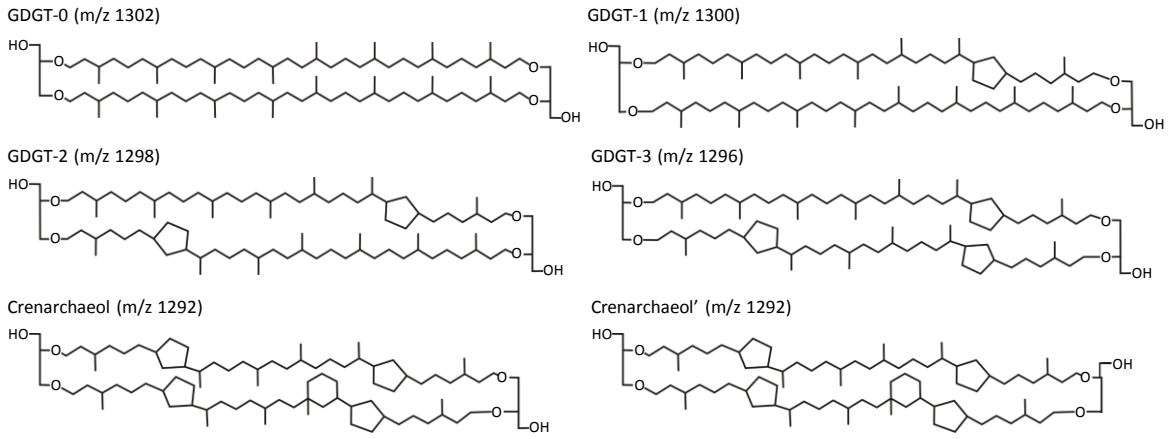

Figure 2.6 Structures of isoprenoid GDGTs (modified after Schouten et al., 2013).

Based on the premise that the number of cyclopentane moieties in the GDGT structure increases with the growth temperature, Schouten *et al*. (2002) defined the TEX_{86} (TetraEther IndeX of membrane lipids consisting of 86 carbon atoms) proxy as:

$$TEX_{86} = \frac{GDGT2 + GDGT3 + crenarchaeol'}{GDGT1 + GDGT2 + GDGT3 + crenarchaeol'} \quad \text{Equation 2.1}$$

As showed in Equation 2.1, the GDGT 0 and crenarchaeol are not included for calculating the TEX_{86} ratio. GDGT 0 is produced by methanogens and crenarchaeol usually presents higher abundance relative to other GDGTS (Schouten *et al*., 2002). Powers *et al*. (2004) applied TEX_{86} in lacustrine setting for the first time to obtain mean annual lake surface temperature by using the marine calibration (Schouten *et al*., 2002). Later, Powers *et al*. (2010) and Tierney *et al*. (2010) presented a TEX_{86} calibration for lakes based on twelve and five samples, respectively. Castañeda and Schouten (2011) combined these calibrations in Equation 2.2, where the mean annual lake surface temperature can be calculated as follows:

$$T°C = 49.032 \times TEX_{86} - 10.989 \quad \text{Equation 2.2}$$

The application of TEX_{86} in lacustrine settings has proved to be a useful tool for continental paleotemperature reconstruction, particularly in large lakes of the East African Rift Valley with abundant isoprenoidal GDGTs such as the Lake Malawi (Powers *et al*., 2005), Lake Tanganyika (Tierney *et al*., 2008), Lake Turkana (Berke *et al*., 2009) and Lake Victoria

(Berke *et al*., 2010) among others. However, TEX_{86} ratio cannot be successfully applied in all lacustrine settings and several factors must be considered such as:

- Not all the lakes present the suitable GDGT assemblage to calculate TEX_{86} ratio (Powers *et al*. 2010; Blaga *et al*., 2009).
- Some isoprenoid GDGTs can be produced in soils by other Archaea (Weijers *et al*., 2006).
- Additional contributions of isoprenoid GDGTs can be from methanogenic Euryarchaeota (Blaga *et al*., 2009).
- Seasonal influence of Thaumarchaeota blooms (Castañeda and Schouten, 2011).
- Thaumarchaeota sub-surface production (Castañeda and Schouten, 2011).
- pH (Pearson *et al*., 2008).
- Different populations of Thamuarchaeota residing in different lakes (Trommer *et al*., 2009).

2.6.2.2 Branched GDGTs

Branched GDGTs (brGDGTs) present methyl substituted C_{28} *n*-alkyl side chains that contain 4, 5 of 6 methyl substitutes rather than isoprenoidal carbon skeleton (Sinninghe Damsté *et al*., 2000; Figure 2.7) and are biosynthesized by anaerobic soil bacteria (Weijers *et al*., 2006a; Sinninghe Damsté *et al*., 2011), although their exact source organism(s) remain unknown. They were first identified in peats (Sinninghe Damsté *et al*., 2000) and later found as ubiquitous and dominant in soils (Weijers *et al*., 2006). They are of interest in reconstructing mean annual air temperature and soil pH (Weijers *et al*., 2007).

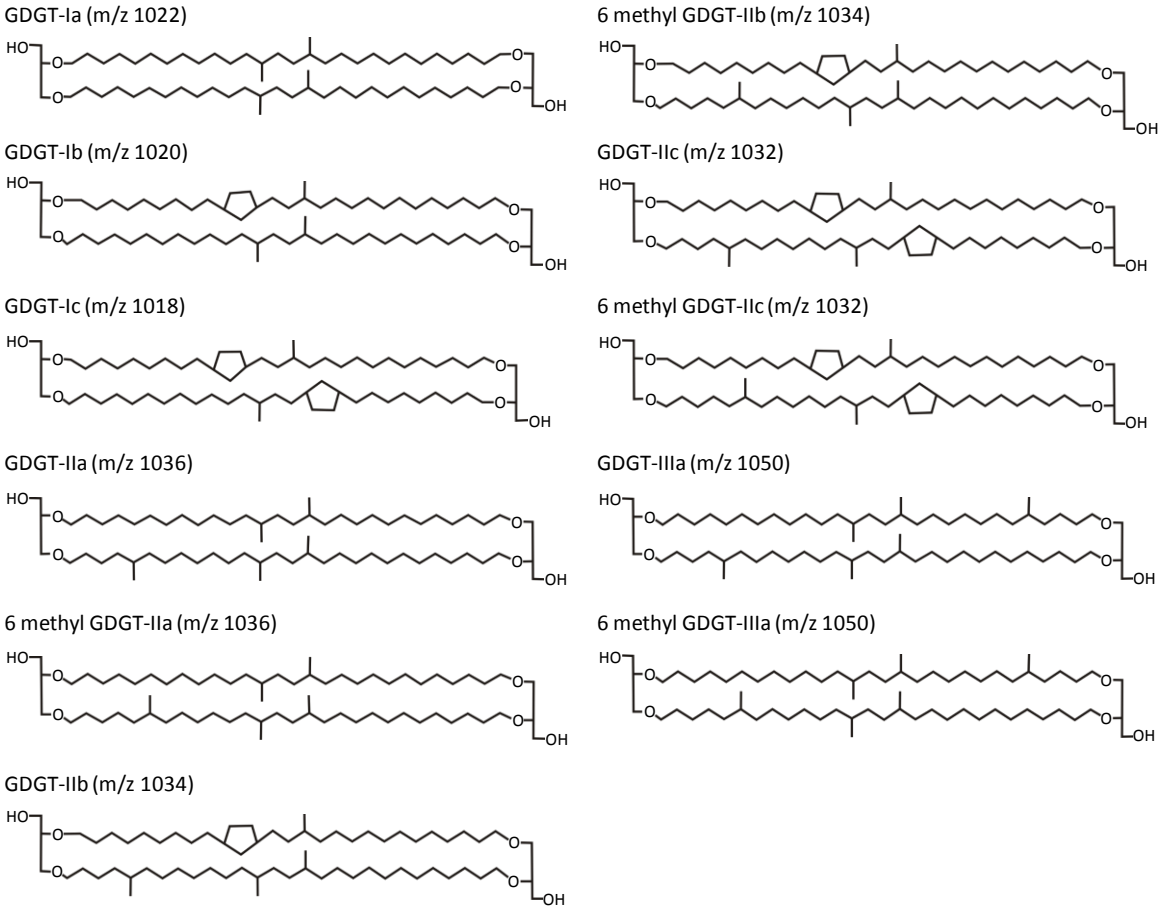

Figure 2.7 Structures of branched GDGTs (modified after Schouten *et al*., 2013).

The Cyclisation of Branched Tetraethers (CBT) represents a pH proxy for soils and it is based on the observation that relative number of cyclopentane moieties of brGDGTs is exponentially negatively correlated with soil pH (Weijers *et al*., 2007). The CBT ratio can be calculated as follows:

$$\mathrm{CBT} = -\mathrm{LOG}\frac{GDGT1b + GDGT2b}{GDGT1a + GDGT2a} \qquad \text{Equation 2.3}$$

The Methylation of Branched Tetraethers (MBT) show positive correlation with the mean annual soil temperature – which in many cases is similar to mean annual air temperature (MAAT). They are also negatively correlated with soil pH (Weijers *et al*., 2007). The MBT ratio can be calculated as follows:

$$\mathrm{MBT} = \frac{GDGT1a + GDGT1b + GDGT1c}{\sum[all\ branched\ GDGTs]}$$ Equation 2.4

Therefore, the mean annual air temperature (MAAT) can be reconstructed by combining the MBT and CBT ratios as follows:

$$\mathrm{CBT} = 3.33 - 0.38 \times \mathrm{pH}$$ Equation 2.5

(Weijers *et al*., 2007; Peterse *et al*., 2012)

$$\mathrm{MAAT} = 0.81 - 5.67 \times \mathrm{CBT} + 31.0 \times \mathrm{MBT}$$ Equation 2.6

(Weijers *et al*., 2007; Peterse *et al*., 2012)

Application of these proxies in lake sediments to reconstruct continental MAAT is currently uncertain as brGDGTs in lacustrine settings reflect mixed sources (Castañeda and Schouten, 2011). The use of local calibrations is highly recommended to improve the MAAT reconstruction based on brGDGTs (e.g. Zink *et al*., 2010; Tierney *et al*., 2010b). Some lakes with mixed sources of brGDGTs may be suitable for reconstructing MAAT when the lake water temperature is correlated with MAAT (Livingstone and Lotter, 1998). Shallow lakes without thermal stratification, usually present water temperatures similar to MAAT, while lakes deep enough to stratify present different water temperature between surface and bottom. Seasonal variations in GDGT production could also influence MAAT reconstructions in some lakes. However, some outstanding questions, remain to be answered by further studies, and their application as proxies needs to be assessed for individual sites (Castañeda and Schouten, 2011).

2.6.2.3 Relationship between iGDGTs and brGDGTs

The Branched and Isoprenoid Tetraether (BIT) index is a proxy for aquatic vs. soil organic matter (OM) input. It is based on relative abundances of soil derived (branched) GDGTs vs. crenarchaeol (Figure 2.4), which is a biomarker for aquatic Thaumarchaeota (Hopmans *et al*., 2004). This ratio is calculated as follows:

$$\text{BIT} = \frac{GDGT1a + GDGT2a + GDGT3a}{crenarchaeol + GDGT1a + GDGT2a + GDGT3a} \quad \text{Equation 2.7}$$

BIT values range from 0 to 1, where 0 indicates pure aquatic source (only crenarchaeol is present) and 1 represents pure soil OM source (Hopmans *et al*., 2004). Although the BIT index represents a useful tool for examining the delivery of soil organic matter to lacustrine (marine) systems, it should be used with other terrestrial proxies for examining the transport of soil organic matter and vegetation to aquatic environments. Additional considerations should be made as crenarchaeol can occur in subordinate abundances in soils (Weijers *et al*., 2006), and brGDGTs can be produced in situ in aquatic settings (Smith *et al*., 2012; Damsté, 2016). Many lakes present high BIT index values as they have larger watersheds and smaller lake surface areas. Powers *et al*. (2010) estimated that >75% of lakes present high BIT values (>0.5). However, the studies of Damsté *et al*. (2009), Tierney and Russell (2009) and Bechtel *et al*. (2010) have concluded that in-situ production of branched GDGTs is very likely to occur in lakes as a result of biosynthesis by anaerobic soil bacteria.

2.6.3 Compound specific isotopes

In addition to biomarker distributions, the carbon isotopic composition of plant wax constituents, such as fatty acids and *n*-alkanes, can be used to distinguish between vegetation using different photosynthetic pathways such as C_3 (Calvin-Benson pathway), C_4 (Hatch-Slack pathway) and Crassulacean Acid Metabolism (CAM) plants (Leng and Henderson, 2013). C_3 plants dominate temperate environments in terrestrial ecosystems and represent approximately 85% of all plant species, whereas C_4 plants grow in extreme environments with high light intensities, high temperatures and high aridity (Ehleringer, 1991). Therefore, $\delta^{13}C$ values of plant biomarkers can act as an environmental proxy, via the ecological response to climatic conditions.

During photosynthesis, the Rubisco (RuBP) enzyme discriminates in favour of the lighter ^{12}C isotope over the heavier ^{13}C isotope from the atmospheric CO_2 (O'Leary, 1988). However, due to physiological and biochemical differences, different plants exhibit different degrees of discrimination. C_3 plants incorporate atmospheric CO_2 through the boundary layer and the stomata into the internal gas space. The internal CO_2 is dissolved in cell sap and

diffuses to the chloroplast for RuBP-mediated carboxylation (Figure 2.8). On the other hand, C_4 photosynthesis pathway involves two carboxylase systems (Figure 2.8). The atmospheric CO_2 enters the leaf through the stomata and then taken up by phosphoenolpyruvate carboxylase in the mesophyll cells. The product of this carboxylation is converted to either malate or aspartate. It is then transported to bundle sheath cells to be cleaved to CO_2 and some other compounds, and the produced CO_2 is taken up by the RuBP carboxylase (O'Leary, 1988).

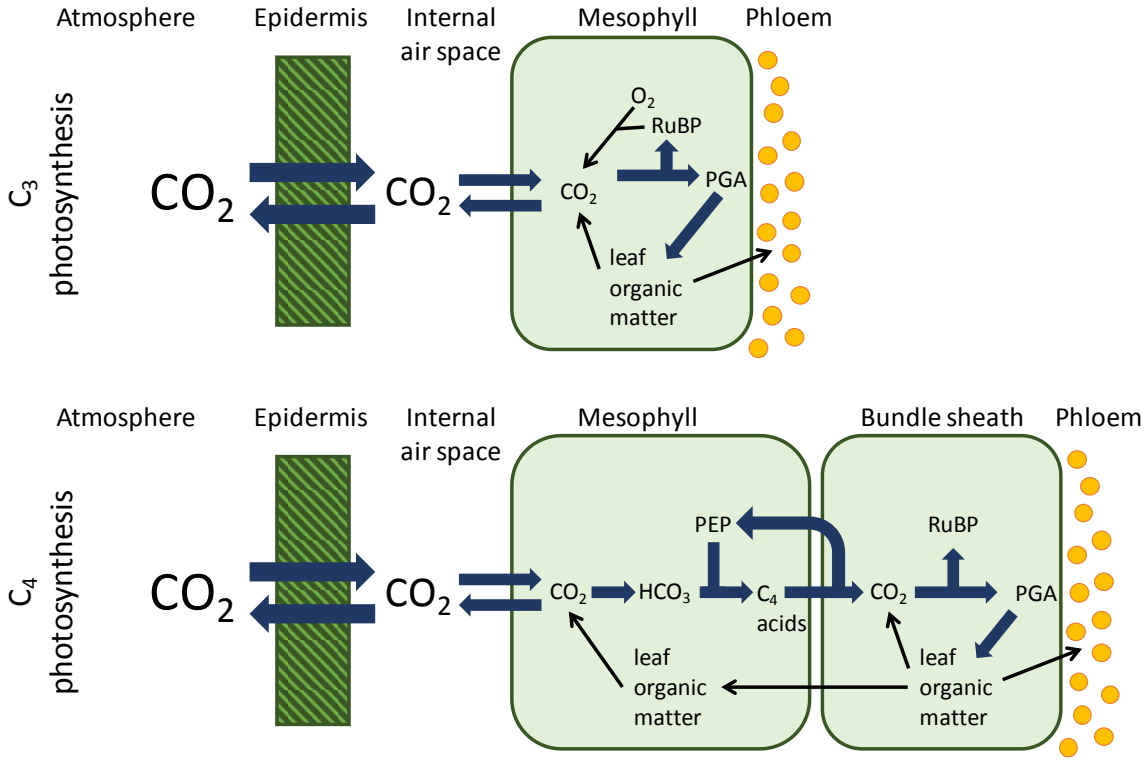

Figure 2.8 Important steps in CO_2 fixation during C_3 and C_4 photosynthesis. Sizes of arrows indicate the relative fluxes through the various steps (modified after O'Leary, 1988).

As a result of their different photosynthesis pathway, C_4 plants are less depleted in ^{13}C than C_3 species. Usually the C_3 plants exhibit $\delta^{13}C$ values between -34 and -22 ‰, whereas C_4 exhibit $\delta^{13}C$ values between -20 and -10 ‰ (Figure 2.9; O'Leary, 1988).

Desert plants and other succulents – approximately 10 % of global flora – absorb CO_2 by the pathway known as Crassulacean acid metabolism (CAM; Osmond *et al.*, 1976; Kluge and Ting 1978; Ehleringer *et al.*, 1991). These plants possess the ability to absorb atmospheric

CO_2 during the day or night, utilising both the C_3 and C_4 photosynthesis pathways (Osmond *et al*., 1976; Kluge and Ting 1978). Therefore, CAM plants can exhibit a wide range of $\delta^{13}C$ values, when the photosynthesis is engaged during daytime, they have $\delta^{13}C$ values of approximately -28 ‰, characteristic of C_3 plants, whereas when this prosses occurs at night, they have $\delta^{13}C$ values of approximately -11 ‰ (Nalborczyk *et al*. 1975, O'Leary 1981).

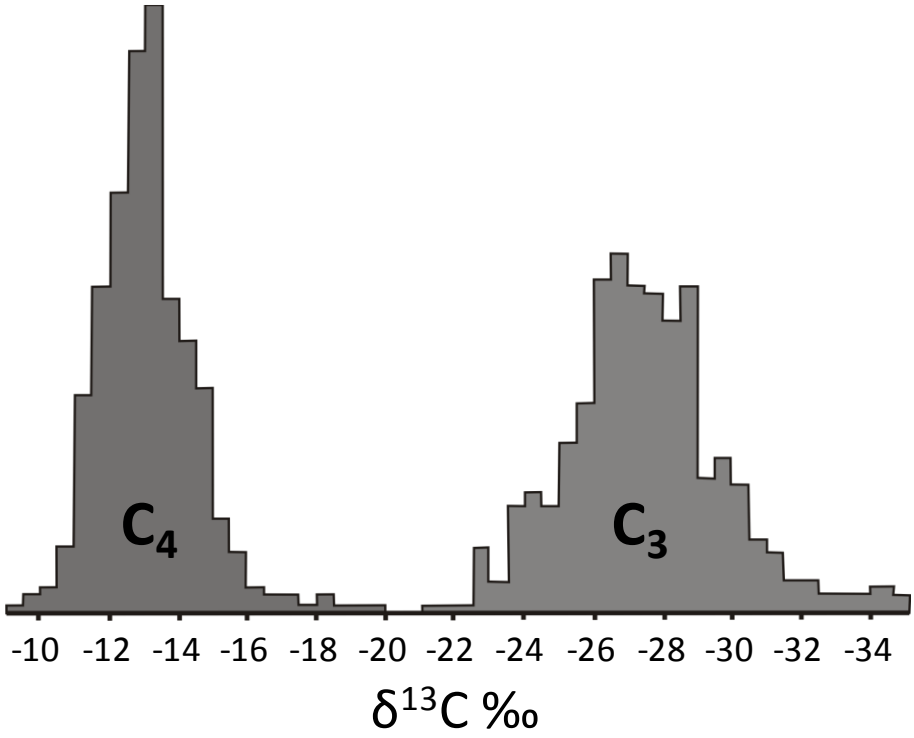

Figure 2.9 Histogram showing the distribution of $\delta^{13}C$ values obtained in different plant materials. Figure based on ~1000 analyses performed in different laboratories (O'Leary, 1988).

The carbon isotopic composition of aquatic biomarkers, such as short- and mid-chain compounds (fatty acids, *n*-alkanes) in lacustrine sediments, can be used to reconstruct changes in primary productivity and the lake's carbon cycle (Leng and Henderson, 2013). Aquatic plants follow the photosynthesis pathway of C_3 plants, but they exhibit $\delta^{13}C$ values between -42 and -26 ‰ as they incorporate CO_2 dissolved in water with more depleted (-20 ‰) $\delta^{13}C$ values than the atmospheric CO_2 (-7.8 ‰; Leng and Marshall, 2004).

2.7 Inorganic Geochemical Proxies

Inorganic geochemical proxies that have been applied in previous studies of the Santiaguillo and El Potosi basins include mineralogy, major and trace element analysis. Moreover, a

recent study of the Santiaguillo Basin (Quiroz-Jiménez *et al*. 2017) includes analysis of carbon and oxygen isotopic composition of endogenic carbonates. However, the authors only focused on the paleoclimate conditions of the six Heinrich events. In this project, I am generating new isotopic data of endogenic carbonates at better resolution and focusing on the late Pleistocene and Holocene from both Satiaguillo and El Potosi basins.

2.7.1 $\delta^{18}O$ in endogenic carbonate

The oxygen isotopic composition of endogenic carbonate precipitates ($\delta^{18}O_{carb}$) is governed by temperature, the source of precipitation and the balance of precipitation/evaporation, the latter two factors via their impact on lake water $\delta^{18}O$ (Figure 2.10). Given a specific $\delta^{18}O$ value for source water (i.e. lake water), the isotopic composition of carbonates precipitated in equilibrium can be predicted by thermodynamics, reflecting the temperature control on $\delta^{18}O_{carb}$. However, the interpretation of $\delta^{18}O_{carb}$ in practice is complicated because $\delta^{18}O_{lakewatr}$ does vary, and in particular can be strongly affected by climate (Leng and Marshall, 2004). This is particularly true in lakes that experience pronounced evaporitic water loss.

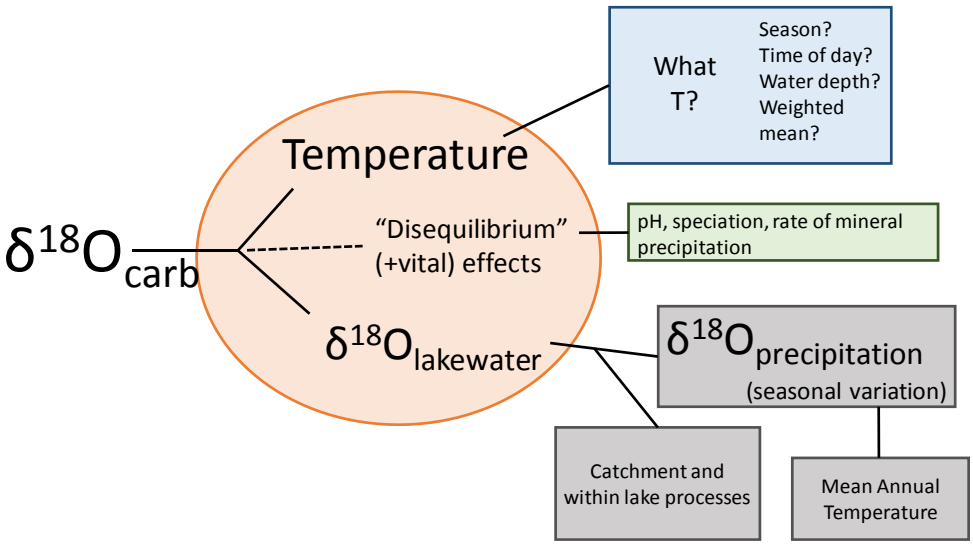

Figure 2.10 Factors that can influence the oxygen isotope composition of a lacustrine carbonate precipitate ($\delta^{18}O_{carb}$) (Leng and Marshall, 2004).

For the carbonates precipitated in equilibrium with the water column, the isotopic composition decreases by about 0.24‰ for each 1˚C increase in temperature (Craig, 1965). Several studies have attempted to determine the empirical relationship between temperature,

oxygen isotope composition of different carbonate minerals and composition of the water from which they precipitated (i.e. Craig, 1965; Anderson and Arthur, 1983; Grossman and Ku, 1986; Kim and O'Neil, 1997; Leng and Marshall, 2004). The following equation proposed by Leng and Marshall (2004) is a more convenient re-expression of the one proposed by Kim and O'Neil (1997):

$$T^{\circ}C = 13.8 - 4.58(\delta c - \delta w) + 0.08(\delta c - \delta w)^2$$

Equation 2.8

Where:

T˚C = temperature in Celsius degrees

$\delta c = \delta^{18}O$ of the carbonate compared to the PDB international standard

$\delta w = \delta^{18}O$ of the water compared to the SMOW international standard

The application of paleotemperature equations should consider the modern relationship between temperature and mineral composition. This would be very useful when interpreting the sediment record and reconstructing the past temperature. Carbonates do not always precipitate in equilibrium, often due to disequilibrium effects (vital effects in biogenic materials) associated with the rates of precipitation, pH, incorporation of metabolic fluids and microenvironment effect (vital offset; Leng and Marshall, 2004). Therefore, it is recommended to avoid bulk carbonate analysis in sediments with a mixture of variable proportions of biogenic and authigenic phases with very different compositions.

Crucially, the oxygen isotope composition of the lake water ($\delta^{18}O_{water}$) also dictates $\delta^{18}O_{carb}$, and strongly depends on the entire hydrological system. Most systems can be divided into two broad types: open lakes (more common at high altitudes) and closed lakes (more common at low altitudes). In open lake systems, with a degree of throughflow, the $\delta^{18}O_{water}$ mostly reflects the isotopic composition of the precipitation. These types of lakes usually present a variable down-core oxygen isotope composition of no more than a few ‰ and that predominantly reflect changes in temperature and the isotopic composition of precipitation (Leng and Marshall, 2004). In closed lake systems, those same factors are important, but $\delta^{18}O_{water}$ values are further impacted by the balance of precipitation and evaporation. Typically, $\delta^{18}O_{water}$ values are enriched due to the loss of water through evaporation. In such cases, analogous to both Santaguillo and El Potosi, long-term changes in the

precipitation/evaporation ratio are typically the main drivers of the isotope composition of authigenic carbonates, with variations of >10 ‰. Closed lakes are often classified as salt lakes and contain abundant endogenic carbonate (Leng and Marshall, 2004).

2.7.2 $\delta^{13}C$ in endogenic carbonate

The carbon isotopic composition of endogenic carbonate ($\delta^{13}C_{carb}$) provides information about the sources of total dissolved inorganic carbon (TDIC) within the lake. Those are typically: (1) dissolved inorganic carbon in inflowing waters; (2) CO_2 exchange between the atmosphere and lake water; and (3) photosynthesis/respiration of aquatic plants of the lake basin (Figure 2.11; Leng and Marshall, 2004). In lakes with strong allochthonous organic matter inputs, respiration of that organic matter provides a further strong control on $\delta^{13}C_{carb}$.

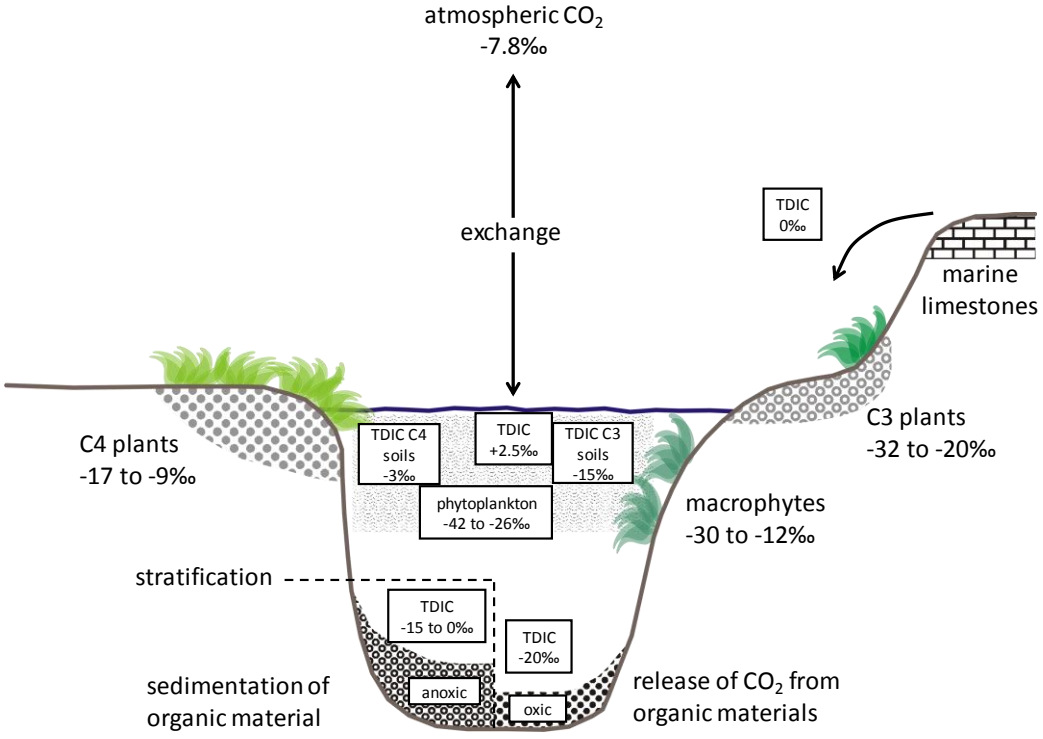

Figure 2.11 Carbon isotope values of main sources of carbon for the lacustrine sediments and resulting $\delta^{13}C_{TDIC}$ ranges (Leng and Marshall, 2004).

The carbon isotopic composition of the inflowing water, such as ground and rivers waters, can have a significant proportion of inorganic carbon derived from the decomposition of plant debris (C_3 vs. C_4 plants) and production of CO_2 in the soil. Thus, the transport path,

amount of vegetation and soil development can have a large effect on the TDIC budget. Moreover, the ground water in karstic regions enriches the inorganic carbon isotope composition of the TDIC due to high proportion of carbon sourced from dissolution of catchment limestones (Leng and Marshall, 2004). In hydrologically closed lakes, especially in non-karstic catchments, the inorganic carbon isotope composition of the TDIC is also strongly controlled by the exchange between atmospheric CO_2 and the lake water, where the (high) values are likely to reflect different equilibration of TDIC with atmospheric CO_2 (Leng and Marshall, 2004).

During periods of enhanced productivity, the carbon pool in water becomes enriched in ^{13}C by aquatic plants discriminating in favour of the lighter ^{12}C isotope during photosynthesis, resulting higher $\delta^{13}C_{TDIC}$ values. Depending on when and where this organic matter is respired (seasonally, at depth, in sediments), this can cause strong isotopic variation both seasonally and with water depth. This can particularly impact the $\delta^{13}C_{carb}$ of carbonates precipitated at different depths in the water column (Leng and Marshall, 2004).

In particular, the Santiaguillo and the El Potosi basins are closed lake systems. Therefore, $\delta^{18}O_{carb}$ values are mainly impacted by the balance of precipitation and evaporation, reflecting associated temperature changes. On the other hand, $\delta^{13}C_{carb}$ values of the Santiaguillo carbonates reflect lake productivity changes during wetter periods, and CO_2 exchange between the atmosphere and lake water during dry periods. While $\delta^{13}C_{carb}$ values of the El Potosi Basin are mainly influenced by dissolved inorganic carbon from catchment limestone during wetter periods, and CO_2 exchange between the atmosphere and lake water during dry periods.

2.8 Unravelling paleoenvironmental conditions

The evaluation of lipid biomarker context in Santiaguillo and El Potosi lake sediments provides information about changing source inputs, aquatic productivity and/or vegetation changes in response to the major climate perturbations that occurred over the late Pleistocene and Holocene. Moreover, GDGT analysis – in particular the application of BIT index – provides further information about soil organic matter input to the lacustrine system.

The carbon isotopic composition of fatty acids in plant wax constituents provides specific information about the type of vegetation for reconstructing past ecosystems in and around the lacustrine basins. Furthermore, the carbon isotopic composition of aquatic biomarkers, such as short- and mid-chain fatty acids is used to reconstruct changes in primary productivity and the lake's carbon cycle.

The oxygen isotopic composition of endogenic carbonates is used as proxy of paleotemperature changes and provides further information for inferring the biological and environmental responses to global climatic events during the late Pleistocene and Holocene at southern part of the Chihuahua Desert of Mexico.

CHAPTER III
Materials and Methodology

3.1 Material

Sediment samples originate from two different areas: the Santiaguillo Basin (state of Durango) and the El Potosi Basin (state of Nuevo Leon) in central northern Mexico (Figure 3.1). The sediments were recovered during two expeditions headed by Prof. Priyadarsi D. Roy between 2009 and 2014. Both sedimentary records were sampled every two centimetres, individually packaged in plastic bags and stored in the freezer room of the Paleoenvionmental and Paleoclimatology Lab at the Institute of Geology of the National Autonomous University of Mexico (UNAM).

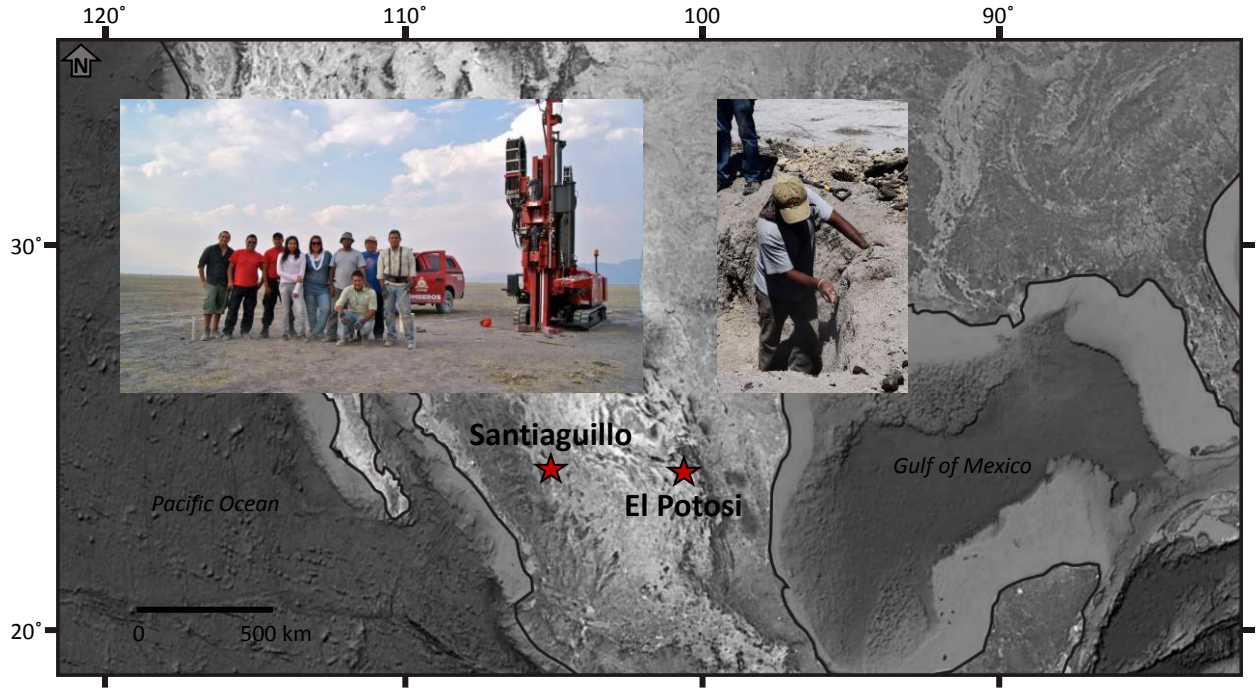

Figure 3.1 Location of the Santiaguillo and the El Potosi lacustrine basins in central northern Mexico.

The sedimentary records were dated using radiocarbon chronology, ensuring the existence of well-developed age models. Accordingly, the sedimentary records from the Santiaguillo and El Potosi basins span the last 27,000 and 20,000 years, respectively, thus recording major climate perturbations from the LGM to the present. In addition, multi-element geochemistry and magnetic susceptibility records have been established, providing crucial information on the depositional environment and sources of the mineral phase of the sediment for each site (Chávez-Lara *et al*., 2015; Roy *et al*., 2015, 2016). This data has been included in this study for comparison and better understanding of the new proxies targeting the complex nature of organic matter inputs and their variability over time. Initially, a total of 62 sediment samples from both basins were selected for this PhD project. Subsequently, a second batch of 62 sediment samples were incorporated for inorganic analysis.

3.2 Methodology

3.2.1 General sample preparation

All glassware used for sample preparation and storage was cleaned first by soaking in water and detergent (Decon 90), followed by rinsing with tap water, distilled water and finally furnacing at 450 °C for at least 4 h. Analytical blanks were handled alongside each batch of samples to track and identify possible contamination. Analytical grade reagents (≥98% purity) and HPLC grade solvents were used in all experiments. All samples were freeze-dried and removed from plastic bags. The sediments were homogenized by hand using a glass mortar and pestle and stored individually in furnaced glass jars.

The following diagram shows the methodology used for the different analyses, every step is described in detail below.

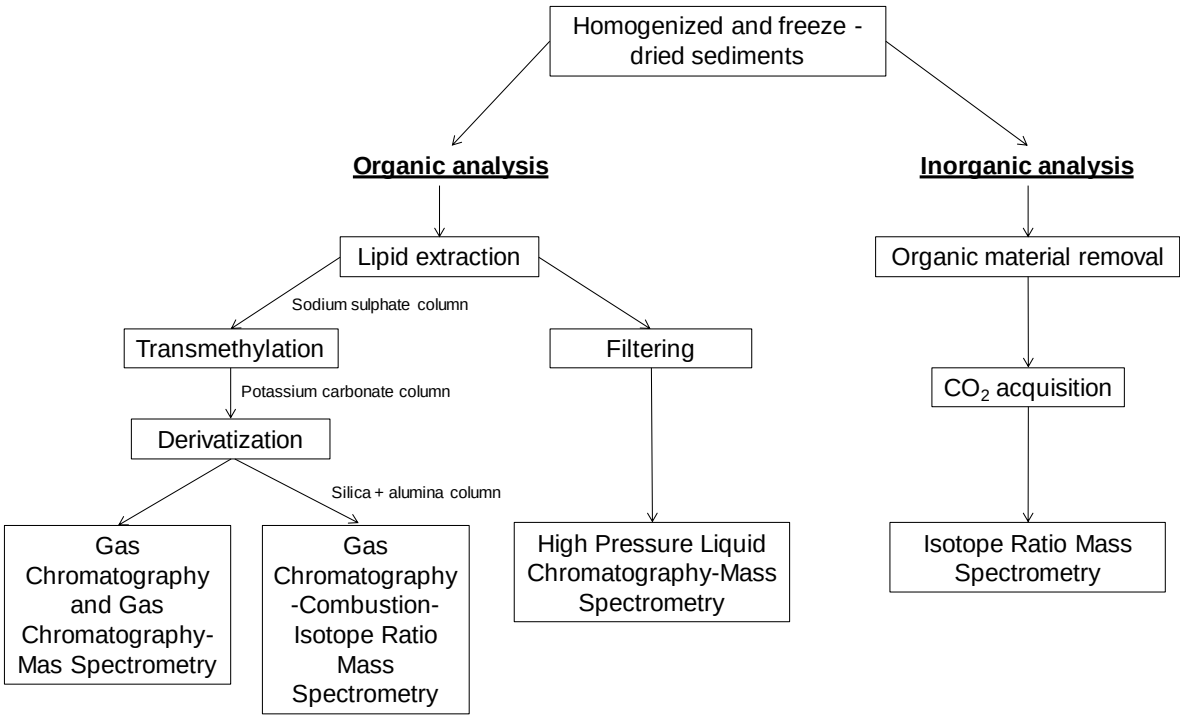

Figure 3.2 Flowchart of the methodologies carried out for analyses in this project.

3.2.2 Organic geochemical analyses

3.2.2.1 Biomarker analysis

3.2.2.1.1 Lipid Extractions

The powdered sediment was weighed and transferred to a clean glass culture tube and 5α-cholestane was added as an internal standard. The amounts of internal standard added to each sediment sample were assessed based on the total organic carbon (TOC) concentrations of the samples. The lipid biomarkers were then extracted from the sediment using a microwave-assisted solvent extraction system (Milestone EthosEX), with a solvent mix of dichloromethane (DCM) and methanol (9:1 v/v). The solvent was heated to 70˚C over 10 minutes and kept at this temperature for another 10 minutes. Once cooled, the samples were centrifuged and the supernatant was pipetted off into round-bottom flasks. The samples were washed with DCM:methanol (9:1 v/v) and centrifuged, again, with the supernatant being collected. This was repeated twice. A rotary evaporator was used to remove most of solvent. The residual solution was then transferred onto small sodium sulphate columns (Pasteur

pipettes) in order to completely remove any residual water from the total lipid extracts (TLEs). The TLEs of samples with sufficiently high yields were then split for various analytical procedures and stored in a freezer at -20˚C.

3.2.2.1.2 Hydrolysis and transmethylation of fatty acids

About 1 mL of acetyl chloride in methanol (1:30 v/v) was added to an aliquot of TLE. Samples were then heated at 45˚C for 12 h. This acid-catalysed procedure splits esters into their fatty alcohol and acid components (hydrolysis) and turns the fatty acids into GC-amenable fatty acid methyl esters (FAMEs). Free fatty acids present in the TLE are also turned into FAMEs (transmethylation). The acetyl chloride-methanol solution was evaporated under a gentle flow of nitrogen. The extracts were then passed through potassium carbonate columns in order to remove any excess acids.

3.2.2.1.3 Derivatisation of hydroxy groups

About 25 µL of N,O-bis(trimethylsilyl)trifluoroacetamide (BSTFA) was added to the transmethylated TLEs. Samples were then heated at 65˚C for 1 h. This procedure replaces hydroxy groups (e.g., of alcohols, sterols, hydroxy acids) with a trimethylsilyl (TMS) group, thus reducing polarity of the molecules and making them GC-amenable. Excess of derivatising agent BSTFA was evaporated under a gentle flow of nitrogen.

3.2.2.1.4 Gas chromatography (GC) and gas chromatography-mass spectrometry (GC-MS)

The derivatised lipid extracts were dissolved in DCM prior to GC and GC/MS analysis. 1 µl was injected on the GC to screen the TLE and to calculate the appropriate concentration for the GC-MS analyses. The equipment used for screening is a Trace 1300 gas chromatograph (ThermoFisher Scientific) fitted with a Restek RTX-1 fused silica column (50 m x 0.32 mm; film: dimethyl polysiloxane, thickness 0.17 µm) and a flame ionization detector (FID). GC-MS analysis was carried out using a Trace 1300 GC linked to an ISQ mass spectrometer (ThermoFisher Scientific), operating with electron ionization at 70 eV and scanning an ion fragment mass range of m/z = 50-650. H_2 was used as carrier gas on the GC and He on the GC-MS. The heating program for both GC and GC-MS analyses was as follows: 60˚C initial

temperature, hold for 1 minute, heating to 170˚C at 6˚C min^{-1}, then to 315˚C at 2.5˚C min^{-1}. The final temperature was hold at for 10 minutes.

3.2.2.2 GDGTs analysis

3.2.2.2.1 Filtering

For GDGTs analysis, TLE aliquots were dissolved in a solvent mix of hexane and isopropanol (99:1) and passed through a 0.45 μm polytetrafluoroethylene (PTFE) filter.

3.2.2.2.2 High Pressure Liquid Chromatography / Mass Spectrometry (HPLC/MS)

The analysis of isoprenoidal and branched glycerol dialkyl glycerol tetraethers (GDGTs) analysis was performed using a ThermoFisher Scientific Accela Quantum Access triple quadrupole MS. 15 μl of sample was automatically injected with partial loop injection setting. The column used was an Alltech Prevail Cyano (150 mm x 2.1 mm; 3 μm i.d.) with a flow rate of 0.2 ml/min (Schouten *et al*., 2002). Samples were eluted isocratically with a solvent mix of hexane and isopropanol (99:1 v/v) for 5 minutes followed by a linear gradient to 88:12 (v/v) hexane:isopropanol.

3.2.2.3 Compound-specific isotopes analysis

3.2.2.3.1 Fractionation

In order to fractionate TLEs for compound-specific carbon isotope analysis, TLEs were taken up by activated alumina and, after gentle removal of the solvent (DCM), transferred onto a silica column (deactivated with 5% H_2O, 1.25 g, 60-120 mesh, column length ~132 mm). The TLEs were separated into 7 fractions, based on polarity using 7 solvent mixtures (3.5 ml of each) of increasing polarity: *n*-hexane, *n*-hexane:toluene (75:25 v/v), *n*-hexane:toluene (50:50 v/v), *n*-hexane:ethyl acetate (95:5 v/v), *n*-hexane:ethyl acetate (90:10 v/v), *n*-hexane:ethyl acetate (85:15 v/v) and *n*-hexane:ethyl acetate (80:20 v/v). Fractions were dried under a gentle flow of nitrogen and dissolved in hexane prior to compound-specific isotope analysis.

3.2.2.3.2 Gas Chromatography-Combustion-Isotope Ratio Mass Spectrometry (GC-C-IRMS)

Stable carbon isotope values of fatty acid methyl esters (FAMEs) were analysed using an Agilent Industries 7890A gas chromatograph coupled to an IsoPrime 100 mass spectrometer. Samples were automatically injected in splitless mode. Helium was used as a carrier gas. The GC oven temperature programme was set to hold at 40 ˚C for 2 minutes, followed by an increase to 300 ˚C at 10 ˚C min^{-1}. The oven temperature was held at 315 ˚C for 10 minutes. The combustion interface consisted of a copper and silver wool reactor maintained at 850 ˚C. A standard FAME mixture (C_{11}, C_{13}, C_{16}, C_{21} and C_{23}) of known isotopic composition was used to determine the instrument accuracy. Samples were analysed in duplicate and the average value was considered for interpretation.

3.2.3 Inorganic analysis

3.2.3.1 Analysis of carbon and oxygen isotopes of carbonates

3.2.3.1.1 Organic matter removal

Around 1 g of powdered sediment was placed in 500 ml glass jars and immersed in 50 ml of 5% sodium hypochlorite for at least 12 hrs. Afterwards, sediments were repeatedly washed with double-distilled water until reaching neutral pH and left to dry at 40 ˚C for 12 hours. The dry sediments were re-homogenised by hand using a glass mortar and pestle.

3.2.3.1.2 CO_2 acquisition

Bulk carbonates were reacted with 100% phosphoric acid to evolve CO_2 under vacuum overnight at a constant 25.5 ˚C. The CO_2 was separated from water vapour by cryogenic cooling with liquid nitrogen under vacuum and collected for analysis.

3.2.3.1.3 VG Optima MS

Carbon and oxygen isotope values ($\delta^{13}C_{calcite}$, $\delta^{18}O_{calcite}$) were determined by a VG Optima dual inlet mass spectrometer at the Stable Isotope Facility of the British Geological Survey.

3.3 Data processing

3.3.1 Identification and quantification of lipids

Compounds were identified by comparing the mass spectra and relative retention times of peaks in the chromatogram/with those in the literature. Fatty acids were determined as their derivatives, fatty acids methyl esters (FAMEs). Alcohols and sterols were determined as their trimethylsilyl (TMS) derivatives. The acquisition and analysis of the MS data was carried out using XCalibur software. Quantification was based on the ratio of the peak areas of the target compound and the internal standard, 5α(H)-cholestane, given through the total ion count (TIC). Since the ionisation potential of distinctly different molecular structures (e.g. sterols and fatty acids) differs this method has to be regarded as semi-quantitative unless peak areas are corrected by response factors. The latter would have to be calculated from the analysis of a standard mixture containing all target compounds. Since this was not available biomarker-based proxies could only be developed for compounds from the same compound class, i.e. with similar structures and, hence, similar ionisation potential. Furthermore, samples were analysed in large batches and within a short timeframe to minimise instrumental drift of the ionisation potential.

3.3.2 GDGT analysis

GDGT analysis was performed in "selective ion monitoring" mode and protonated molecular ion GDGT peaks (Table 3.1) were integrated manually defining the peak area as the area above the baseline. In order to track instrumental sensitivity and accuracy, analysis of laboratory standard containing isoprenoidal and branched GDGTs were performed every four samples.

Table 3.1 Molecular ions (m/z) of isoprenoidal and branched GDGTs analysed by HPLC/MS.

GDGT structure	m/z
GDGT-0	1302
GDGT-1	1300
GDGT-2	1298
GDGT-3	1296
GDGT-4	1294
Crenarchaeol and Cren. isomer	1292
brGDGT-Ia	1022
brGDGT-Ib	1020
brGDGT-Ic	1018
brGDGT-IIa and IIa’	1036
brGDGT-IIb and IIb’	1034
brGDGT-IIc and IIc’	1032
brGDGT-IIIa and IIIa’	1050
brGDGT-IIIb and IIIb’	1048
brGDGT-IIIc and IIIc’	1046

3.3.3 $\delta^{13}C$ values of FAMEs

Data processing was carried out using Ion Vantage software (version 1.5.6.0, IsoPrime). The $\delta^{13}C$ values are calculated relative to the international Vienna Pee Dee Belemnite (VPDB) standard, based on the following equation:

$$\delta^{13}C_{sample} = \frac{R_{sample} - R_{standard}}{R_{standard}} \quad \text{Equation 3.1}$$

where:

$\delta^{13}C_{sample}$ = $\delta^{13}C$ values of the sample (in ‰),

R_{sample} = $^{13}C/^{12}C$ in the sample,

$R_{standard}$ = $^{13}C/^{12}C$ in the standard.

$\delta^{13}C$ values for individual fatty acids were then corrected for the carbon atom added during transmethylation using the mass balance equation from Rieley (1994) as follows:

$$\delta^{13}C_{FA} = \frac{(\text{no.}\,C_{\text{FAME}} \times \delta^{13}C_{FAME}) - \delta^{13}C_{CH3OH}}{\text{no.}\,C_{\text{FA}}} \quad \text{Equation 3.2}$$

where:

$\delta^{13}C_{FA}$ = $\delta^{13}C$ of the original fatty acid (in ‰),

$\delta^{13}C_{FAME}$ = measured $\delta^{13}C$ of the FAME (in ‰),

$\delta^{13}C_{CH3OH}$ = measured $\delta^{13}C$ value of the CH_3OH used for methylation,

no.C_{FAME} = total number of carbon atoms in the FAME,

no.C_{FA} = total number of carbon atoms in the fatty acid.

3.3.4 $\delta^{13}C$ and $\delta^{18}O$ values of calcite

Based on equation 3.1, the isotope values are reported as per mil (‰) deviation from the isotopic ratios ($^{13}C/^{12}C$, $^{18}O/^{16}O$) of the VPDB standard, using within-run laboratory and international standards. Analytical reproducibility was <0.1‰ for $\delta^{13}C$ and $\delta^{18}O$.

3.4 Uncertainty evaluation

About 250 compounds per sample were quantified using a single response factor of an internal standard like 5α(H)-cholestane. Therefore, it is reasonable to assume that missing response factors introduce an error as the exact absolute amounts of a specific compound cannot be calculated. However, response factors within a specific compound class, e.g., *n*-fatty acids, tend to differ very slightly (Holtvoeth, unpublished data from analyses of external standard mixtures). Larger differences in detector response are typically observed between different compound classes, e.g., *n*-fatty acids compared to *n*-alkanes. This means that chain-length distributions are barely affected by detector selectivity. However, the amounts of different compound classes such as the amounts of *n*-alkanes relative to *n*-fatty acids, will not reflect actual proportions. Still, relative changes in these proportions between samples

are real. Therefore, in this thesis I am presenting proxies that are based on ratios of compounds from the same compound class, only. In order to minimise the impact of changes in detector sensitivity from instrument reconfiguration and tuning that can also affect different compound classes to different degrees, I analysed the samples in large batches within a short period of time. Nevertheless, the lipid data as a whole has to be viewed as semi-quantitative.

CHAPTER IV
The Santiaguillo Basin

A 27cal ka biomarker-based record of ecosystem changes from lacustrine sediments of the Chihuahua Desert of Mexico

Published in: Quaternary Science Reviews, 191, pp.132-143.

Chávez-Lara, C.M., Holtvoeth, J., Roy, P.D. and Pancost, R.D., 2018.

https://doi.org/10.1016/j.quascirev.2018.05.013

Photo by C.M. Chávez-Lara of the Santiaguillo Basin

4.1 Abstract

Hydroclimate variation of the northwest Mexico during the late Pleistocene and Holocene is an active area of debate, with uncertainty in the nature and sources of precipitation. Previous research has inferred the influences of winter storms, summer monsoonal rain and autumn tropical cyclones. The impacts on regional and local ecosystems, however, are not well constrained. Here, we investigate the response of lacustrine and terrestrial habitats of the Santiaguillo Basin in the Chihuahua Desert (Mexico) to hydrological changes occurring since the late last glacial. Biomarkers from the sediments reflect variable input of organic matter (OM) from algal and bacterial biomass, aquatic microfauna and surrounding vegetation, revealing distinct stages of ecosystem adaption over the last 27 cal ka. Based on previously published and new data, we show that a perennial productive lake was present during the late glacial and it persisted until 17.5 cal ka BP. Coinciding with Heinrich event 1, OM supply from deteriorating wetland soils may have been caused by early dry conditions. Further phases of increasing aridity and a shrinking water body drove changing OM quality and biomarker composition during the early and mid-Holocene. A pronounced shift in biomarker distributions at 4 cal ka BP suggests that the supply of plant litter from resinous trees and grasses increased, likely reflecting the establishment of modern vegetation. Our results illustrate the potential of biomarker applications in the area, adding to the evidence of hydroclimate variability and enabling reconstructions of local ecosystem dynamics.

Keywords: Organic Geochemistry; Continental Biomarkers; North America; Paleoclimatology; Paleolimnology; Pleistocene; Holocene

4.2 Introduction

The Chihuahua Desert is located between 22-32º N and 100-109º W and is the largest desert in North America. Its area of ~ 450,000 km^2 extends through the northern Mexican states of Chihuahua, Durango, Zacatecas, Nuevo Leon and San Luis Potosi and the southern USA states of New Mexico, Texas and Arizona (Palacios-Fest *et al*., 2002). Reconstructions of past climate variations in this desert have received significant attention over the last few decades, particularly with respect to the North American Monsoon (NAM) during the Late Quaternary. Previous records include lacustrine sediments, aeolian deposits, packrat middens

and speleothems, producing proxy data through the distributions of pollen, diatoms and ostracods, inorganic geochemistry (X ray fluorescence, X ray diffraction, magnetic susceptibility) and stable isotopes (e.g. Lozano-García *et al*., 2002; Metcalfe *et al*., 2002; Roy *et al*., 2012, 2013, 2016; Chávez-Lara *et al*., 2015; Quiroz-Jimenez *et al*, 2017). These records have provided insight into past climatic change but the carbon cycling and vegetation responses to those changes are still poorly understood (Metcalfe *et al*., 2015).

Recent publications have presented different hypotheses with regard to the role of the NAM, winter storms and tropical cyclones in regional precipitation patterns during the last glacial maximum (LGM). Oster *et al*. (2015) argued that the location and strength of the contemporary pressure system were responsible for a higher contribution of winter precipitation from the Pacific Ocean to the southwestern USA during the LGM. In Northwest Mexico, however, the NAM was weaker during the LGM due to high latitude cooling that shifted the westerlies south, causing changes in the main wind direction and cold and dry conditions in the region (Bhattacharya *et al*., 2017). Furthermore, Roy *et al*. (2015) observed humid conditions in the Santiaguillo Basin in central northern Mexico during the LGM but concluded that, although the NAM was inactive or weaker, the frequent formation of tropical cyclones in the eastern North Pacific brought more albeit regionally restricted autumn rainfall. By contrast, based on speleothem record from tropical Southwest Mexico, Lachniet *et al*. (2013) argued that the NAM was active and attributed this to an active but shallow Atlantic Meridional Overturning Circulation and the proximity of their study site to the northern limits of the Intertropical Convergence Zone (ITCZ). Although the exact causes of climatic change in the Chihuahua Desert thus remain uncertain, it is still useful to explore how those changes impacted local ecosystems. The development of the vegetation, for example, can also reflect changes in the seasonality of rainfall and, hence, may provide clues towards changes in the moisture source since the LGM. For the late glacial, pollen records indicate the presence of cold climate species, in contrast to the current dominance of desert shrublands in the southwestern USA (Van Devender, 1990; McAuliffe and Van Devender, 1998; Holmgren *et al*., 2003, 2006). Similarly, close to the Mexican border, packrat middens indicate the presence of summer-flowering annuals and the absence or minimal proportions of desert shrublands (Holmgren *et al*., 2007). During the early Holocene, the belt of greater winter precipitation shifted north. Associated with this was a migration of cold weather

vegetation to higher latitudes and elevations over 2,000 m a.s.l., being replaced by shrub and desert species during the establishment of the North American deserts (Van Devender, 1990; Holmgren *et al*., 2003). For the mid to late Holocene, as the conditions became drier in northwestern Mexico, paleovegetation records become scarce due to fossil pollen being poorly preserved and sediments becoming organic lean, leaving unclear much of the overall biome development from the last glacial to today (e.g. Lozano-García *et al*., 2002; Metcalfe *et al*., 2002).

Lipid biomarkers in lacustrine sediments can be used to fill this gap (Meyers, 2003). The organic matter (OM) of lacustrine sediments is derived from the particulate detritus of aquatic plants and algae as well as vegetation present in the surrounding lake catchment. It contains a range of biomarkers that represent input of OM from different sources and subsequent diagenetic alteration (Perry *et al*., 1979). Both of these characteristics can be used to reconstruct environmental changes in ancient ecosystems (Meyers and Benson, 1988). In this paper, we present the lipid biomarkers in organic-poor sediments (total organic carbon concentration/TOC: 0.2-1.2%) deposited over the last 27 cal ka in the Santiaguillo Basin of central-northern Mexico. This is the first biomarker-based investigation of late Quaternary lacustrine sediments from Mexico, and we use these data to identify changes in the sources of organic carbon to the lake system during the late Pleistocene and Holocene, with implications for carbon cycling, and to reconstruct the paleovegetation of the Chihuahua Desert of Mexico.

4.3 Regional Setting

The Santiaguillo Basin is located in central-north Mexico (Figure 4.1), in the rain shadow of the Sierra Madre Occidental hills. It has an area of 1,964 km^2 within 24°30' to 25°00' N and from 104°40' to 105°00' W. Tectonic movements formed this basin during the Cenozoic, and its bedrock is composed of Cretaceous to Quaternary metamorphic, igneous, and sedimentary rocks (Nieto-Samaniego *et al*., 2012). The most recent deposits are lacustrine sediments and Quaternary alluvium (Nieto-Samaniego *et al*., 2012). A nearby meteorological station (Guatimape: 24°48'25" N, 104°55'19" W; Figure 4.2) provides mean monthly temperature and precipitation data from 1981 to 2010 AD (Source: Servicio Meteorologico Nacional, Mexico). The basin receives around 394 mm of its average annual precipitation of 445 mm

between June and October and the rest of the year contributes around 51 mm of precipitation (Figure 4.1).

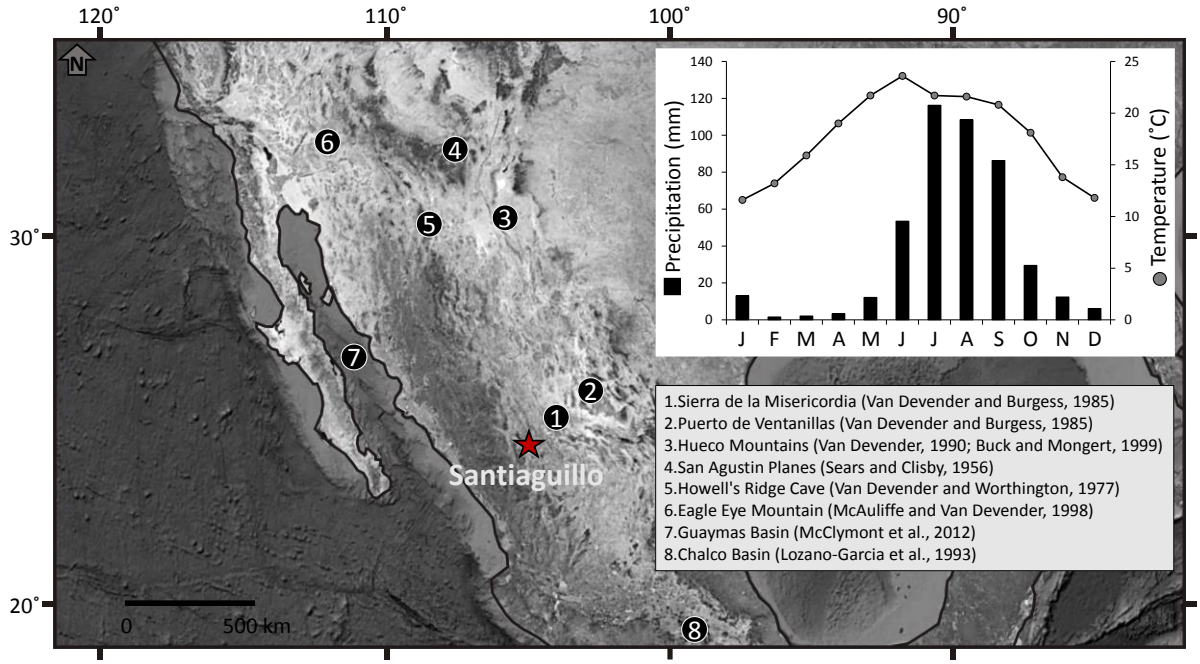

Figure 4.1 The Santiaguillo Basin (red star) is located in the central-northern Mexico. Location of other records used here for comparison (circles). Mean monthly temperature and precipitation from 1981 to 2010 AD are calculated from data obtained from the nearest meteorological station at Guatimape.

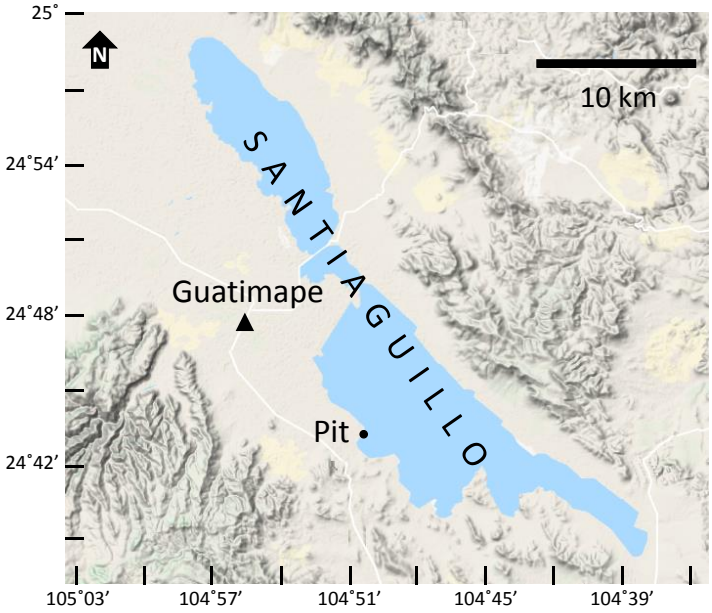

Figure 4.2 The Santiaguillo catchment area, sampling location (circle) and nearest meteorological station (triangle) at Guatimape.

4.4 Materials and Methodology

Sediments were collected from a 3 m deep pit at the western border (24° 44′ N, 104° 48′ W, 1960 m a.s.l.) of the Santiaguillo Basin (Figure 4.2). The sedimentary record was divided in 2 cm intervals and stored in the Paleoenvironment and Paleoclimatology Lab at the Institute of Geology of the National Autonomous University of Mexico. This sequence was previously studied for ostracod paleoecology, TOC contents, TOC/TN ratios (Chávez-Lara *et al*., 2015) and inorganic geochemistry (Roy *et al*., 2015) in order to reconstruct paleosalinity of the water column and the paleohydrological conditions of the basin. The stratigraphy of the sediment profile is from Roy *et al*. (2015): clay and calcareous silt represent the bottom 22 cm (300-278 cm depth), overlain by silty-clay (278-265 cm depth); intercalations of silty-sand and silt occur from 265 to 60 cm depths, and vertical desiccation fissures (~65 cm long) are preserved in sediments at 75 cm depth; on top of this large block of intercalations is a 10 cm layer of silty-clay (60-50 cm depth), and the upper 50 cm are composed of darker massive silty-sand with abundant root remnants. Occasional carbonate nodules are present from the bottom of the record to 75 cm depth. The chronology of the sequence is based on 7 radiocarbon (AMS) dates of organic carbon present in the bulk sediment (Table 4.1), and we have improved the previously presented age model (Roy *et al*., 2015) by including another radiocarbon date at 11 cm depth. Since all of the surrounding rocks are of igneous or metamorphic origin and are carbonate-free, we can rule out significant contributions of fossil/dead organic carbon and (old) dissolved inorganic carbon from the catchment and incorporation into the lacustrine biomass. We cannot exclude supply of pre-aged terrestrial organic carbon from soils in the catchment but synchronous responses of speleothems of southwest Mexico (Uranium–thorium dating; Lachniet *et al*., 2013) and the paleohydrology of the Santiaguillo Basin suggests that this effect might be minimal. Dates were calibrated by the online software Calib, version 7.0.2 (Reimer *et al*., 2013), within the 2σ interval and using the date of the highest probability. Accordingly, the sediment record represents the last 27,000 cal. years (27 cal ka; Figure 4.3) and sedimentation rates are relatively invariant at the resolution measured, between 0.01 to 0.013 cm $year^{-1}$.

Table 4.1 Radiocarbon dates of bulk sediment samples from different depths of the sedimentary record, Santiaguillo Basin. *Calib 7.0.2

Lab. code	Depth (cm)	AMS ^{14}C age (yr BP)	*Modeled calibrated age (2σ, cal yr BP)	*Probability (%)	*Age of highest prob. (cal yr BP)
ICA15OS/0506	11	1,100±40	929-1,085	98	979
Beta-299072	49	3,610±30	3,838-3,984	99	3,905
Beta-299073	73	5,250±30	5,925-6,030	67	5,980
Beta-321663	111	8,900±40	9,897-10,189	100	10,043
Beta-299074	167	13,360±60	15,854-16,267	100	16,082
Beta-299075	205	14,610±60	17,603-17,976	100	17,807
Beta-299076	279	20,790±100	24,622-25,391	100	25,110

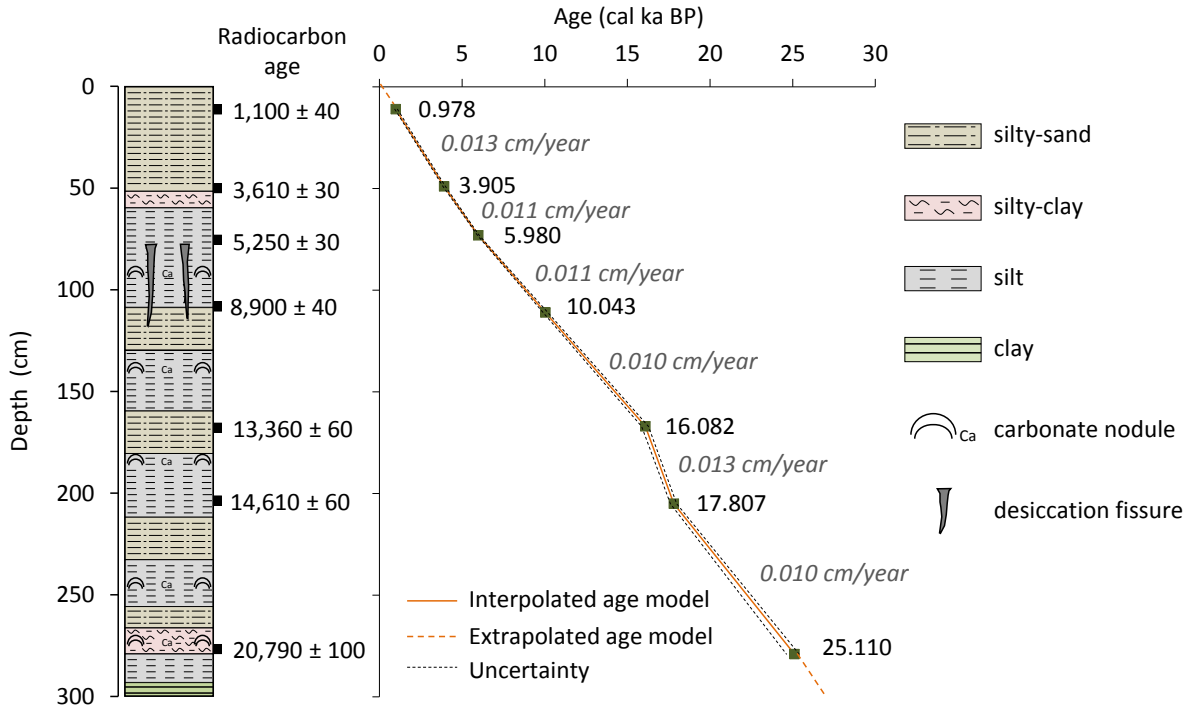

Figure 4.3 Stratigraphy of the sedimentary record and radiocarbon dates at different depths (black boxes). The age model is constructed using the calibrated values and suggests that sediments from the Santiaguillo Basin represent the depositional history of the last 27,000 cal. years.

All samples were freeze-dried and homogenized with mortar and pestle. Total lipid extraction, transmethylation of fatty acids, derivatisation and lipid analysis were carried out as described in Chapter III.

4.5 Results

4.5.1 Lipid concentrations

The total lipid concentration fluctuates between 0.4 and 34 $\mu g/g_{sed}$ (Figure 4.4) with an average of 7.5 $\mu g/g_{sed}$. Higher concentrations (3.5-34 $\mu g/g_{sed}$) occur in sediments at the bottom of the record, from 299-201cm (27-17.6 cal ka BP), and in the uppermost 31 cm (last 2.5 cal ka). Abundances of individual lipids are presented as percentages of the sum of all quantified lipids ($\%_{lipids}$).

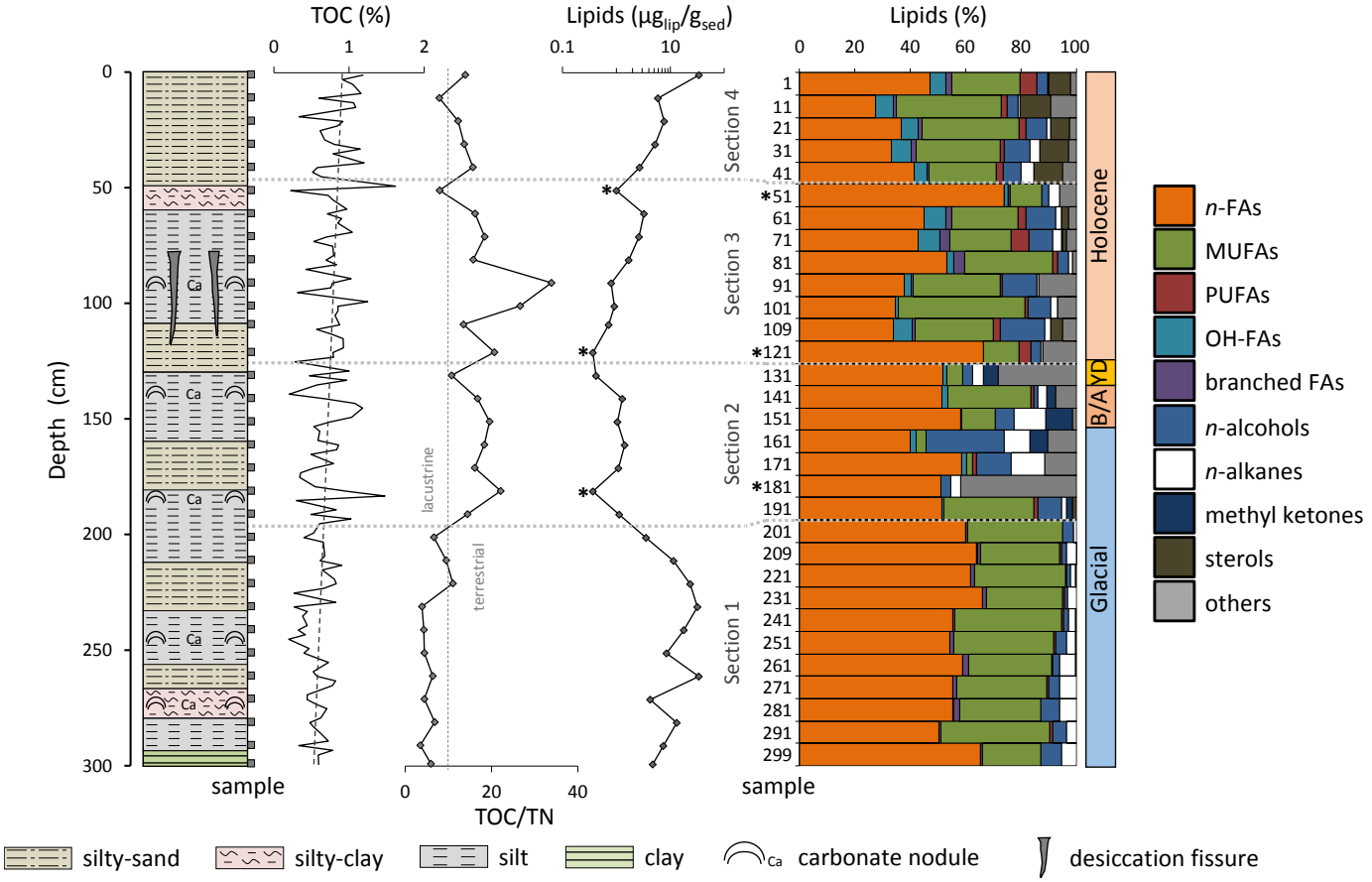

Figure 4.4 Stratigraphic profile of the sedimentary record and geochemical data from elemental (total organic carbon: TOC, in weight%; total organic carbon to total nitrogen ratio: TOC/TN) and biomarker analyses (lipid concentration in µg per g sediment; lipid composition: bar diagram), with sample distributions (gray boxes) over depth. The elemental data (TOC, TOC/TN) are taken from Chávez-Lara *et al*. (2015). Note that he total lipid concentration ($\mu g/g_{sed}$) is presented on logarithmic scale. The record is divided into four sections based on geochemical characteristics and biomarker distributions as described in the discussion. The asterisk (*) marks sediments with highly anomalous lipid compositions resulting from very low lipid concentrations, leaving many compounds below the detection limit. These samples have not been considered for further interpretation.

4.5.2 Lipid composition (compound class inventory)

We quantified saturated *n*-fatty acids, mono- and poly-unsaturated fatty acids, hydroxy fatty acids, branched fatty acids, *n*-alcohols, *n*-alkanes, methyl ketones, sterols, and a range of miscellaneous compounds, mainly β-amyrin, α-amyrin and methoxy acids (Figure 4.4, summary in Table 4.2, for complete compound list see Appendix 1). In general, these include the vast majority of GC-amenable compounds in the TLEs. Glycerol dialkyl glycerol tetraethers (GDGTs) were present but in abundances too low for quantification.

Table 4.2 Summary of the quantified compound classes found in 31 sediment samples collected from the Santiaguillo sedimentary record. The concentrations are expressed as $\%_{lipids}$. (*sediments with extremely low lipid concentrations and resulting anomalous composition, ignored for further interpretation)

Depth (cm)	Age (cal ka BP)	*n*-FAs	short *n*-FA	mid *n*-FA	long *n*-FA	OH-FAs	α-OH-FAs	ω-OH-FAs	branched FAs	MUFAs	PUFAs	OHs	*n*-alkanes	methyl ketones	sterols	others
1	0.1	47.1	19.8	16.5	10.8	5.8	1.0	4.6	2.3	24.5	6.3	3.9	0.4	-	7.6	2.2
11	1.0	27.4	17.3	6.4	3.8	6.5	5.5	1.0	0.9	38.2	2.1	3.9	0.7	-	11.2	9.0
21	1.8	36.9	16.1	6.1	14.8	6.0	2.0	4.0	1.4	35.1	2.3	7.5	1.6	-	6.8	2.2
31	2.5	33.4	12.0	5.5	15.9	7.1	2.1	4.6	1.8	30.3	1.4	9.2	3.6	-	10.4	2.9
41	3.3	41.4	19.1	11.0	11.2	4.9	3.1	1.8	0.5	24.3	2.6	6.4	4.8	-	10.4	4.9
*51	4.1	74.1	24.0	21.8	28.3	1.4	1.4	-	0.5	11.4	-	2.6	4.2	-	-	5.8
61	4.9	45.0	23.7	7.5	13.9	8.1	5.1	-	2.1	23.9	2.8	10.9	1.8	-	2.6	2.7
71	5.8	42.8	30.2	7.7	4.9	8.2	6.1	1.4	3.4	22.2	6.3	8.6	3.5	0.1	1.6	3.4
81	6.8	53.3	39.8	9.7	3.8	2.4	2.4	-	3.8	31.8	1.9	3.8	1.4	-	-	1.5
91	7.9	37.9	9.6	16.8	11.4	2.7	2.3	0.4	0.4	31.6	0.8	12.2	0.8	-	-	13.6
101	9.0	34.8	12.1	9.9	12.9	0.8	0.8	-	0.3	45.7	0.9	8.2	2.5	-	-	6.8
109	10.0	33.8	16.3	12.3	5.3	7.1	5.4	1.6	1.0	28.0	2.5	16.2	2.3	-	4.2	4.8
*121	11.1	66.4	36.9	21.7	7.8	-	-	-	-	13.0	4.1	3.8	0.7	-	-	11.9
131	12.2	51.8	15.1	22.0	14.7	1.5	1.5	-	-	5.7	-	3.3	4.0	5.4	-	28.2
141	13.3	51.5	14.1	11.6	25.9	2.0	1.7	0.3	-	30.1	1.2	1.2	3.2	3.4	-	7.4
151	14.4	58.4	3.7	17.7	37.0	0.3	0.3	-	-	12.0	-	6.8	11.7	9.6	-	1.2
161	15.4	40.1	3.7	16.3	20.2	2.2	0.2	2.0	-	3.6	-	28.0	9.3	6.5	-	10.3
171	16.3	58.7	16.2	14.9	27.7	1.6	1.1	0.5	-	2.3	1.1	12.7	12.2	-	-	11.3
*181	16.7	51.0	27.0	10.4	13.6	-	-	-	-	-	-	3.7	3.7	-	-	41.7
191	17.2	51.4	17.7	15.8	17.9	0.8	0.8	-	-	32.6	1.2	8.7	1.7	2.2	1.3	-
201	17.6	60.2	55.8	3.4	1.0	-	-	-	0.8	34.3	-	3.7	1.0	-	-	-
211	18.4	64.0	62.7	1.2	0.1	0.2	0.2	-	1.3	28.5	0.7	1.8	3.4	-	-	-
221	19.4	61.8	60.2	1.2	0.4	-	-	-	1.4	33.0	0.4	1.4	1.8	0.1	-	-
231	20.4	66.2	65.4	0.6	0.2	-	-	-	1.3	27.7	0.6	1.2	3.0	-	-	-
241	21.4	55.4	50.9	2.6	1.9	-	-	-	0.9	38.5	0.7	1.6	2.6	0.3	-	-
251	22.4	54.2	49.8	2.4	2.0	-	-	-	1.5	36.2	0.6	4.0	3.4	0.1	-	-
261	23.3	58.9	57.4	1.2	0.4	0.1	-	0.1	2.2	29.7	0.6	2.5	5.7	0.2	-	-
271	24.3	55.4	51.5	3.1	0.9	-	-	-	1.4	32.4	1.0	3.8	6.0	-	-	-
281	25.3	55.3	49.5	2.6	3.1	0.5	0.5	-	2.1	29.3	-	6.9	6.0	-	-	-
291	26.3	50.5	43.4	4.5	2.6	-	-	-	0.7	39.4	0.8	5.0	3.5	-	-	-
299	27.1	65.3	56.8	3.8	4.8	-	-	-	1.0	21.1	-	7.4	5.3	-	-	-

4.5.2.1 Saturated n-fatty acids (n-FAs)

Saturated *n*-fatty acids (*n*-FAs) represent the major lipid group, with the summed abundance fluctuating between 27 to 74 $\%_{lipids}$ (average 51 $\%_{lipids}$). Higher proportional abundances (> average) occur in the deepest sediments, from 299-201 cm (27-17.6 cal ka BP), although

discrete sediment horizons at depths of 121 cm (11.1 cal ka BP) and 51 cm (4.1 cal ka BP) have abundances of 66 $\%_{lipids}$ and 74 $\%_{lipids}$ respectively.

4.5.2.2 Mono- and polyunsaturated fatty acids (MUFAs and PUFAs)

Monounsaturated FAs (MUFAs) comprise the second major lipid group, and relative abundances fluctuate between 2 and 46 $\%_{lipids}$ (average 26 $\%_{lipids}$). Higher abundances (> average) typically occur in the deepest sediments, from 299-191 cm (27-17.2 cal ka BP), and in the top 109 cm (last 10 cal ka). Only the sediment at 181 cm depth (16.7 cal ka BP) contained no detectable MUFAs. Polyunsaturated FA (PUFAs) proportional abundances are < 6.3 $\%_{lipids}$ (average 1.4 $\%_{lipids}$). Higher abundances (> average) occur in sediments from the upper 121 cm depths (last 11.1 cal ka).

4.5.2.3 Hydroxy acids (OH-FAs)

Hydroxy fatty acid (OH-FAs) relative abundances are < 8.2 $\%_{lipids}$ (average 2.3 $\%_{lipids}$). Higher abundances (> average) occur in sediments from the upper 109 cm depths (last 10 cal ka).

4.5.2.4. Branched fatty acids

Branched FA relative abundances – mainly *iso*- and *anteiso*- C_{15}, *iso*-C_{16} and *iso*- and *anteiso*- C_{17} components – are < 3.8 $\%_{lipids}$ (average 1.1 $\%_{lipids}$). Higher abundances (> average) occur in the deepest sediments, from 299-211 cm (27-18.4 cal ka BP), and in the upper 81 cm (last 6.8 cal ka).

4.5.2.5 n-Alkanes

n-Alkane relative abundances fluctuate between 0.4 and 12 $\%_{lipids}$ (average 3.7 $\%_{lipids}$). Higher abundances (> average) typically occur in the lower half of the core, from 299-131 cm (27-12.2 cal ka BP), and in sediments from the upper 51 cm (last 4.1 cal ka). Distributions of n-alkanes differ significantly (Figures 4.4 and 4.5) and are interpreted below.

4.5.2.6 n-Alcohols (OH)

n-Alcohol (OH) relative abundances fluctuate between 1.2 to 28 $\%_{lipids}$ (average 3.7 $\%_{lipids}$). Higher abundances (> average) occur in most of the sediments but particularly high abundances (10 to 28 $\%_{lipids}$) occur in sediments at 171 cm (16.3 cal ka BP), 161 cm (15.4 cal ka BP), 109 cm (10 cal ka BP), 91 cm (7.9 cal ka BP) and 61 cm (4.9 cal ka BP).

4.5.2.7 Methyl ketones

Methyl ketone relative abundances are < 10 $\%_{lipids}$ (average 1.1 $\%_{lipids}$). Higher contents (> average) occur in sediments at 191 cm depth (17.2 cal ka BP) and from depths of 161-131 cm (15.4-12.2 cal ka BP).

4.5.2.8 Sterols

Sterol relative abundances – mainly sitosterol, stigmasterol and campesterol – are < 11 $\%_{lipids}$ (average 1.8 $\%_{lipids}$). Higher abundances (> average) occur at 191 cm (17.2 cal ka BP), 109 cm (10 cal ka BP) and in the upper 71 cm of the profile (last 5.8 cal ka).

4.5.2.9 Others

Other identified compounds include β-amyrin (< 11 $\%_{lipids}$, average 1.6 $\%_{lipids}$), α-amyrin (< 1.6 $\%_{lipids}$, average 0.1 $\%_{lipids}$) and 13-methoxyheneicosanoic acid (< 42 $\%_{lipids}$, average 3 $\%_{lipids}$). They occur only in sediments between 181 and 0 cm (last 16.7 cal ka). Sediments at 181 cm depth (16.7 cal ka BP) contain a particularly high relative abundance (42 $\%_{lipids}$) of 13-methoxyheneicosanoic acid.

4.6 Discussion

4.6.1 Degradation

We did not observe any correlation of lipid concentrations with previously published TOC contents (Chávez-Lara *et al.*, 2015), and there is no indication of a significant down-core degradation of lipids. Moreover, the summed lipid abundances vary by at least an order of magnitude more than TOC contents (Figure 4.4). This suggests that a persistent background of reworked lipid-poor organic matter dominates the litter and changes in lipid concentrations

reflect the more dynamic organic pool, including ecosystem and biogeochemical changes in source inputs. Although there does not appear to be downcore degradation of all lipids, it is possible that the reactive lipids (i.e. PUFAs and MUFAs) were preferentially degraded which would partially explain their high proportional abundances in the shallowest sediments; therefore, their profiles are interpreted cautiously. TOC/TN ratios do appear to vary with lipid concentrations, with low TOC/TN ratios corresponding to higher lipid concentrations and vice versa (Figure 4.3). Apart from the aquatic and terrestrial vegetation, it is likely that some of the TN in this organic-poor system was sourced from clay-associated ammonium (Freudenthal *et al*., 2001; Calvert., 2004), such that organic C/N ratios are likely higher.

Three sediments at 181 cm (16.7 ka cal BP), 121 cm (11.1 ka cal BP) and 51 cm (4.1 ka cal BP) depths have highly anomalous lipid compositions and very low lipid concentrations (Figure 4.4). They could have experienced particularly intense oxidative degradation. For example, the 181 cm sample is present at the lithological boundary between silty-clay and darker silty-sand and is associated with root remnants. It might have experienced a variety of episodic or transitory processes, including diagenetic changes (e.g. Meyers *et al*., 1984), associated with drying. Therefore, we avoided these three samples in our interpretations and focussed on generalised broader trends in lipid composition to evaluate environmental processes.

4.6.2 Inferred paleoenvironment from lipid assemblages

Based on the lipid assemblages and concentrations, the sediment sequence can be divided into four sections as described below and shown in Figures 4.5 and 4.6.

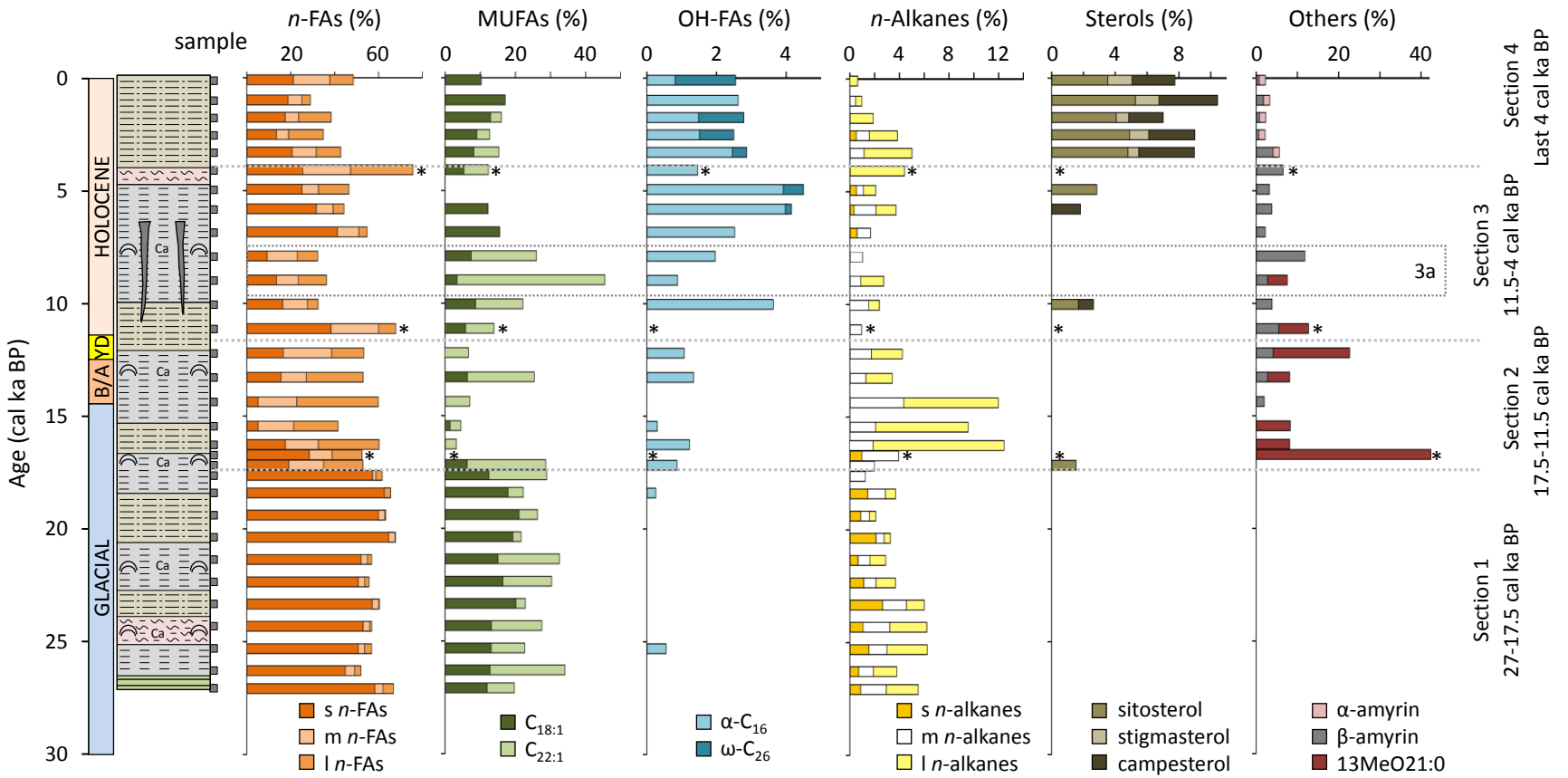

Figure 4.5 Stratigraphic profile of the sedimentary record (boxes on side of profile are sampled layers) compared to lipid biomarker distributions over time. Key compositional changes (%) of n-fatty acids (n-FAs), monounsaturated FAs (MUFAs), hydroxy acids (OH-FAs), n-alkanes, sterols and other compounds are shown, as well as sections defined in the text: Section 1 (27-17.5 cal ka BP), Section 2 (17.5-11.5 cal ka BP), Section 3 (11.5-4 cal ka BP) and Section 4 (last 4 cal ka). Section 3 has a subsection (3a). *Sediments with extremely low lipid concentrations and resulting anomalous composition, ignored for further interpretation.

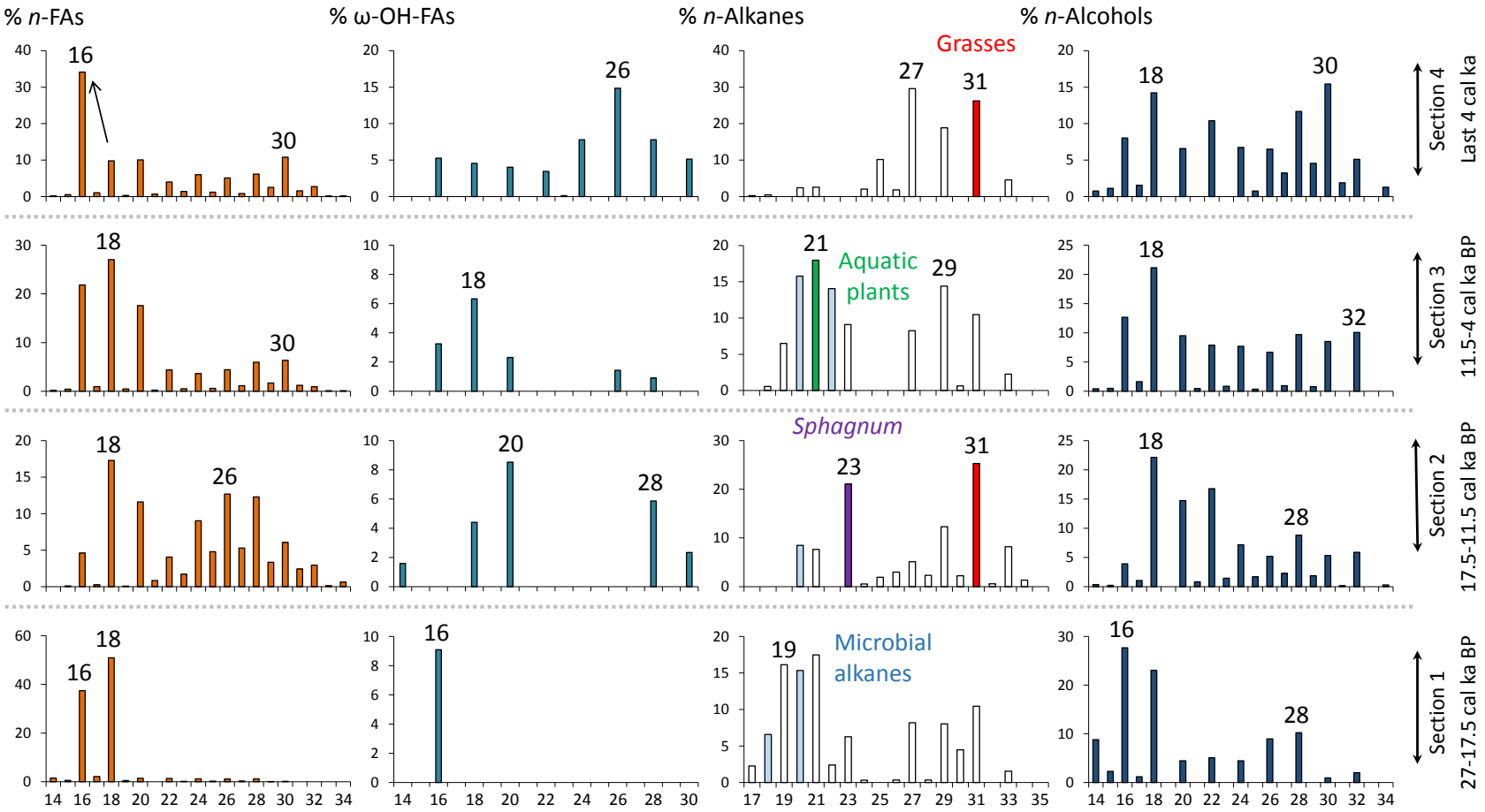

Figure 4.6 Averaged (by section) distributions, by chain length, of n-fatty acids, ω-hydroxy acids, n-alkanes and n-alcohols from section 1 (27-17.5 cal ka BP), section 2 (17.5-11.5 cal ka BP), section 3 (11.5-4 cal ka BP) and section 4 (last 4 cal ka BP). Average values (y axis) are percentages of the total amount of each compound class, i.e. $\%_{n\text{-FAs}}$, $\%_{\omega\text{-OH-FAs}}$, etc.

Section 1 (299-201 cm, 27-17.5 cal ka BP): Section 1 includes sediments at the bottom of the sequence and is characterized by high total lipid concentrations and higher proportions of short-chain fatty acids (s *n*-FAs) such as C_{16} and C_{18}. This is expressed in the ratio of short-chain C_{16} and C_{18} over the long chain C_{26} to C_{32} *n*-FA ($C_{16,18}/C_{26-32}$ FA, Fig. 6). These short-chain compounds are near ubiquitous in the environment, deriving from membrane lipids of all eukaryotes and most bacteria (Matsuda and Koyama, 1977), but also being part of biopolyesters such as cutin and suberin (Kolattukudy, 1981). In this section we inferred C_{16} and C_{18} *n*-FAs derive from phytoplankton and bacteria, based on the general geochemical fingerprint of the sediments that represent this interval. Short-chain *n*-FAs are dominated by C_{18} FA, which is rather unusual given that most algal FA is dominated by C_{16} (Brooks *et al*., 1976). We attribute high proportions of C_{18} *n*-FA to an increased contribution of bacterial biomass, consistent with a short chain *n*-alkane distribution (C_{17-21}) with high proportions of even-numbered *n*-alkanes. Section 1 also contains high proportions of C_{17} and C_{19} *n*-alkanes, generally considered as indicators of algae and photosynthetic bacteria (Han *et al*., 1968; Han and Calvin, 1969; Cranwell *et al*., 1987; Meyers, 2003). Typically, *n*-alkanes have odd carbon-number predominance (Debyser *et al*., 1975; Dastillung and Corbet, 1978), but in some settings even-numbered *n*-alkanes, especially the C_{14}-C_{22} homologues, occur in elevated proportions and have been attributed to a bacterial source (Grimalt *et al*., 1986; Grimalt and Albaigés, 1987). Similarly, the short chain OHs (primarily the C_{16} and C_{18} homologues) are mainly derived from phytoplankton and bacteria (Meyers and Ishiwatari, 1993). High proportions of $C_{18:1}$ MUFA also could derive from phytoplankton and bacteria (Bobbie and White, 1980; Kattner *et al*., 1983; Ahlgren *et al*., 1992). However, the near absence of hydroxy acids (OH-FAs) – except from small amounts of α- and ω-C_{16} OH-FA at 25.3 cal ka BP, 18.4 cal ka BP (α-) and 23.3 cal ka BP (ω-) – suggests a minimal relative contribution from bacterial biomass (Bobbie and White, 1980; Kattner *et al*., 1983; 273 Ahlgren *et al*., 1992). One possible explanation for the near absence of OH-FAs and the lack of sterols is that cyanobacteria are the main lipid source in this section. However, these photosynthetic prokaryotes have higher proportions of C_{16} over C_{18} saturated *n*-FAs, as well as C_{16} over C_{18} MUFA (Cohen and Vonshak, 1991; Singh *et al*., 2002). Therefore, a cyanobacterial source of the LMW components remains equivocal. Overall, we suggest a mixed aquatic origin of organic matter that includes some significant bacterial contributions

to specific compound classes. The absence of sterols, amyrins and methoxy acids, as well as low abundances of long-chain *n*-FAs, *n*-alkanes and *n*-OH, indicate minimal terrestrial vegetation input to the core site.

Section 2 (201-131 cm, 17.5-11.5 cal ka BP): Section 2 is characterised by significantly higher proportions of long-chain *n*-FAs, *n*-alkanes and *n*-OHs. This is expressed by a decrease in $C_{16,18}/C_{26-32}$ *n*-FA ratios and C_{16-24}/C_{25-34} *n*-alkane ratios (Fig. 6). Long-chain *n*-FAs, OHs and n-alkanes are derived nearly exclusively from leaf waxes of terrestrial plants (Eglinton and Hamilton, 1967; Řezanka and Sigler, 2009) (Maffei, 1996; Ficken *et al*., 2002). Between 16.3 and 14.4 ka, the proportion of *n*-alkanes was significantly higher (8.6 vs. 1.4 $\%_{lipids}$ on average of the entire record), with C_{31} being the dominant chain-length. This suggests input from a grassy environment since grasses contain higher amounts of *n*-alkanes as a proportion of the total lipids compared to leaf litter (Rommerskirchen *et al*., 2006; Cui *et al*., 2008; Holtvoeth *et al*., 2016; Bliedtner *et al*., 2017) and are frequently dominated by the C_{31} *n*-alkane, but we recognise the complexity of inferring sources of specific *n*-alkanes, especially in the absence of detailed reference plant analyses. Despite the long-chain *n*-alkane predominance, the distribution is bimodal with a high proportion of C_{23} *n*-alkane. Although *n*-alkanes are derived from a wide range of sources, some mid-chain *n*-alkanes can indicate input from more specific sources if present in a greater proportion, such is the case of C_{23} *n*-alkane which is abundant and frequently the dominant *n*-alkane in many *Sphagnum* species (Baas *et al*., 2000; Nott *et al*., 2000). The absence of α-amyrin but low amounts of β-amyrin could be indicative of minimal leaf, bark and resin inputs (Volkman, 2005; Hernández-Vázquez *et al*., 2012). The near absence of $C_{18:1}$ MUFA, and only small amounts of OH-FAs and short-chain *n*-alkanes (except at 16.7 cal ka BP) indicate low inputs from phytoplankton, bacteria or microalgae (Bobbie and White, 1980; Kattner *et al*., 1983; Ahlgren *et al*., 1992). This section is also characterised by the highest proportions of 13-methoxyheneicosanoic (13MeO21:0), which is rare in lacustrine ecosystems. This methoxy acid has been identified in the red alga *Schizymenia dubyi* (Barnathan *et al*., 1998) in the Mediterranean and waters of Japan and Australia but has never been reported from lacustrine ecosystems (Ramirez *et al*., 2012). Kerger *et al*. (1986) identified a series of methoxy acids (10MeO18:0, 11MeO18:0, 12MeO20:0, 13MeO20:0) and interpreted them as biomarkers from sulphur bacteria (*Thiobacillus* spp.). This organism is halophilic and the optimal conditions for

growing are in hypersaline lakes (Wood and Kelly, 1991). However, ostracod assemblages suggest that the Santiaguillo Basin hosted a lacustrine system with oligohaline to mesohaline water (Chávez-Lara *et al*., 2015). On the other hand, methoxy acids are also likely products from chemical alteration of FAs containing a cyclopropane unit (CFAs) during catalysed transmethylation (Orgambide *et al*., 1993). CFAs are major phospholipid components of many bacteria species (Grogan and Cronan, 1997) and appear to stabilize bacterial membranes under adverse conditions such as enhanced osmotic pressure or higher temperatures (Poger and Mark, 2015). It is thus reasonable to assume that the 13-methoxyheneicosanoic acid found in the Santiaguillo sediments were derived from a C_{22} CFA of bacterial origin, potentially growing under elevated salinity.

Section 3 (131-51 cm, 11.5-4 cal ka BP): This section largely coincides with the youngest silt layer and contains highly variable lipid distributions. It has lower proportions of mid- and long-chain *n*-FA compared to the under- and over-lying sections. This and other lipid biomarkers suggest a decrease in the contribution of terrestrial vegetation and an increase of bacterial and microalgal input (high proportions of short-chain *n*-FA and high relative abundance of even-numbered *n*-alkanes). Overall, this section shows high proportions of C_{21} *n*-alkane, likely indicative of aquatic plants (Cranwell, 1984), and contains the highest amounts of OH-FA in the sequence, with α-C_{16} OH-FA, likely sourced from bacteria (Yano *et al*., 1971), being the dominant compound.

Subsection 3a corresponds to an interval from 9 to 7.9 cal ka BP (101-91 cm), and it is characterised by a decrease in bacterial and microalgal input (low proportions of short-chain *n*-FAs, short- and mid-chain *n*-alkanes and α-C_{16} OH-FA), and the highest amounts of $C_{22:1}$ MUFA, which is a major compound produced by copepods to maximize the buoyancy effect of their wax esters (Arts *et al*., 2001). However, it also contains high amounts of β-amyrin (despite low leaf wax inputs), potentially indicating lower leaf wax inputs but stronger bark and resin inputs. This subsection coincides with the highest TOC/TN ratios (> 20) from the record.

Section 4 (51-0 cm, last 4 cal ka BP): Section 4 is characterised by the highest proportions of sitosterol, campesterol and stigmasterol. Sterols occur in a range of sources, being present in all eukaryote organisms (Volkman, 1986); as such they derive from both algal and aquatic

and higher plant inputs, with the latter typically associated with a dominance of C_{29} and sometimes C_{28} components, i.e. the Santiaguillo sterols are the three major sterols in higher plants (Goad and Goodwin, 1972). Moreover, this section is the only one from the Santiaguillo record that contains both α- and β-amyrin, continuing the trend from Section 3 of increasing higher plant bark and resin inputs. Particularly high amounts of α-amyrin have been found in the resins of *Bursera* and *Protium* species of the *Burseraceae* family (Hernández-Vázquez *et al*., 2012), which are common in the modern subtropical dry forest vegetation of the region (Porter, 1974; Espinosa *et al*, 2006). Diagenetically modified counterparts, i.e. *des*-A-triterpenoids (*des*-A-lupane, *des*-A-ursenes, *des*-A-oleanenes), reported from sediments of Lake Challa (East Africa; van Bree *et al.*, 2016) were not detected here. Compared with the Section 3, Section 4 has higher proportions of long-chain *n*-alkanes that mainly peak at C_{27} and C_{31}, possibly indicating higher inputs from woody angiosperms (dry forest vegetation) dominated by the C_{27} *n*-alkane and grasses dominated by the C_{31} *n*-alkane rather than two types of woody angiosperm species (e.g. Bush and McInerney, 2013). Higher proportions of long-chain ω-OH-FAs, mainly peaking at C_{26}, are also indicative of terrestrial plants. The ω-OH-FAs are major components of plant macromolecules such as cutin, and suberin (Baker and Martin, 1963; Kunst and Samuels, 2003; Samuels *et al*., 2008). A unique feature of this section is the shift in short-chain *n*-FAs dominance from C_{18} to C_{16} *n*-FA (Figure 4.6).

4.6.3 Interpretation of Changing Ecosystems and Land Surface Processes

The hydroclimate of the Santiaguillo Basin and its catchment was controlled by dynamics of the North American Monsoon and tropical cyclones over the last 27 cal ka (Roy *et al*., 2015). Both regional and local factors would have influenced the development of the limnic ecosystem as well as the surrounding terrestrial habitats. The biomarker record shows four different sections that represent a combination of biogeochemical, earth surface and ecosystem developments in response to changes in the local hydrological regime. In the following, we interpret the multi-proxy dataset with respect to ecosystem changes in chronological order and compare the results with previously published proxies such as a titanium (Ti)-based runoff record and TOC/TN ratios (Chávez-Lara *et al*., 2015; Roy *et al*., 2015; Figure 4.7). Previous regional (Figure 4.1) paleovegetation reconstructions from pollen

archives (Sears and Clisby, 1956; Lozano-García *et al*., 1993), packrat middens (Van Devender, 1990; McAuliffe and Van Devender, 1998) and vertebrate fossils (Van Devender and Worthington, 1977) are used for comparison. For clarity in the discussion below, we divide the Holocene into early Holocene (11.7- 8.2 ka BP), mid Holocene (8.2-4.2 ka BP) and late Holocene (last 4.2 ka) after Walker *et al*. (2012).

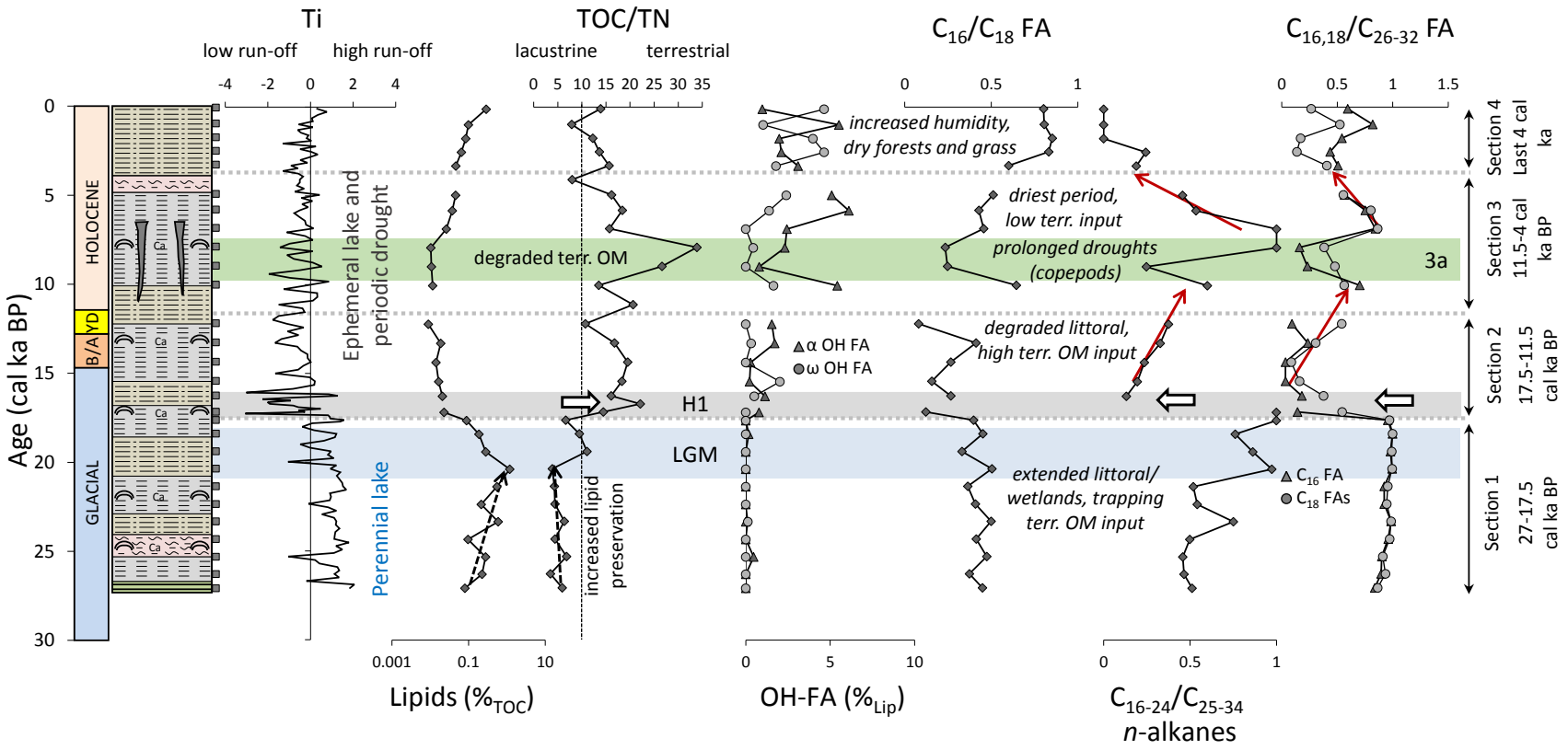

Figure 4.7 Comparison of proxy records of (inorganic) terrestrial runoff (Ti; Roy et al., 2015), lipid concentration relative to the total organic carbon ($\%_{TOC}$), total organic carbon to total nitrogen ratio (TOC/TN; Chavez-Lara et al., 2015), α and ω hydroxy acid (OH-FA) concentration ($\%_{Lip}$), C_{16}/C_{18} FA ratio, $C_{16\text{-}24}/C_{25\text{-}34}$ n-alkane ratio and $C_{16,18}/C_{26\text{-}32}$ FA ratio the Santiaguillo sedimentary profile, with the 4 Sections shown alongside basic interpretations. Note, e.g., the sharp changes in n-alkane and n-fatty acid distributions during Heinrich Stadial 1 (H1), the maximum TOC/TN ratios of Section 3a and the inversion of the relation between α- and ω-hydroxy acids in Section 4. H1 = Heinrich Stadial 1; LGM = last glacial maximum.

Section 1 (27 - 17.5 cal ka BP):

The early phase of this section corresponds to the later stages of the last glacial and it includes the last glacial maximum (LGM) lasting from ca. 21 to 18 cal ka BP. This section is characterised by aquatic (algal or bacterial) biomarkers (i.e. short-chain *n*-FAs) and relatively low abundances of terrestrial biomarkers (i.e. long-chain *n*-FAs). Collectively, all biomarker evidence is indicative of a system that sustained a perennial, highly productive lake with considerable input of bacterial biomass. There is hardly any evidence for input from the surrounding vegetation, which is surprising considering the fact that the basin received above average runoff during this interval (Roy *et al*., 2015), consistent with the existence of a perennial lake (Chávez-Lara *et al*., 2015). Plant remains from packrat middens indicate that the region was dominated by woodland species until 11.5 cal ka BP, including pinyon pines, juniper and shrub oak (Van Devender, 1990). We considered two hypotheses for explaining the lack of input from higher terrestrial vegetation. The first one is high in-lake productivity diluting the terrestrial inputs. However, the concentration of terrestrial biomarkers in this section is genuinely low (< 0.4 $\mu g/g_{sed}$,) and similar to the ranges observed in sections 2 and 3 and slightly lower than the biomarker concentration of section 4. The second and favoured hypothesis is that extended littoral zones trapped OM sourced from the catchment (Figure 4.8). Relatively high Ti concentration in sediments from this section reflects a high contribution of detrital materials into the basin, despite the lack of input from higher terrestrial vegetation. Mafic and heavy minerals like ilmenite, magnetite or biotite present higher Ti concentration than felsic minerals, and they can be better sorted in the finer fraction of the sediments (e.g. Roy *et al*., 2012). In the Santiaguillo Basin, similarities in geochemical characteristics between the lacustrine sediments and western watershed rhyolite are evident (Roy *et al*., 2015), suggesting that the lacustrine sediments were mainly sourced from erosion of the western rhyolite. We do not exclude the possibility that extended littoral zones also trapped some of the Ti input. However, we suggest that most of mafic and heavy minerals in the finer fraction of the sediments could have filtered from the littoral zones and/or travelled by suspension to the sampling site. The finding that, during the period from 27 to 17.5 cal ka BP, the Santiaguillo Basin harboured a year-round productive lake, with a stable water column and extended littoral zones contrasts a pollen record from the Chalco Basin in central Mexico (Figure 4.1). There, the data suggests a desert climate during the last glacial (Lozano-

García *et al*., 1993), implying a hydrological disconnect between the western Chihuahua Desert and central Mexico. Furthermore, the Community Earth System Model applied by Bhattacharya *et al*. (2017) for the LGM produces an East-West gradient in summer precipitation anomalies across central Mexico depending on ice-sheet extent and sea surface temperature, with the West experiencing drier conditions. Bhattacharya *et al*. (2017) hypothesize that local differences in the moist static energy budget are responsible for asymmetric extension of monsoonal convection over continental areas. It appears that regional hydrological boundaries and their lateral displacement over time cannot be sufficiently addressed based on the current slim paleoenvironmental data base. In order to resolve the apparent patchiness in glacial moisture distribution across Mexico more evidence from paleoenvironmental archives is needed.

Section 2 (17.5 - 11.5 cal ka BP):

Section 2 corresponds to the deglaciation and it is characterised by much higher input from terrestrial vegetation compared to the glacial. More *Sphagnum* biomarkers (i.e. C_{23} *n*-alkane and methyl ketones) indicate the presence of ombrotrophic bogs in the surrounding catchment especially during 16- 11.7 cal ka BP. That would imply wetter conditions, but the Ti-based record suggests decreased runoff (Roy *et al*., 2015). Moreover, ostracod assemblages (Chávez-Lara *et al*., 2015) indicate that the lake level had dropped. Therefore, we suggest that these biomarker signatures reflect the exposure of wetland soils in the littoral zone and their erosion and transfer into the Santiaguillo Basin. During this interval, the vegetation of the Chihuahua Desert appears dominated by pinyon-juniper-oak woodland as suggested by packrat midden data from the northern (Van Devender, 1990) and southern parts of the desert (Van Devender and Burgess, 1985), with the latter records being closest to the Santiaguillo. While the long-chain *n*-FAs support an enhanced contribution of leaf waxes from a woodland environment to the Santiaguillo Basin, the increased proportions of *n*-alkanes (peaking at C_{31}), the supply of the C_{23} *n*-alkane (*Sphagnum*) and low amounts of lipids relative to TOC suggest a dominant supply of degraded OM mainly from a grassy (former) wetland area.

The onset of this section coincides with the Heinrich event 1 (H1: 17.2-16.3 cal ka BP; Figure 4.7). Interestingly, the paleoclimatic records from more northerly areas (e.g., the Gulf of

California, Figure 4.1; McClymont *et al*., 2012) do not show a clear response to this cooling event, nor to the Younger Dryas (YD). In contrast, the records towards the south in central Mexico (i.e. Chalco Basin) indicate a distinct shift towards more humid conditions (16.5 ka, Lozano-García *et al*., 1993). At Santiaguillo, the H1 event is reflected by high-amplitude fluctuations in terrestrial runoff (Ti, Roy *et al*., 2015) and also abrupt shifts in both the amount and composition of the lipids supplied to the sediment. Specifically, the amount of lipids relative to the total organic carbon concentration dropped significantly to values below 0.1 $\%_{TOC}$ (minimum of 0.002 $\%_{TOC}$ at 16.7 cal ka BP), and compounds such as long-chain *n*-FAs, *n*-alkanes and, notably, 13-methoxyheneicosanoic acid increased sharply, with the latter reaching up to 41.7 $\%_{lipids}$ at 16.7 cal ka BP, indicating proportionally high input from bacterial biomass. Very similar conditions of high bacterial contributions (18.5 $\%_{lipids}$ of 13-methoxyheneicosanoic acid) were observed during the YD (12.2 cal ka BP). Therefore, compared to the glacial, the lake level in the Santiaguillo Basin appears to have dropped during the period of 17.5-11.5 cal ka BP or potentially fluctuated, causing degradation of former wetlands and associated supply of degraded OM (Figure 4.8).

Section 3 (11.5 - 4 cal ka BP):

This section corresponds to the early and mid-Holocene. In general, the biomarkers indicate reduced leaf wax inputs (long-chain *n*-FAs). Instead, contributions from woody plant tissues, as indicated by high C/N ratios but also consistent with bark and resin inputs (β-amyrin), appear to have increased. There is also evidence for significant inputs from bacterial biomass (short-chain *n*-FAs, α-C_{16} OH-FA) and aquatic plants (C_{21} *n*-alkane). The early phase of section 3 (11.5 – 9 cal ka BP) overlaps with expansion of modern grassland and provides evidence for increasing aridity beginning at 10 cal ka BP located towards the north, in the San Augustin Planes (Figure 4.1) (Sears and Clisby, 1956). This trend towards drier conditions appears to set in later, at about 9 cal ka BP in the Chihuahua Desert as seen in packrat midden records (Van Devender, 1990). In the Santiaguillo Basin, the input of terrestrial OM appears to maximise from 9 cal ka BP to 7.9 cal ka BP (subsection 3a) but it appears to be associated with predominantly woody material rather than leaf litter (Figure 4.8). The onset of this phase also coincides with a decrease in the abundance of ostracods (Chávez-Lara *et al*., 2015) and a contemporaneous increase in the abundance of copepods as

implied by maximum relative amounts of the $C_{22:1}$ MUFA. This indicates a shift in the microfaunal community, probably as a response to a shallowing of the lake and the onset of seasonal droughts to which copepods tend to be more resistant than ostracods (Pillay and Perissinotto, 2009). The ostracod assemblage during this period (9-3.5 cal ka BP) also indicates the presence of an ephemeral lake with humid conditions only during summer months (Chávez-Lara *et al*., 2015). Enhanced aridity from about 9 cal ka BP is further documented by the disappearance of woodland plants, a decline of C_4 grasses and the establishment of desert scrubs in the Chihuahua Desert and, finally, expansion of desert grasslands at 8.3 ka (Van Devender, 1990; Buck and Monger, 1999).

Further aridification and extended periods of drought between 6.8 and 4.9 cal ka BP are indicated by the appearance of desiccation fissures at 6.2 cal ka BP (Figure 4.7), lower than average terrestrial runoff as inferred from the Ti record (Roy *et al*., 2015; Figure 4.7) and the disappearance of copepods as the source of the $C_{22:1}$ MUFA. During this phase, desert grassland in the northern part of the Chihuahua desert appeared more mesic than today (8.3-4.2 cal ka BP; Van Devender, 1990), while in the Sonora Desert winters were warmer than present (6.4-4.5 cal ka BP; McAuliffe and Van Devender, 1998). Towards the south, in central Mexico (Chalco Basin), the vegetation also declined (9-3 cal ka BP; Lozano-García *et al*., 1993). As aridity across the wider area generally increased and terrestrial OM inputs declined, relative contributions from algal and bacterial biomass to the Santiaguillo record increased (short-chain *n*-FAs, α-C_{16} OH-FA, C_{21} *n*-alkane), indicating at least short-lived occurrences of a water body during the summer season. Thus, from 11.5 to 4 cal ka BP (section 3), distinct phases of increasing aridity affecting the Santiaguillo ecosystem can be distinguished, in particular, the transition to a shallower, ephemeral lake with extended drought periods and associated microfaunal adaption between 9 and 7.9 cal ka BP (subsection 3a) and to even drier conditions supporting only a short-lived water body after 7.9 cal ka BP.

Section 4 (last 4 cal ka):

This uppermost section represents the late Holocene and it is marked by a change of sediment grain size from silty-clay to silty-sand. In terms of biomarkers, almost all higher plant biomarkers (long-chain ω-OH-FAs, *n*-alkanes, *n*-alcohols, sterols, and to a lesser degree, *n*-fatty acids) become more dominant. Modern subtropical dry forest vegetation, relying on

seasonal moisture supply and with species rich in α-amyrin such as the *Burseraceae* family, might have been established at the beginning of this phase. This was apparently accompanied by the expansion of grasses growing among the open dry forest vegetation, as suggested by the bimodal *n*-alkane distribution with an enhanced proportion of the C_{31} *n*-alkane. At the same time, comparable vegetation change is reported from the north of the Chihuahua Desert, with more open habitats dominated by shrubs and succulents (3.9 cal ka BP; Van Devender and Worthington, 1977) and a recovery of the C_4 grasses (4 cal ka BP; Buck and Monger, 1999). The Sonora Desert experienced the establishment of modern desert scrub (4 cal ka BP; McAuliffe and Van Devender, 1998). The expansion of the C_4 grasses, in this particular context, provides evidence for less severe aridity during the late Holocene summers as these grasses largely depend on summer precipitation (Throop *et al*., 2012; Báez *et al*., 2013). However, an increase in frequency and magnitude of the El Niño Southern Oscillation (ENSO) has been reconstructed over the last 4.2 cal ka (Moy *et al*., 2002; Conroy *et al*., 2008), which is typically associated with a general decrease in summer precipitation in the wider area (Magaña *et al*., 2003). However, during El Niño years, the north of Mexico also experiences more humid winters as a result of the increased sea surface temperatures in the NE Pacific (Ropelewski and Halpert, 1987) as well as an increased inflow of humid air masses from tropical Pacific cyclones in the autumn (Reyes and Mejia-Trejo, 1991; Rodgers *et al*., 2000; Englehart and Douglas, 2001; Jáuregui, 2003; Magaña *et al*., 2003; Larson *et al*., 2005), and both of these factors could have compensated for the drier summers. Thus, the reduced seasonal contrast in precipitation and the supply of moisture in autumn and winter during the late Holocene appeared to have supported an expansion of subtropical dry forests and grass lands that also represent the modern vegetation (Figure 4.8).

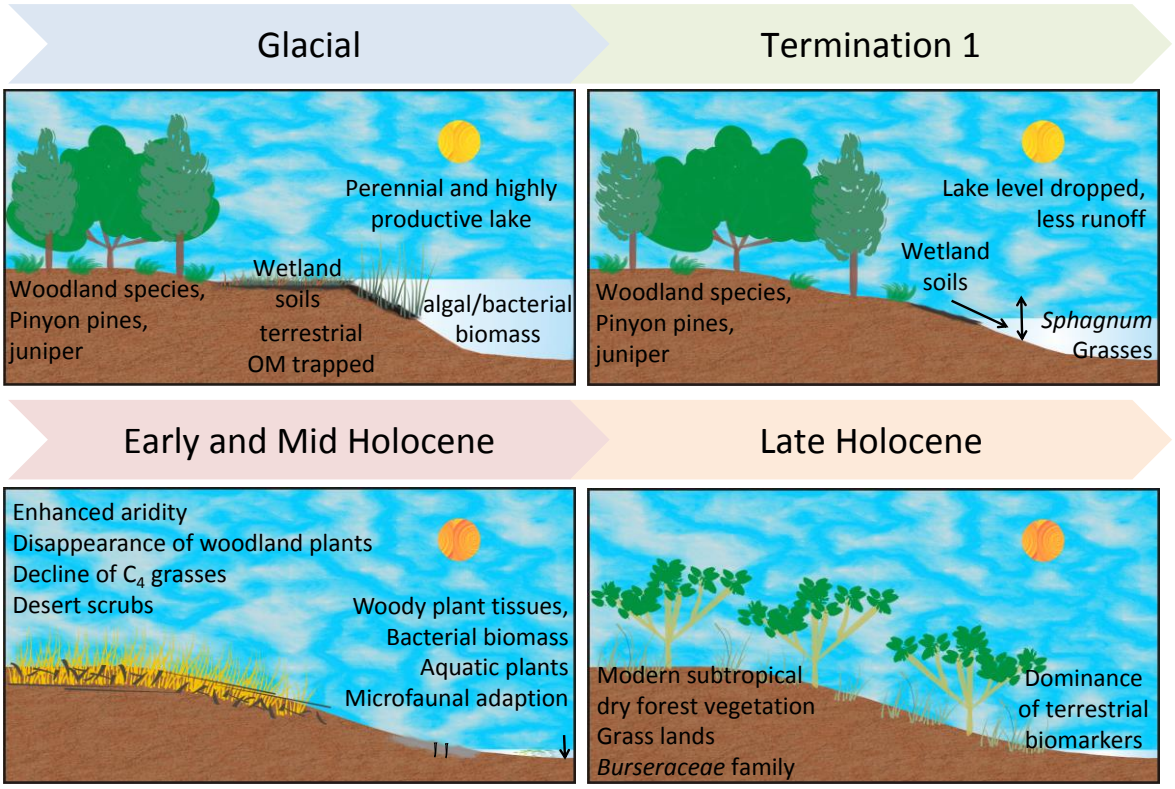

Figure 4.8 Cartoon representing the environmental evolution of the Santiaguillo Basin during the last Glacial, Termination 1 and Holocene. Interpretation is based on previous studies as well as the presented biomarker data.

4.7 Conclusions

In this study, we used biomarker-based proxy data to reconstruct changes of the lacustrine and terrestrial environment of the Santiaguillo Basin in the western Chihuahua Desert (central-northern Mexico) over the past 27 cal ka. The lipid biomarker records reveal clearly distinguishable phases from a perennial lake with an extended littoral zone to an ephemeral lake and, ultimately, a dry basin. Furthermore, differences in the amount and composition of terrestrial biomarkers document the vegetation changes in the catchment, responding to the dynamics of the hydrological regime. Accordingly, during the last glacial period, the basin sustained a productive lake, with a stable water table and extended littoral zones that trapped most of the input from the surrounding terrestrial vegetation, which was probably dominated by woodland species. During the deglaciation, the lake level appears to have dropped and/or fluctuated, causing the degradation of the littoral wetlands and erosion of material from wetland soils into the lake. During the early Holocene, increasing aridity with extending

periods of drought affected the aquatic ecosystem, turning the lake into a shallower, ephemeral lake and causing a shift in the macrofaunal community at 9 cal ka BP. After 7.9 cal ka BP, the Santiaguillo Basin appears to have sustained only a short-lived water body and significant proportions of the deposited organic matter appear to have derived from bacterial biomass and the resin-rich bark litter from the surrounding desertscrubs. Over the last 4 cal ka, the distinctive modern vegetation of a subtropical dry forest along with grasses were established as a response to a reduced seasonal contrast in moisture supply, resulting from an increased frequency and magnitude of El Niño events.

Our study illustrates the great potential of biomarker applications for paleoenvironmental reconstructions that use depositional archives with poor preservation of pollen and other fossil particulate matter. It also confirms observations from paleoenvironmental studies in the wider area, i.e. the deserts of Northern Mexico and the Southwest of the USA. In particular, it supports and expands our understanding of the distinct climatic shift at about 4 cal ka BP that is related to the major reorganisation of atmospheric heat and moisture distribution observed across the Northern Hemisphere. Although the biomarker data from the Santiaguillo Basin provides evidence of changes in seasonality, other fundamental questions such as the source of precipitation, remain unresolved. We suggest that the determination of hydrogen isotope composition of terrestrial leaf-wax compounds (i.e., long-chain alkyl lipids), although not possible in this study due to the small sample size and low biomarker concentrations, could provide additional insight in future studies; such work, however, would have to recognise the complex changes in the sources of higher plant biomarkers as identified here.

CHAPTER V
The El Potosi Basin

Lipid biomarkers in lacustrine sediments of the subtropical northeast Mexico and inferred ecosystem changes during the late Pleistocene and Holocene

In collaboration with J. Holtvoeth, P.D. Roy and R.D. Pancost

Photo by P.D. Roy showing the El Potosi Basin and hills of the Sierra Madre Oriental mountains.

5.1 Abstract

The evolution of ecosystems in northeastern since the Last Glacial Maximum and through the Holocene have yet to be fully characterised, creating a gap in our understanding of the ecological response to climate change in this sensitive area. Here we explore the response of lacustrine and surrounding terrestrial habitats of the El Potosi Basin, northeastern Mexico, to hydrological changes during the late Pleistocene and especially the Holocene. Biomarker-based proxy data indicates a dynamic and variable input of organic matter (OM) into the basin, with sources including the surrounding vegetation, bacterial biomass and aquatic microfauna. Changes in these inputs reveal distinct stages of ecosystem development over the last 20,000 years. Overall, low lipid abundances (as a proportion of TOC), mainly from aquatic/*in-situ* microbial biomass and degraded terrestrial OM occur from 20-19 cal ka BP and are attributed to relatively low runoff. The deglaciation, from 19 to 15 cal ka BP, was characterized by increasing lipid proportions, mostly derived from terrestrial sources including woodland vegetation, soil and wetland vegetation, which we attribute to increased rainfall and runoff. Subsequently, the wetland biomarkers disappeared, and woodland input began to dominate the OM assemblage from 15 to 11.7 cal ka BP. During the early- and mid-Holocene, after about 11.7 ka, putative woodland and grass inputs decreased and the dominant vegetation appeared to shift to subtropical desert shrub, which could have been due to increasing regional aridity. The onset of the dry late Holocene was characterized by gradual environmental transition and ecosystem adaption, especially from 4.2 to 2.8 cal ka BP. The terrestrial vegetation comprised increasing proportions of C_4 grasses, documented by changes in leaf wax carbon isotopic compositions, and potentially more open vegetation, while the in-lake bacterial production increased. From 2.8 cal ka BP, with increasing desertification, terrestrial productivity decreased substantially and the lake became shallower/ephemeral, and the surrounding soils became more alkaline. Changes of the limnic habitat from algal towards microbial communities occurred ~300 years after the onset of terrestrial habitat changes. Finally, during the last millennium, the vegetation again became C_3 dominated, implying an enhanced moisture supply, either natural or anthropogenic. Overall, this work shows the marked sensitivity of northeastern Mexico ecosystems to the climatic shifts of the past 20 kyr, including the relatively subtle climatic changes of the Holocene, and perhaps indicates their vulnerability to future climate change.

5.2 Introduction

Paleovegetation reconstruction plays an important role in understanding the nature and influence of past climate systems (e.g. Lozano-García and Ortega-Guerrero, 1998; Metcalfe *et al*., 2000; Ortega-Rosas *et al*., 2016). The prevailing vegetation communities are directly influenced by atmospheric temperature, but are also affected by evaporation and precipitation. The terrestrial biosphere can also release or absorb greenhouse gases, such that it has an important role in regulating atmospheric composition and climate (e.g. Gifford and Howden, 2001; Justino *et al*., 2016). Consequently, paleoenvironmental records are crucial for understanding past climate change and the co-evolution of ecosystems, but also for developing understanding of future environmental conditions and ecological responses.

Paleovegetation records from subtropical northeast Mexico are scarce and poorly dated. The first study focused on sediments from the Cuatro Ciénegas Basin (Figure 5.1), representing the last 30 ka BP (4 radiocarbon dates) with the pollen record revealing gaps for the Holocene (Meyers, 1973). Subsequently, packrat midden analysis from Puerto de Ventanillas and Cañon de la Fragua (Van Devender and Burgess, 1985; Betancourt *et al*., 1990; Figure 5.1) revealed the vegetation changes during the early Holocene and deglaciation, respectively. Beyond these studies, however, paleoenvironmental reconstructions of northeastern Mexico during the Holocene remains sparse.

A recent study from El Potosi Basin suggests that paleohydrological conditions of the area were controlled by sea-surface temperature (SST) in the Gulf of Mexico (GoM; Roy *et al*., 2016). The Ti abundance, interpreted as a runoff and precipitation record, shows a first order positive correlation with the June (summer) insolation and SST of the GoM (Flower *et al*., 2004; Ziegler *et al*., 2008) for the Last Glacial Maximum (LGM) and deglaciation, with enhanced moisture transported during warmer conditions, and vice versa (Roy *et al*., 2016). However, during the early- and mid- Holocene, the precipitation record and SST of the GoM became decoupled, and the authors suggested that further evaluation was necessary to understand this hydrological disconnection.

In this study, we present a paleoenvironmental and paleoecological reconstruction of the El Potosi Basin – based on molecular organic geochemical proxies – over the last 20 ka with a

particular focus on the Holocene. Molecular organic geochemical proxies can be used to reconstruct environmental conditions and organic matter inputs, commonly applied to modern lakes across the world (e.g. Meyers *et al*., 2003; Theissen *et al*., 2005; Xiong *et al*., 2010; Holtvoeth *et al*., 2016; van Bree *et al*., 2018). Lipid biomarkers can distinguish between terrestrial and aquatic components, providing insight into environmental conditions in the water column and the surrounding watershed. For example, long-chain fatty acids (*n*-FAs) derive nearly exclusively from leaf waxes of terrestrial plants (Eglinton and Hamilton, 1967), whereas C_{17} and C_{19} *n*-alkanes are generally considered to be indicators of algae and photosynthetic bacteria (Han *et al*., 1968; Han and Calvin, 1969; Cranwell *et al*., 1987; Meyers, 2003). The C_{27}, C_{29} and C_{31} *n*-alkanes are also leaf wax constituents of terrestrial plants, with the C_{31} *n*-alkane frequently being the most abundant *n*-alkane in grasses (Maffei, 1996; Ficken *et al*., 2002). Microbial biomarkers include the branched FAs (Goossens *et al*., 1989) and the isoprenoidal (i) and branched (br) glycerol dialkyl glycerol tetraether (GDGT) lipids (Sinninghe Damsté *et al*., 2000). Because the iGDGT crenarchaeol derives from primarily aquatic Thaumarchaeota and brGDGTs derive primarily from soil bacteria, the ratio of these two compound classes can also be used to assess the varying contributions of aquatic vs. terrestrial organic matter, via the Branched and Isoprenoid Tetraether (BIT) index (Hopmans *et al*., 2004).

The carbon isotopic composition of biomarkers can provide further insights into organic matter inputs; in particular, the carbon isotopic composition of the aforementioned leaf waxes can be used to distinguish between C_3 and C_4 plants (O'Leary, 1988; Leng and Henderson, 2013). C_3 plants, which represent approximately 85% of all plant species, dominate in temperate environments, whereas C_4 plants, largely but not exclusively grasses, grow in extreme environments with high light intensities, high temperatures and high aridity (Ehleringer, 1991). Crucially, C_4 plants are enriched in ^{13}C relative to C_3 plants (O'Leary, 1988), such that leaf wax $\delta^{13}C$ values can act as an environmental proxy, via the ecological response to climatic conditions. Moreover, the carbon isotopic composition of aquatic biomarkers – such as short- and mid-chain fatty acids – can be used to evaluate changes in lake conditions; this is because their $\delta^{13}C$ values are governed by dissolved inorganic carbon $\delta^{13}C$ values (Hollander and McKenzie 1991; Leng and Marshall, 2004) as well as the range

of apparent fractionation values arising during algal photosynthesis (e.g. Bidigare *et al*., 1997).

The application of lipid biomarkers for environmental reconstruction in arid regions is generally poorly developed because the associated lacustrine sediments often lack significant quantities of organic matter (OM). Nonetheless, organic-poor sediments of a paleo-lake located within the Santiaguillo Basin did yield a variety of biomarkers, allowing us to reconstruct ecosystem changes of the Chihuahua Desert of Mexico over the late Quaternary (Chapter IV). This provided insight into the temporal evolution of this lacustrine system and its catchment area through changes the aquatic and terrestrial OM inputs.

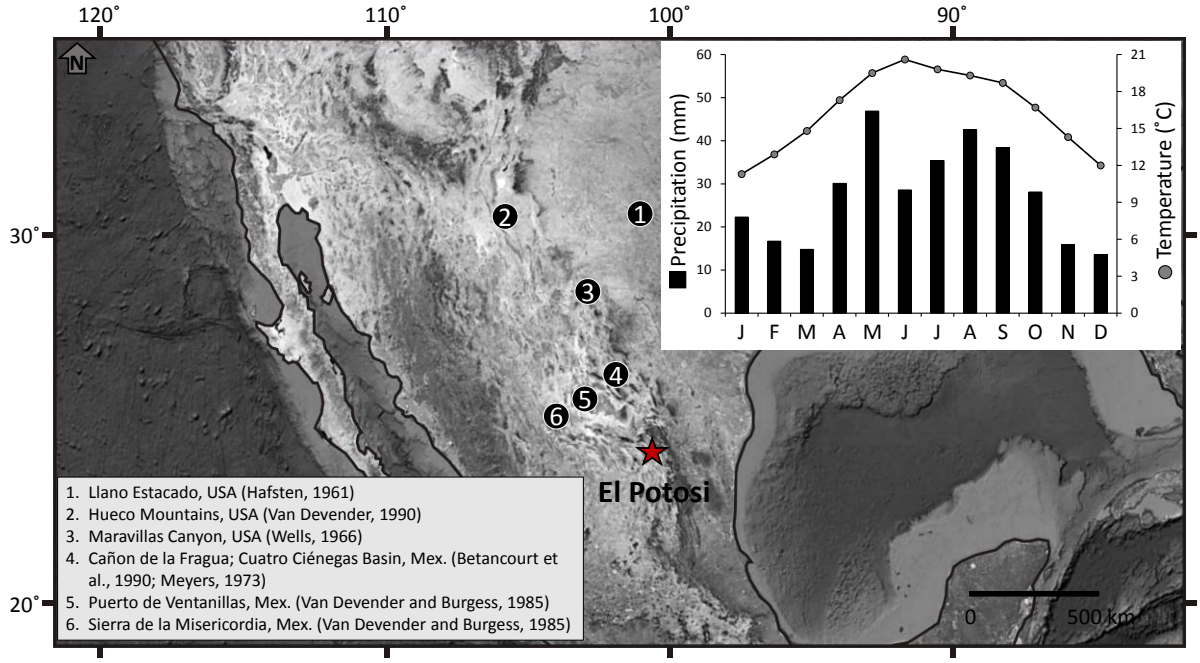

Figure 5.1 The El Potosi Basin (red star) is located in the central-northern Mexico. Location of other records used here for comparison are presented as circles. Mean monthly temperature and precipitation from 1981 to 2010 AD are calculated from data obtained from the nearest meteorological station at El Potosi hills.

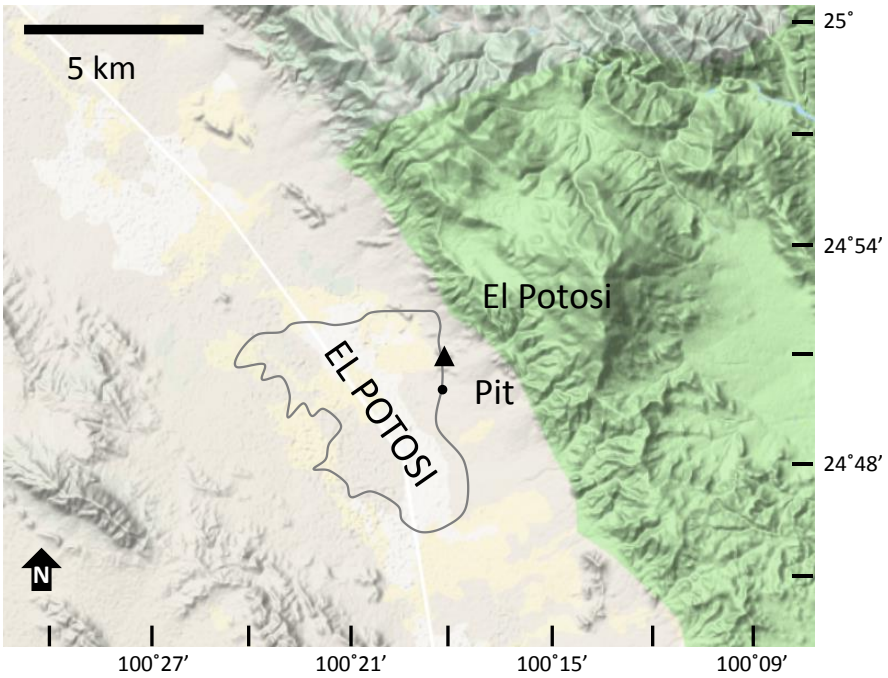

Figure 5.2 The El Potosi catchment area, sampling location (circle) and nearest meteorological station (triangle) at the El Potosi hills.

5.3 Regional Settings

The El Potosi Basin is located in subtropical northeast Mexico (Nuevo Leon State), in the rain shadow of the Sierra Madre Oriental Mountains (Figure 5.1). There was an endorheic and ephemeral lacustrine basin within this semi-graben (24˚50'25" N and 100˚20'08" W), but it has been dry for the last three decades. This is probably due to over-exploitation of groundwater from this drought-prone basin and agricultural practices, including burning the surface plants to prepare the land for cultivation, both of which have caused subsidence and sub-surface peat fire (Roy *et al*., 2014). The Jurassic to Neogene sedimentary bedrock of the watershed includes limestone, sandstone, siltstone and conglomerate (Eguiluz *et al*., 2000; Servicio Geológico Mexicano, 2000).

A nearby meteorological station on the El Potosi hills (24˚ 50' 36" N, 100˚ 19' 15" W, 1890 m a.s.l.; Figure 5.2) provides mean monthly temperature and precipitation data from 1981 to 2010 AD (Source: Servicio Meteorologico Nacional, Mexico). It recorded an average annual temperature of ~16 ˚C (Figure 5.1). The average annual precipitation was 330 mm and most of it (~250 mm) occurred between April and October, with a bimodal distribution peaking in

May and August. Precipitation for the rest of the year was 83 mm. Most of the modern day vegetation has been altered by agricultural activities, and the unaffected vegetation consists of xeric shrubland and halophilic grassland, including juniper (*Juniperus monosperma*), yuca (*Yuca* sp.), mesquite (*Prosopis glandulosa*), creosote bush (*Larrea tridentata*), prickly pear (*Opuntia* sp.), club chollas (*Cylindropuntia* sp.), lechuguilla (*Agave lechuguilla*), maguey (*Agave* sp.) and grasses (*Oordeas* sp., *Bouteloa* sp., *Aristida* sp.) (Amezcua-Torres, 2003).

5.4 Sediment and analysis

Sediment samples were collected up to 310 cm depth in a pit dug at the eastern border of the basin (Figure 5.2), in a natural part that had been unaffected by subsidence and peat fire. This sequence was previously studied for inorganic geochemistry, including total organic carbon (TOC), in order to reconstruct the paleohydrological conditions (Roy *et al*., 2016). This profile includes a unit of clay at the bottom (310-200 cm depth) that includes a 42-cm section of organic rich clay (282-240 cm). Overlaying the clay is a calcareous silt unit, from 200 to 48 cm depth, and then an upper silty-sand unit, from 48 to 0 cm depth. Both the silt and silty-sand units contain ~3-10 cm long desiccation fissures (Figure 5.3). Sediments have TOC contents varying from 0.02 to 27.5 %, with the higher values (7.1-27.5 %) associated with the organic rich clay at 282-240 cm (Roy *et al*., 2016).

The chronology of the sequence is based on 9 different radiocarbon (AMS) dates previously reported by Roy *et al*. (2016) (Table 5.1). The radiocarbon values were calibrated by the online software Calib version 7.0.2 (Reimer *et al*., 2013) and the dates of highest probability within a 2σ interval were used for the chronological control (age vs. depth model shown in Figure 5.3). Collectively, the sediment sequence down to 301 cm depth represents the last 20,000 calendar years (20 cal. ka).

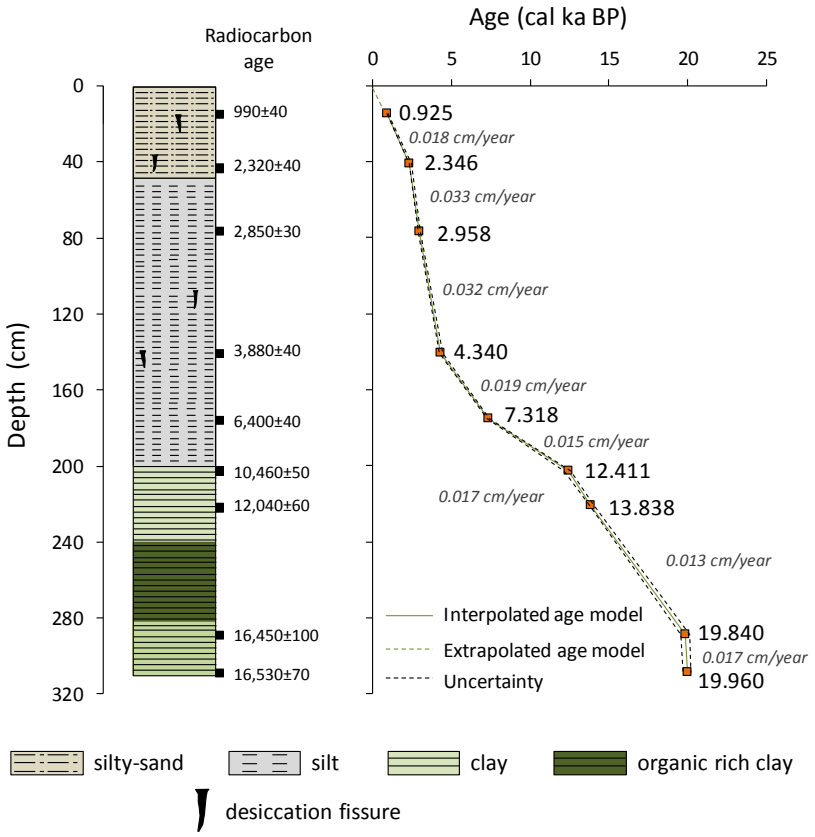

Figure 5.3 Stratigraphy of the sedimentary sequence from the El Potosi Basin and radiocarbon dates at different depths (black boxes). The age model is constructed using calibrated values and indicates that sediments from the El Potosi Basin represent the depositional history of the last 20,000 years.

Table 5.1 Radiocarbon dates of bulk sediment samples from different depths of the sedimentary profile, El Potosi Basin. *Calib 7.0.2

Lab. code	**Depth** (cm)	**AMS ^{14}C age** (yr BP)	***Modeled calibrated age** (2σ, cal yr BP)	***Probability** (%)	***Age of highest prob.** (cal yr BP)
OS-0502	15	990±40	890-963	53	925
OS-0411	41	2320±40	2302-2459	85	2,346
Beta-360653	77	2850±30	2876-3059	100	2,958
OS-0412	141	3880±40	4225-4419	93	4,340
OS-0503	175	6400±40	7267-7419	100	7,318
Beta-356261	203	10 460±50	12131-12552	100	12,411
14OS/1002	221	12040±60	13751-14060	100	13,838
OS-0413	289	16450±100	19573-20104	100	19,840
Beta-360655	309	16 530±70	19688-20157	100	19,960

*Calib 7.0.2

Total nitrogen (TN) contents were measured in 30 samples in duplicate (0.004 mean std. deviation) using a Thermo Scientific Flash Smart Organic Elemental Analyser at the School of Environmental Sciences of the University of Liverpool.

For lipid biomarker analysis, 31 samples were collected at 10 cm interval up to 301 cm depth. The samples were freeze-dried, homogenized, microwave extracted, transmethylated and derivatised prior to Gas Chromatography-Mass Spectrometry (GC-MS) analysis. Total lipid extracts (TLEs) were fractionated and fatty acids were analysed by Gas Chromatography-Combustion-Isotope Ratio Mass Spectrometry (GC-C-IRMS). See Chapter III for more detail information about the methodology. $\delta^{13}C$ values are expressed relative to the international VPDB (Vienna Pee Dee Belemnite) standard.

The Carbon Preference Index of *n*-alkyl leaf wax consitituents (CPI), including *n*-FAs (Equation 2; Bray and Evans, 1961) can be used to explore the nature and degradation of terrigenous inputs. Sediments containing non-degraded and immature organic matter have high indices, reflecting the primary biological signature, whereas low CPIs indicate that the inherited biological signature has been altered by secondary processes, such as degradation. CPI is defined as:

$$\mathrm{CPI} = \frac{\frac{C22 + C24 + C26 + C28}{C21 + C23 + C25 + C27} + \frac{C22 + C24 + C26 + C28}{C23 + C25 + C27 + C29}}{2} \quad \text{Equation 5.1,}$$

where the numbers reflect the number of atoms in the *n*-FA carbon chain.

For GDGT analyses, a second TLE aliquot was filtered. GDGTs were determined using HPLC -MS as described in Chapter III. No response factors were determined as we only focus on GDGT proxy ratios such as Branched and Isoprenoid Tetraether (BIT) index (Hopmans *et al*., 2004; Equation 2.7, Chapter II).

5.5 Results

5.5.1 TOC contents, TOC/TN ratios and lipid concentration

The TOC concentration is highly variable, and the highest percentages (7.1-27.5 %) are associated with organic rich clay at depths between 282 and 240 cm. Clay sediments between

240 and 200 cm have intermediate TOC concentration (1.5-4.8%). Silt and silty-sand sediments have the lowest concentration (< 2.1 %). The TOC percentages are taken from Roy *et al*. (2016).

TOC/TN values range from 6.7 to 23 (Figure 5.4). Clay sediments at the bottom-most part of the sediment archive (301-282 cm, 20-19.2 cal. ka) have the lowest ratios (6.7-7.9), and the organic rich clay sediments (282-240 cm, 19.2-15.5 cal. ka) have the highest ratios (18-23). In the rest of the sediment archive (240-0 cm, last 15.5 cal. ka), TOC/TN ratios range between 8.8 and 18.

Lipid content is < 3.9 % relative to the total organic carbon ($\%_{TOC}$) and has an average of 0.7 % (Figure 5.4). Higher concentrations (0.5-3.9 %) occur in the organic rich clay unit (282-240 cm, 19.2-15.5 cal ka BP) and the overlying clay unit at 240-200 cm (15.5-11.8 cal ka BP). The bottom-most clay unit (301-282 cm, 20-19.2 cal ka BP) and the sediments of the upper 91 cm (last 3.3 cal ka) have lower lipid concentrations (<0.3 %), indicating that a significant proportion of the TOC is recalcitrant and potentially reworked.

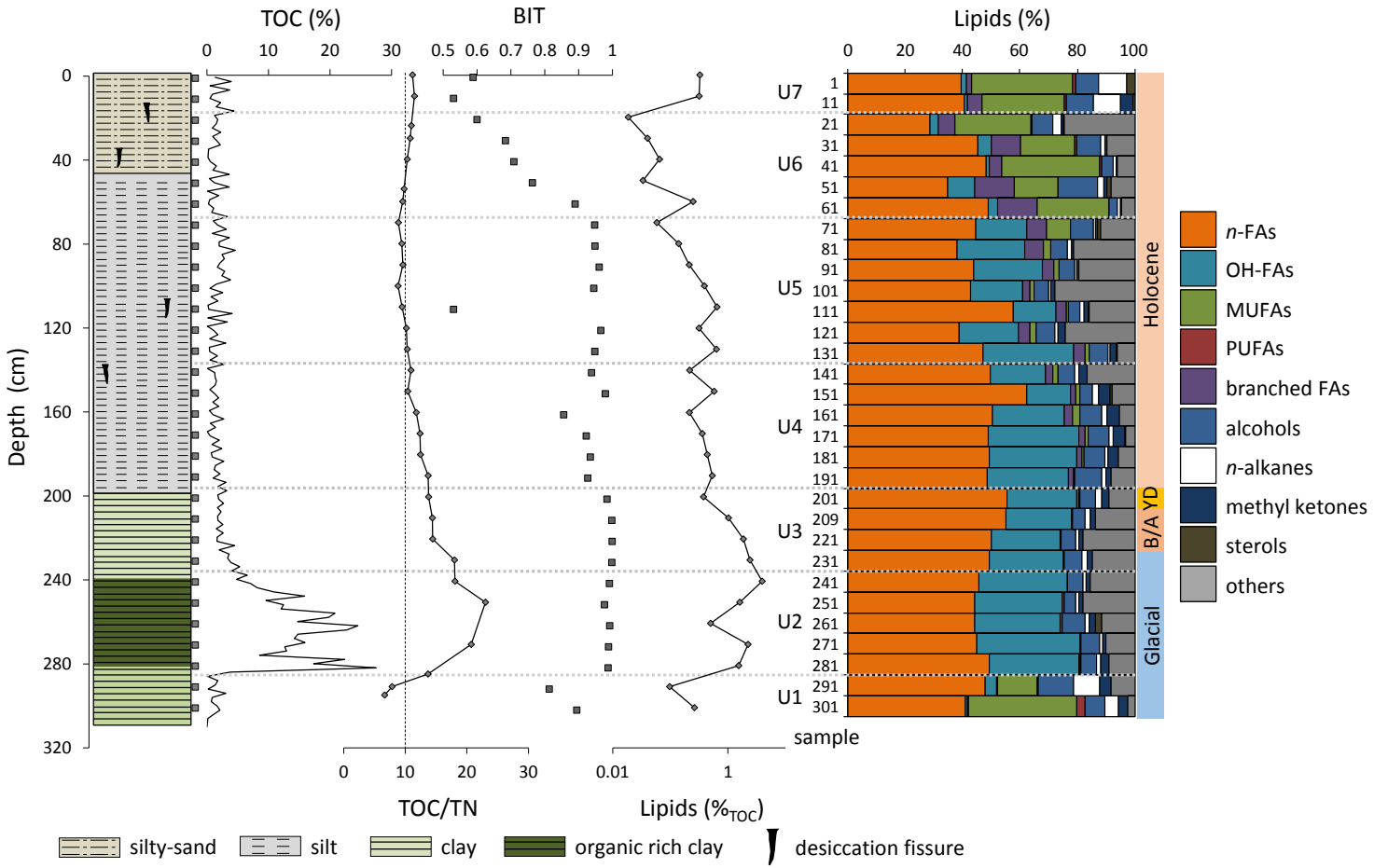

Figure 5.4 Stratigraphic profile with sample depths (grey boxes), geochemical data from elemental (TOC, total organic carbon content in weight%; and TOC to total nitrogen, TN, ratio) and biomarker analyses (BIT index; lipid concentration relative to TOC; lipid composition: bar diagram) over depth. Note that the total lipid concentration ($\%_{TOC}$) is presented on a logarithmic scale. The record is divided into seven units (grey bars) based on geochemical characteristics and biomarker distributions as described in the discussion.

5.5.2 GDGTs

BIT indices range from 0.5 to 1 with an average of 0.9 (Figure 5.5). Only the uppermost sediments (51-0 cm, last 2.5 cal ka) and a single horizon 111 cm depth (3.7 cal ka BP) have values below 0.8. A second GDGT analysis was performed for sample 111 cm, in order to make sure that BIT index is genuinely low (Figure 5.4; Appendix 3). Samples from rest of the sediment archive have high values (0.8-1), indicating a dominance of either allochthonous soil inputs or a lack of Thaumarchaeotal production. The BIT index includes only crenarchaeol among the isoprenoidal GDGTs, but other isoprenoidal GDGTs do occur; these are less dominant and consequently the ratio of total br-GDGTs to total iso-GDGTs parallels the BIT profile. GDGT-0 is the most significant iGDGT, even over crenarchaeol (high GDGT-0/cren ratio; Figure 5.5), and it could originate from lake surface-dwelling crenarchaeota as well as from methanogenic archaea residing in the deeper and anoxic part of the water column (Blaga *et al*., 2009; Sinninghe Damsté *et al*., 2009). Cyclopentane-bearing GDGTs also occur; typically, this is GDGT-1 (i.e. a single ring) but in some sediments the proportions of GDGT-2 are relatively higher than GDGT-1. Like BIT indices, however, total abundances of iGDGTs that include these other components are low compared to total abundances of brGDGTs (Figure 5.6).

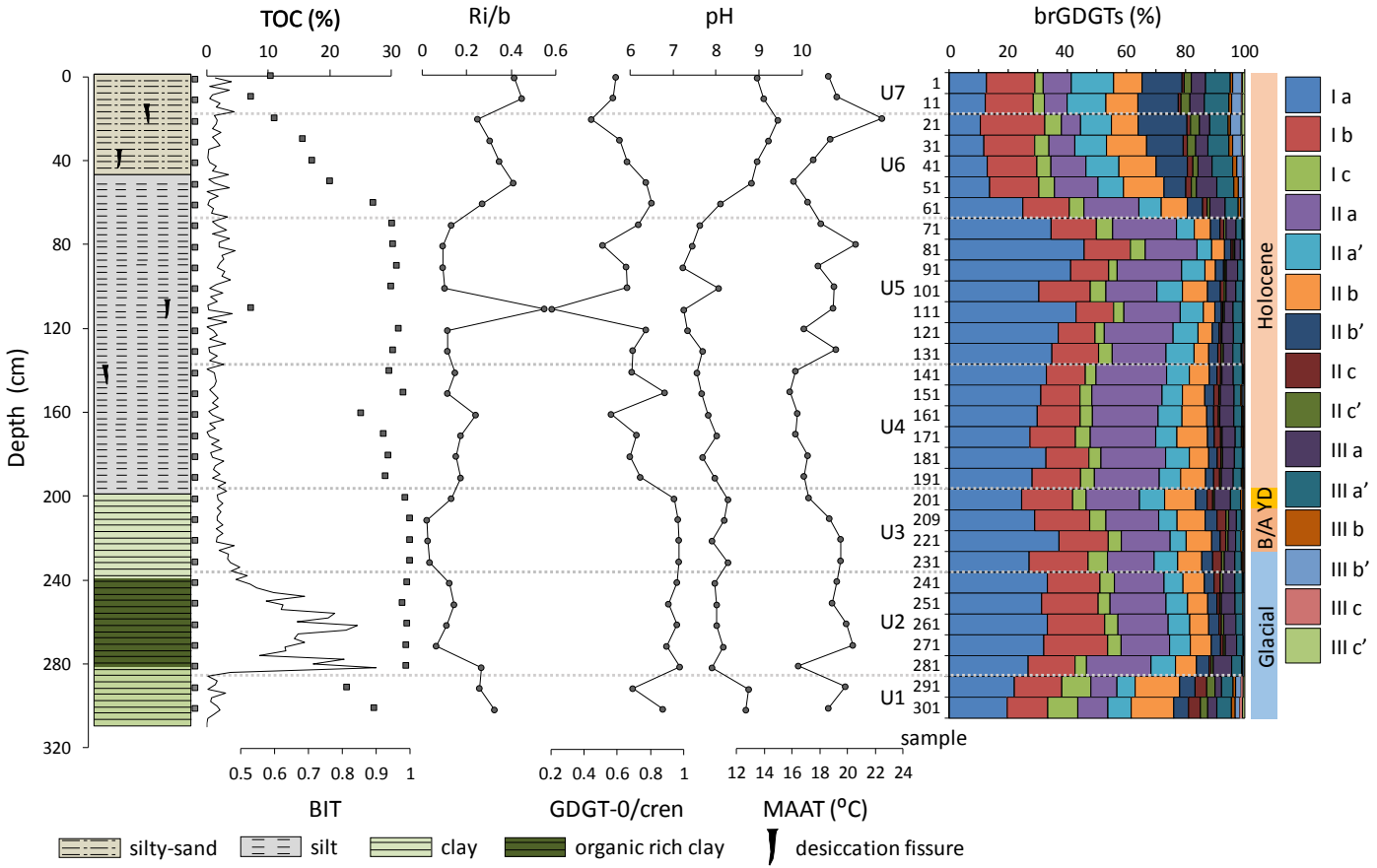

Figure 5.5 Stratigraphic profile with sample depths (grey boxes), total organic carbon content (TOC) in weight% and biomarker analyses (BIT index; total iGDGTs to total brGDGTs ratio (Ri/b); GDGT-0 to crenarchaeol ratio; pH and mean annual air temperature (˚C) calculated using the calibration of Peterse *et al*., 2012; and brGDGT composition: bar diagram) over depth. NOTE: the calculated temperatures are not thought to be robust, as discussed in the text but included to facilitate consideration of the GDGT distributions. The record is divided into seven units (grey bars) based on geochemical characteristics and biomarker distributions as described in the discussion.

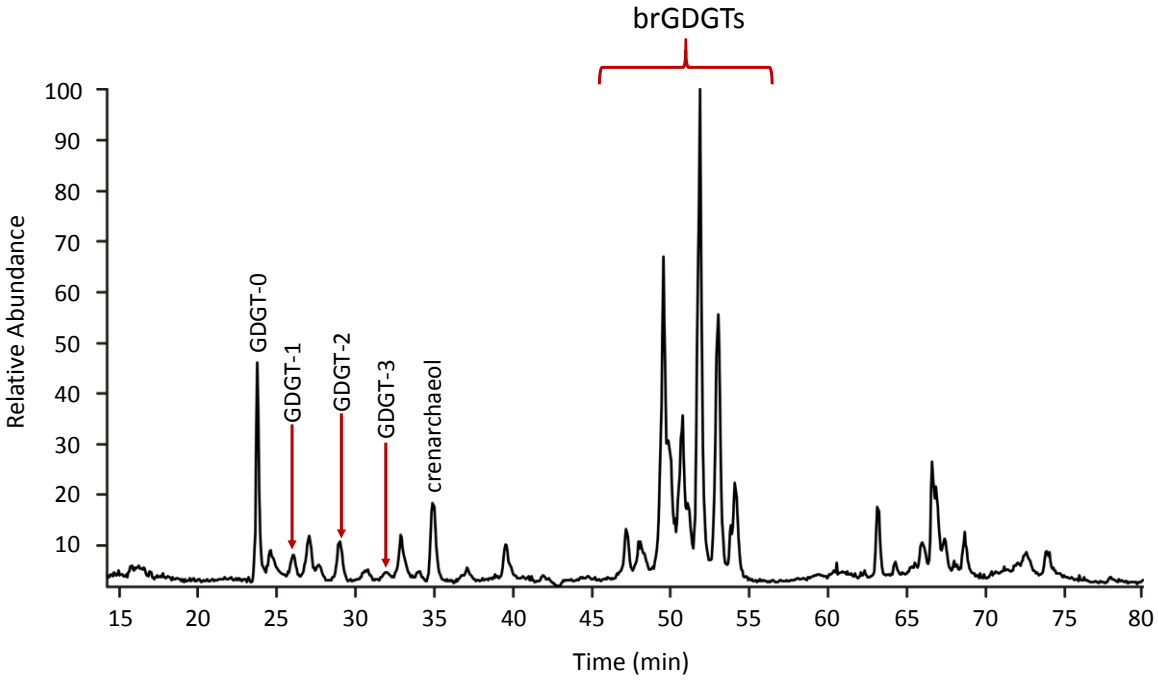

Figure 5.6 Representative total ion count (TIC) of the HPLC/APCI/MS chromatogram of a representative sample, showing both br- and iGDGTs with their respective m/z. Note that the brGDGT are particularly dominant than iGDGT.

The high BIT indices preclude application of the TEX_{86} proxy (Weijers *et al*., 2006; Schouten *et al*., 2013). The MBT' and CBT ratios, used for estimating the mean annual air temperature and pH (Weijers *et al*., 2007; Peterse *et al*., 2012), could be determined but are also deemed unreliable despite the dominance of brGDGTs, because they indicate LGM temperatures that are greater than those of the Holocene. This could reflect seasonal or other impacts, but we suggest that it arises from changes in aridity and soil moisture, which are known to strongly impact the MBT' proxy (Xie *et al*., 2012).

5.5.3 Lipid composition (compound class inventory)

Amounts of individual lipids are presented as percentages of the sum of all quantified lipids ($\%_{lipids}$). Saturated *n*-fatty acids, mono- and poly-unsaturated fatty acids, hydroxy fatty acids, branched fatty acids, *n*-alcohols, *n*-alkanes, methyl ketones, sterols, and a range of miscellaneous compounds including α-amyrin and β-amyrin are semi-quantified (summary in Table 5.2, for complete compound list see Appendix 2) and presented in Figure 5.4

(complete compound list is in the supplement). In general, these represent the vast majority of GC-amenable compounds in the TLEs. The lipid record is divided into seven units based on geochemical characteristics and biomarker distributions as discussed in section 5.6.1.

Saturated *n*-fatty acids (*n*-FAs) represent the major lipid group, and their summed concentration fluctuates between 29 to 62 $\%_{lipids}$, albeit with no clear trend with depth or among units (average 46 $\%_{lipids}$). Hydroxy fatty acids (OH-FAs) comprise the second major lipid group and their concentration fluctuates between 0.8 and 36 $\%_{lipids}$ (average 19 $\%_{lipids}$), with that range largely arising from low abundances at the base of the section (Unit 1) and in the shallowest sediments (Units 6 and 7). The concentration of monounsaturated FAs (MUFAs) is highly variable, up to 37 $\%_{lipids}$ (average 9.3 $\%_{lipids}$), with the highest concentration at the base of the record (Unit 1) and in the shallowest sediments (Units 6 and 7). Polyunsaturated FA (PUFAs) concentration is < 3.2 $\%_{lipids}$ (average 0.8 $\%_{lipids}$) with the highest concentration at the deepest sediments (Unit 1). Branched FA – mainly *anteiso*- C_{15}, *iso*- C_{16} and *iso*- and *anteiso*- C_{17} components – concentration is < 14 $\%_{lipids}$ (average 3.4 $\%_{lipids}$), with that value decreasing from top (Units 6 and 7) to bottom (Unit 1) sediments. The *n*-alkane concentration varies from 0.6 $\%_{lipids}$ and 9.7 $\%_{lipids}$ (average 2.3 $\%_{lipids}$), with the highest concentration in sediments from Units 1 and 7.

The concentrations of other compound groups vary but do not exhibit any clear trends with depth or among units: the *n*-alcohol (*n*-OH) concentration varies from 2.3 to 14 $\%_{lipids}$ (average 6.7 $\%_{lipids}$), the methyl ketone concentration is < 4.5 $\%_{lipids}$ (average 2.1 $\%_{lipids}$), and the concentration of summed sterols – mainly sitosterol – is < 2.7 $\%_{lipids}$ (average 0.3 $\%_{lipids}$). Finally, the concentration of other identified compounds – mainly amyrins – is < 28 $\%_{lipids}$ (average 12 $\%_{lipids}$), varying significantly through Units 1 to 6 and being absent in the uppermost Unit 7.

Table 5.2 Summary of the quantified compound classes in 31 sediment samples collected from the El Potosi sedimentary record. The concentrations are expressed as $\%_{lipids}$.

Depth (cm)	Age (cal ka BP)	*n*-FAs	short *n*-FA	mid *n*-FA	long *n*-FA	OH-FAs	α-OH-FAs	ω-OH-FAs	branched FAs	MUFAs	PUFAs	*n*-OHs	*n*-alkanes	methyl ketones	sterols	others
1	0.1	40	13	7.9	19	1.9	1.2	0.6	1.7	35	1.2	8.1	9.7	-	2.7	-
11	0.7	41	12	10	19	1.0	0.1	0.5	5.1	29	0.7	9.4	9.7	4.5	0.4	-
21	1.3	29	18	9.2	1.4	2.8	1.6	1.1	6.0	26	0.5	7.2	3.0	0.4	0.6	24
31	1.8	45	26	14	4.9	4.5	2.9	1.6	10	19	0.6	8.4	1.6	0.7	-	9.6
41	2.3	48	24	21	3.1	1.3	0.9	0.5	4.2	34	0.6	3.9	1.2	0.4	-	6.0
51	2.5	35	18	13	4.2	9.2	3.0	5.9	14	15	-	14	2.1	0.9	1.6	8.2
61	2.7	49	27	19	3.0	3.1	2.3	0.9	14	25	0.2	2.9	1.1	0.4	-	4.5
71	2.9	45	9.6	12	23	18	0.4	18	6.8	8.5	-	7.8	0.7	0.6	1.3	12
81	3.0	38	6.0	13	20	24	-	24	6.7	2.3	-	5.9	1.3	0.9	-	21
91	3.3	44	4.4	16	24	24	0.2	24	3.8	1.7	-	5.5	0.8	0.6	-	19
101	3.5	43	4.3	15	24	18	0.1	18	2.5	1.2	-	5.3	0.6	1.4	-	28
111	3.7	58	8.7	24	25	15	-	15	3.7	0.9	-	4.0	1.4	1.6	0.4	16
121	3.9	39	4.5	13	21	21	0.1	20	4.1	2.1	-	6.8	1.0	2.6	-	24
131	4.1	47	5.0	18	24	32	0.1	32	3.9	1.6	0.1	6.3	0.8	2.3	0.2	6.1
141	4.3	50	5.7	21	23	19	0.1	19	2.6	1.5	-	6.0	1.4	3.1	-	16
151	5.2	62	3.7	25	34	15	-	15	1.8	1.2	-	4.7	2.1	3.9	0.6	8.0
161	6.1	51	4.7	20	26	25	-	25	2.9	2.5	-	7.7	1.6	4.4	-	5.4
171	7.0	49	3.5	18	28	31	-	31	2.3	1.2	-	7.2	1.6	3.8	0.5	3.1
181	8.4	50	3.1	19	28	30	0.1	30	1.9	0.8	-	7.2	1.1	3.6	-	5.7
191	10.2	49	3.6	17	28	28	0.1	28	1.7	0.6	-	9.1	1.6	1.9	-	8.1
201	12.0	55	3.3	17	35	24	-	24	0.9	0.2	-	5.5	2.2	2.6	-	9.0
211	13.0	55	2.7	18	35	23	0.3	22	0.3	0.0	-	4.5	1.7	2.1	-	14
221	13.8	50	3.4	16	31	24	0.3	23	0.3	-	-	5.1	1.3	1.4	-	18
231	14.7	49	2.3	17	30	26	-	26	0.4	0.1	-	6.2	1.7	1.8	-	15
241	15.6	46	2.9	14	29	31	3.2	27	0.2	-	-	5.2	1.1	1.6	-	15
251	16.5	44	6.9	15	22	31	0.7	30	0.6	-	-	3.8	1.2	1.4	-	18
261	17.4	44	5.0	22	17	30	0.1	29	0.7	0.3	-	7.9	1.4	2.4	2.2	11
271	18.3	45	3.3	13	29	36	0.7	35	0.5	0.1	-	6.4	1.0	1.2	-	10
281	19.1	49	4.6	22	23	31	0.6	31	0.4	0.1	-	5.5	1.4	2.9	-	9.1
291	19.9	48	12	10	26	4.1	-	4.1	0.4	14	0.3	12	9.1	3.9	-	8.3
301	20.0	41	14	13	14	0.8	-	0.8	0.5	37	3.2	6.9	4.5	3.4	-	2.3

5.5.4 Carbon isotopes of fatty acids

Carbon isotopic composition of *n*-FAs ($\delta^{13}C_{FA}$, Figure 5.7, Table 3), vary significantly with both carbon number and depth. However, there appear to be three general patterns of behaviour, although within each group there are intriguing variations: 1) short-chain C_{16} and C_{18} *n*-FAs, which exhibit high variability in Units 3 and 4; 2) the C_{20} *n*-FA, which is unexpectedly decoupled from other mid-chain *n*-FAs and is often the most ^{13}C-enriched *n*-FA in the entire sequence; and 3) mid-chain C_{22} and C_{24} *n*-FAs, which intriguingly exhibit similar carbon isotopic trends as the long-chain even-numbered *n*-FAs. The odd-chain C_{23}, C_{25} and C_{27} *n*-FAs appear to exhibit similar behaviour to those in group (3), suggesting a similar source and suggesting that they derive from diagenetic alteration (Meyers and Ishiwatari, 1993).

Short-chain C_{16} and C_{18} *n*-FAs $\delta^{13}C$ values exhibit a similar trend among Unit 2 and from Unit 5 to 7, where the values range from -31 ‰ to -24.7 ‰. In Units 3 and 4, their $\delta^{13}C$ values exhibit profound variability and a larger range from -32.2 ‰ to -22.6 ‰. However, excluding

Units 3 and 4, these short-chain compounds record a general trend of ^{13}C-enrichment from the deepest sediments to the shallowest sediments (Figure 5.7).

Overall, mid-chain C_{22} and C_{24} *n*-FAs exhibit a similar isotopic composition among all the units, and their $\delta^{13}C$ values range from -31.3 ‰ to -25.3 ‰. Interestingly, the counterpart C_{20} *n*-FA presents a unique trend and more enriched isotopic composition with $\delta^{13}C$ values fluctuating from -30.2 ‰ to -19.2 ‰, where the lower values are observed in Unit 2, gradually increasing in Unit 3 and remaining high from Unit 4 to 7. The heavy $\delta^{13}C$ values of the C_{20} FA of up to -19.2 $\delta^{13}C$ suggest an aquatic (algal) source, which is supported by the covariation of the $\delta^{13}C$ values of the C_{20} and C_{16} FAs during the C_{16} isotope excursion in Units 3 and 4 (Figure 5.7).

Long-chain C_{26}, C_{28} and C_{30} *n*-FAs $\delta^{13}C$ values are variable but generally low in Units 2 and 3 within a range from -32.6 ‰ to -30 ‰. In Unit 4, they exhibit a larger range (from -32.2 ‰ to -26 ‰) which increases to higher $\delta^{13}C$ values (from -33.8 ‰ to -21.2 ‰) in Unit 6. Generally, C_3 plants exhibit $\delta^{13}C$ bulk values between -35 and -21 ‰, whereas C_4 exhibit $\delta^{13}C$ bulk values between -20 and -9 ‰ (O'Leary, 1988). Most lipids found in plant tissue such as leaf waxes have depleted values, by up to 4-6 ‰, relative to C_3 plant bulk vegetation values and up to 8-10 ‰ relative to C_4 bulk values (Hobbie and Werner, 2004). Thus, $\delta^{13}C$ values in leaf waxes can range from -40 to -27 ‰ in C_3 plants and from -30 to -19 ‰ in C_4 plants. Accordingly, higher $\delta^{13}C$ values of some long-chain FAs suggest an increase in the proportion of ^{13}C-enriched C_4 plants within the terrestrial plant community.

The dominant chain length of long-chain leaf wax FAs can vary between different plant species (e.g. Holtvoeth *et al*., 2016), and this means that mixing ratios between C_3 and C_4 members can differ for different FAs; this appears to be the case at El Potosi (Figure 5.7). In Unit 4, C_{26} and C_{30} FAs have elevated $\delta^{13}C$ values; in Unit 5, mainly C_{30} FA has an elevated $\delta^{13}C$ value; and in Unit 6 it is only the C_{26} FA and, in one case, the C_{28} FA that has an elevated value. Collectively, this indicates that there were significant C_4 inputs in Units 4, 5 and especially 6, but the C_4 plant source appears to have varied. Long-chain *n*-FA $\delta^{13}C$ values are lower in the shallowest unit (Unit 7) compared to previous units, with a range from -29.2 ‰ to -26.8 ‰. $\delta^{13}C_{FA}$ values in the bottom-most clay unit (Unit 1) could not be determined due to low concentrations.

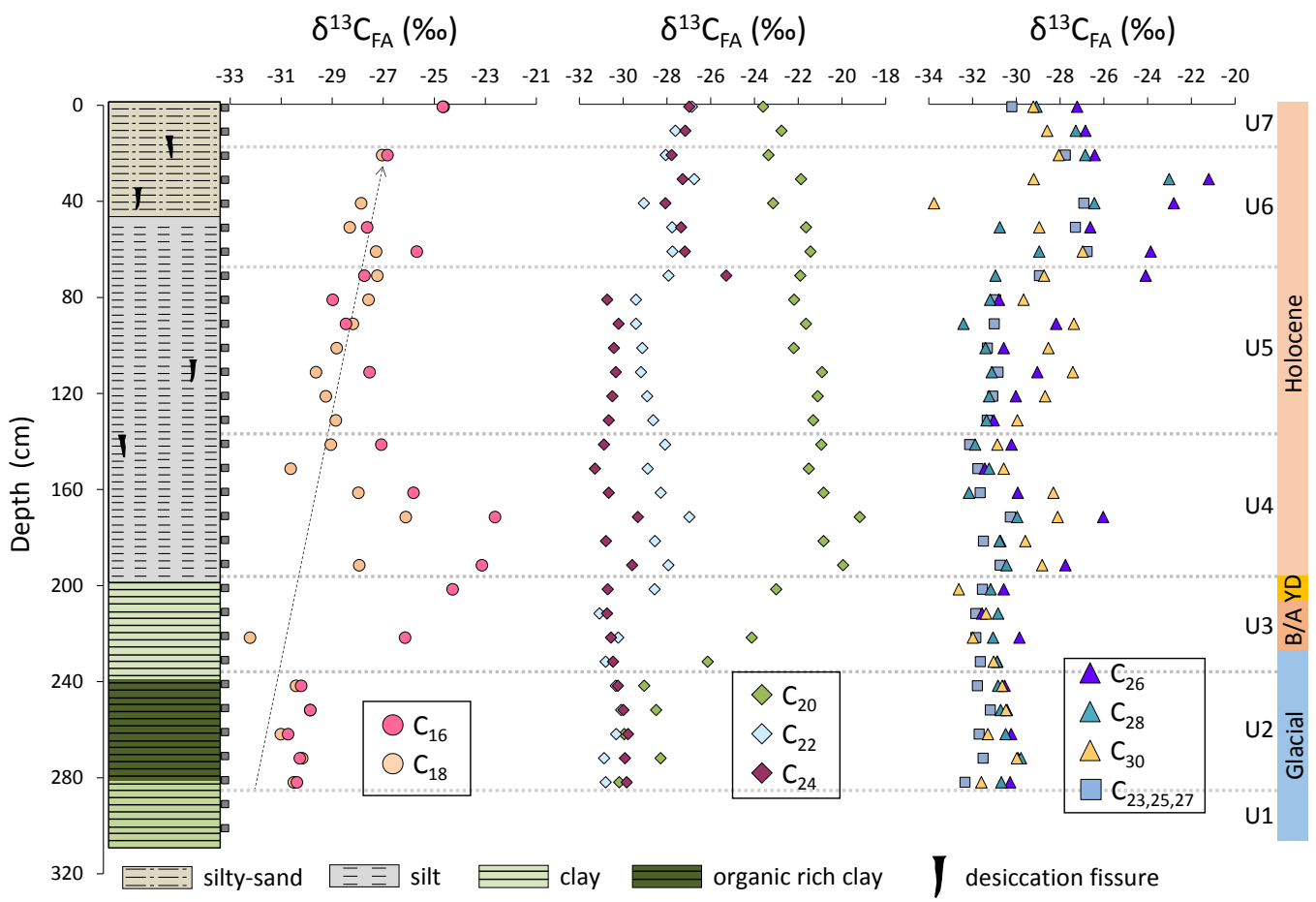

Figure 5.7 Stratigraphic profile with sample depths (grey boxes) and the carbon isotopic compositions of short-chain C_{16} and C_{18} *n*-FAs (circles), mid-chain C_{20}, C_{22} and C_{24} *n*-FAs (diamonds), long-chain C_{26}, C_{28} and C_{30} *n*-FAs (triangles), and odd-numbered C_{23}, C_{25} and C_{27} *n*-FAs (average, squares). The values are expressed as ‰ relative to the international Vienna Pee Dee Belemnite standard. The record is divided into seven units (grey bars) based on geochemical characteristics and biomarker distributions as described in the discussion.

Table 5.3 Carbon isotopic composition of *n*-fatty acids for 31 sediments collected from the El Potosi sedimentary record. The values are expressed as ‰ relative to the international Vienna Pee Dee Belemnite standard.

Depth (cm)	Age (cal ka BP)	FA C16	FA C18	FA C20	FA C21	FA C22	FA C23	FA C24	FA C25	FA C26	FA C27	FA C28	FA C29	FA C30	FA C31	FA C32
1	0.1	-24.7	-24.6	-23.6	-	-26.9	-32.3	-27.0	-29.4	-27.2	-28.9	-29.1	-30.3	-29.2	-31.6	-26.2
11	0.7	-	-	-22.8	-	-27.6	-	-27.2	-	-26.8	-	-27.3	-	-28.6	-	-24.9
21	1.3	-26.8	-27.0	-23.4	-	-28.1	-27.7	-27.8	-28.2	-26.4	-27.4	-26.9	-27.8	-28.1	-	-25.6
31	1.8	-	-	-21.9	-	-26.8	-	-27.3	-	-21.2	-	-23.0	-	-29.2	-	-
41	2.3	-	-27.9	-23.1	-	-29.1	-28.0	-28.1	-25.8	-22.8	-	-26.4	-	-33.8	-	-
51	2.5	-27.6	-28.3	-21.6	-	-27.8	-26.0	-27.4	-27.0	-26.6	-28.9	-30.8	-30.3	-29.0	-	-
61	2.7	-25.7	-27.3	-21.4	-	-27.8	-26.3	-27.2	-27.3	-23.9	-	-29.0	-	-27.0	-	-
71	2.9	-27.7	-27.2	-21.9	-	-27.9	-27.2	-25.3	-31.3	-24.1	-28.3	-31.0	-	-28.7	-	-
81	3.0	-29.0	-27.6	-22.2	-	-29.4	-30.9	-30.7	-31.4	-30.8	-30.6	-31.2	-32.0	-29.7	-	-
91	3.3	-28.5	-28.2	-21.6	-	-29.4	-30.2	-30.2	-32.6	-28.2	-30.2	-32.4	-	-27.4	-	-
101	3.5	-	-28.8	-22.2	-	-29.1	-31.6	-30.4	-31.9	-30.6	-30.5	-31.4	-	-28.5	-	-
111	3.7	-27.5	-29.6	-20.9	-	-29.2	-29.8	-30.3	-31.9	-29.0	-30.8	-31.1	-	-27.4	-	-
121	3.9	-	-29.3	-21.1	-	-28.9	-30.3	-30.5	-32.0	-30.0	-31.0	-31.2	-	-28.7	-	-
131	4.1	-	-28.9	-21.3	-	-28.6	-30.7	-30.7	-32.1	-31.0	-31.3	-31.4	-	-30.0	-	-
141	4.3	-27.1	-29.1	-20.9	-	-28.1	-30.8	-30.9	-33.4	-30.2	-32.1	-31.9	-	-30.9	-	-
151	5.2	-	-30.6	-21.5	-	-28.9	-31.6	-31.3	-32.4	-31.4	-31.3	-31.2	-	-30.6	-	-
161	6.1	-25.8	-28.0	-20.8	-	-28.3	-30.7	-30.7	-32.3	-29.9	-32.0	-32.2	-	-28.3	-	-
171	7.0	-22.6	-26.1	-19.2	-	-27.0	-29.3	-29.3	-31.1	-26.0	-30.4	-30.0	-	-28.1	-	-
181	8.4	-	-	-20.8	-	-28.6	-30.9	-30.8	-32.1	-30.7	-31.5	-30.8	-30.9	-29.6	-	-
191	10.2	-23.1	-28.0	-20.0	-	-27.9	-30.2	-29.6	-31.5	-27.8	-30.5	-30.4	-30.7	-28.8	-	-
201	12.0	-24.3	-	-23.0	-	-28.6	-32.3	-30.7	-32.1	-30.6	-30.2	-31.2	-32.2	-32.6	-	-
211	13.0	-	-	-	-23.7	-31.1	-32.2	-30.7	-31.8	-31.6	-31.6	-30.8	-32.1	-31.4	-31.6	-30.8
221	13.8	-26.2	-32.2	-24.1	-32.4	-30.2	-32.4	-30.6	-31.7	-29.9	-31.4	-31.1	-32.5	-32.0	-	-
231	14.7	-	-	-26.1	-	-30.8	-31.3	-30.5	-31.8	-30.9	-31.9	-30.9	-32.1	-31.0	-31.3	-30.7
241	15.6	-30.2	-30.4	-29.0	-31.4	-30.3	-31.2	-30.2	-31.7	-30.5	-32.4	-30.8	-32.6	-30.6	-32.7	-30.2
251	16.5	-29.9	-29.9	-28.5	-30.4	-30.1	-30.9	-30.0	-30.8	-30.4	-31.8	-30.7	-32.4	-30.5	-	-30.2
261	17.4	-30.7	-31.0	-30.0	-28.3	-30.3	-31.2	-29.8	-31.5	-30.2	-32.3	-30.5	-33.2	-31.3	-33.3	-30.2
271	18.3	-30.3	-30.2	-28.3	-29.2	-30.9	-31.9	-29.9	-31.3	-29.9	-31.3	-29.8	-31.9	-30.0	-31.5	-28.9
281	19.1	-30.4	-30.5	-30.2	-31.0	-30.8	-32.3	-29.8	-32.0	-30.3	-32.7	-30.7	-35.5	-31.6	-	-30.1
291	19.9	-	-	-	-	-	-	-	-	-	-	-	-	-	-	-
301	20.0	-	-	-	-	-	-	-	-	-	-	-	-	-	-	-

5.6 Discussion

5.6.1 Ecosystem evolution

Based on the changing biomarker distributions and concentrations (see Figures 5.8 and 5.9), we divided the sediment sequence into seven different geochemical units, with each of these units representing a distinct stage of ecosystem development in the El Potosi Basin. In the following section, they are interpreted in terms of changing organic matter sources (in chronological order).

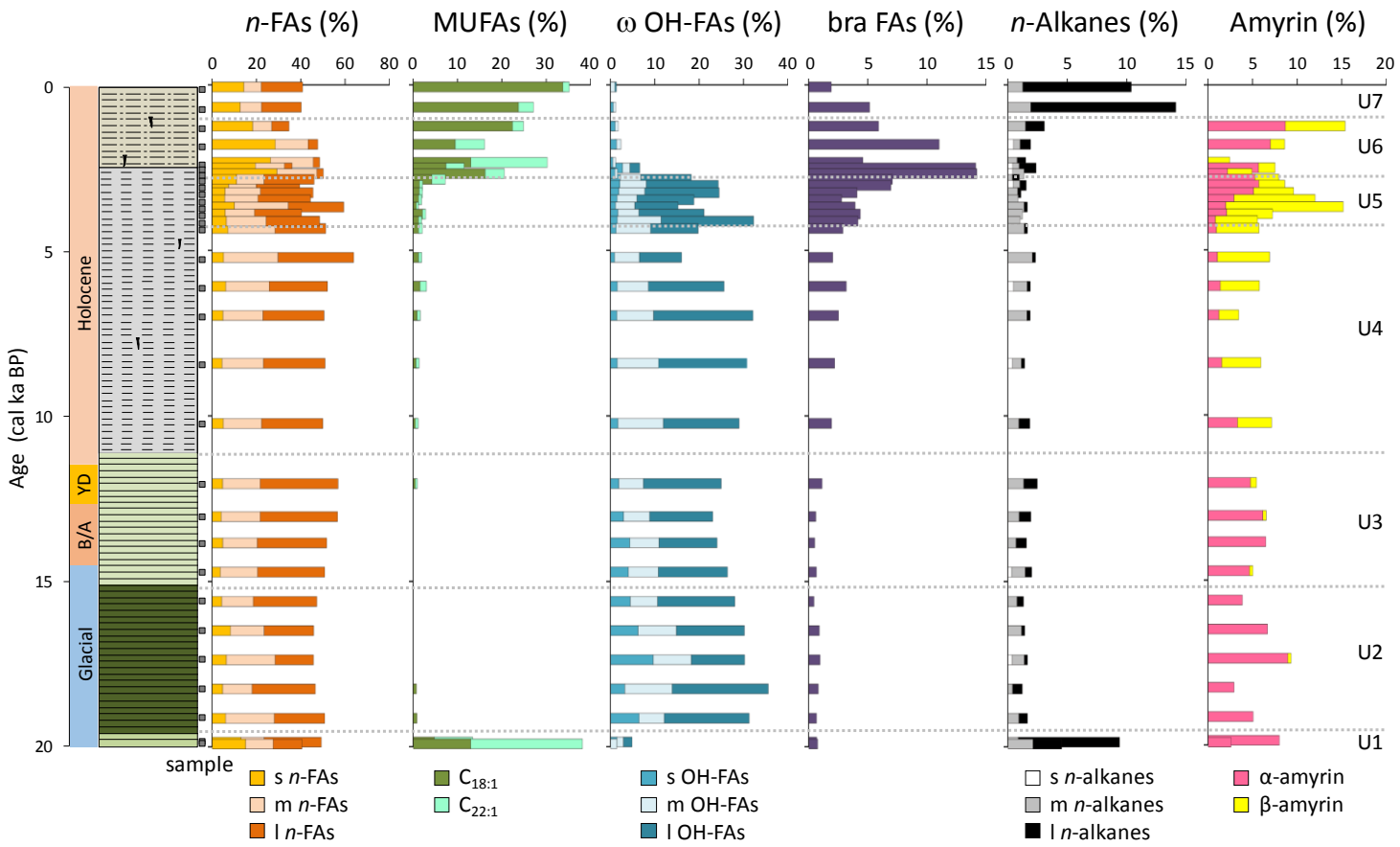

Figure 5.8 Stratigraphic profile of the sedimentary record (boxes on side of profile are sampled layers) alongside lipid biomarker distributions over time. Key compositional changes (%) of *n*-fatty acids (*n*-FAs), monounsaturated FAs (MUFAs), hydroxy acids (ω-OH-FAs), branched FAs, *n*-alkanes and amyrins are shown, as well as units defined in the text: Unit 1 (20-19 cal ka BP), Unit 2 (19-15 cal ka BP), Unit 3 (15-11.7 cal ka BP), Unit 4 (11.7-4.2 cal ka BP), Unit 5 (4.2-2.8 cal ka BP), Unit 6 (2.8-1 cal ka BP) and Unit 7 (last 1 cal ka). For *n*-alkyl components, s = short-chain (C_{16} to C_{19}), m = mid-chain (C_{20} to C_{25}), and l = long-chain (C_{26} to C_{32}) homologues.

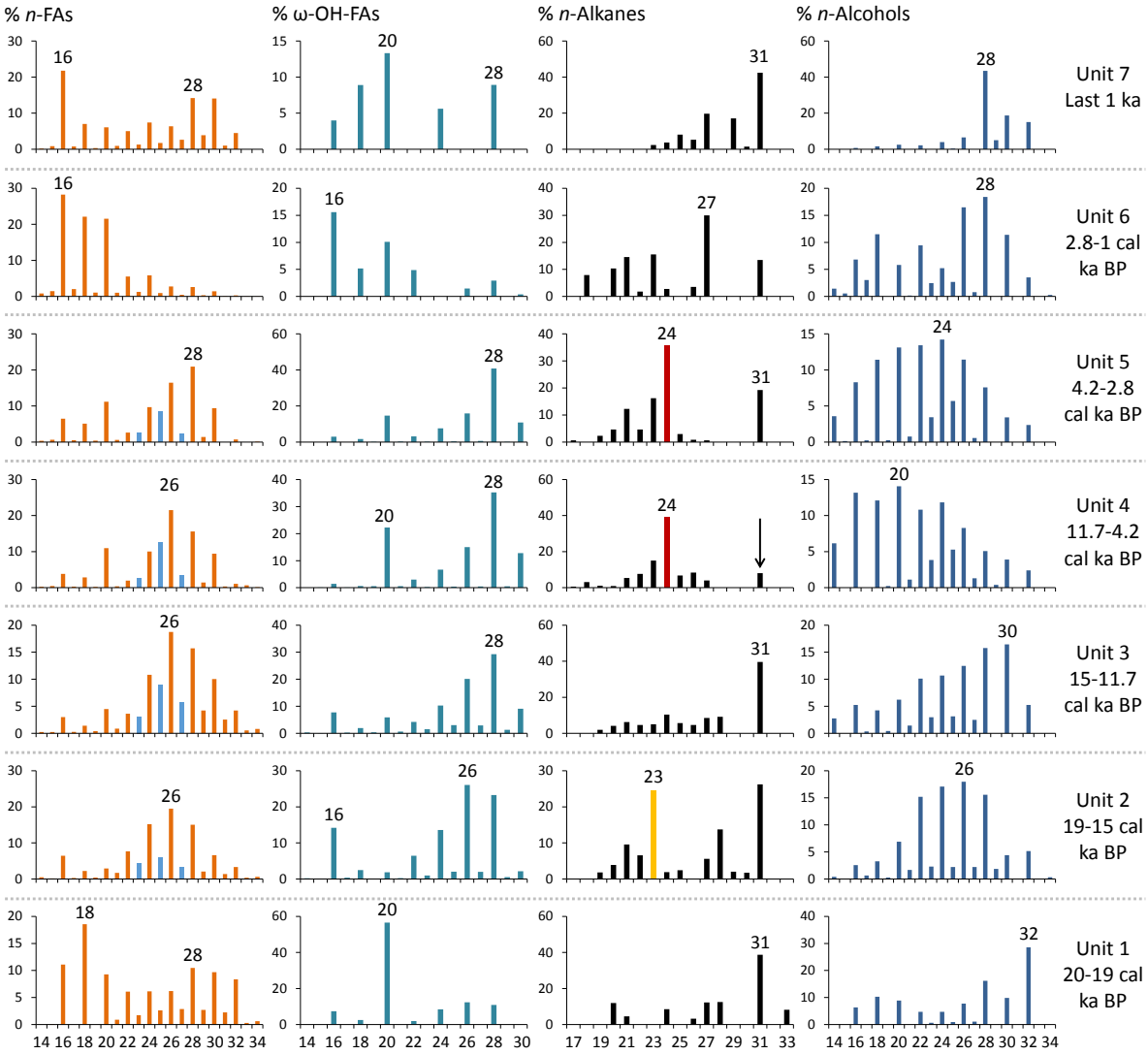

Figure 5.9 Averaged (by unit) chain length distributions of *n*-fatty acids, ω-hydroxy acids, *n*-alkanes and *n*-alcohols from Unit 1 (20-19 cal ka BP), Unit 2 (19-15 cal ka BP), Unit 3 (15-11.7 cal ka BP), Unit 4 (11.7-4.2 cal ka BP), Unit 5 (4.2-2.8 cal ka BP), Unit 6 (2.8-1 cal ka BP) and Unit 7 (last 1 cal ka). Average values (*y* axis) are percentages of the total amount of each compound class, i.e. $\%_{n\text{-FAs}}$, $\%_{\omega\text{-OH-FAs}}$, etc.

Unit 1 (20-19 cal ka BP, n=2): This unit is contemporary to the latest phase of the LGM and is characterized by very low lipid concentrations. Compound class distributions exhibit high proportions of MUFAs ($C_{18:1}$ and $C_{22:1}$) and *n*-alkanes, and among the *n*-FAs, the short-chain homologues are elevated relative to mid- and long-chain ones. The $C_{22:1}$ MUFA could derive from zooplanktonic copepods that produce this compound as part of protective wax esters (Arts *et al.*, 2001). The proportion of ω-OH-FAs, on the other hand, is very low. These

compounds may result from *in-situ* microbial oxidation of fatty acids (Eglinton *et al*., 1968; Cranwell, 1982), in which case they would be expected to show a distribution similar to the fatty acids. However, the distributions of *n*-FAs and ω-OH-FAs appear unrelated in this unit. The unusually high relative amounts of MUFAs and presence of some PUFAs in one of the samples suggest an *in-situ* source since unsaturated compounds are more susceptible to microbial degradation (electrophile attack on double bonds) compared to saturated compounds. The high proportions of $C_{18:1}$ MUFA could be related to the comparably enhanced proportions of short-chain *n*-FAs, notably the C_{18} *n*-FA. This makes a plant source seem unlikely as this would typically be associated with elevated amounts of C_{16} *n*-FA as the main fatty acid in plant tissue (e.g., Matsuda and Koyama, 1977; Desvilettes *et al*., 1997; Holtvoeth *et al*., 2010). Low TOC/TN ratios are also consistent with a contribution from *in-situ* bacterial and/or algal biomass (TOC/TN: 4-6; Nagata, 1986; Lee and Fuhrman, 1987), and low BIT indices (Figure 5.10) suggest some contribution of archaeal isoprenoidal GDGTs from the water column.

Terrestrial inputs are evident but are dominated by more recalcitrant components. In particular, the low proportion of long-chain ω-OH-FA and long-chain *n*-FAs and enhanced proportions of long-chain *n*-alkanes (l *n*-alkanes) suggests that terrestrial OM was degraded on land, i.e. before being exported towards the sediment. The dominance of the C_{31} *n*-alkane suggests input from a grassy environment since grasses tend to show a distribution maximum at this chain length (Rommerskirchen *et al*., 2006; Cui *et al*., 2008; Holtvoeth *et al*., 2016; Bliedtner *et al*., 2018). The *n*-alcohols have a trimodal distribution, peaking at C_{18}, C_{28} and C_{32}, with the latter compounds indicating input of terrestrial plant leaf waxes (Eglinton and Hamilton, 1967; Řezanka and Sigler, 2009) from two distinct sources. This implies that the asymmetrical distribution of the long-chain *n*-FAs potentially also results from input of *n*-FAs from two sources.

Overall, Unit 1 appears to represent a period with low organic matter burial in the lake, with production and/or export of terrestrial OM being relatively low and degraded and the contribution of lipids from aquatic/*in-situ* microbial biomass being relatively higher.

Unit 2 (19-15 cal ka BP, n=5): Unit 2, by contrast, is characterized by significantly higher lipid concentrations, with higher proportions of mid- and long-chain *n*-FAs, ω-OH-FAs and

long-chain OHs. Mid- and long-chain *n*-FAs derive nearly exclusively from leaf waxes of terrestrial plants, as indicated by their low $\delta^{13}C$ values (Figure 5.10). The ω-OH-FA distribution in this unit appears to match that of the *n*-FAs, suggesting that, unlike in Unit 1, the ω-OH-FAs are mainly *in-situ* degradation products of *n*-FAs. Moreover, this unit shows enhanced proportions of odd-numbered *n*-FAs, peaking at C_{25}; based on their carbon isotopic compositions, they also appear to be of terrestrial provenance, suggesting OM input from a peculiar terrestrial source with unusual high proportions of odd-numbered *n*-FAs or enhanced degradation of the FAs. The *n*-alkane distribution in this unit is bimodal with pronounced peaks at the C_{23} and C_{31} *n*-alkanes. The C_{23} *n*-alkane is the major *n*-alkane in many *Sphagnum* species (Baas *et al*., 2000; Nott *et al*., 2000), and also occurs in the roots of sedges (Ronkainen *et al*., 2013). Thus, its abundance could be indicative of a wetland environment within the catchment of the lake. The C_{31} *n*-alkane is typically associated with grasses (Rommerskirchen *et al*., 2006; Cui *et al*., 2008; Holtvoeth *et al*., 2016; Bliedtner *et al*., 2018), which may have flourished in a wetland environment as well as in the hinterland. The *n*-alcohol distribution differs significantly from Unit 1, with the long-chain *n*-OHs now peaking at C_{26} and significant contributions of the mid-chain C_{22} and C_{24} *n*-OHs. The latter can derive from suberin, a biopolyester and major compound in root material (Molina *et al*., 2006), thus, representing inputs of soil OM (Holtvoeth *et al*., 2016).

Regardless of those nuanced biomarker interpretations, Unit 2 clearly represents a stage of significantly higher terrestrial OM input to the lake sediments compared to Unit 1, with the biomarkers evidently deriving from a range of terrestrial materials including leaf waxes, degradation products of macromolecules (suberin and cutin) and wetland vegetation. Such an interpretation is also consistent with high TOC/TN ratios and BIT indices (Figure 5.10).

Unit 3 (15-11.7 cal ka BP, n=4): Sediments of this unit represent the deglaciation and the Pleistocene-Holocene transition. While the general lipid composition in Unit 3 appears to be similar to the previous Unit 2 (Figures 5.4 and 5.8), there are, in fact, subtle but meaningful differences in the chain-length distributions of the individual alkyl compound classes (Figure 5.9) as well as in the isotopic composition of the C_{20} *n*-FA. FAs are still dominated by the long-chain homologues, peaking at C_{26}, but the proportion of odd-numbered *n*-FAs, specifically C_{23}, C_{25} and C_{27} *n*-FA (peaking at C_{25}), continues to increase leading to slightly

lower *n*-FA CPIs (Figure 5.10). Slightly elevated abundances of C_{20} *n*-FA result in a trimodal FA distribution that is also recognisable in the distribution of ω-OH-FAs, corroborating the assumption that the ω-OH-FAs result from *in-situ* degradation of *n*-FAs. However, the chain-length distribution maximum shifts from C_{26} to C_{28} ω-OH-FA, thus diverging from the *n*-FA distribution, peaking at C_{26}. This could result from different susceptibility of the mixture of plant tissue types to microbial degradation. As in Unit 2, the *n*-alcohols comprise high proportions of long-chain *n*-OHs, derived from terrestrial wax esters. However, a shift towards longer chain lengths occurs, with the dominant compounds now being C_{28} and C_{30} *n*-OH. The asymmetrical distribution clearly indicates a supply of *n*-OHs from a range of sources, which could again include suberin (C_{22} *n*-OH) and possibly reeds with high proportions of the C_{30} and C_{28} *n*-OH on leaves (Holtvoeth *et al*., 2016). In contrast to Unit 2, the pronounced C_{23} *n*-alkane peak is nearly absent, leaving the C_{31} *n*-alkanes as the main, probably grass-derived compound. Finally, the $\delta^{13}C$ values of the C_{16} and C_{20} *n*-FAs increase during this stage, suggesting increasing supply of this short-chain compounds from a ^{13}C-enriched aquatic source (Hollander and McKenzie 1991; Leng and Marshall 2004).

The organic matter of Unit 3, therefore, and like that of Unit 2, is dominated by terrigenous inputs. However, the distribution of terrestrial and littoral habitats appears to have changed, with the loss of wetlands but persistence of grasses. In addition, the C_{20} *n*-FA carbon isotopic shift indicates the emergence of a distinct aquatic yet unidentified source, and the shift in C_{16} *n*-FAs $\delta^{13}C$ values provides additional evidence for an increase in aquatic contributions.

Unit 4 (11.7-4.2 cal ka BP, n=6): Unit 4 comprises sediments deposited during the early and middle Holocene. There, the proportion of the aquatic C_{20} *n*-FA further increases relative to the long-chain terrestrial *n*-FAs (Figure 5.10). The ω-OH-FA distribution is also similar to that of the *n*-FAs, again suggesting that the former are degradation products of the latter. The abundances of odd-numbered *n*-FAs also increases, again resulting in low CPIs (Figure 5.10); higher proportions of odd-chain C_{23}, C_{25} and C_{27} alcohols provide additional evidence for increased degradation of leaf waxes. The odd-numbered FAs and the C_{28} *n*-FA appear to derive from a common terrestrial source(s) as indicated by their $\delta^{13}C$ values (Figure 5.10), but the $\delta^{13}C$ values of the C_{26} and C_{30} *n*-FA exhibit slightly different profiles and become variable in this interval. This suggests that there are at least two terrestrial long-chain *n*-FA

sources: one with variable $\delta^{13}C$ values, contributing mainly C_{26} and C_{30} FA, and other with non-variable $\delta^{13}C$ values, providing the C_{28} *n*-FA and the odd-numbered *n*-FAs (Figure 5.10).

The *n*-alkane distribution exhibits a remarkable decrease in the amount of the C_{31} *n*-alkane, suggesting a decrease in grass inputs. At the same time, the amount of β-amyrin relative to α-amyrin increases in Unit 4, expressed as the sharp drop in the α/β-amyrin ratio (Figure 5.10). This also indicates a change in the type of terrestrial plant tissue supplied to the lake which could result from a change in the composition of the terrestrial vegetation. In land plant tissue, β-amyrin is typically found in higher proportions in bark tissue, whereas α-amyrin is the major triterpenoid in resin (Hernández-Vázquez *et al*., 2012). Thus, a decrease in the α/β-amyrin ratio implies a shift towards a type of vegetation that contains less resinous material and produces relatively more bark litter.

The $\delta^{13}C$ values of the C_{16} and C_{20} *n*-FAs become even more positive in the lower part of Unit 4, confirming the persistence of their aquatic source. Assuming that this increase no longer represents a change in a source mixing ratio, i.e. from a ^{13}C-depleted higher plant source to a ^{13}C-enriched aquatic one, and that these values reflect solely the aquatic end-member, then the increase in $\delta^{13}C$ values could reflect a combination of low dissolved carbon dioxide in the lake, more ^{13}C-enriched dissolved inorganic carbon and/or higher algal growth rates (Leng and Marshall., 2004). The $\delta^{13}C$ values of carbonate (Chapter VI) do not change in this interval, and we attribute the increase in $\delta^{13}C$ values to an increase in algal growth – although a change in source cannot be precluded. Intriguingly, in the upper part of Unit 4, the C_{16} and C_{20} *n*-FA $\delta^{13}C$ values become decoupled with the former decreasing to values similar to those of the putative higher plant long-chain *n*-FAs.

This unit also contains increased proportions of short- and mid-chain *n*-OHs, dominated by the C_{16} and C_{20} homologues that possibly derive from phytoplankton and bacteria (Fukushima and Ishiwatari, 1984). The $C_{18:1}$ and $C_{22:1}$ MUFAs are also slightly more abundant, also indicative of phytoplankton and bacteria (e.g. Bobbie and White, 1980; Kattner *et al*., 1983; Ahlgren *et al*., 1992) and also consistent with higher proportions of bacteria-derived branched FAs (Goossens *et al*., 1989). The mid-chain *n*-alkane, notably, are dominated by the even-numbered C_{24} *n*-alkane. Elevated proportions of even-numbered *n*-alkanes are typically attributed to bacterial sources (Grimalt *et al*., 1986; Grimalt and

Albaigés, 1987). At the same time, the GDGT-0 to crenarchaeaol ratio decreases, which could reflect either higher temperatures (Schouten *et al*., 2002) or a change in archaeal assemblages, with lower abundances of methanogens associated with lower TOC contents.

Altogether, the supply of terrestrial OM appears to have decreased relative to aquatic/bacterial biomass in Unit 4. This is also indicated by lower TOC/TN values and slightly lower BIT indices (Figure 5.10). Furthermore, the composition of the terrestrial OM sources appears to have changed compared to Unit 3, with the relative contribution of the C_{31} *n*-alkane from grasses decreasing and the change in the α/β-amyrin ratio suggesting a lower proportional input from resinous plant inputs. The terrestrial OM fraction also appears to be more degraded, with fatty acid and *n*-alcohols characterised by low CPIs.

Unit 5 (4.2-2.8 cal ka BP, n=7): The transition to Unit 5 marks the onset of the late Holocene. Sediments of this unit contain slightly higher proportions of short-chain C_{16} and C_{18} *n*-FA relative to the long-chain terrestrial *n*-FAs, which could indicate greater proportions of aquatic OM sources. However, as discussed above, their $\delta^{13}C$ values converge somewhat, such that both could be of terrestrial provenance. The average *n*-FA distribution of this unit shows a distinct shift in the dominant compound from C_{26} to C_{28} *n*-FA, indicating decreasing *n*-FA supply from the terrestrial source characterised by variable $\delta^{13}C$ values of the C_{26} and C_{30} *n*-FAs (Figure 5.10). The odd-numbered terrestrial *n*-FAs are still present in this unit as well as their odd-chain C_{23}, C_{25} and C_{27} *n*-alcohol counterparts, albeit in slightly lower relative abundance compared to Unit 4. Thus, the CPI $FA_{22\text{-}28}$ values increase. The α/β-amyrin ratio sharply increases, suggesting that the proportions of resin-derived α-amyrin increases relative to β-amyrin from bark-type plant tissue.

The $\delta^{13}C$ values of the C_{28}, C_{30} and especially C_{26} *n*-FAs increase through Unit 5, which could be due to a shift between C_3 and C_4 vegetation. The large increase in the C_{26} *n*-FA $\delta^{13}C$ value, especially at the top of Unit 5 (-24.1 ‰) and into Unit 6, provides particularly strong evidence for the presence of C_4 plants in the catchment.

In general, the biomarker data of this unit reflects a period of gradual environmental transition and ecosystem adaption during the first 1.5 ka of the late Holocene. The findings imply a phase of gradual change in the terrestrial vegetation, including a higher proportion of C_4

grasses and potentially more open vegetation, as the overall terrestrial input decreases relative to bacterial/aquatic input. The latter is also indicated by slightly lower TOC/TN ratios. The sample at 3.7 ka appears to represent a short interval of enhanced aquatic productivity as indicated by enhanced proportions of C_{20} *n*-FA, C_{20} ω-OH-FA and isoprenoidal GDGTs (low BIT index, Figure 5.10).

Unit 6 (2.8-1 cal ka BP, n=5): The most pronounced change in the overall character of OM input occurs from 2.8 ka, apparently suggesting significant ecosystem shifts. The input of soil bacteria-derived branched GDGTs decreases abruptly relative to aquatic isoprenoidal GDGTs, as reflected by the BIT index (Figure 5.10), due to either a decrease in branched GDGT supply and/or enhanced production of isoprenoidal GDGTs. However, we note that an increase in the ratio of isoprenoidal to branched GDGTs in soils also occurs in alkaline soils formed under particularly arid conditions (Ri/b ratio; Xie *et al*., 2012). Given that the CBT-derived pH (Weijers *et al*., 2007; Peterse *et al*., 2012) also increases to values >8, increased soil alkalinity seems an additional or alternative explanation for the observed trends in BIT.

Further evidence for the shift towards a predominantly aquatic source of the extractable OM is the fact that Unit 6 is the only time slice where the C_{20} *n*-FA is far more abundant than the long-chain leaf-wax derived *n*-FAs (high C_{20}/C_{28} *n*-FAs ratio; Figure 5.10). Furthermore, the proportion of MUFAs ($C_{18:1}$ and $C_{22:1}$) increases significantly. High $C_{18:1}$ MUFA concentrations could reflect contributions from bacterial biomass, which is corroborated by enhanced proportions of microbial branched FAs and slightly higher amounts of the $C_{18:1}$ trans-isomer that tends to be more abundant in bacteria (Bobbie and White, 1980). The $C_{22:1}$ MUFA could derive from copepods (Arts *et al*., 2001). The total proportions of ω-OH-FAs – particularly of long-chain ω-OH-FAs – decrease markedly, also in line with reduced terrestrial OM supply.

The now dominant C_{16} ω-OH-FA is likely to be of bacterial origin rather than a degradation product of C_{16} *n*-FA. This is supported by enhanced proportions of C_{16} α-OH-FA (Table 5.2), which also probably derives from an *in-situ* bacterial source (Eglinton *et al*., 1968; Yano *et al*., 1971; Fukushima *et al*., 1992). Leaf wax-derived long-chain *n*-FAs not only have become sparse but also at the base of Unit 6 appear to have been significantly degraded (low l *n*-FA/l

OH-FA ratio; Figure 5.10), suggesting reduced productivity and potentially deterioration of the vegetation cover. Similarly, FA CPIs decrease.

Changes in vegetation, as inferred from biomarker distributions, appear to be complex. The α/β-amyrin ratio fluctuates as do the *n*-OH distributions. Such fluctuations are not observed in the *n*-alkane distributions, but the upper three samples of Unit 6 are dominated by the C_{27} *n*-alkane, which was largely absent in Units 3-5. Moreover, there is isotopic evidence that the C_{26} *n*-FA derives from a C_4 plant source. Intriguingly, the short-chain C_{16} and C_{18} *n*-FA $\delta^{13}C$ values shift to slightly lower values of -26.7 and -27.6 ‰, respectively, deviating from those of the C_{20} *n*-FA of presumed aquatic origin (-22.3 ‰) towards the $\delta^{13}C$ values of long-chain *n*-FAs. Thus, these also could derive from degraded terrestrial inputs. Collectively, this suggests a general change in the terrestrial vegetation inputs, but it is unclear if this reflects ecosystem change or variability in delivery mechanism.

Overall, the proxy data in Unit 6 reflects an ecosystem with decreasing and variable terrestrial OM inputs, and associated variability in the character of those inputs. The ecosystem could have been near a transition state, making the supply of OM from various sources sensitive to low-amplitude climatic fluctuations. This could be expected for a shallow or ephemeral water body, with a limited catchment; indeed, evidence for a smaller and shallower lake comes from coarser lithogenic material (change from silt to silty sand), although the lithogenic change appears to have lagged those recorded by the biomarkers by about 700 years. It is also consistent with high Ri/b ratios, potentially indicating very arid conditions and alkaline soils. This change in lacustrine conditions did not appear to adversely impact aquatic production, as the OM is still associated with persistent inputs from presumably aquatic (algal and microbial) sources. However, it is possible that the production became more microbially driven, as suggested by the decreased contribution of aquatic (algal) sources to the short-chain FAs (as reflected in their $\delta^{13}C$ values).

Unit 7 (last 1 cal ka, n=2): The uppermost and most recent unit contains higher lipid concentrations compared to the previous unit; it also appears, like Unit 6, to be dominated by aquatic inputs although the changes in higher plant inputs are complex and contradictory (although we note that Unit 1 comprises only two samples). The major changes with regard to lipid composition are the re-occurrence of abundant leaf wax-derived (long-chain) fatty

acids and the highest proportions of long-chain *n*-alkanes, dominated again by the C_{31} *n*-alkane, but also the absence of the amyrins. BIT indices have their lowest values in the entire sequence, reflecting a combination of persistent aquatic inputs and low soil OM inputs – or highly alkaline soils. The $\delta^{13}C$ values of terrestrial *n*-FAs are slightly lower than in the previous unit, specifically for the C_{26} and C_{30} *n*-FA, suggesting a decreased C_4 plant contribution to both and especially the C_{26} *n*-FA. The short-chain FAs, on the other hand, now seem to originate primarily from an aquatic source, whereas in Unit 6 they appeared to be of terrestrial origin.

It is possible that the contradictory terrestrial plant biomarker trends (i.e. the complete absence of amyrins and the minimum amounts of long-chain ω-OH-FAs but the highest proportions of long-chain *n*-alkanes and l-FAs) arises from a low quality of the terrestrial OM, potentially related to OM degradation during soil storage or transport to the sediments. However, evidence for the preservation state of the OM is equivocal. The l *n*-FA/l OH-FA ratio increases, suggesting better preservation of leaf wax-derived *n*-FAs (Figure 5.10), but those ratios are not as high as in the fine-grained lower sections of the sediment core. Moreover, higher proportions of short chain ω-OH-FAs peaking at C_{20} indicate enhanced *in situ* degradation of the aquatic C_{20} *n*-FA, which now is present in significantly lower proportions; however, it also has a lighter isotopic composition (Figure 5.10), implying an increasing contribution from terrestrial sources.

Evidence for significant aquatic inputs comes from the abundant short-chain FAs, with high $\delta^{13}C$ values that are clearly distinct from those of the long-chain FAs, as well as low BIT indices and the maximum relative amounts of the $C_{18:1}$ MUFA in the entire section, with higher proportions of the *trans*-isomer.

In general, the lipid composition of Unit 7 appears to reflect a combination of aquatic and minimal terrestrial inputs. The findings imply an ecosystem with some aquatic/bacterial productivity and degraded terrestrial vegetation shifting from C_4 to C_3 type. Moreover, the putative terrestrial source(s) for resinous material and bark litter (α- and β-amyrins) seems to have been lost.

5.6.2 Ecosystem response to regional hydroclimate

It has been argued that the hydroclimate of the El Potosi Basin was controlled by sea-surface temperature (SST) of the Gulf of Mexico (GoM) with enhanced moisture transported during warmer conditions, and vice versa (Roy *et al*., 2016). It influenced the evolution of the limnic ecosystem as well as the surrounding terrestrial habitats. Seven different units have been distinguished, based on biomarker assemblages and representing different stages of the ecosystem development. We compare the ecosystem changes inferred by the biomarker proxies with the previous published Ti-based runoff record (Roy *et al*., 2016) for the late Pleistocene as well as Holocene in Figure 5.10. Some of the fossil pollen and midden-based paleovegetation records from the southeastern USA and northeastern Mexico (Figure 5.1) are also incorporated into our interpretation (Hafsten, 1961; Wells, 1966; Van Devender and Burgess, 1985; Betancourt *et al*., 1990; Van Devender, 1990).

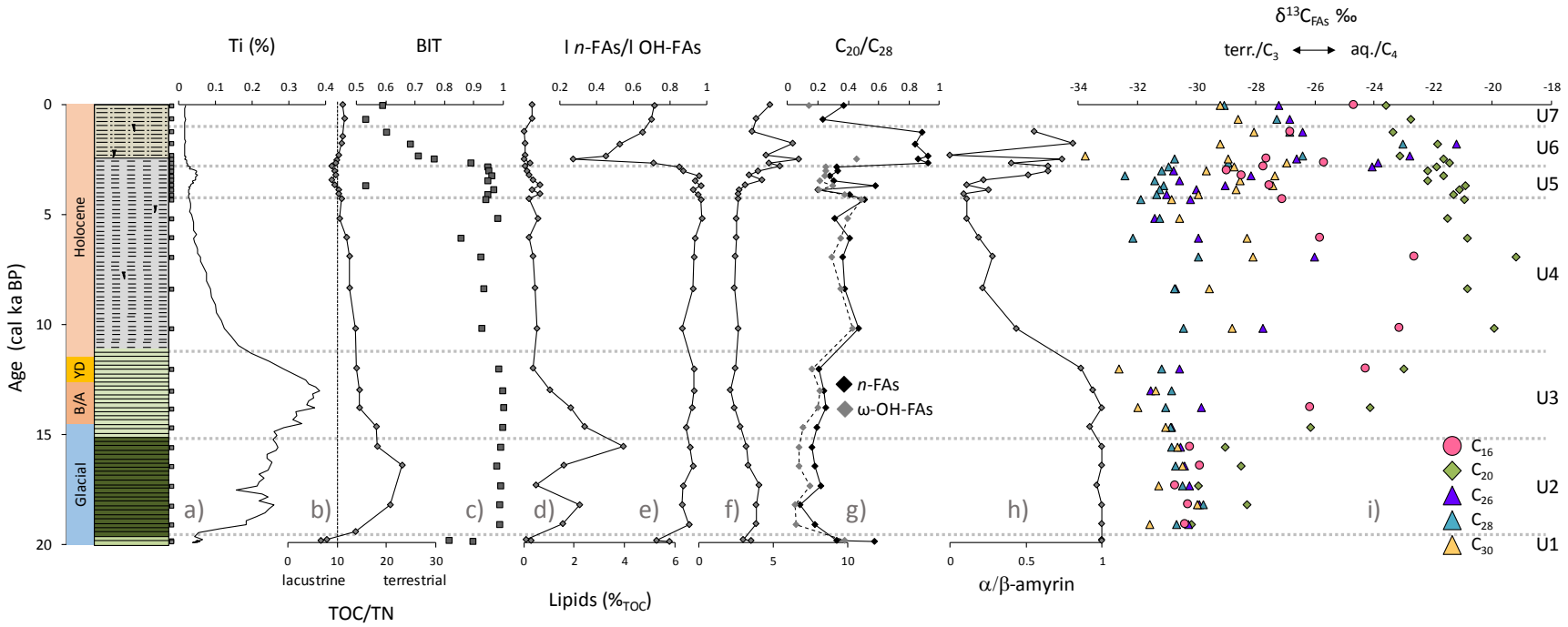

Figure 5.10 Proxy record comparison of a) inorganic terrestrial runoff (Ti; Roy *et al*., 2016), b) total organic carbon to total nitrogen ratio, c) branched and isoprenoid tetraether (BIT) index, d) lipid concentration relative to the total organic carbon ($\%_{TOC}$), e) long chain *n*-fatty acids to long chain hydroxy acids ratio, f) carbon preference index from C_{22} to C_{28} *n*-fatty acids, g) C_{20} to C_{28} *n*-fatty acid ratio and C_{20} to C_{28} ω-hydroxy acid ratio, h) α-amyrin to β-amyrin ratio and i) $\delta^{13}C$ values of *n*-fatty acids. The record is divided into seven units (grey bars) as defined in the text: Unit 1 (20-19 cal ka BP), Unit 2 (19-15 cal ka BP), Unit 3 (15-11.7 cal ka BP), Unit 4 (11.7-4.2 cal ka BP), Unit 5 (4.2-2.8 cal ka BP), Unit 6 (2.8-1 cal ka BP) and Unit 7 (last 1 cal ka).

5.6.2.1 Late Pleistocene

During the final stage of the LGM (20-19 cal ka BP; Unit 1), dry conditions are inferred from low terrestrial runoff input as indicated by low Ti concentration (Roy *et al*., 2016). Moreover, lipid biomarkers suggest a period with relatively low terrestrial OM production and evidence for degraded terrestrial biomass (unrelated distributions of *n*-FAs and ω-OH-FAs; low l *n*-FAs/l OH-FAs ratio). However, the lake did seem well developed, with a strong contribution of aquatic/*in-situ* microbial biomass ($C_{18:1}$ MUFA, TOC/TN, BIT index) as well as inferred copepod abundance which are highly adapted to survive periods of droughts (Hairston and Walton, 1986).

During the deglaciation, the SST of the GoM increased and concurrently runoff to the El Potosi basin increased between 19 and 12 cal ka BP (Roy *et al*., 2016). The paleovegetation record – based on packrat middens – suggests abundant woodland species including pinyon, juniper and some succulents (Wells, 1966; Betancourt *et al*., 1990). These findings seem to correlate with the lipid results. During the earlier part of the wetter deglaciation (19-15 cal ka BP; Unit 2), the lipid concentration increased significantly. Crucially, it appears to have been derived mostly from terrestrial materials (woodland) such as protective leaf wax esters and cutin (mid- and long-chain *n*-FAs), wetland vegetation and grasses (C_{23} and C_{31} *n*-alkane, respectively) and potentially suberin from soil OM (C_{22} and C_{24} *n*-OH). Moreover, there was a high contribution of terrestrial *in-situ* degradation products (ω-OH-FAs), and the in-lake productivity seems to have been diluted. We do not exclude the possibility of a rapid erosive event that might have formed sedimentary Unit 2. Unfortunately, no radiocarbon dates for this section were available to rule out this hypothesis. However, for our interpretation, the adjacent calibrated dates are interpolated in the age model (Figure 5.3) and sedimentary Unit 2 is considered as part of the lake record. Moreover, our interpretation correlates well with regional records (e.g. Ziegler *et al*., 2008; Roy *et al*., 2016) suggesting that warming and increased rainfall in the El Potosi Basin from 19 to 15 cal ka BP brought about the growth of extensive and diverse terrestrial ecosystems and associated runoff that flushed the OM into the ancient lake.

During the latter part of deglaciation (15-11.7 cal ka BP; Unit 3), the contribution of wetland material disappeared, whereas the proportions of leaf wax esters, cutin and soil OM remain

high, reflecting the woodland influence. This could reflect somewhat much wetter conditions, especially as it is associated with an increased lipid preservation or terrigenous OM. Moreover, the aquatic contributions (C_{16} and C_{20} *n*-FA) appear to have been proportionally higher, although their specific source was not recognizable.

5.6.2.2 Holocene

The early- and mid-Holocene represent a drier period in the El Potosi Basin. Reduced runoff after 13 cal ka BP was possibly due to lower SST in the Gulf of Mexico (Flower *et al*., 2004; Ziegler *et al*., 2008;) as a result of larger pulses of the Laurentide ice sheet melt water into the Atlantic Ocean (Roy *et al*., 2016). The decrease in moisture evidently affected the vegetation cover and runoff into the basin. Fossil pollen and plant remains of packrat middens suggest the woodland disappeared from the Llano Estacado and Maravillas Canyon (southern USA; Figure 5.1) from 11.2 to 10 cal ka BP (Hafsten, 1961; Wells, 1966). Paleovegetation records from the Canyon de la Fragua, Puerto de Ventanilas and Sierra de la Misericordia suggest that the woodlands also disappeared in northeastern Mexico from 12.6 to 8.7 cal ka BP (Van Devender and Burgess, 1985; Betancourt *et al*., 1990). Based on lower lipid concentrations and a changing terrestrial vegetation biomarker distribution (C_{20}/C_{28} ω-OH-FA, α/β-amyrin ratio, $\delta^{13}C_{FA}$ values), we suggest the woodland withdrew from the El Potosi Basin after 11.7 ka (Unit 4). The in-land vegetation became less resinous and grassy, but produced relatively more bark litter during 11.7-4.2 cal ka BP. The abundance of grasses was evidently lower than during the deglaciation period, but an increase in long-chain *n*-FA $\delta^{13}C$ values suggests an increasing proportion of C_4 plants. Coincident with these terrestrial ecosystem changes, the proportion of aquatic OM increased. During 10.3-4.6 cal ka BP the paleovegetation record from the Maravillas Canyon indicates an interval of dominant subtropical desert shrub with many grasses (Wells, 1966); despite the apparent lack of biomarker evidence for grasses, compositional changes in the terrestrial vegetation of the El Potosi Basin might also be the result of a subtropical desert shrub ecosystem.

During the late Holocene, aridity increased in the El Potosi Basin, possibly as a result of intensification of the El Niño Southern Oscillation activity and a relatively cooler GoM (Flower *et al*., 2004; Ziegler *et al*., 2008; Roy *et al*., 2016). This considerable reduction in the moisture flux triggered a shift in the vegetation type to a more xeric habitat in the

Chihuahua Desert (e.g. Van Devender, 1990; Chapter IV), characterised by the appearance of Big Bend silver leaf and C_4 chino grass at the Maravillas Canyon at 4.6 cal ka BP (Wells, 1966). The lipid biomarker data also indicate a period of gradual environmental transition and ecosystem adaption from 4.2 to 2.8 cal ka BP (Unit 5). The terrestrial vegetation shifted gradually (α/β-amyrin ratio, CPI $FA_{22\text{-}28}$, $\delta^{13}C$ values) to enhanced proportions of C_4 grasses and potentially more open vegetation. Runoff continued to decrease as indicated by lower Ti concentrations and decreasing proportions of terrigenous relative to inferred aquatic OM (Figure 5.10). Slightly enhanced terrestrial mineral runoff at ~3.5-3 cal ka BP, indicated by enhanced Ti concentrations, could have resulted from temporarily destabilised soils during vegetation recession.

After 2.8 cal ka BP (Unit 6), as climate continued to dry, terrestrial productivity decreased substantially and the lake became shallower and ephemeral, with OM characterised by high contributions from microbes ($C_{18:1}$ MUFA, branch FAs, isoGDGTs) and possibly copepods ($C_{22:1}$ MUFA), both of which are resistant to drought. Periodic drying is also indicated by the presence of desiccation fissures in the sedimentary record. At least two types of vegetation, the relative contributions of which vary, occur in Unit 6: one with enhanced proportions of long-chain C_{30} and C_{32} *n*-OH and reduced amounts of β-amyrin, and the other with higher amounts of β-amyrin and degraded FA distributions (low CPI). The fluctuations could reflect changes in the climatically controlled supply mechanisms, including episodic runoff through transient and poorly connected fluvial systems or an increased role for aeolian input under these drier conditions. Such variability is supported by higher concentrations of Si-bearing sediments with higher amplitude changes after ~2.7 cal ka BP (Roy *et al*., 2016) as well as coarser, sandy sediments.

The last millennium (Unit 7) represents a period of relatively higher lipid concentration, better preservation of leaf wax-derived compounds and terrestrial vegetation with lighter isotopic composition (C_3). All of this suggests enhanced moisture supply. Likewise, the vegetation of Maravillas Canyon became more mesic during the last thousand years (Wells, 1966). However, terrestrial mineral runoff (Ti) remains low (Roy *et al*., 2016), and it is unclear what the natural forcing mechanism would be for a reversal in the long-term Holocene drying trend. One possible explanation for these somewhat divergent

characteristics is modern human influence. During the pre-Columbian era, the north of Mexico (Aridoamerica) was occupied by the Guachichiles, nomadic and non-agrarian people (Powell, 1945). Hence, the agricultural activity in the El Potosi area is relatively recent and started during the Spanish conquest about 400 years ago (SEGOB, 1988) and nowadays, most of the modern vegetation has been altered (mainly for tomato, chili and pepper farming; FIDESUR, 2018). Agriculture could also explain the loss of amyrins, possibly derived from the xeric shrubland, from the sedimentary record and the enhanced proportions of the C_{31} *n*-alkane. Determination of the biomarker distribution in modern day vegetation in the El Potosi Basin would help explore this hypothesis.

5.7 Conclusions

This study represents the first paleoenvironmental reconstruction based on lipid biomarkers from sediments of the El Potosi Basin that represent the last 20,000 years. The biomarker-based proxy data reflects seven units that represent the environmental transition of this basin during the Late Pleistocene and Holocene, but also representing the first Holocene environmental reconstruction of northeastern Mexico. Our findings correlate and complement previous studies such as the paleohydrological reconstruction of the El Potosi Basin and the paleovegetation reconstruction of southeastern USA. Generally, during 20-19 cal ka BP, dry conditions are reflected by low lipid concentration and degraded terrestrial OM previous to sedimentation, whereas the contribution of aquatic/*in-situ* microbial biomass was relatively enhanced. The wetter deglaciation was characterized by increasing lipid concentration to lake sediments mostly derived from terrestrial vegetation such as woodland, soil and wetland from 19 to 15 cal ka BP. After this period, the wetland disappeared and the woodland input dominated the organic material during 15-11.7 cal ka BP. During the early- and mid-Holocene, the aridity increased and the woodland habitat possibly disappeared after 11.7 ka. The proportion of grasses decreased, and the dominant vegetation shifted to subtropical desert shrub with higher proportions of bark litter during 11.7-4.2 cal ka BP. The onset of the dry late Holocene is characterized by gradual environmental transition and ecosystem adaption from 4.2 to 2.8 cal ka BP. The terrestrial vegetation shifted gradually to enhanced proportions of C_4 grasses and potentially more open vegetation, and the in-lake productivity relatively increased. After 2.8 cal ka BP, the terrestrial productivity decreased

substantially and the lake became shallower/ephemeral and more sensitive to changes in the climatically controlled supply mechanisms. Changes of the limnic habitat from algal towards microbial communities occurred ~300 years after the onset of terrestrial habitat changes. Finally, during the last thousand years the vegetation shifted back to C_3 conditions, and the lipid concentration and preservation increased, implying enhanced moisture supply, either natural or anthropogenic.

CHAPTER VI
Paleoclimatic implications for the Chihuahua Desert

Paleohydrological responses to climatic variability

In collaboration with P.D. Roy, J. Holtvoeth, R.D. Pancost and M.J. Leng.

Photo by A. Rivero-Navarrete of an unspecific location at the Chihuahua Desert on the Nuevo Leon state.

6.1 Abstract

The Chihuahua Desert hydrological response to climatic variability during the late Pleistocene and Holocene is not fully understood, but is of great importance to understanding the impact of North American Monsoon variablity. In this Chapter, we present oxygen and carbon isotope data from endogenic lacustrine carbonates deposited in the Santiaguillo and El Potosi basins over the last 27,000 and 20,000 years, respectively. These data provide insight into the hydroclimate conditions and the carbon cycling of these lacustrine basins at the Chihuahua Desert of Mexico. Moreover, we integrate these data with our previous biomarker and elemental composition investigations, developing a deeper understanding of the spatio-temporal climatic variations of the region during the late Pleistocene and Holocene. Overall, we observe different stages of aridity and humidity with variable evaporation/precipitation rate. In particular, the new isotopic data reveal lower temperatures associated with low evaporation rate and well developed lake system during the LGM at the Santiaguillo Basin. On the other hand, conditions were drier at the El Potosi Basin during 20-19 cal ka BP, however, the isotopic record could suggest a wetter LGM onset. During the deglaciation, conditions were drier at the Santiaguillo Basin than at the El Potosi Basin, but it seems that the extended geographical expansion of the NAM prior to 9 cal ka BP did also allow the existence of a water body, forming during summer and evaporating during spring. After 9 cal ka BP, the Santiaguillo Basin experienced extended periods of drought, with a water body forming during summer/autumn and evaporating during winter as a result of a weaker NAM with restricted geographical expansion. Drier conditions with low moisture supply are also inferred at the El Potosi Basin from 11 to 4.6 cal ka BP. Finally, increasing aridity for both Santiaguillo and El Potosi basins occurred during the late Holocene.

6.2 Introduction

Characterization of the paleoenvironment allows us to explore the responses of local ecosystems to regional changes in hydroclimate conditions and, hence, improving our ability to understand the associated climate forcings (such as the NAM and tropical cyclones). A variety of atmospheric factors appear to have caused complex and spatially-varying changes in climate and ecology between the last glacial maximum (LGM) climate of SW North America and that of today. Firstly, the Laurentide Ice Sheet (LIS) and relatively southern location of the Intertropical Convergence Zone allowed the formation of a unique pressure system responsible for a higher contribution of winter precipitation from the Pacific Ocean to the southwestern USA (Oster *et al*., 2015). However, a recent modelling study by Bhattacharya *et al*. (2017) suggests that changes in the main wind direction weakened the North America Monsoon (NAM) and caused cold and dry conditions in the north of Mexico during the last glacial maximum (LGM). This Community Earth System Model produces an East-West gradient in summer precipitation anomalies across north and central Mexico, with western areas experiencing drier conditions. Local differences in the moist static energy budget seem to be responsible for asymmetric extension of monsoonal convection over continental areas (Bhattacharya *et al*., 2017).

Such an interpretation is consistent with many proxy records, which also indicate that northern Mexico was drier during the LGM (e.g. Lozano-García *et al*., 2002; Roy *et al*., 2013) but also indicate a strong spatial gradient; in fact many sites appear to have been characterised by wetter conditions (e.g. Lachniet *et al*., 2013; Roy *et al*., 2015). Most of these paleoclimate inferences for climate evolution in northern Mexico since the LGM are based on palynological characterisation (Lozano-Garcia *et al*., 2002; Metcalfe *et al*., 2002) and inorganic geochemistry of lacustrine sedimentary archives (e.g. Roy *et al*., 2010, 2013, 2015). Such data suggest spatio-temporal variations in hydroclimate conditions related to the dynamics of the NAM and tropical cyclones between the late last glacial to early Holocene. During the deglaciation, conditions in the central-northern Mexico remained drier overall, whilst there was more summer precipitation in northern Mexico (Roy *et al*, 2013). Northward expansion of summer moisture brought more humidity up to the Great Basin in western USA (Lyle *et al.*, 2012).

The Santiaguillo sequence has been previously analysed for ostracod species, TOC and TOC/TN ratios (Chávez-Lara *et al*., 2015), inorganic geochemistry (Roy *et al*., 2015), and lipid biomarkers (Chapter IV) to understand palaeoenvironment. Overall, these records reveal distinguishable phases from a perennial productive lake with an extended littoral zone to an ephemeral lake and, ultimately, a dry basin. Similarly, the El Potosi sequence has been analysed for TOC contents, inorganic geochemistry (Roy *et al*., 2016), and lipid biomarkers (Chapter V) to understand palaeoenvironment. Generally, these records show characteristics of a wet deglaciation followed by Holocene aridification. The paleo-precipitation reconstruction of these sedimentary sequences in the subtropical Mexico is mainly based on estimations of erosion in the lacustrine watersheds through temporal variation on Ti concentration. However, erosion is not only controlled by precipitation, other factors such as the vegetation cover in the watershed can influence this proxy (Li *et al*., 1991; Simon and Collison, 2002; Zhou and Shangguan, 2005; Reubens *et al*., 2007; Durán-Zuazo and Rodríguez-Pleguezuelo, 2008). Molecular organic compounds (biomarkers) can deepen the understanding gleaned from the Ti based precipitation proxy and have been applied for reconstructing the paleoecological conditions and identifying the sources of terrestrial and aquatic organic matter from the Santiaguillo and the El Potosi basins (Chapter IV and V). Those records reveal variable inputs of algal and bacterial biomass, aquatic microfauna and surrounding vegetation during distinct stages of ecosystem adaption. However, questions remain about the hydrological response of these lacustrine basins to climatic variability during the late Pleistocene and Holocene. To explore this, we present new oxygen ($\delta^{18}O$) and carbon ($\delta^{13}C$) isotope data from endogenic lacustrine carbonates deposited in the Santiaguillo and El Potosi basins over the last 27,000 and 20,000 years, respectively.

$\delta^{18}O$ values of endogenic carbonates are dependent on temperature and the $\delta^{18}O$ of the water in which they form, the latter governed by the precipitation ($\delta^{18}O$) and the balance of precipitation/evaporation (Leng and Marshall, 2004). Crucially, the entire hydrological system strongly affects the $\delta^{18}O$ of the lake water which dictates $\delta^{18}O$ values of carbonates. Furthermore, the $\delta^{13}C$ values provide further insight about the source of dissolved bicarbonate in the water column, the influx of allochthonous ^{13}C-depleted organic carbon, utilisation and burial of carbon during organic productivity, and exchange with atmospheric CO_2 (e.g. Andrews *et al*., 1997; Leng and Marshall, 2004; Soper *et al*., 2017).

6.3 Previous studies

Ostracod assemblages (Chávez-Lara *et al*., 2015), inorganic geochemistry (Roy *et al*., 2015), and lipid biomarkers (Chapter IV) suggest that the Santiaguillo Basin hosted an oligohaline perennial lake with high productivity and extended littoral zone during the late glacial until 17.5 cal ka BP. After this period, salinity conditions of the lake water became variable – from oligohaline to mesohaline – and an OM inputs from deteriorating surrounding wetland soils may have been caused by early dry conditions. During the early and mid-Holocene, increasing aridity and a shrinking water body brought about mesohaline conditions in the lake, with the vegetation also responding to a much drier climate. Finally, biomarker data suggests the establishment of modern vegetation during the last 4 cal ka – consistent with arid conditions, albeit less arid than during the earlier Holocene.

Similarly, inorganic geochemistry (Roy *et al*., 2016) and lipid biomarkers (Chapter V) suggest that from 20-19 cal ka BP, El Potosi Basin received low runoff and OM was mainly from aquatic/*in-situ* microbial biomass and degraded terrestrial OM. The much wetter deglaciation was characterized by increasing lipid proportions, mostly derived from terrestrial sources including woodland vegetation, soil and wetland vegetation. During the early- and mid-Holocene, the dominant vegetation appeared to shift to subtropical desert shrub. Finally, the much drier late Holocene was characterized by varying environmental change including gradual ecosystem adaption, increasing proportions of C_4 grasses and further aridification.

Multi-element geochemistry (including carbonate content; Roy *et al*., 2015, 2016), in particular, has been determined at centennial-scale resolution (181 years, on average) for both sediment sequences and provides a crucial context with respect to the depositional environment and sediment sources. The abundance of Ca is positively correlated (r^2=0.9) to CO_3 contents, and is therefore interpreted to reflect the abundance of carbonate minerals in both sediment sequences (Figure 6.2). Furthermore, the negative correlation (r^2=0.7; 0.9) of $CaCO_3$ to Ti (an inferred runoff proxy) suggests that higher deposition of $CaCO_3$ occurred during intervals of lower precipitation. The negative correlation also suggests that $CaCO_3$ was formed in lake (endogenic), rather than being detrital. Finally, X ray diffraction analysis

suggests that $CaCO_3$ present in both sedimentary records occurs as calcite, whereas other mineralogical polymorphs such as aragonite and dolomite are absent.

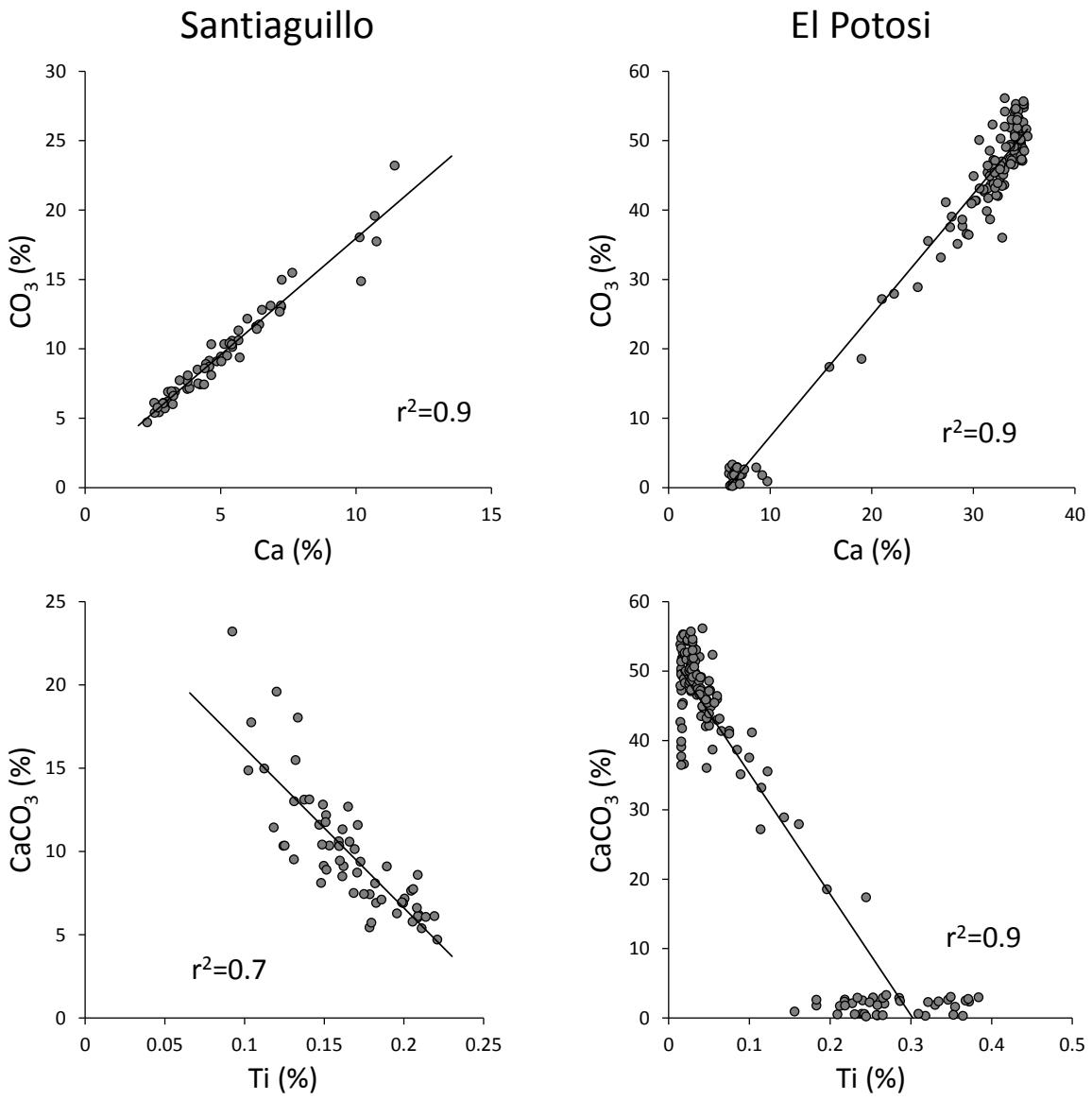

Figure 6.2 Positive correlation between concentration (%) of Ca vs. CO_3 and negative correlation between concentration (%) of $CaCO_3$ vs. Ti for the Santiaguillo and El Potosi sedimentary records.

The goal, of this chapter, therefore is to determine the carbon and oxygen isotopic composition of the endogenic carbonates of both lakes and use them to refine our understanding of their hydrological history. These data are integrated with the biomarker and elemental data to test our previous interpretations, in particular to global climatic responses

such as the last glacial gaximum, termination I, the Holocene thermal maximum and neoglaciation.

6.4 Materials and Methodology

Sampling, stratigraphy and chronology of the sedimentary records from the Santiaguillo and El Potosi basins are described in Chapter IV and V, respectively.

The isotope analysis of calcite ($CaCO_3$) was carried out on 122 sediment samples (61, from each basin). The methodology for the organic material removal, CO_2 acquisition and the isotopic analysis is described in Chapter III. Carbon and oxygen isotopic results are presented as ‰ deviation from the Vienna Pee Dee Belemnite standard (Figure 6.3; Table 6.1).

Table 6.1 Carbon ($\delta^{13}C$) and oxygen ($\delta^{18}O$) isotopic values of endogenic calcite from the Santiaguillo and the El Potosi sedimentary records. Values are expressed as ‰ relative to the international Vienna Pee Dee Belemnite standard.

Santiaguillo				El Potosi			
Depth (cm)	Age (cal ka BP)	$\delta^{13}C$ (‰)	$\delta^{18}O$ (‰)	Depth (cm)	Age (cal ka BP)	$\delta^{13}C$ (‰)	$\delta^{18}O$ (‰)
1	0.1	-3.9	-3.6	1	0.1	-4.6	-7.4
5	0.4	-4.5	-5.0	5	0.3	-4.7	-7.6
11	1.0	-4.7	-4.9	11	0.7	-4.8	-7.8
15	1.3	-4.5	-4.8	15	0.9	-4.8	-8.1
21	1.7	-4.3	-5.1	21	1.3	-4.6	-8.5
25	2.1	-4.2	-4.9	25	1.5	-4.5	-8.6
31	2.5	-4.0	-4.7	31	1.8	-4.4	-8.9
35	2.8	-3.8	-4.6	35	2.0	-4.3	-8.9
41	3.3	-3.7	-4.6	41	2.3	-4.5	-9.0
45	3.6	-3.4	-4.5	45	2.4	-4.3	-9.0
51	4.1	-3.7	-4.7	51	2.5	-4.4	-9.1
55	4.4	-3.3	-4.6	55	2.6	-4.6	-9.0
61	4.9	-2.7	-3.9	61	2.7	-4.4	-9.2
65	5.3	-3.1	-4.3	65	2.8	-4.2	-9.2
71	5.8	-2.9	-3.7	71	2.9	-3.9	-9.2
75	6.2	-4.1	-4.7	75	2.9	-3.8	-9.2
81	6.8	-2.1	-3.0	81	3.0	-3.7	-9.1
85	7.3	-2.1	-2.9	85	3.1	-3.6	-9.0
91	7.9	-2.7	-3.3	91	3.3	-3.4	-9.2
95	8.3	-2.4	-3.2	95	3.3	-3.2	-9.2

Santiaguillo				El Potosi			
Depth (cm)	Age (cal ka BP)	$\delta^{13}C$ (‰)	$\delta^{18}O$ (‰)	Depth (cm)	Age (cal ka BP)	$\delta^{13}C$ (‰)	$\delta^{18}O$ (‰)
101	9.0	-2.6	-3.6	101	3.5	-3.1	-9.1
105	9.4	-1.1	-0.6	105	3.6	-2.9	-9.3
111	10.0	-0.7	-0.5	111	3.7	-2.7	-9.4
115	10.5	-0.9	-0.6	115	3.8	-2.4	-9.3
121	11.1	-1.4	-1.1	121	3.9	-2.0	-9.4
125	11.6	-2.8	-4.1	125	4.0	-1.5	-9.4
131	12.2	-1.1	-1.0	131	4.1	-1.3	-9.4
135	12.6	-1.6	-1.6	135	4.2	-1.0	-9.6
141	13.3	-3.7	-4.8	141	4.3	-0.8	-9.5
145	13.7	-2.3	-2.3	145	4.7	-0.7	-9.6
151	14.4	-2.3	-3.2	151	5.2	-0.8	-9.4
155	14.8	-1.9	-3.0	155	5.6	-0.8	-9.5
161	15.4	-1.7	-2.4	161	6.1	-0.8	-9.5
165	15.9	-1.9	-2.5	165	6.4	-0.8	-9.3
171	16.3	-0.3	0.0	171	7.0	-0.8	-9.4
175	16.4	-1.6	-0.9	175	7.3	-0.8	-9.2
181	16.7	-2.7	-2.2	181	8.4	-0.8	-9.2
185	16.9	-0.8	0.4	185	9.1	-0.8	-9.1
191	17.2	-1.4	-0.7	191	10.2	-0.8	-9.1
195	17.4	-0.7	0.9	195	11.0	-0.7	-9.1
201	17.6	-1.6	-1.0	201	12.0	-	-
205	17.8	-2.1	-2.1	205	12.6	-	-
211	18.4	-2.5	-2.6	211	13.0	-	-
215	18.8	-3.1	-3.6	215	13.4	-	-
221	19.4	-1.9	-1.6	221	13.8	-	-
225	19.8	-2.7	-3.4	225	14.2	-	-
231	20.4	-2.0	-2.5	231	14.7	-	-
235	20.8	-2.5	-3.0	235	15.1	-	-
241	21.4	-1.8	-1.9	241	15.6	-	-
245	21.8	-1.1	-0.2	245	16.0	-	-
251	22.3	-1.7	-2.0	251	16.5	-	-
255	22.7	-1.9	-1.2	255	16.8	-	-
261	23.3	-1.0	-0.4	261	17.4	-	-
265	23.7	-1.2	-0.9	265	17.7	-	-
271	24.3	-0.8	-0.9	271	18.3	-	-
275	24.7	-0.3	0.0	275	18.6	-	-
281	25.3	-1.3	-1.6	281	19.1	-	-
285	25.7	-0.3	-0.2	285	19.5	-2.8	-9.2
291	26.3	-0.4	-0.6	291	19.9	-1.3	-9.4
295	26.7	-1.9	-3.0	295	19.9	-1.3	-9.5
299	27.1	-1.8	-2.5	301	20.0	-0.6	-9.8

6.5 Results

6.5.1 Endogenic calcite isotope data from the Santiaguillo Basin

Values of $\delta^{18}O$ fluctuate between -5.1 ‰ and 0.9 ‰ (average -2.5 ‰), and values of $\delta^{13}C$ fluctuate between -4.7 ‰ and -0.3 ‰ (average -2.2 ‰). $\delta^{18}O$ and $\delta^{13}C$ are positively correlated (r^2=0.9) which is often interpreted as evidence for an evaporating basin that is hydrologically closed (Leng and Marshall, 2004). Overall, the $\delta^{18}O$ and $\delta^{13}C$ values in the bottom 194 cm of the sequence are higher than those in the upper 101 cm, with dramatic (>1 ‰) variability through the sequence.

6.5.2 Endogenic calcite isotope data from the El Potosi Basin

Values of $\delta^{18}O$ are much lower than at Santaguillo, fluctuating between -9.7 ‰ and -7.4 ‰ (average of -9.1 ‰). However, $\delta^{13}C$ are similar, fluctuating between -4.8 ‰ and -0.6 ‰ (average -2.6 ‰). Isotope values from sediments at the interval of 281-201 cm depth were could not be determined, due to carbonate concentration being lower than instrumental sensitivity. A moderate negative correlation (r^2=0.4) occurs between $\delta^{18}O$ and $\delta^{13}C$ values in these sediments, which is surprising given that this hydrologically closed tectonic basin is expected, like Santaguillo, to also be governed by the P-E balance.

This could be a function of limestone in the catchment, such that the balance between atmospheric CO_2 and allochthonous dissolved carbonate inputs have the greater control on $\delta^{13}C$ values. Most of the sediments have homogeneous $\delta^{13}C$ values that can be categorized into two distinct end-members (-5 to -4 ‰ and -1 to 0 ‰), while the rest of the sediments have intermediate $\delta^{13}C$ values. Average values of each cluster are close to $\delta^{13}C$ values of the atmospheric CO_2 (-7.8 ‰) and limestone (0 ‰) (Leng and Marshall, 2004).

Generally, the $\delta^{18}O$ values are similar through most of the record – but very low. Sediments from the bottom 16 cm have even lower than the average values, whereas the upper 31 cm top have higher than average values.

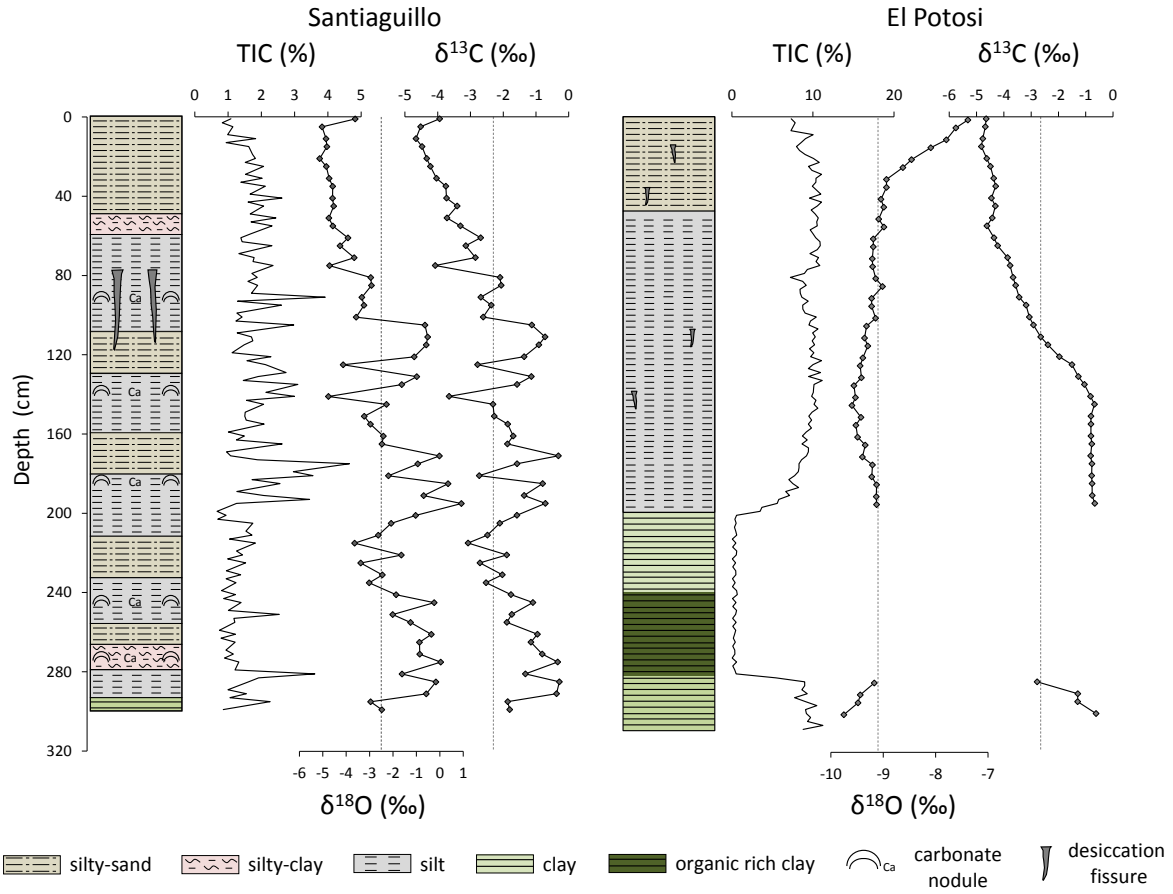

Figure 6.3 Total inorganic carbon (TIC) as percentage, carbon ($\delta^{13}C$) and oxygen ($\delta^{18}O$) isotopic compositions of endogenic calcite along the stratigraphic profiles of the Santiaguillo and the El Potosi basins. Values are expressed as ‰ relative to the international Vienna Pee Dee Belemnite standard.

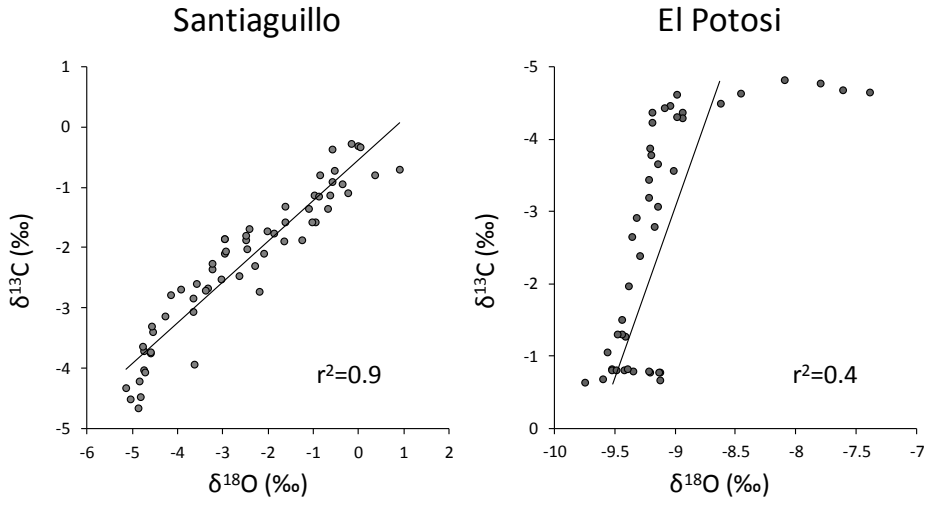

Figure 6.4 Correlation between carbon ($\delta^{13}C$) and oxygen ($\delta^{18}O$) isotopic compositions of endogenic calcite of the Santiaguillo and the El Potosi basins.

6.6 Discussion

6.6.1 Carbonate precipitation and dissolution in lakes

Lakes have the ability to consume atmospheric carbon which is closely linked to internal biological processes such as photosynthesis (Schindler *et al.*, 1997). Bacteria and plant decay in soils releases CO_2 into surface runoff, which, when converted into carbonic acid, can dissolve available carbonate minerals present in the bedrock or soil, forming bicarbonates (Cohen, 2003). This can be expressed as the following reaction:

$$CaCO_3 + H_2O + CO_2 \rightarrow Ca(HCO_3)_2$$

Equation 6.1

In lake waters, the previous reaction is readily reversible and is expressed as an equilibrium relationship; the direction in which the reaction is driven being controlled by CO_2 availability (Cohen, 2003). The addition of CO_2 leads to $CaCO_3$ dissolution until equilibrium is re-established with $Ca(HCO_3)_2$. On the other hand, the removal of CO_2 has the opposite effect, causing precipitation of $CaCO_3$. There are two primary mechanisms for causing $CaCO_3$ precipitation (CO_2 removal); photosynthesis and CO_2 degassing (Cohen, 2003). In some lakes, the increase of temperature and salinity may also cause loss of CO_2 through reduced solubility and calcite precipitation. These mechanisms are important sources for the accumulation of calcium carbonate minerals in lake sediments (Cohen, 2003). Lake waters often remain supersaturated with respect to calcium carbonate, and massive precipitation may not occur until a triggering mechanism develops, such as the presence of abundant nucleating surfaces provided by phytoplankton (Cohen, 2003). On the other hand, respiration and decomposition of organic matter are the primary means for CO_2 addition, causing $CaCO_3$ dissolution in lakes. When the deposition rate of organic matter increases, CO_2 production increases as well and eventually accumulated calcite is dissolved (Dean, 1999).

6.6.2 Unravelling the isotopic signature of lacustrine carbonates

The Santiaguillo basin is a closed lake system, with no input of groundwater and only precipitation/runoff being the source of the lake water (Figure 6.5). El Potosi is somewhat more complicated; its water also predominantly derives from precipitation/runoff, but the carbonate appears to partially derive from dissolution of carbonates in the catchment (Figure 6.6).

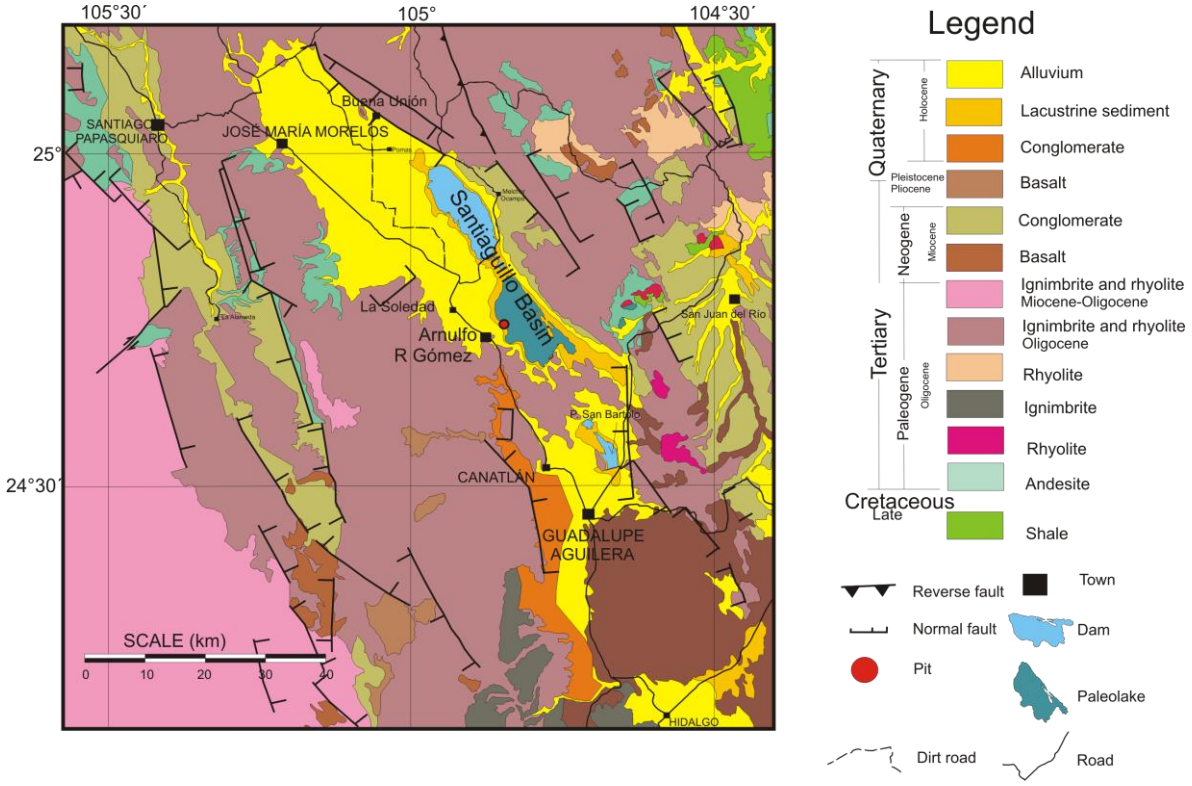

Figure 6.5 Geology map of the Santiaguillo Basin and sampling location.

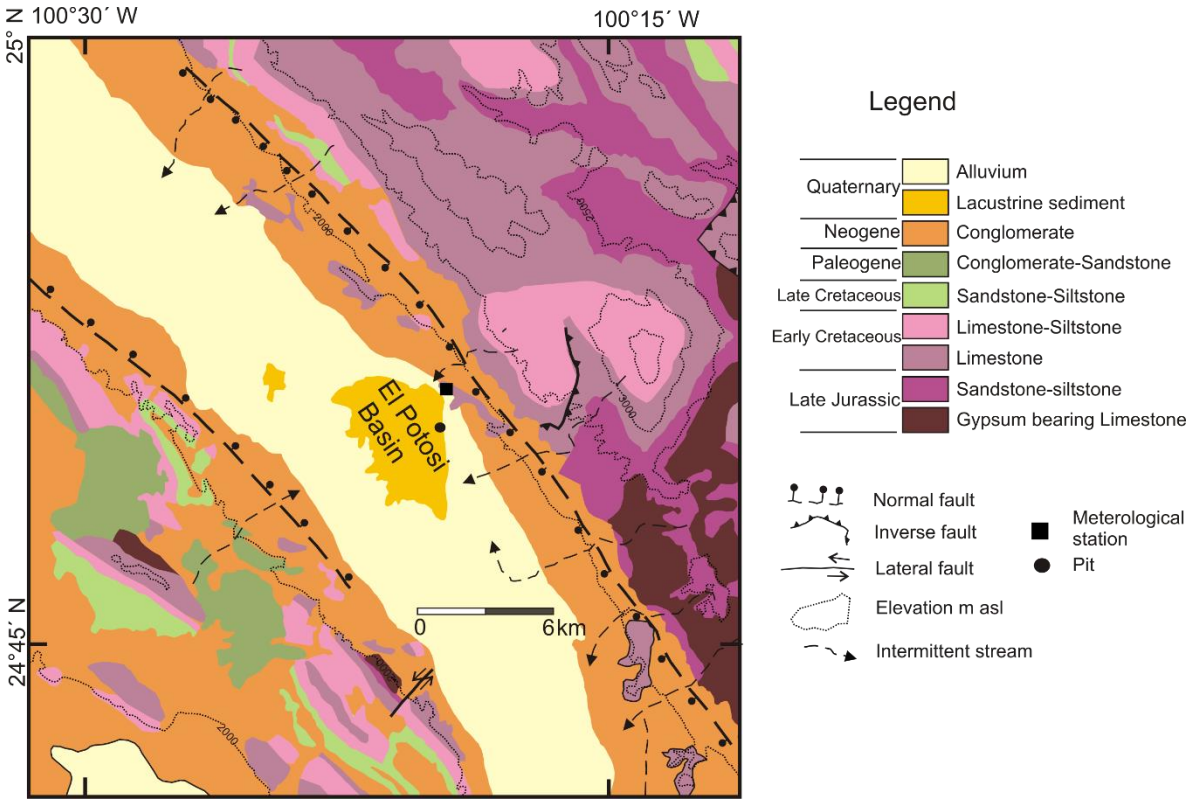

Figure 6.6 Geology map of the El Potosi Basin and sampling location.

The $\delta^{18}O$ values of endogenic carbonates depend on oxygen isotope composition of the rainwater, which is then mediated by the precipitation/evaporation balance (Leng and Marshall, 2004). Calcium carbonate $\delta^{18}O$ values are also governed by fractionation during precipitation, which is influenced by temperature, the carbonate mineralogy (i.e. dolomite exhibit higher values compared to calcite and aragonite) and vital effect of different organisms (Land, 1980; Al-Aasm *et al*., 1990; Leng and Marshall, 2004). Sediments from both basins contain only calcite (Roy *et al*., 2015; 2016), and the biogenic carbonate estimated through ostracod abundance is minimal for the Santiaguillo sedimentary record (< 125 valves/g; Chávez-Lara *et al*., 2015). Moreover, there is no correlation between total inorganic carbonate (TIC) concentration and ostracods abundance (Figure 6.7). We suggest that the ostracode influence in the isotopic signature might be minimal/absent in sediments from the Santiaguillo Basin, considering the fact that all quantified valves are embedded with authigenic carbonates. This ruled out the possibility for analysing the ostracod isotopic signature in previous works (Chávez-Lara *et al*., 2015). Ostracods are absent in El Potosi.

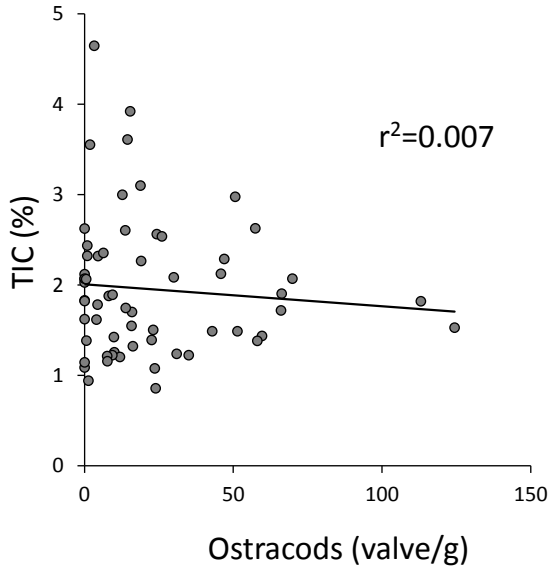

Figure 6.7 Correlation between total inorganic carbon (TIC) concentration (%) and ostracode abundance (valve/g) in sediments from the Santiaguillo basin.

Therefore, we relate the variation in $\delta^{18}O$ endogenic calcite values – of ~6‰ (Santiaguillo) and ~2.5‰ (El Potosi) – mainly to changes in the evaporation/precipitation ratio and to atmospheric temperature during carbonate precipitation. We consider the rainwater $\delta^{18}O$ values to have a minimal influence in these closed systems (Leng and Marshall, 2004). Consistent with that is the fact that the observed $\delta^{18}O$ values are higher than those of meteoric water in this region (-9.6 ‰), likely reflecting intense evaporation and associated enrichment of the lakes with the 'heavy' isotope. However, it is impossible to translate $\delta^{18}O$ values of endogenic carbonates of closed systems into absolute temperature variation as these are influenced by a wide range of interlinked environmental processes rather than a single factor (Leng and Henderson, 2013).

$\delta^{13}C$ values of endogenic carbonates reflect the source of dissolved bicarbonate in the water column, utilisation during organic productivity and exchange with atmospheric CO_2 (e.g. Andrews *et al*., 1997; Leng and Marshall, 2004; Soper *et al*., 2017). In lakes with significant input of terrestrial organic matter, the $\delta^{13}C$ values can be low due to remineralisation and release of more ^{12}C (e.g. -18 ‰; Colleta *et al*., 2001). Both the Santiaguillo and the El Potosi basins are located in arid environments, and previous research suggests that the sediments representing the Pleistocene-Holocene are poor in organic carbon in both basins. The

lacustrine carbonates precipitated in these arid settings have high $\delta^{13}C$ values due to exchange with isotopically heavier atmospheric CO_2 due to less terrestrial vegetation cover and lower organic carbon content in the watershed. Additionally, the lighter ^{12}C isotope in water are used for photosynthesis by aquatic plants during periods of enhanced organic productivity. Thus, the carbonates precipitating from the water column are enriched in ^{13}C and present high $\delta^{13}C$ values (Leng and Marshall, 2004). In case of the El Potosi Basin, the dissolution of catchment limestones also enhances the $\delta^{13}C$ values of the dissolved bicarbonate.

The Santiaguillo Basin

Over the last 27 cal ka, the Santiaguillo Basin has hosted a closed lake system, as explained before. Ostracod assemblage (Chávez-Lara *et al*., 2015) and Ti concentration (Roy *et al*., 2015) indicate perennial conditions with low lake water salinity between 27 and 17.5 cal ka BP, an interpretation consistent with biomarker assemblage indicative of a highly productive lake. Superficially, such conditions are inconsistent with the relatively high $\delta^{13}C$ and $\delta^{18}O$ values, at least compared to the late Holocene, which suggests a strongly evaporitic situation. Instead, we suggest that these reflect a combination of lower temperatures ($\delta^{18}O$) and high aquatic productivity ($\delta^{13}C$). Noticeably, during this time (27-17.5 cal ka BP), there is a decreasing trend of $\delta^{13}C$ and $\delta^{18}O$ values during the LGM (Figure 6.8), suggesting decreasing productivity (photosynthesis activity) and lower evaporation rate, perhaps as the result of lower lake water temperatures. However, reduced aquatic productivity is not reflected in the biomarker nor ostracod record. Instead, increasing proportions of bacteria derived lipids were detected for the LGM (Chapter IV; Figure 6.8), suggesting enhanced respiration and recycling of ^{13}C-depleted organic matter (e.g. Blair *et al*., 1985; Lehmeier *et al*., 2016). Thus, we suggest that decreasing temperatures, accompanied by increased inputs and respiration of OM resulted in declining carbonate $\delta^{13}C$ and $\delta^{18}O$ values during the LGM.

After 17.5 cal ka BP, lower than the average Ti concentration suggest runoff – and by extension, the rainfall - decreased (Roy *et al*., 2015); similarly, ostracod assemblages suggest ephemeral conditions with fluctuating salinity from oligohaline to mesohaline conditions from 17.5-9 cal ka BP (Chávez-Lara *et al*., 2015). This means that the Santiaguillo Basin hosted a contracted and saline water body for only few months. Consistent with this, biomarker assemblages reflect the exposure of wetland soils in the littoral zone and their

erosion as consequence of a dropping lake level (Chapter IV). Overall, higher than the average $\delta^{13}C$ and $\delta^{18}O$ values from 17.5 to 9 cal ka BP are consistent with this being an interval of intense evaporation. In particular, we suggest high productivity by aquatic plants occurred during a dry season associated with evaporative enrichment, likely in the spring given evidence for enhanced NAM-influenced summer precipitation (Barron *et al*., 2012).

After 9 cal ka BP, progressively lower $\delta^{18}O$ values (Figure 6.8) suggest lower evaporation and fresher lake water conditions. However, the ostracod record reflects increasing salinity and the persistence of ephemeral conditions (Chávez-Lara *et al*., 2015), and the Ti record suggests that precipitation reduced further (Roy *et al*., 2015). Moreover, lipid biomarkers indicate the transition to a shallower lake with extended drought periods from 9 to 7.9 cal ka BP, and much drier conditions after 7.9 cal ka BP (Chapter IV). Therefore, we again invoke seasonal atmospheric processes to explain the isotopic signature of carbonates precipitating during the last 9 cal ka. We suggest lower $\delta^{13}C$ values reflect lower productivity and increasing influence of atmospheric CO_2 to dissolved bicarbonate as result of a shallower ephemeral lake evaporating during a cold season such as winter, based on lower $\delta^{18}O$ values. Nowadays, the natural water body is less than 1 m at the deepest part during summer and autumn months when it is recharged by the rains, but evaporates and remains dry during the rest of the year. Thus, the isotopic record of the Santiaguillo Basin reflects the hydrological transition of this evaporative system.

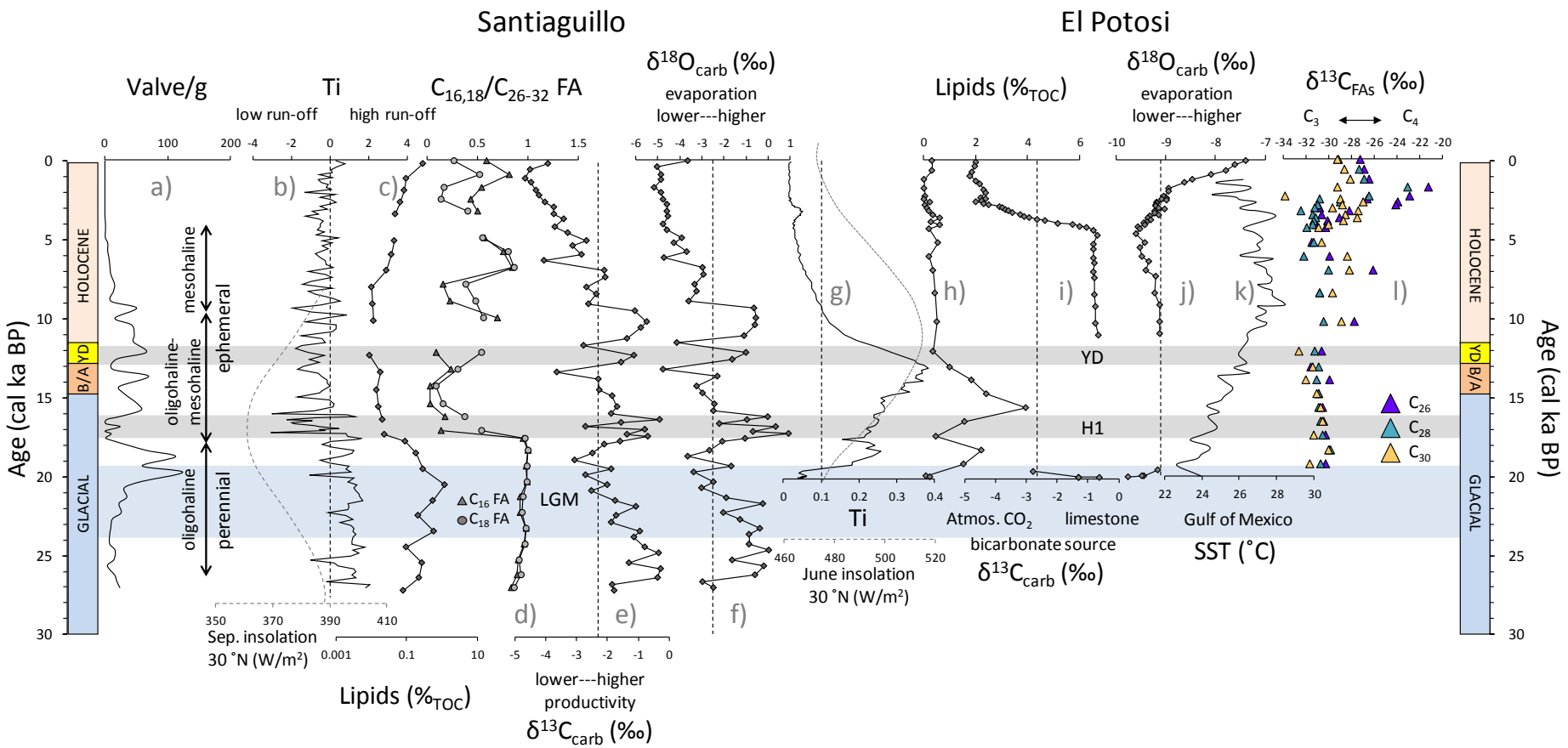

Figure 6.8 Santiaguillo proxy record comparison of a) water column salinity (Chávez-Lara *et al*., 2015), b) inorganic terrestrial runoff and (Ti) and autumn insolation (Roy *et al*., 2015), c) lipid concentration relative to the total organic carbon (‰TOC; Chapter IV), d) short-chain C_{16} and C_{18} *n*-FAs to long-chain C_{26-32} *n*-FAs ratio (Chapter IV), e) carbon and f) oxygen isotopic composition of endogenic carbonates. Similarly, El Potosi proxy record comparison of g) inorganic terrestrial runoff (Ti) and summer insolation (Roy *et al*., 2016), h) lipid concentration relative to the total organic carbon (‰TOC; Chapter V), i) carbon and j) oxygen isotopic composition of endogenic carbonates, k) Gulf of Mexico sea surface temperature (˚C; Ziegler *et al*., 2008), l) carbon isotopic composition of leaf waxes fatty acids (Chapter V).

The El Potosi Basin

The El Potosi Basin is geologically closed, although there is a poor and negative correlation between $\delta^{18}O$ and $\delta^{13}C$ values (Figure 6.3), possibly due to the presence of limestone in the catchment that might have contributed dissolved bicarbonate into the lake through runoff. The isotopic record of the El Potosi Basin for the LGM is limited to three samples from its final stage (20-19 cal ka BP). There, $\delta^{13}C$ values of endogenic carbonates decrease, suggesting a higher influence of the atmospheric CO_2 to dissolved bicarbonate (lake water), and $\delta^{18}O$ values increase, suggesting increasing evaporation (Figure 6.8). Dry conditions are also supported by low Ti and lipid concentrations (Roy *et al*., 2016; Chapter V; Figure 6.8). Further evaluation of longer records from this basin would be necessary to explore climate variation during the LGM.

The hiatus in the $\delta^{13}C$ and $\delta^{18}O$ records (Figure 6.8) occurs during a putatively wetter interval, from 19 to 11 cal ka BP, characterised by high Ti concentrations and high lipid abundances. Therefore, the low carbonate abundances are due to a combination of dilution by lithogenic inputs and perhaps suppression of authigenic carbonate precipitation in a wetter environment.

From 11 to 4.6 cal ka BP, $\delta^{13}C$ and $\delta^{18}O$ values are remarkably constant. The high $\delta^{13}C$ values likely indicate a predominance of contributions from dissolved limestone from the catchment area, and the low $\delta^{18}O$ values likely reflect a positive precipitation/evaporation rate. Both are consistent with relatively high rainfall and greater runoff. This is apparently inconsistent with relatively lower rainfall and runoff, as well as the biomarker and other elemental proxies, which exhibit profound variability; we interpret this as evidence for a relatively persistent lake during the early Holocene, even as rainfall declined and dramatic changes occurred in the surrounding ecosystems (Chapter V). This was maintained until 4.6 cal ka BP, after which $\delta^{18}O$ values dramatically increase (Figure 6.8) indicating less precipitation and/or higher evaporation. At the same time, $\delta^{13}C$ values decrease dramatically, suggesting greater contribution of atmospheric CO_2 during this drier interval and decreased inputs from the surrounding catchment. This is consistent with the biomarker data that reflects a period of gradual environmental transition to drier conditions after 4.2 cal ka BP (Chapter V).

6.6.2 Climate forcings

Our new records allow us to interpret the environmental and paleohydrological responses from the Santiaguillo and the El Potosi basins in the context of atmospheric and NAM changes

associated with the major climatic events of the last 20 cal ka, including the last glacial maximum, Termination 1, the Holocene thermal maximum and neoglaciation. For such a comparison, we integrate all of the data presented in this thesis as well as previous work carried out in the Santiaguillo and El Potosi sedimentary sequences and throughout the NAM-influenced region.

The Last Glacial Maximum

High lake levels and the presence of woodland domains (Van Devender, 1990) in the southwestern USA during the LGM have been attributed to enhanced moisture supply by winter storms caused by a strengthened and southward displaced jet stream, forced by the Laurentide Ice Sheet (LIS) (COHMAP members, 1988). However, more recent evidence has questioned this hypothesis (e.g. Lyle *et al*., 2012; Ibarra *et al*., 2014) and further investigations have tried to explain more complex patterns of moisture anomalies for this period. For example, Oster *et al*. (2015) propose that the location and strength of the contemporary pressure system were responsible for a higher contribution of winter precipitation with a northwest-southeast trend from the Pacific Ocean to southwestern USA (Figure 6.9), instead of the jet stream position. A recent paleoclimate simulation suggests that hydroclimate changes during the LGM over North America were largely due to dynamical mechanisms, such as the reorientation of westerly and southwesterly flow, implying a significant reorientation of the atmospheric circulation (Lora, 2018). This PMIP3 paleoclimate simulation also suggests that precipitation in the NAM region during the LGM was slightly enhanced from May to October in agreement with a speleothem record from tropical Southwest Mexico (Lachniet *et al*., 2013; location in Figure 6.9). However, the Community Earth System Model (CESM1.2) applied by Bhattacharya *et al*. (2017), forced by ice-sheet extent and sea surface temperature, suggests a weaker LGM monsoon. Moreover, evidence for drier conditions has been observed in northwestern Mexico as well as in the NAM region (Lozano-García *et al*., 2002; Metcalfe *et al*., 2002; Roy *et al*., 2014; Figure 6.9).

The Santiaguillo Basin is located at the central part of the NAM area defined between 18˚-33˚N and 112˚-102˚W by Bhattacharya *et al*. (2017). The sediments from this basin indicate wetter conditions during the LGM (Chávez-Lara *et al*., 2015; Roy *et al*., 2015; Chapter IV and VI) and apparently contradict the paleoclimate simulation of Bhattacharya *et al*. (2017). However, enhanced moisture in the Santiaguillo area has been attributed to the moisture contribution from tropical cyclones (Roy *et al*., 2015), which agrees with the PMIP3 paleoclimate

simulation by Lora (2018) while being compatible with a weaker NAM. Both paleoclimate simulations applied by Bhattacharya *et al*. (2017) and Lora (2018) produce an East-West gradient in summer precipitation anomalies across north and central Mexico. And in both, the East experienced wetter conditions compared to the preindustrial period. It is unclear if this extended as far East as El Potosi (Lora *et al*., 2018), where low Ti concentrations and low concentrations of degraded lipids suggest dry conditions during the final stage of the LGM (Roy *et al*., 2016; Chapter V). Our new isotopic data suggest that the LGM onset was more humid than during 20-19 cal ka BP and potentially quite variable. As such, higher resolution and additional records are required to probe the hydrological state of eastern N Mexico, which could have been quite dynamic.

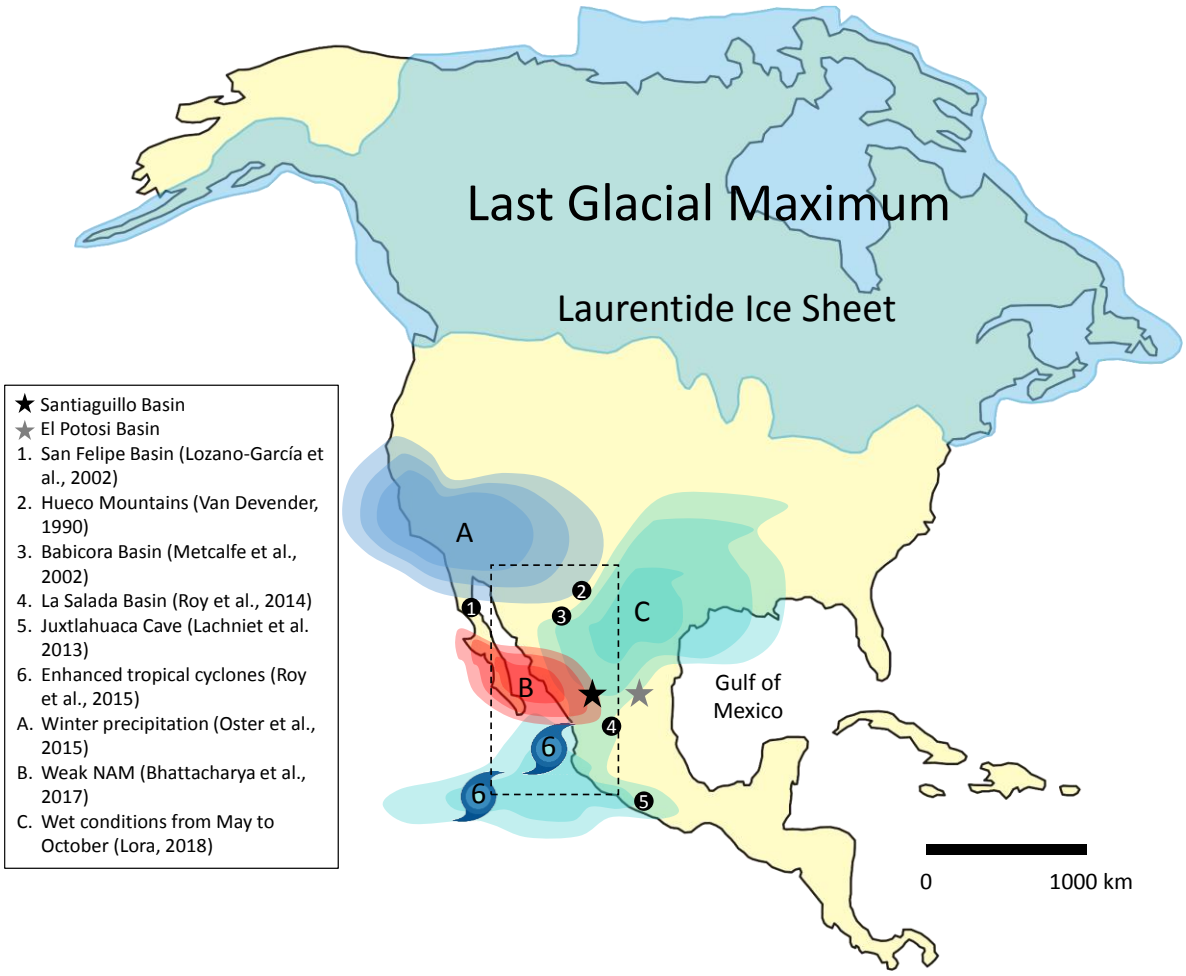

Figure 6.9 Compilation of paleohydrological conditions during the Last Glacial Maximum in North America. Coloured areas denoted by letters (A, B, C) represent the geographical expansion of different hydrological conditions based on paleoclimate simulations. The Santiaguillo and the El Potosi basins (stars) are located in central-northern Mexico. Location of other records used here for comparison are presented as circles. Dashed box represents the North America Monsoon area after Bhattacharya *et al*. (2017).

Termination 1

As with the LGM, hydrological changes across the deglaciation and through the early Holocene are spatially and temporally variable. Sediments at the Santiaguillo Basin record a significant hydrological change from a highly productive perennial lake to ephemeral conditions with seasonal droughts after the onset of the H1 (Chávez-Lara *et al*., 2015; Roy *et al*., 2015; Chapter IV; Figure 6.8). The Santiaguillo runoff record (based on Ti abundances and inferred to reflect precipitation intensity) exhibits a first order positive correlation with the autumn insolation (September), with low precipitation coinciding with an interval of low autumn insolation during the deglaciation (Roy *et al*., 2015; Figure 6.8). In contrast, a runoff record (also based on Ti concentration) at the more northern Babicora Basin shows a positive correlation with summer insolation, with inferred wetter conditions between 18 and 10 cal ka BP (Roy *et al*., 2013). Similarly, a vegetation record based on packrat middens at the southwestern USA also suggests wetter conditions during the deglaciation (Van Devender, 1990). We suggest that this reflects the role of the Gulf of California (GoC) as a moisture source to the more northern sites (Figure 6.10). TEX_{86}-derived SSTs from the Guaymas Basin of the GoC (Figure 6.10) document increasing temperatures after the onset of the H1 (McClymont *et al*., 2012), which the authors attribute to a relatively northward position of the ITCZ in the Pacific, especially during the H1 and YD stadials. Thus, relatively enhanced summer precipitation reflected in northwestern Mexico and south western USA (Figure 6.10) were likely fed by a GoC warm pool, while the Santiaguillo area shifted to drier conditions during Termination 1.

On the other hand, the ecosystem at the El Potosi Basin experienced a much wetter Termination 1 and very low evaporation (Roy *et al*., 2016; Chapter V; VI). During the onset of H1 the conditions were slightly drier, but the general trend of increasing runoff continued until the YD (Figure 6.8). The El Potosi runoff record (based on Ti abundances) shows a positive correlation with summer insolation and GoM SST based on $\delta^{18}O$ foraminifera values from the Florida margin (Ziegler *et al*., 2008) until the YD (Figure 6.8). Therefore, Roy *et al*. (2016) suggested that summer precipitation at El Potosi area gradually increased as the GoM became warmer during the deglaciation. A vegetation record based on packrat middens from the Cañon de la Fragua at northeastern Mexico also suggests wetter conditions during this period (Betancourt *et al*., 1990). Furthermore, a speleothem oxygen isotope record of a stalagmite from a Cave Without A Name near Boerne (Texas) shows a positive correlation with $\delta^{18}O$ foraminifera values from the Orca Basin at the GoM during the deglaciation (Flower *et al*., 2004; Feng *et al*., 2014). All of this evidence suggests that the main moisture supply to northeastern Mexico

and the southeastern USA was mainly sourced from the GoM until the onset of the YD. After the onset of the YD, decreasing precipitation is inferred from the El Potosi Basin Ti record, which could be consistent with cooler GoM temperatures during the YD. However, the SST od the GoM reported Ziegler *et al*. (2008) shows a continuous correlation with the summer insolation curve (Figure 6.8).

The lack of paleoclimate simulations focusing on the GoM dynamics affecting the eastern area during Termination 1 is evident. More environmental records are needed to develop reliable simulations.

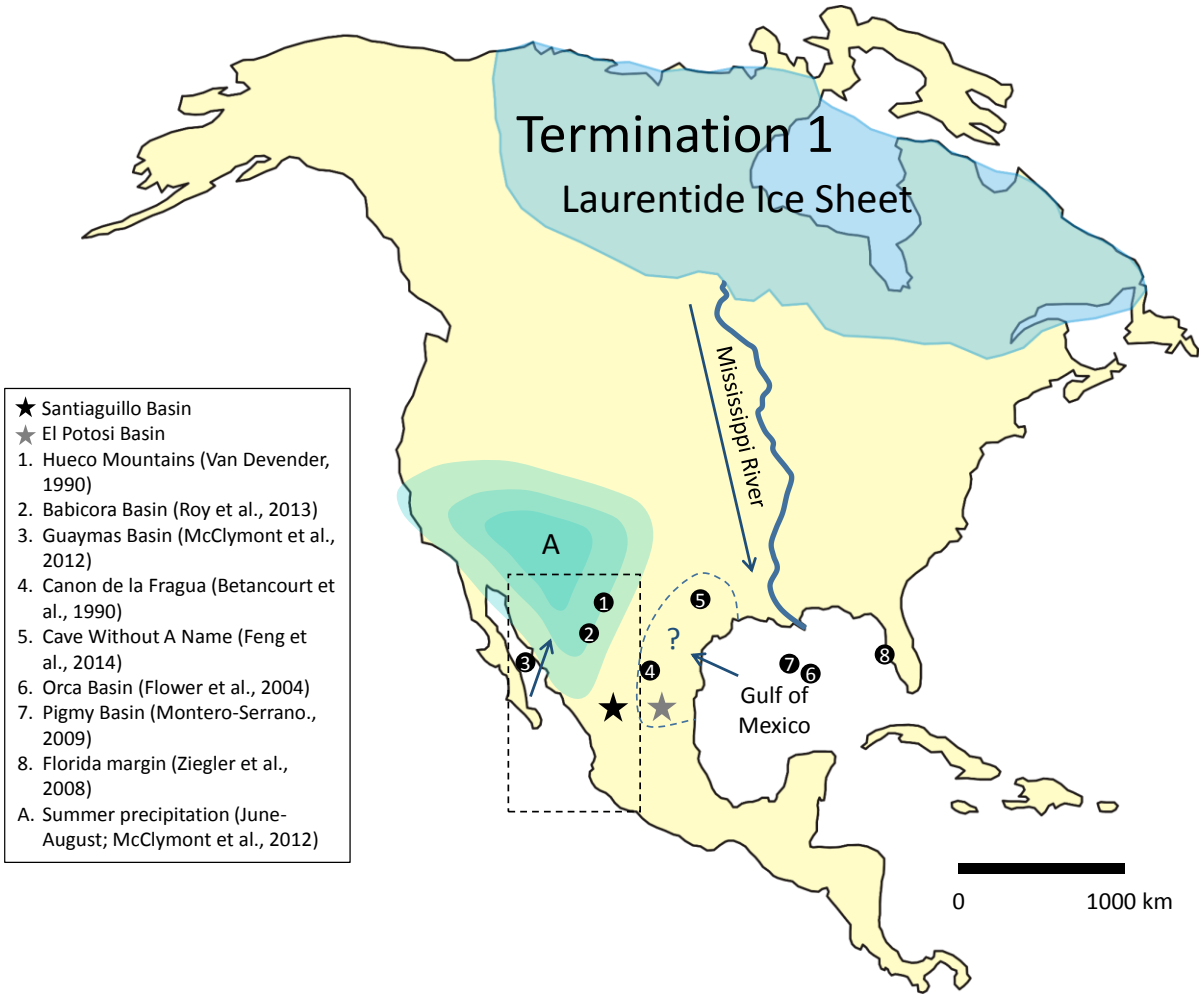

Figure 6.10 Compilation of paleohydrological conditions during Termination 1 in North America. Coloured area denoted by letter A represents the geographical expansion of summer precipitation based on McClymont *et al*. (2012) paleoclimate simulation. The Santiaguillo and the El Potosi basins (stars) are located in central-northern Mexico. Location of other records used here for comparison are presented as circles. Dashed box represents the North America Monsoon area after Bhattacharya *et al*. (2017).

Holocene thermal maximum

After ~11 cal ka BP, most of the world entered a period of warmer conditions and NH continental ice sheets disappeared (Deevey and Flint, 1957). The Scandinavian ice sheet had almost completely disintegrated by about 7 cal ka BP, the last remnants of the once huge Laurentide ice sheet melted away at 5 cal ka BP, and glaciers in alpine areas throughout the world also reduced in size or disappeared entirely (Denton and Porter, 1970). This relatively warmer period has been defined as the "hypsithermal" interval (Deevey and Flint, 1957) or commonly known as Holocene thermal maximum (HTM). However, several paleoclimatic reconstructions around the world have demonstrated that the timing and magnitude of this warming phase vary substantially between different regions, suggesting the contribution of regional feedbacks and forcings (Renssen *et al*., 2009). In the north of Mexico and south USA, most of the paleoclimate records reflect drier conditions for the early- and mid-Holocene. The expansion of modern grassland in southwestern USA provides evidence for increasing aridity after 10 cal ka BP (Sears and Clisby, 1956). In northern areas of the Chihuahua Desert, enhanced aridity is suggested after 9 cal ka BP by packrat midden records (Van Devender, 1990). However, some records in northwestern Mexico suggest the return of wetter conditions after a relatively dry YD (e.g. Lozano-García *et al*., 2002; Metcalfe *et al*., 2002; Roy *et al*., 2013). This increased moisture has been attributed to enhanced summer precipitation suggesting that the NAM became well established after 9 cal ka BP (Metcalfe *et al*., 2015). Moreover, Barron *et al*., (2012) suggest the NAM geographical expansion was enlarged, reaching southern locations prior to 8 cal ka BP.

In the central western Chihuahua Desert, lipid biomarkers in sediments from the Santiaguillo Basin reflect microfaunal adaption as a response of a shallower lake and onset of extended seasonal droughts from 9 to 7.9 cal ka BP (Chapter IV). Moreover, based on the oxygen isotope data of endogenic carbonates presented in this Chapter, we estimate the drought season at the Santiaguillo Basin shifted from spring-summer to winter-summer after 9 cal ka BP, as discussed on section 6.6.1. Hence, we suggest that the NAM enlarged scope area included the Santiaguillo Basin prior to 9 cal ka BP, while after this period it migrated to northern locations.

The HTM at the El Potosi Basin is not as clear as in western areas. Lipid biomarkers (Chapter V) as well as the isotopic composition of carbonates here presented reveal a relatively dry and stable period from 11 to 4.7 cal ka BP. The carbon isotopic composition of fatty acids in terrestrial leaf waxes exhibit higher proportions of C_4 vegetation at ~7 cal ka BP (Chapter V),

possibly suggesting that the HTM was reached at this time in northeastern Mexico. However, this assumption is only based on one data point and interpretation must be treated cautiously. Comparably, the pollen record of sediments from the Chalco Basin in central Mexico suggest increasing mean annual temperatures with subhumid-humid conditions from about 7.5 cal ka BP (Lozano-García *et al*., 1993). Overall, we suggest that the HTM in the Chihuahua Desert is manifesting itself without a clear spatiotemporal trend due to influence of regional forcings such as the NAM and the GoM dynamics. Unfortunately, paleoenvironmental records from northeastern Mexico become more limited from the early Holocene onwards.

Neoglaciation

The expansion of alpine glaciers throughout the World between 5.5 and 4.5 cal ka BP, as well as pollen records from many locations indicating a cooler and wetter climate from about 6.5-4.5 cal ka BP suggest a worldwide shift to cooler global temperatures, following the culmination of the Holocene climatic optimum (Denton and Porter, 1970). In the Sonora Desert, the modern desert scrub was established from about 4 cal ka BP (McAuliffe and Van Devender, 1998). Similarly, more open habitats dominated by shrubs and succulents are reported in the northern Chihuahua Desert at 3.9 cal ka BP (Van Devender and Worthington, 1977) and a recovery of C_4 grasses at 4 cal ka BP (Buck and Monger, 1999). At the same time, the modern dry forest vegetation became established and grasses expanded among the open vegetation in the Santiaguillo Basin (Chapter IV). Packrat middens from the southeastern USA reflect similar changes but earlier than in the western areas, characterised by the appearance of Big Bend silver leaf and C_4 chino grass at the Maravillas Canyon at 4.6 cal ka BP (Wells, 1966). Similarly, lipid biomarker proxies at the El Potosi Basin suggest the onset of gradual environmental transition and ecosystem adaption at 4.2 cal ka BP with enhanced proportions of C_4 grasses and more open vegetation (Chapter V). Drier conditions for the eastern area are associated with a relatively cooler GoM (Roy *et al*., 2016). In southern areas, towards central Mexico, the most arid conditions at the Etzatlán-Magdalena Basin were reached at 4.8 cal ka BP (Vázquez *et al*., 2017), likewise in the Lerma Basin a shallower lake associated with marsh environment is reported at 4.6 cal ka BP (Metcalfe *et al*., 1991; Caballero *et al*., 2002). Hence, dry conditions are associated with the Neoglaciation for most part of Mexico and the southern USA, with the first environmental changes documented in central Mexico, followed by the northeast Mexico-southeast USA and finally occurring in the northwest Mexico-southwest USA.

However, the expansion of C_4 grasses in northern Mexico-southern USA provides evidence for less severe aridity during the late Holocene than during the HTM, as these grasses largely depend on summer precipitation (Throop *et al*., 2012; Báez *et al*., 2013). Moreover, the last 4.2 cal ka have been characterized by enhanced frequency and magnitude of the El Niño Southern Oscillation (ENSO; Moy *et al*., 2002; Conroy *et al*., 2008). In the modern era, during El Niño years, summer precipitation decreases significantly in the north of Mexico (Magaña *et al*., 2003). Moreover, some parts of northwestern Mexico experience more humid winters as a result of increased SST in the north eastern Pacific (Ropelewski and Halpert, 1987), as well as increased inflow of humid air masses from tropical Pacific cyclones during autumn (Reyes and Mejia-Trejo, 1991; Rodgers *et al*., 2000; Englehart and Douglas, 2001; Jáuregui, 2003; Magaña *et al*., 2003; Larson *et al*., 2005). Hence, the moisture supply during autumn and winter could have supported the expansion of C_4 grasses (Chapter IV).

6.7 Conclusions

The oxygen isotopic composition of endogenic carbonates from the Santiaguillo and the El Potosi basins are mainly impacted by the balance of precipitation and evaporation as both basins are closed lake systems. The carbon isotopic composition for the Santiaguillo Basin mainly reflects utilisation during organic productivity and exchange with atmospheric CO_2, while for the El Potosi Basin the carbon isotopic composition is mainly controlled by the balance between allochthonous dissolved carbonate inputs from the catchment during relatively wet periods, and by atmospheric CO_2 exchange during relatively dry periods. The isotope data here presented supports previous environmental interpretation and helps to understand regional spatio-temporal climatic variations in the region during the late Pleistocene and Holocene. More specific, our conclusions are:

a) Lower temperatures at the Santiaguillo Basin during the LGM is associated with low evaporation rate, enhanced respiration and recycling of ^{13}C-depleted organic matter.

b) The isotopic record supports previous interpretation of dry conditions during the final stage of the LGM (20-19 cal ka BP) at the El Potosi Basin with decreasing $\delta^{13}C$ values suggesting higher influence of the atmospheric CO_2 to dissolved bicarbonate in the lake water as a result of increasing evaporation. However, these conditions could suggest a wetter LGM onset, we recommend further evaluation to longer records of El Potosi Basin to determine this.

c) The deglaciation period caused a reduction of moisture supply at the Santiaguillo Basin shifting from a perennial lake to an ephemeral one. However, the geographical expansion of the NAM prior to 9 cal ka BP supported the existence of a water body forming during the summer and evaporating during spring.

d) Much wetter conditions at the El Potosi Basin during the deglaciation period are supported by a hiatus on the $\delta^{13}C$ and $\delta^{18}O$ records indicating minimal evaporation rate, thus endogenic carbonated did not precipitate from 19 to 11 cal ka BP. We link enhanced precipitation from the GoM to lower oxygen isotopic composition of sea water as a result of more depleted meltwater pulses from the LIS channel by the Mississippi River.

e) After 9 cal ka BP, drier conditions with extended periods of drought at the Santiaguillo Basin are inferred from the isotopic records and associated to a weaker NAM with restricted geographical expansion. We suggest formation of the water body during summer/autumn and evaporating during winters.

f) Drier conditions from 11 to 4.6 cal ka BP at the El Potosi Basin are reflected by precipitation of carbonates. We infer a constant moisture supply with an increasing trend among the early- and mid-Holocene that washed in limestone from the catchment area. There is no clear evidence of the HTM during this period.

g) The isotopic records for both Santiaguillo and El Potosi basins reflect increasing aridity during the late Holocene, despite the C_4 evidence based on lipid biomarkers, which suggests seasonal precipitation derived by tropical cyclones during autumn in response to enhanced ENSO activity.

h) Finally, we notice a deficit of paleoclimatic records from the northeastern Mexico, which are key for developing more precise paleoclimate simulations. We suggest future investigations should also focus on this area as much as they do for the northwestern region.

CHAPTER VII
Conclusions and Final remarks

Photo by C.M. Chávez-Lara

This final chapter summarises and integrates the conclusions from the previous data chapters (Chapters IV, V and VI) and addresses the general and specific aims of this thesis. Recapitulating, the main goal of this work is to explore and understand the responses of lacustrine ecosystems and their environment in subtropical Mexico to the major climate changes of the late Pleistocene and Holocene and to document spatio-temporal climatic variations in the region that may help identifying the mechanisms behind NAM variability.

7.1 Conclusions

7.1.1 Records of environmental changes from subtropical Mexico

The Santiaguillo Basin

Lipid biomarkers from the Santiaguillo Basin are indicative of a system that sustained a perennial, highly productive lake with considerable input of bacterial biomass during the last glacial (27 to 17.5 cal ka BP). However, although such a feature clearly suggests humid conditions, there is hardly any evidence for input from the surrounding vegetation. Still, plant remains from packrat middens indicate that the wider region was in fact dominated by woodland species until 11.5 cal ka BP, including pinyon pines, juniper and shrub oak (Van Devender, 1990). The striking absence of significant amounts of lipids from terrestrial plants may be explained by extended littoral zones surrounding the open lake that trapped OM sourced from the catchment.

By contrast, the deglaciation was characterised by much higher input from terrestrial vegetation. *Sphagnum* biomarkers (i.e. C_{23} *n*-alkane and methyl ketones) reflect the exposure of wetland soils in the littoral zone, their erosion and transfer into the Santiaguillo Basin. During this interval, the vegetation of the Chihuahua Desert was dominated by pinyon-juniper-oak woodland as suggested by packrat midden data (Van Devender, 1990; Van Devender and Burgess, 1985). Long-chain *n*-FAs support an enhanced contribution of leaf waxes from a woodland environment to the Santiaguillo Basin. However, increased proportions of C_{31} *n*-alkane, C_{23} *n*-alkane (*Sphagnum*) and low amounts of lipids suggest a dominant supply of degraded OM mainly from a grassy (former) wetland area. Furthermore, increasing proportions of 13-methoxyheneicosanoic acid suggests relatively high input from bacterial biomass mainly at 16.7 cal ka BP (~H1) and 12.2 cal ka BP (~YD). Therefore,

compared to the glacial, the lake level in the Santiaguillo Basin appears to have dropped during the period of 17.5-11.5 cal ka BP or potentially fluctuated, causing degradation of former wetlands and associated supply of degraded OM.

During the early- and mid-Holocene, the biomarkers indicate reduced leaf wax inputs but contributions from woody plant tissues, consistent with bark and resin inputs (β-amyrin), appear to have increased. The early Holocene provides evidence for increasing aridity, with expansion of modern grassland appearing to set in at about 9 cal ka BP. The input of terrestrial OM appears to maximise from 9 cal ka BP to 7.9 cal ka BP and seems to be associated to predominantly woody material rather than leaf litter. This period coincides with a decrease in the abundance of ostracods (Chávez-Lara *et al*., 2015) and a contemporaneous increase in the abundance of copepods as implied by maximum relative amounts of the $C_{22:1}$ MUFA. This suggests a shift in the microfaunal community, probably as a response to a shallowing of the lake and the onset of seasonal droughts to which copepods tend to be more resistant than ostracods (Pillay and Perissinotto, 2009). Further aridification and extended periods of drought between 6.8 and 4.9 cal ka BP are indicated by the appearance of desiccation fissures, lower than average terrestrial runoff as inferred from the Ti record (Roy *et al*., 2015) and the disappearance of copepods as the source of the $C_{22:1}$ MUFA. Aridity across the wider area increased and terrestrial OM inputs declined, while enhanced relative contributions from algal and bacterial biomass (short-chain *n*-FAs, α-C_{16} OH-FA, C_{21} *n*-alkane) indicate at least short-lived occurrences of a water body during the summer season.

During the late Holocene higher plant biomarkers (long-chain ω-OH-FAs, *n*-alkanes, *n*-alcohols, sterols and, to a lesser degree, *n*-fatty acids) become more dominant. Modern subtropical dry forest vegetation, relying on seasonal moisture supply and with species rich in α-amyrin such as the *Burseraceae* family, might have established at the beginning of this period. This was apparently accompanied by the expansion of grasses growing among the open dry forest vegetation, as suggested by *n*-alkane distributions with an enhanced proportion of the C_{31} *n*-alkane. At the same time, the vegetation in the North of the Chihuahua Desert shifted to more open habitats dominated by shrubs, succulents and C_4 grasses (Van Devender and Worthington, 1977; Buck and Monger, 1999). The expansion of the C_4 grasses

provides evidence for less severe aridity during the late Holocene, as these grasses largely depend on summer precipitation (Throop *et al*., 2012; Báez *et al*., 2013).

The El Potosi Basin

The final stage of the LGM (20-19 cal ka BP) at the El Potosi Basin is characterized by dry conditions inferred from low terrestrial runoff input (low Ti concentration; Roy *et al*., 2016). Lipid biomarkers reflect a period with relatively low terrestrial OM production and evidence for degraded terrestrial biomass (unrelated distributions of *n*-FAs and ω-OH-FAs; low l *n*-FAs/l OH-FAs ratio). However, at least an ephemeral lake seems to have existed, resulting in a strong contribution of OM from aquatic/*in-situ* microbial biomass ($C_{18:1}$ MUFA, low TOC/TN, lower BIT index) as well as inferred copepod abundance ($C_{22:1}$ MUFA), which are highly adapted to survive periods of droughts (Hairston and Walton, 1986).

During the deglaciation, lipid biomarkers reflect much wetter conditions. The OM appears to have been derived mostly from terrestrial materials (woodland) such as protective leaf wax esters and cutin (mid- and long-chain *n*-FAs), wetland vegetation and grasses (C_{23} and C_{31} *n*-alkane, respectively) and potentially suberin from soil OM (C_{22} and C_{24} *n*-OH) between 19 and 15 cal ka BP. Subsequently, from 15 to 11.7 cal ka BP, the contribution of wetland material disappeared, but the proportions of leaf wax esters, cutin and soil OM remain high, reflecting enhanced woodland influence. Moreover, aquatic contribution ($\delta^{13}C$ of C_{16} and C_{20} *n*-FA) appears to have been proportionally higher.

The early- and mid-Holocene was characterized by lower Ti concentrations, lower lipid concentrations and a changing terrestrial vegetation biomarker distribution (C_{20}/C_{28} ω-OH-FA, α/β-amyrin ratio, $\delta^{13}C_{FA}$ values) that may be interpreted to reflecta recession of woodland from the El Potosi Basin after 11.7 ka. The vegetation appears to have become less resinous and grassy, but produced relatively more bark litter between 11.7 and 4.2 cal ka BP. The abundance of grasses was evidently lower than during the deglaciation period, but an increase in long-chain *n*-FA $\delta^{13}C$ values suggests an increasing proportion of C_4 plants. These compositional changes in the terrestrial vegetation of the El Potosi Basin might reflect the development of a subtropical desert shrub ecosystem. Coincident with these terrestrial ecosystem changes, the proportion of aquatic OM increased.

At the onset of the late Holocene, the biomarkers indicate a period of gradual environmental transition and ecosystem adaption from 4.2 to 2.8 cal ka BP. The terrestrial vegetation shifted gradually (α/β-amyrin ratio, CPI $FA_{22\text{-}28}$, $\delta^{13}C$ values) to enhanced proportions of C_4 grasses and potentially more open vegetation. Runoff continued to decrease as indicated by lower Ti concentrations and decreasing proportions of terrigenous relative to inferred aquatic OM. After 2.8 cal ka BP, as aridity increased, terrestrial productivity decreased substantially and the lake became shallower and again ephemeral, with OM characterised by high contributions from microbes ($C_{18:1}$ MUFA, branched FAs, isoGDGTs) and possibly copepods ($C_{22:1}$ MUFA), both of which are resistant to drought. Periodic drying is also indicated by the presence of desiccation fissures in the sedimentary record. Two types of vegetation with variable relative contributions were detected: one with enhanced proportions of long-chain C_{30} and C_{32} *n*-OH and reduced amounts of β-amyrin, and the other with higher amounts of β-amyrin and degraded FA distributions (low CPI). The fluctuations could reflect changes in the climatically controlled supply mechanisms, including episodic runoff through transient and poorly connected fluvial systems or an increased role for aeolian input under these drier conditions.

The last millennium represents a period of relatively higher lipid concentration, better preservation of leaf wax-derived compounds and terrestrial vegetation with lighter isotopic composition (C_3), suggesting enhanced moisture supply. However, terrestrial mineral runoff (Ti) remains low (Roy *et al*., 2016) and it is unclear what the natural forcing mechanism would be for a reversal in the long-term Holocene drying trend. Modern human influence could be the cause of these divergent characteristics.

7.1.2 Climatic forcing

Lipid biomarkers from the Santiaguillo sedimentary record reveal characteristics of a highly productive perennial lake with an extended littoral zone during the last glacial. The isotopic composition of endogenic carbonates suggests decreasing temperatures and evaporation rates enhanced the productivity of the lake, especially during the LGM. However, some records from northwestern Mexico suggest dry conditions (e.g. Lozano-García et al., 2002; Metcalfe et al., 2002;) and agree with a recent paleoclimate simulation that reflects a weak NAM during this period (Bhattacharya *et al*., 2017). Enhanced moisture in the Santiaguillo area has

therefore been attributed to moisture contribution from Pacific tropical cyclones (Roy *et al*., 2015), which agrees with the PMIP3 paleoclimate simulation by Lora (2018). It is unclear if increased cyclone-sourced summer precipitation reached as far east as El Potosi where low Ti concentrations and low concentrations of lipids from apparently degraded OM suggest dry conditions during the final stage of the LGM, comparable to the northwest Mexican records. This contrasting development of the lake basins continues into the deglaciation, when drier conditions affect the Santiaguillo ecosystem while the El Potosi Basin experiences increasingly humid conditions. During the deglacial, decreasing terrestrial runoff in the Santiaguillo Basin correlates to decreasing September insolation. At the same time, northwestern Mexico and the southwestern USA experience relatively enhanced summer precipitation, which is likely fed by a GoC warm pool. Also the ecosystem of the El Potosi Basin experienced a much wetter deglaciation and very low evaporation rates. Roy *et al*. (2016) suggested that, in this case, summer precipitation gradually increased as the GoM became warmer during the deglaciation. Similarly, wetter conditions are observed from Cañon de la Fragua in northeastern Mexico (Betancourt *et al*., 1990) and from Boerne (Texas) in the southeast USA during this period, suggesting that the main moisture supply to the eastern regions was mainly sourced from the GoM until the onset of the YD.

The HTM was characterized by much drier conditions in the North Mexico and the southern USA, most of the paleoclimate records reflect drier conditions for the early- and mid-Holocene. However, some records in northwestern Mexico suggest the return of wetter conditions after a relatively dry YD (e.g. Lozano-García *et al*., 2002; Metcalfe *et al*., 2002; Roy *et al*., 2013), which has been attributed to enhanced summer precipitation from a well-established NAM after 9 cal ka BP (Metcalfe *et al*., 2015). Moreover, Barron *et al*. (2012) suggest the NAM geographical expansion was enlarged, reaching southern locations prior to 8 cal ka BP. In the central western Chihuahua Desert, the geochemical records from the Santiaguillo Basin suggests that the enlarged NAM region included the Santiaguillo Basin prior to 9 cal ka BP, whereas after this period it migrated to northern locations. There is no clear evidence for a Holocene temperature maximum in the El Potosi Basin and the eastern Chihuahua Desert. Rather, the data reveals a relatively dry and stable period from 11 to 4.7 cal ka BP, although the carbon isotopic composition of fatty acids in terrestrial leaf waxes suggest temporarily higher proportions of C_4 vegetation at ~7 cal ka BP. Still, there appears

to be no consistent spatiotemporal trend in the early to mid-Holocene climatic development in the Chihuahua Desert, which is most likely due to the influence of different regional forcing factors such as the dynamics of the NAM and temperature and evaporation over the GoM. By contrast, both records from the Chihuahua Desert show some impacts of the Neoglaciation that correspond to the climatic development of the wider area. Dry conditions are associated with the Neoglaciation for most parts of Mexico and the southern USA, with the first environmental changes documented in central Mexico (~4.8 cal ka BP), followed by northeastern Mexico and the southeastern USA and, finally, northwestern Mexico and the southwestern USA. However, the expansion of C_4 grasses in northern Mexico and the southern USA provides evidence for less severe aridity during the late Holocene than during the HTM, as these grasses largely depend on summer precipitation (Throop *et al*., 2012; Báez *et al*., 2013). This can be attributed to enhanced ENSO activity over the last 4.2 cal ka which has caused more humid winters to some parts of northwestern Mexico as well as increased inflow of humid air masses from tropical Pacific cyclones during autumn.

7.2 Final remarks

The biomarker data from the Santiaguillo Basin provides evidence of changes in seasonality, however, the source of precipitation remains unresolved. The determination of hydrogen isotope composition of terrestrial leaf-wax compounds (i.e., long-chain alkyl lipids) could provide additional insight in future studies. For this, I recommend the acquisition of large sediment samples (i.e. ~30 g of sediment per sample), as sediments from the area are low in TOC, in order to obtain sufficiently high amounts of lipids required for compound-specific isotope analyses.

Additional records at higher resolution with reliable age models are required to probe the hydrological and environmental state of eastern North Mexico, which could have been highly dynamic during the glacial. Furthermore, additional environmental records are needed to determine the western limits of GoM influence and to develop reliable simulations of GoM dynamics affecting the eastern areas during the late Pleistocene and Holocene, which so far are very scarce.

Lipid characterization of modern-day Chihuahua Desert vegetation, i.e. the determination of its geochemical fingerprint, would support the development and calibration of paleoenvironmental proxies in a region, where depositional archives exhibit poor preservation of pollen and other fossil particulate matter.

APPENDIX

Appendix 1: Complete list of the quantified compound classes found in 31 sediment samples collected from the Santiaguillo sedimentary record. The concentrations are expressed as $\%_{lipids}$.

Appendix 2: Complete list of the quantified compound classes found in 31 sediment samples collected from the El Potosi sedimentary record. The concentrations are expressed as $\%_{lipids}$.

Appendix 3: Complete list of the quantified GDGTs found in 31 sediment samples collected from the El Potosi sedimentary record. The concentrations are expressed as $\%_{GDGT}$.

Appendix 1

		FAMEs																				
Depth (cm)	Age cal ka BP	C14	C15	C16	C17	C18	C19	C20	C21	C22	C23	C24	C25	C26	C27	C28	C29	C30	C31	C32	C33	C34
1	0.1	0.38	0.48	14.73	0.40	3.64	0.18	5.12	0.52	3.25	1.53	5.33	0.75	3.83	0.15	2.39	0.00	3.01	0.37	0.86	0.00	0.13
11	1.0	0.00	0.13	13.57	0.13	3.28	0.18	3.21	0.32	0.99	0.24	1.41	0.19	0.00	0.00	0.84	0.59	1.69	0.24	0.46	0.00	0.00
21	1.8	0.11	0.33	13.14	0.22	2.28	0.00	2.35	0.18	0.86	0.46	1.70	0.52	2.24	0.50	2.81	1.66	4.80	0.93	1.29	0.31	0.28
31	2.5	0.00	0.16	9.28	0.72	1.87	0.00	2.36	0.00	1.01	0.36	1.31	0.46	1.91	0.50	2.67	2.03	5.85	1.32	1.58	0.00	0.00
41	3.3	0.00	0.00	10.96	0.59	7.29	0.31	5.89	0.36	1.82	0.34	2.13	0.49	2.36	0.48	2.96	0.00	4.52	0.00	0.88	0.00	0.00
51	4.1	0.00	0.00	4.79	0.00	19.24	0.00	14.26	0.00	3.51	0.00	4.00	0.00	3.33	0.00	7.28	3.23	10.21	2.33	1.95	0.00	0.00
61	4.9	0.13	0.25	11.45	0.36	10.94	0.52	4.00	0.00	1.23	0.35	1.46	0.44	1.19	0.51	2.68	2.58	3.75	1.32	1.15	0.36	0.36
71	5.8	0.13	0.31	12.20	0.59	16.28	0.66	4.82	0.00	1.12	0.34	1.18	0.25	0.92	0.28	1.38	0.00	1.72	0.57	0.00	0.00	0.00
81	6.8	0.27	0.58	17.39	0.86	20.69	0.00	6.84	0.00	1.60	0.00	1.29	0.00	0.88	0.58	1.15	0.00	1.23	0.00	0.00	0.00	0.00
91	7.9	0.00	0.00	2.15	0.43	7.05	0.00	13.14	0.00	2.22	0.00	1.47	0.00	2.76	0.00	3.66	0.00	4.96	0.00	0.00	0.00	0.00
101	9.0	0.00	0.00	2.96	0.09	9.01	0.00	5.34	0.00	2.80	0.00	1.72	0.00	1.98	0.82	3.85	1.30	3.06	0.97	0.92	0.00	0.00
109	10.0	0.00	0.12	10.27	0.15	5.65	0.07	7.68	0.50	1.34	0.49	1.57	0.70	2.38	0.53	1.25	0.28	0.58	0.08	0.18	0.00	0.00
121	11.1	0.00	0.00	10.26	0.00	26.61	0.00	18.27	0.00	3.43	0.00	0.00	0.00	4.43	0.00	3.39	0.00	0.00	0.00	0.00	0.00	0.00
131	12.2	0.00	0.00	1.20	0.00	13.93	0.00	13.03	0.00	2.92	0.00	3.93	2.13	5.44	1.58	5.30	1.18	1.18	0.00	0.00	0.00	0.00
141	13.3	0.00	0.18	5.59	0.32	7.99	0.00	3.38	0.00	1.53	0.84	3.33	2.47	6.47	2.95	6.83	2.05	3.86	1.36	1.08	0.00	1.25
151	14.4	0.00	0.00	0.97	0.00	2.69	0.00	3.46	0.00	1.08	1.20	7.04	4.89	12.39	4.99	9.33	2.21	4.39	1.36	2.37	0.00	0.00
161	15.4	0.00	0.00	0.55	0.00	2.94	0.20	5.39	0.00	2.09	1.38	5.20	2.20	5.54	2.14	5.11	1.23	3.12	1.34	1.67	0.00	0.00
171	16.3	0.00	0.12	4.27	0.00	11.76	0.00	4.11	2.96	1.84	0.71	3.40	1.89	5.15	2.87	6.63	2.31	4.50	1.75	3.26	0.40	0.80
181	16.7	0.00	0.00	9.15	0.53	17.33	0.00	4.60	0.00	3.07	0.00	2.71	0.00	4.68	2.08	4.15	0.74	1.95	0.00	0.00	0.00	0.00
191	17.2	0.00	0.00	2.10	0.50	15.07	0.00	5.93	0.00	2.82	0.99	4.74	1.35	4.76	2.09	5.22	1.51	1.85	1.63	0.87	0.00	0.00
201	17.6	0.19	0.00	21.50	1.41	32.67	0.00	1.23	0.00	1.23	0.00	0.95	0.00	1.01	0.00	0.00	0.00	0.00	0.00	0.00	0.00	0.00
211	18.4	0.44	0.30	27.23	1.60	33.17	0.00	0.54	0.00	0.27	0.00	0.42	0.00	0.06	0.00	0.00	0.00	0.00	0.00	0.00	0.00	0.00
221	19.4	0.24	0.25	18.99	1.41	38.51	0.82	0.50	0.00	0.42	0.00	0.26	0.00	0.41	0.00	0.00	0.00	0.00	0.00	0.00	0.00	0.00
231	20.4	1.92	0.51	30.82	1.56	30.35	0.27	0.30	0.00	0.16	0.00	0.11	0.00	0.21	0.00	0.00	0.00	0.00	0.00	0.00	0.00	0.00
241	21.4	0.00	0.18	18.06	1.17	31.49	0.00	0.90	0.00	1.11	0.00	0.61	0.00	0.72	0.41	0.77	0.00	0.00	0.00	0.00	0.00	0.00
251	22.4	0.28	0.21	19.31	1.24	28.05	0.70	0.93	0.00	0.74	0.00	0.73	0.00	0.68	0.40	0.93	0.00	0.00	0.00	0.00	0.00	0.00
261	23.3	2.53	0.65	25.98	1.72	26.05	0.44	0.49	0.00	0.25	0.14	0.28	0.00	0.39	0.00	0.00	0.00	0.00	0.00	0.00	0.00	0.00
271	24.3	0.34	0.48	20.26	1.04	28.83	0.53	1.14	0.00	1.29	0.00	0.63	0.00	0.86	0.00	0.00	0.00	0.00	0.00	0.00	0.00	0.00
281	25.3	2.46	0.59	21.50	1.12	23.88	0.00	0.89	0.00	0.90	0.00	0.53	0.33	0.72	0.41	0.95	0.36	0.69	0.00	0.00	0.00	0.00
291	26.3	0.37	0.26	15.70	0.74	26.31	0.00	0.89	0.00	1.27	0.51	1.10	0.78	0.00	0.76	1.85	0.00	0.00	0.00	0.00	0.00	0.00
299	27.1	1.00	0.00	24.62	1.01	30.16	0.00	1.01	0.00	0.83	0.00	1.95	0.00	2.12	0.00	2.63	0.00	0.00	0.00	0.00	0.00	0.00

Appendix 1

		OH-FA																				
Depth (cm)	Age cal ka BP	*i*-α-C15	*ai*-α-C15	α-C15	C14	α-C16	C15	α-C17	C16	α-C18	un. α-C18	C17	un. α-C19	α-C19	C18	un. α-C20	α-C20	C19	α-C21	C20	α-C22	C21
1	0.1	0.11	0.06	0.00	0.00	0.73	0.00	0.18	0.26	0.00	0.00	0.00	0.00	0.00	0.15	0.00	0.00	0.00	0.00	0.18	0.00	0.00
11	1.0	0.00	0.00	0.00	0.00	2.53	0.00	0.25	0.41	0.30	0.00	0.00	0.00	0.00	0.35	0.00	0.00	0.00	0.00	0.27	0.00	0.00
21	1.8	0.00	0.00	0.00	0.00	1.40	0.00	0.28	0.40	0.30	0.00	0.00	0.00	0.00	0.46	0.00	0.00	0.00	0.00	0.25	0.00	0.00
31	2.5	0.00	0.00	0.00	0.00	1.42	0.00	0.30	0.25	0.21	0.00	0.00	0.00	0.00	0.20	0.00	0.00	0.00	0.00	0.31	0.17	0.00
41	3.3	0.00	0.00	0.00	0.00	2.37	0.00	0.43	0.27	0.29	0.00	0.00	0.00	0.00	0.21	0.00	0.00	0.00	0.00	0.21	0.00	0.00
51	4.1	0.00	0.00	0.00	0.00	1.37	0.00	0.00	0.00	0.00	0.00	0.00	0.00	0.00	0.00	0.00	0.00	0.00	0.00	0.00	0.00	0.00
61	4.9	0.60	0.00	0.16	0.00	3.83	0.00	0.53	0.51	0.00	0.00	0.00	0.00	0.00	0.49	0.00	0.00	0.00	0.00	0.36	0.00	0.00
71	5.8	0.51	0.17	0.00	0.00	3.95	0.00	0.89	0.60	0.87	0.00	0.00	0.00	0.00	0.66	0.00	0.00	0.00	0.00	0.00	0.00	0.00
81	6.8	0.00	0.00	0.00	0.00	2.43	0.00	0.00	0.00	0.00	0.00	0.00	0.00	0.00	0.00	0.00	0.00	0.00	0.00	0.00	0.00	0.00
91	7.9	0.00	0.00	0.00	0.00	2.31	0.00	0.00	0.00	0.00	0.00	0.00	0.00	0.00	0.44	0.00	0.00	0.00	0.00	0.00	0.00	0.00
101	9.0	0.00	0.00	0.00	0.00	0.80	0.00	0.00	0.00	0.00	0.00	0.00	0.00	0.00	0.00	0.00	0.00	0.00	0.00	0.00	0.00	0.00
109	10.0	0.00	0.00	0.00	0.00	3.87	0.00	1.56	0.41	0.00	0.00	0.00	0.00	0.00	0.55	0.00	0.00	0.00	0.00	0.67	0.00	0.00
121	11.1	0.00	0.00	0.00	0.00	0.00	0.00	0.00	0.00	0.00	0.00	0.00	0.00	0.00	0.00	0.00	0.00	0.00	0.00	0.00	0.00	0.00
131	12.2	0.00	0.00	0.00	0.00	0.98	0.00	0.56	0.00	0.00	0.00	0.00	0.00	0.00	0.00	0.00	0.00	0.00	0.00	0.00	0.00	0.00
141	13.3	0.00	0.00	0.00	0.00	1.25	0.00	0.45	0.00	0.00	0.00	0.00	0.00	0.00	0.00	0.00	0.00	0.00	0.00	0.31	0.00	0.00
151	14.4	0.00	0.00	0.00	0.00	0.00	0.00	0.28	0.00	0.00	0.00	0.00	0.00	0.00	0.00	0.00	0.00	0.00	0.00	0.00	0.00	0.00
161	15.4	0.00	0.00	0.00	0.21	0.21	0.00	0.00	0.00	0.00	0.00	0.00	0.00	0.00	0.59	0.00	0.00	0.00	0.00	0.79	0.00	0.00
171	16.3	0.00	0.00	0.00	0.00	1.13	0.00	0.00	0.00	0.00	0.00	0.00	0.00	0.00	0.00	0.00	0.00	0.00	0.00	0.00	0.00	0.00
181	16.7	0.00	0.00	0.00	0.00	0.00	0.00	0.00	0.00	0.00	0.00	0.00	0.00	0.00	0.00	0.00	0.00	0.00	0.00	0.00	0.00	0.00
191	17.2	0.00	0.00	0.00	0.00	0.78	0.00	0.00	0.00	0.00	0.00	0.00	0.00	0.00	0.00	0.00	0.00	0.00	0.00	0.00	0.00	0.00
201	17.6	0.00	0.00	0.00	0.00	0.00	0.00	0.00	0.00	0.00	0.00	0.00	0.00	0.00	0.00	0.00	0.00	0.00	0.00	0.00	0.00	0.00
211	18.4	0.00	0.00	0.00	0.00	0.17	0.00	0.00	0.00	0.00	0.00	0.00	0.00	0.00	0.00	0.00	0.00	0.00	0.00	0.00	0.00	0.00
221	19.4	0.00	0.00	0.00	0.00	0.00	0.00	0.00	0.00	0.00	0.00	0.00	0.00	0.00	0.00	0.00	0.00	0.00	0.00	0.00	0.00	0.00
231	20.4	0.00	0.00	0.00	0.00	0.00	0.00	0.00	0.00	0.00	0.00	0.00	0.00	0.00	0.00	0.00	0.00	0.00	0.00	0.00	0.00	0.00
241	21.4	0.00	0.00	0.00	0.00	0.00	0.00	0.00	0.00	0.00	0.00	0.00	0.00	0.00	0.00	0.00	0.00	0.00	0.00	0.00	0.00	0.00
251	22.4	0.00	0.00	0.00	0.00	0.00	0.00	0.00	0.00	0.00	0.00	0.00	0.00	0.00	0.00	0.00	0.00	0.00	0.00	0.00	0.00	0.00
261	23.3	0.00	0.00	0.00	0.00	0.00	0.00	0.00	0.12	0.00	0.00	0.00	0.00	0.00	0.00	0.00	0.00	0.00	0.00	0.00	0.00	0.00
271	24.3	0.00	0.00	0.00	0.00	0.00	0.00	0.00	0.00	0.00	0.00	0.00	0.00	0.00	0.00	0.00	0.00	0.00	0.00	0.00	0.00	0.00
281	25.3	0.00	0.00	0.00	0.00	0.47	0.00	0.00	0.00	0.00	0.00	0.00	0.00	0.00	0.00	0.00	0.00	0.00	0.00	0.00	0.00	0.00
291	26.3	0.00	0.00	0.00	0.00	0.00	0.00	0.00	0.00	0.00	0.00	0.00	0.00	0.00	0.00	0.00	0.00	0.00	0.00	0.00	0.00	0.00
299	27.1	0.00	0.00	0.00	0.00	0.00	0.00	0.00	0.00	0.00	0.00	0.00	0.00	0.00	0.00	0.00	0.00	0.00	0.00	0.00	0.00	0.00

Appendix 1

		OH-FA													Branched Fas									
Depth (cm)	Age cal ka BP	α-C23	C22	α-C24	C23	α-C25	C24	α-C26	C25	C26	C27	C28	C29	C30	C14	*i*-C15:0	*a*-C15:0	*i*-C16:0	*a*-C16:0	*i*-C17:0	*a*-C17:0	C18	C19	C20
1	0.1	0.00	0.37	0.00	0.04	0.06	0.85	0.00	0.00	1.73	0.00	0.87	0.00	0.18	0.00	0.47	0.31	0.35	0.00	0.52	0.70	0.00	0.00	0.00
11	1.0	0.44	0.00	2.00	0.00	0.00	0.00	0.00	0.00	0.00	0.00	0.00	0.00	0.00	0.00	0.20	0.18	0.51	0.00	0.00	0.00	0.00	0.00	0.00
21	1.8	0.00	0.36	0.00	0.00	0.00	0.47	0.00	0.00	1.30	0.00	0.00	0.00	0.74	0.07	0.39	0.34	0.62	0.00	0.00	0.00	0.00	0.00	0.00
31	2.5	0.00	0.34	0.00	0.00	0.00	0.50	0.00	0.00	0.99	0.00	1.33	0.00	0.72	0.00	0.18	0.22	0.56	0.00	0.39	0.47	0.00	0.00	0.00
41	3.3	0.00	0.00	0.00	0.00	0.00	0.45	0.00	0.00	0.41	0.00	0.24	0.00	0.00	0.00	0.06	0.09	0.37	0.00	0.00	0.00	0.00	0.00	0.00
51	4.1	0.00	0.00	0.00	0.00	0.00	0.00	0.00	0.00	0.00	0.00	0.00	0.00	0.00	0.00	0.00	0.00	0.29	0.00	0.00	0.25	0.00	0.00	0.00
61	4.9	0.00	0.00	0.57	0.00	0.00	0.00	0.00	0.00	0.58	0.00	0.44	0.00	0.00	0.00	0.24	0.38	0.57	0.00	0.90	0.00	0.00	0.00	0.00
71	5.8	0.00	0.00	0.40	0.00	0.00	0.00	0.00	0.00	0.12	0.00	0.00	0.00	0.00	0.00	0.28	0.47	0.81	0.00	0.58	0.84	0.41	0.00	0.00
81	6.8	0.00	0.00	0.00	0.00	0.00	0.00	0.00	0.00	0.00	0.00	0.00	0.00	0.00	0.00	0.47	0.59	0.88	0.00	1.12	0.76	0.00	0.00	0.00
91	7.9	0.00	0.00	0.00	0.00	0.00	0.00	0.00	0.00	0.00	0.00	0.00	0.00	0.00	0.00	0.00	0.00	0.03	0.00	0.14	0.21	0.00	0.00	0.00
101	9.0	0.00	0.00	0.00	0.00	0.00	0.00	0.00	0.00	0.00	0.00	0.00	0.00	0.00	0.00	0.00	0.00	0.06	0.00	0.10	0.14	0.00	0.00	0.00
109	10.0	0.00	0.00	0.00	0.00	0.00	0.00	0.00	0.00	0.00	0.00	0.00	0.00	0.00	0.00	0.12	0.01	0.45	0.00	0.21	0.25	0.00	0.00	0.00
121	11.1	0.00	0.00	0.00	0.00	0.00	0.00	0.00	0.00	0.00	0.00	0.00	0.00	0.00	0.00	0.00	0.00	0.00	0.00	0.00	0.00	0.00	0.00	0.00
131	12.2	0.00	0.00	0.00	0.00	0.00	0.00	0.00	0.00	0.00	0.00	0.00	0.00	0.00	0.00	0.00	0.00	0.00	0.00	0.00	0.00	0.00	0.00	0.00
141	13.3	0.00	0.00	0.00	0.00	0.00	0.00	0.00	0.00	0.00	0.00	0.00	0.00	0.00	0.00	0.00	0.00	0.00	0.00	0.00	0.00	0.00	0.00	0.00
151	14.4	0.00	0.00	0.00	0.00	0.00	0.00	0.00	0.00	0.00	0.00	0.00	0.00	0.00	0.00	0.00	0.00	0.00	0.00	0.00	0.00	0.00	0.00	0.00
161	15.4	0.00	0.00	0.00	0.00	0.00	0.00	0.00	0.00	0.00	0.00	0.42	0.00	0.00	0.00	0.00	0.00	0.00	0.00	0.00	0.00	0.00	0.00	0.00
171	16.3	0.00	0.00	0.00	0.00	0.00	0.00	0.00	0.00	0.00	0.00	0.27	0.00	0.23	0.00	0.00	0.00	0.00	0.00	0.00	0.00	0.00	0.00	0.00
181	16.7	0.00	0.00	0.00	0.00	0.00	0.00	0.00	0.00	0.00	0.00	0.00	0.00	0.00	0.00	0.00	0.00	0.00	0.00	0.00	0.00	0.00	0.00	0.00
191	17.2	0.00	0.00	0.00	0.00	0.00	0.00	0.00	0.00	0.00	0.00	0.00	0.00	0.00	0.00	0.00	0.00	0.00	0.00	0.00	0.00	0.00	0.00	0.00
201	17.6	0.00	0.00	0.00	0.00	0.00	0.00	0.00	0.00	0.00	0.00	0.00	0.00	0.00	0.00	0.00	0.07	0.16	0.00	0.00	0.55	0.00	0.00	0.00
211	18.4	0.00	0.00	0.00	0.00	0.00	0.00	0.00	0.00	0.00	0.00	0.00	0.00	0.00	0.00	0.00	0.00	0.00	0.00	0.49	0.82	0.00	0.00	0.00
221	19.4	0.00	0.00	0.00	0.00	0.00	0.00	0.00	0.00	0.00	0.00	0.00	0.00	0.00	0.00	0.00	0.00	0.00	0.00	0.65	0.74	0.00	0.00	0.00
231	20.4	0.00	0.00	0.00	0.00	0.00	0.00	0.00	0.00	0.00	0.00	0.00	0.00	0.00	0.00	0.00	0.00	0.00	0.00	0.32	0.84	0.17	0.00	0.00
241	21.4	0.00	0.00	0.00	0.00	0.00	0.00	0.00	0.00	0.00	0.00	0.00	0.00	0.00	0.00	0.00	0.00	0.00	0.00	0.30	0.59	0.00	0.00	0.00
251	22.4	0.00	0.00	0.00	0.00	0.00	0.00	0.00	0.00	0.00	0.00	0.00	0.00	0.00	0.00	0.00	0.11	0.18	0.00	0.38	0.79	0.00	0.00	0.00
261	23.3	0.00	0.00	0.00	0.00	0.00	0.00	0.00	0.00	0.00	0.00	0.00	0.00	0.00	0.00	0.00	0.00	0.46	0.00	0.65	1.10	0.00	0.00	0.00
271	24.3	0.00	0.00	0.00	0.00	0.00	0.00	0.00	0.00	0.00	0.00	0.00	0.00	0.00	0.00	0.00	0.00	0.44	0.00	0.39	0.54	0.00	0.00	0.00
281	25.3	0.00	0.00	0.00	0.00	0.00	0.00	0.00	0.00	0.00	0.00	0.00	0.00	0.00	0.00	0.00	0.00	0.50	0.00	0.86	0.73	0.00	0.00	0.00
291	26.3	0.00	0.00	0.00	0.00	0.00	0.00	0.00	0.00	0.00	0.00	0.00	0.00	0.00	0.00	0.00	0.00	0.13	0.00	0.18	0.35	0.00	0.00	0.00
299	27.1	0.00	0.00	0.00	0.00	0.00	0.00	0.00	0.00	0.00	0.00	0.00	0.00	0.00	0.00	0.00	0.19	0.16	0.00	0.00	0.64	0.00	0.00	0.00

Appendix 1

		Unsaturated Fas																			
Depth (cm)	Age cal ka BP	C14:1 (cis9)	C15:1 (cis-10)	C16:2	C16:1 isomere	C16:1 (cis-9)	C16:1 isomere	C17:1 isomere	C17:1 (cis-10)	C17:1 isomere	C18:3 (cis-6)	C18:3 isomere	C18:2 (cis-9)	C18:3 (cis-9)	C18:1 (cis-	C18:2 (tr-9)	C18:1 (tr-9)	C18:1 isomere	C18:1 isomere	C20:4 (cis-5)	C20:5 (cis-8)	C20:4 isomere
1	0.1	0.00	0.00	0.00	1.71	7.91	0.00	0.52	0.70	0.00	0.07	0.00	5.75	0.28	9.37	0.00	3.73	0.26	0.28	0.10	0.11	0.00
11	1.0	0.00	0.00	0.00	5.86	3.00	0.00	0.34	0.69	0.00	0.00	0.00	1.69	0.00	16.23	0.00	12.05	0.00	0.00	0.00	0.00	0.00
21	1.8	0.00	0.00	0.28	6.64	2.31	0.00	0.61	0.00	0.00	0.00	0.00	1.30	0.00	12.03	0.00	8.49	0.83	0.00	0.00	0.00	0.00
31	2.5	0.00	0.00	0.00	0.25	2.51	4.05	0.31	0.42	0.37	0.00	0.00	0.52	0.00	8.13	0.85	8.80	0.34	0.27	0.00	0.00	0.00
41	3.3	0.00	0.00	0.21	1.70	2.40	0.00	0.00	0.00	0.38	0.00	0.98	0.48	0.00	7.26	0.00	3.19	0.92	0.00	0.00	0.92	0.00
51	4.1	0.00	0.00	0.00	0.00	0.00	0.00	0.00	0.00	0.00	0.00	0.00	0.00	0.00	4.46	0.00	0.00	0.00	0.00	0.00	0.00	0.00
61	4.9	0.00	0.00	0.11	0.44	0.40	1.05	1.65	0.00	0.00	0.00	0.44	0.00	2.28	0.00	0.00	0.90	11.38	1.81	0.00	0.00	0.00
71	5.8	0.00	0.00	0.00	1.01	0.37	1.66	0.70	0.00	0.00	0.53	2.44	1.29	0.00	11.32	2.04	0.02	0.00	0.00	0.00	0.00	0.00
81	6.8	0.00	0.00	0.00	2.23	1.35	2.13	0.00	0.00	0.00	0.00	0.00	0.00	0.00	14.66	1.91	0.00	0.00	0.00	0.00	0.00	0.00
91	7.9	0.00	0.00	0.00	0.00	0.00	0.00	0.00	0.00	0.00	0.00	0.00	0.00	0.00	8.03	0.00	0.78	0.00	0.00	0.00	0.00	0.00
101	9.0	0.00	0.00	0.00	0.00	0.00	0.00	0.00	0.00	0.00	0.00	0.00	0.42	0.00	2.51	0.43	0.00	0.00	0.00	0.00	0.00	0.00
109	10.0	0.00	0.00	0.00	0.62	1.71	0.00	0.00	0.00	0.00	0.00	0.00	1.28	0.00	8.51	1.25	0.00	0.00	0.00	0.00	0.00	0.00
121	11.1	0.00	0.00	0.00	0.00	0.00	0.00	0.00	0.00	0.00	4.14	0.00	0.00	0.00	4.92	0.00	0.00	0.00	0.00	0.00	0.00	0.00
131	12.2	0.00	0.00	0.00	0.00	0.00	0.00	0.00	0.00	0.00	0.00	0.00	0.00	0.00	0.00	0.00	0.00	0.00	0.00	0.00	0.00	0.00
141	13.3	0.00	0.17	0.00	0.33	0.78	0.59	0.00	0.00	0.00	0.00	0.00	0.00	0.00	5.46	0.00	0.72	0.00	0.00	1.21	0.00	0.00
151	14.4	0.00	0.00	0.00	0.00	0.00	0.00	0.00	0.00	0.00	0.00	0.00	0.00	0.00	0.00	0.00	3.96	0.00	0.00	0.00	0.00	0.00
161	15.4	0.00	0.00	0.00	0.00	0.00	0.00	0.00	0.00	0.00	0.00	0.00	0.00	0.00	0.54	0.00	0.00	0.00	0.00	0.00	0.00	0.00
171	16.3	0.00	0.00	0.00	0.00	0.00	0.00	0.00	0.00	0.00	0.00	0.00	0.00	0.00	0.00	0.00	0.00	0.00	0.00	0.00	0.00	0.00
181	16.7	0.00	0.00	0.00	0.00	0.00	0.00	0.00	0.00	0.00	0.00	0.00	0.00	0.00	0.00	0.00	0.00	0.00	0.00	0.00	0.00	0.00
191	17.2	0.00	0.00	0.00	0.00	0.00	0.00	0.00	0.00	0.00	0.00	0.00	0.00	0.00	5.42	1.22	0.00	0.00	0.00	0.00	0.00	0.00
201	17.6	0.00	0.00	0.00	0.00	0.00	0.00	0.00	0.00	0.00	0.00	0.00	0.00	0.00	11.56	0.00	4.50	0.00	0.00	0.00	0.00	0.00
211	18.4	0.00	0.00	0.00	0.00	0.00	0.00	0.00	0.00	0.00	0.00	0.00	0.71	0.00	17.01	0.00	2.13	4.46	0.36	0.00	0.00	0.00
221	19.4	0.00	0.00	0.00	0.41	0.00	0.00	0.00	0.00	0.00	0.00	0.00	0.43	0.00	20.16	0.00	1.95	4.71	0.26	0.00	0.00	0.00
231	20.4	0.00	0.00	0.18	0.55	0.00	0.00	0.00	0.00	0.00	0.00	0.00	0.44	0.00	18.39	0.00	1.54	4.69	0.19	0.00	0.00	0.00
241	21.4	0.00	0.00	0.00	0.00	0.00	0.00	0.00	0.00	0.00	0.00	0.00	0.66	0.00	14.12	0.00	1.87	2.25	1.99	0.00	0.00	0.00
251	22.4	0.00	0.00	0.00	0.00	0.00	0.00	0.00	0.00	0.00	0.00	0.00	0.64	0.00	15.55	0.00	1.95	2.65	1.40	0.00	0.00	0.00
261	23.3	0.00	0.00	0.00	0.20	1.03	0.00	0.00	0.00	0.00	0.00	0.00	0.59	0.00	19.26	0.00	2.06	2.76	1.77	0.00	0.00	0.00
271	24.3	0.00	0.00	0.00	0.47	0.36	0.00	0.00	0.00	0.00	0.00	0.00	1.03	0.00	12.28	0.00	1.37	1.32	1.07	0.00	0.00	0.00
281	25.3	0.00	0.00	0.00	1.27	0.75	0.00	0.00	0.00	0.00	0.00	0.00	0.00	0.00	12.20	0.00	1.80	1.64	1.53	0.00	0.00	0.00
291	26.3	0.00	0.00	0.00	0.85	0.00	0.00	0.00	0.00	0.00	0.00	0.00	0.80	0.00	11.88	0.00	1.57	1.22	1.11	0.00	0.00	0.00
299	27.1	0.00	0.00	0.00	0.00	0.00	0.00	0.00	0.00	0.00	0.00	0.00	0.00	0.00	11.09	0.00	1.50	0.76	0.00	0.00	0.00	0.00

Appendix 1

		Unsaturated Fas											Alcohols									
Depth (cm)	Age cal ka BP	C20:3 (cis-8)	C20:2(cis-11)	C20:3(cis-11)	C20:1 (cis-11)	C20:1 isomere	C22:6 (cis-9)	C22:2 (cis-13)	C22:1 isomere	C22:1 (cis-13)	C24:1 isomere	C24:1 (cis-15)	C12	C13	C14	C15	C16	C17	C18	C19	C20	C21
1	0.1	0.00	0.00	0.00	0.00	0.00	0.00	0.00	0.00	0.00	0.00	0.00	0.00	0.00	0.12	0.17	0.55	0.16	0.37	0.00	0.32	0.00
11	1.0	0.00	0.00	0.00	0.00	0.00	0.37	0.00	0.00	0.00	0.00	0.00	0.00	0.00	0.00	0.00	0.19	0.00	1.10	0.00	0.25	0.00
21	1.8	0.00	0.00	0.00	0.56	0.00	0.78	0.00	3.10	0.22	0.34	0.00	0.00	0.00	0.06	0.10	0.44	0.27	1.10	0.00	0.46	0.00
31	2.5	0.00	0.00	0.00	0.86	0.00	0.00	0.00	3.63	0.00	0.34	0.00	0.00	0.00	0.00	0.00	0.40	0.00	0.84	0.00	0.40	0.00
41	3.3	0.00	0.00	0.00	0.97	0.00	0.00	0.00	7.16	0.28	0.00	0.00	0.00	0.00	0.00	0.00	0.71	0.00	0.64	0.00	0.51	0.00
51	4.1	0.00	0.00	0.00	0.00	0.00	0.00	0.00	6.97	0.00	0.00	0.00	0.00	0.00	0.00	0.00	0.00	0.00	1.15	0.00	0.00	0.00
61	4.9	0.00	0.00	0.00	0.00	0.00	0.00	0.00	0.00	6.25	0.00	0.00	0.00	0.00	0.13	0.20	1.18	0.36	1.52	0.00	0.66	0.00
71	5.8	0.00	0.00	0.00	0.00	0.00	0.00	0.00	0.00	6.47	0.65	0.00	0.00	0.00	0.12	0.09	1.06	0.58	1.95	0.00	1.23	0.00
81	6.8	0.00	0.00	0.00	0.00	3.58	0.00	0.00	0.00	7.88	0.00	0.00	0.00	0.00	0.00	0.00	0.95	0.00	1.38	0.00	0.38	0.00
91	7.9	0.00	0.84	0.00	0.00	0.00	0.00	0.00	22.79	0.00	0.00	0.00	0.00	0.00	0.00	0.00	0.72	0.00	0.95	0.00	1.18	0.00
101	9.0	0.00	0.00	0.00	0.00	0.00	0.00	0.00	42.04	1.18	0.00	0.00	0.00	0.00	0.00	0.00	0.81	0.00	1.55	0.00	0.71	0.00
109	10.0	0.00	0.00	0.00	1.64	0.00	0.00	0.00	14.65	0.86	0.00	0.00	0.00	0.00	0.00	0.00	1.95	0.00	4.42	0.00	1.35	0.45
121	11.1	0.00	0.00	0.00	0.00	0.00	0.00	0.00	8.10	0.00	0.00	0.00	0.00	0.00	0.00	0.00	0.00	0.00	2.68	0.00	0.00	0.00
131	12.2	0.00	0.00	0.00	0.00	0.00	0.00	0.00	5.74	0.00	0.00	0.00	0.00	0.00	0.00	0.00	0.00	0.00	0.91	0.00	1.11	0.00
141	13.3	0.00	0.00	0.00	1.73	0.00	0.00	0.00	19.04	1.30	0.00	0.00	0.00	0.00	0.00	0.00	0.00	0.00	0.53	0.00	0.21	0.00
151	14.4	0.00	0.00	0.00	1.91	0.00	0.00	0.00	6.14	0.00	0.00	0.00	0.00	0.00	0.00	0.00	0.00	0.43	1.05	0.00	0.39	0.00
161	15.4	0.00	0.00	0.00	0.00	0.00	0.00	0.00	3.07	0.00	0.00	0.00	0.00	0.00	0.00	0.00	0.43	0.00	0.92	0.00	1.40	0.00
171	16.3	0.00	0.00	0.00	0.00	0.00	0.00	1.13	2.35	0.00	0.00	0.00	0.00	0.00	0.27	0.16	1.54	0.00	0.99	0.00	0.93	0.24
181	16.7	0.00	0.00	0.00	0.00	0.00	0.00	0.00	0.00	0.00	0.00	0.00	0.00	0.00	0.00	0.00	0.76	0.00	1.26	0.00	0.00	0.00
191	17.2	0.00	0.00	0.00	1.99	0.00	0.00	0.00	22.31	2.86	0.00	0.00	0.00	0.00	0.00	0.00	0.86	0.00	3.17	0.00	1.72	0.26
201	17.6	0.00	0.00	0.00	0.00	0.00	0.00	0.00	16.42	1.80	0.00	0.00	0.00	0.00	0.27	0.00	1.49	0.00	1.09	0.00	0.15	0.00
211	18.4	0.00	0.00	0.00	0.00	0.00	0.00	0.00	4.36	0.18	0.00	0.00	0.00	0.00	0.15	0.06	0.51	0.07	0.42	0.00	0.09	0.00
221	19.4	0.00	0.00	0.00	0.00	0.00	0.00	0.00	5.20	0.28	0.00	0.00	0.00	0.00	0.00	0.00	0.38	0.00	0.46	0.00	0.10	0.00
231	20.4	0.00	0.00	0.00	0.00	0.00	0.00	0.00	2.30	0.00	0.00	0.00	0.00	0.00	0.18	0.10	0.34	0.00	0.25	0.00	0.05	0.00
241	21.4	0.00	0.00	0.00	0.00	0.00	0.00	0.00	17.53	0.72	0.00	0.00	0.00	0.00	0.00	0.00	0.42	0.00	0.54	0.00	0.25	0.00
251	22.4	0.00	0.00	0.00	0.00	0.00	0.00	0.00	13.86	0.75	0.00	0.00	0.00	0.00	0.17	0.00	0.88	0.21	0.80	0.00	0.00	0.00
261	23.3	0.00	0.00	0.00	0.00	0.00	0.00	0.00	2.65	0.00	0.00	0.00	0.14	0.00	0.33	0.12	0.50	0.00	0.46	0.00	0.07	0.00
271	24.3	0.00	0.00	0.00	0.00	0.00	0.00	0.00	14.36	1.22	0.00	0.00	0.00	0.00	0.27	0.00	1.11	0.00	0.84	0.00	0.00	0.00
281	25.3	0.00	0.00	0.00	0.00	0.00	0.00	0.00	9.56	0.55	0.00	0.00	0.33	0.00	0.85	0.32	1.38	0.27	0.99	0.00	0.26	0.00
291	26.3	0.00	0.00	0.00	0.00	0.00	0.00	0.00	21.31	1.49	0.00	0.00	0.00	0.00	0.37	0.17	1.07	0.00	0.85	0.00	0.32	0.00
299	27.1	0.00	0.00	0.00	0.00	0.00	0.00	0.00	7.72	0.00	0.00	0.00	0.00	0.00	1.53	0.00	3.07	0.00	1.66	0.00	0.00	0.00

Appendix 1

		Alcohols															n-Alkanes					
Depth (cm)	Age cal ka BP	C22	C23	C24	C25	C26	C27	C28	C29	C30	C31	C32	C33	C34	C35	C36	C16	C17	C18	C19	C20	C21
1	0.1	0.61	0.00	0.31	0.00	0.13	0.00	0.22	0.00	0.26	0.00	0.55	0.00	0.12	0.00	0.00	0.00	0.00	0.00	0.00	0.00	0.00
11	1.0	0.59	0.00	0.29	0.00	0.32	0.00	0.51	0.00	0.69	0.00	0.00	0.00	0.00	0.00	0.00	0.00	0.00	0.00	0.00	0.00	0.00
21	1.8	0.58	0.00	0.43	0.15	0.30	0.35	0.83	0.58	1.24	0.35	0.00	0.00	0.26	0.00	0.00	0.00	0.00	0.00	0.00	0.00	0.00
31	2.5	0.43	0.00	0.48	0.17	0.57	0.70	1.50	0.98	2.32	0.45	0.00	0.00	0.00	0.00	0.00	0.13	0.05	0.09	0.00	0.44	0.16
41	3.3	0.56	0.00	0.48	0.00	0.69	0.26	0.80	0.29	0.71	0.00	0.72	0.00	0.00	0.00	0.00	0.00	0.00	0.00	0.00	0.00	0.40
51	4.1	0.00	0.00	0.00	0.00	0.00	0.00	1.42	0.00	0.00	0.00	0.00	0.00	0.00	0.00	0.00	0.00	0.00	0.00	0.00	0.00	0.00
61	4.9	0.41	0.15	0.55	0.00	0.67	0.33	1.20	0.53	1.36	0.00	1.64	0.00	0.00	0.00	0.00	0.00	0.00	0.06	0.22	0.30	0.26
71	5.8	0.66	0.00	0.34	0.00	0.37	0.24	0.72	0.00	0.48	0.00	0.80	0.00	0.00	0.00	0.00	0.00	0.00	0.00	0.10	0.22	0.36
81	6.8	0.22	0.00	0.22	0.00	0.08	0.00	0.22	0.00	0.17	0.00	0.16	0.00	0.00	0.00	0.00	0.00	0.00	0.00	0.35	0.43	0.64
91	7.9	0.97	0.00	1.02	0.00	1.03	0.00	1.87	0.00	2.07	0.00	2.43	0.00	0.00	0.00	0.00	0.00	0.00	0.00	0.00	0.33	0.00
101	9.0	0.60	0.00	0.92	0.00	0.95	0.00	0.92	0.00	0.72	0.00	1.00	0.00	0.00	0.00	0.00	0.00	0.00	0.00	0.00	0.00	0.21
109	10.0	2.40	0.62	1.89	0.35	1.21	0.00	1.05	0.00	0.47	0.00	0.00	0.00	0.00	0.00	0.00	0.00	0.00	0.00	0.00	0.00	0.69
121	11.1	0.48	0.00	0.66	0.00	0.00	0.00	0.00	0.00	0.00	0.00	0.00	0.00	0.00	0.00	0.00	0.00	0.00	0.00	0.00	0.00	0.70
131	12.2	1.29	0.00	0.00	0.00	0.00	0.00	0.00	0.00	0.00	0.00	0.00	0.00	0.00	0.00	0.00	0.00	0.00	0.00	0.00	1.50	0.00
141	13.3	0.31	0.00	0.15	0.00	0.04	0.00	0.00	0.00	0.00	0.00	0.00	0.00	0.00	0.00	0.00	0.00	0.00	0.00	0.00	0.30	0.00
151	14.4	0.25	0.11	0.29	0.42	0.39	0.59	1.12	0.64	1.11	0.00	0.00	0.00	0.00	0.00	0.00	0.00	0.00	0.00	0.00	0.00	0.97
161	15.4	2.92	1.35	3.01	0.72	3.24	0.76	5.30	0.51	2.69	0.27	4.54	0.00	0.00	0.00	0.00	0.00	0.00	0.00	0.00	0.00	0.56
171	16.3	0.71	0.00	1.05	0.00	0.88	0.27	2.22	0.00	0.77	0.00	2.41	0.00	0.22	0.00	0.00	0.00	0.00	0.00	0.00	0.49	0.00
181	16.7	0.89	0.00	0.38	0.00	0.15	0.00	0.21	0.00	0.00	0.00	0.00	0.00	0.00	0.00	0.00	0.00	0.00	0.00	0.72	0.49	1.01
191	17.2	1.47	0.19	0.68	0.10	0.29	0.00	0.00	0.00	0.00	0.00	0.00	0.00	0.00	0.00	0.00	0.00	0.00	0.00	0.00	0.00	0.55
201	17.6	0.32	0.00	0.18	0.00	0.24	0.00	0.00	0.00	0.00	0.00	0.00	0.00	0.00	0.00	0.00	0.00	0.00	0.00	0.00	0.00	1.01
211	18.4	0.17	0.00	0.08	0.00	0.16	0.00	0.12	0.00	0.00	0.00	0.00	0.00	0.00	0.00	0.00	0.00	0.11	0.46	0.63	0.64	0.56
221	19.4	0.10	0.00	0.07	0.00	0.16	0.00	0.09	0.00	0.08	0.00	0.00	0.00	0.00	0.00	0.00	0.00	0.00	0.00	0.64	0.75	0.00
231	20.4	0.05	0.00	0.06	0.00	0.08	0.00	0.05	0.00	0.00	0.00	0.00	0.00	0.00	0.00	0.00	0.00	0.37	0.68	0.82	0.51	0.35
241	21.4	0.09	0.00	0.10	0.00	0.14	0.00	0.07	0.00	0.00	0.00	0.00	0.00	0.00	0.00	0.00	0.00	0.00	0.00	0.42	0.52	0.43
251	22.4	0.00	0.00	0.25	0.00	0.38	0.00	0.93	0.00	0.00	0.00	0.36	0.00	0.00	0.00	0.00	0.00	0.00	0.33	0.54	0.64	0.00
261	23.3	0.15	0.00	0.15	0.00	0.28	0.00	0.25	0.00	0.00	0.00	0.00	0.00	0.00	0.00	0.00	0.00	0.53	0.94	0.92	0.75	0.54
271	24.3	0.00	0.00	0.00	0.00	0.81	0.00	0.77	0.00	0.00	0.00	0.00	0.00	0.00	0.00	0.00	0.00	0.00	0.00	0.81	0.78	0.52
281	25.3	0.36	0.00	0.39	0.00	0.43	0.00	0.46	0.00	0.31	0.00	0.51	0.00	0.00	0.00	0.00	0.00	0.00	0.62	0.67	0.52	0.40
291	26.3	0.46	0.00	0.33	0.00	0.41	0.00	0.78	0.00	0.00	0.00	0.29	0.00	0.00	0.00	0.00	0.00	0.00	0.00	0.47	0.00	0.55
299	27.1	0.00	0.00	0.00	0.00	0.00	0.00	1.10	0.00	0.00	0.00	0.00	0.00	0.00	0.00	0.00	0.00	0.00	0.00	0.63	1.02	0.40

Appendix 1

		n-Alkanes														Methyl Ketones						
Depth (cm)	Age cal ka BP	C22	C23	C24	C25	C26	C27	C28	C29	C30	C31	C32	C33	C34	C35	C19	C20	C21	C22	C23	C24	C25
1	0.1	0.00	0.00	0.00	0.00	0.00	0.09	0.00	0.10	0.00	0.19	0.00	0.00	0.00	0.00	0.00	0.00	0.00	0.00	0.00	0.00	0.00
11	1.0	0.00	0.00	0.00	0.27	0.00	0.44	0.00	0.00	0.00	0.00	0.00	0.00	0.00	0.00	0.00	0.00	0.00	0.00	0.00	0.00	0.00
21	1.8	0.00	0.00	0.00	0.00	0.00	0.60	0.00	0.52	0.00	0.53	0.00	0.00	0.00	0.00	0.00	0.00	0.00	0.00	0.00	0.00	0.00
31	2.5	0.00	0.00	0.00	0.45	0.00	0.69	0.00	0.79	0.00	0.78	0.00	0.00	0.00	0.00	0.00	0.00	0.00	0.00	0.00	0.00	0.00
41	3.3	0.00	0.00	0.50	0.00	0.45	0.35	0.00	0.70	0.00	1.28	0.00	1.09	0.00	0.00	0.00	0.00	0.00	0.00	0.00	0.00	0.00
51	4.1	0.00	0.00	0.00	0.00	0.00	0.37	0.00	0.35	0.00	2.54	0.00	0.89	0.00	0.00	0.00	0.00	0.00	0.00	0.00	0.00	0.00
61	4.9	0.00	0.00	0.00	0.00	0.00	0.40	0.00	0.60	0.00	0.00	0.00	0.00	0.00	0.00	0.00	0.00	0.00	0.00	0.00	0.00	0.05
71	5.8	0.90	0.28	0.00	0.00	0.00	0.30	0.00	0.00	0.13	0.71	0.00	0.47	0.00	0.00	0.00	0.00	0.00	0.00	0.00	0.00	0.04
81	6.8	0.00	0.00	0.00	0.00	0.00	0.00	0.00	0.00	0.00	0.00	0.00	0.00	0.00	0.00	0.00	0.00	0.00	0.00	0.00	0.00	0.00
91	7.9	0.46	0.00	0.00	0.00	0.00	0.00	0.00	0.00	0.00	0.00	0.00	0.00	0.00	0.00	0.00	0.00	0.00	0.00	0.00	0.00	0.00
101	9.0	0.00	0.41	0.00	0.00	0.00	0.00	0.00	0.82	0.00	1.05	0.00	0.00	0.00	0.00	0.00	0.00	0.00	0.00	0.00	0.00	0.04
109	10.0	0.00	0.70	0.00	0.00	0.00	0.45	0.00	0.48	0.00	0.00	0.00	0.00	0.00	0.00	0.00	0.00	0.00	0.00	0.00	0.00	0.00
121	11.1	0.00	0.00	0.00	0.00	0.00	0.00	0.00	0.00	0.00	0.00	0.00	0.00	0.00	0.00	0.00	0.00	0.00	0.00	0.00	0.00	0.00
131	12.2	0.00	0.00	0.00	0.00	0.00	0.00	0.00	1.10	0.00	1.39	0.00	0.00	0.00	0.00	0.00	0.00	0.00	0.00	4.74	0.00	0.66
141	13.3	0.00	0.74	0.00	0.00	0.35	0.38	0.00	0.00	0.00	1.41	0.00	0.00	0.00	0.00	0.00	0.00	0.00	0.00	0.00	0.44	0.85
151	14.4	0.00	1.79	0.00	1.34	0.78	0.92	0.79	1.33	0.74	1.78	0.00	1.29	0.00	0.00	0.00	0.00	0.00	0.00	1.35	1.19	2.89
161	15.4	0.00	1.26	0.00	0.00	0.00	1.03	0.00	1.72	0.00	3.04	0.00	1.69	0.00	0.00	0.00	0.00	0.00	0.38	1.12	1.02	1.95
171	16.3	0.00	0.73	0.39	0.00	0.00	0.00	0.87	1.99	0.88	3.01	0.42	2.44	0.97	0.00	0.00	0.00	0.00	0.00	0.00	0.00	0.00
181	16.7	0.00	1.47	0.00	0.00	0.00	0.00	0.00	0.00	0.00	0.00	0.00	0.00	0.00	0.00	0.00	0.00	0.00	0.00	0.00	0.00	0.00
191	17.2	0.00	1.19	0.00	0.00	0.00	0.00	0.00	0.00	0.00	0.00	0.00	0.00	0.00	0.00	0.00	0.00	0.00	0.00	0.51	0.29	0.93
201	17.6	0.00	0.00	0.00	0.00	0.00	0.00	0.00	0.00	0.00	0.00	0.00	0.00	0.00	0.00	0.00	0.00	0.00	0.00	0.00	0.00	0.00
211	18.4	0.00	0.21	0.00	0.00	0.00	0.44	0.00	0.38	0.00	0.00	0.00	0.00	0.00	0.00	0.00	0.00	0.00	0.00	0.00	0.00	0.03
221	19.4	0.00	0.20	0.00	0.00	0.00	0.25	0.00	0.00	0.00	0.00	0.00	0.00	0.00	0.00	0.00	0.00	0.00	0.00	0.09	0.00	0.02
231	20.4	0.21	0.00	0.00	0.00	0.00	0.08	0.00	0.00	0.00	0.00	0.00	0.00	0.00	0.00	0.00	0.00	0.00	0.00	0.00	0.00	0.00
241	21.4	0.00	0.00	0.00	0.00	0.00	0.00	0.00	0.34	0.29	0.64	0.00	0.00	0.00	0.00	0.00	0.00	0.00	0.00	0.24	0.00	0.05
251	22.4	0.00	0.35	0.00	0.00	0.00	0.00	0.00	0.56	0.45	0.56	0.00	0.00	0.00	0.00	0.00	0.00	0.00	0.00	0.00	0.00	0.06
261	23.3	0.28	0.16	0.19	0.00	0.21	0.27	0.21	0.00	0.00	0.36	0.00	0.38	0.00	0.00	0.00	0.00	0.00	0.00	0.07	0.07	0.05
271	24.3	0.86	0.00	0.00	0.00	0.00	1.71	0.00	1.28	0.00	0.00	0.00	0.00	0.00	0.00	0.00	0.00	0.00	0.00	0.00	0.00	0.00
281	25.3	0.00	0.54	0.00	0.00	0.00	0.55	0.00	0.60	0.58	0.89	0.00	0.62	0.00	0.00	0.00	0.00	0.00	0.00	0.00	0.00	0.00
291	26.3	0.00	0.63	0.00	0.00	0.00	0.64	0.00	0.00	0.54	0.71	0.00	0.00	0.00	0.00	0.00	0.00	0.00	0.00	0.00	0.00	0.00
299	27.1	0.00	0.64	0.00	0.00	0.00	0.00	0.00	0.84	0.00	1.73	0.00	0.00	0.00	0.00	0.00	0.00	0.00	0.00	0.00	0.00	0.00

Appendix 1

		Methyl Ketones								Sterols												
Depth (cm)	Age cal ka BP	C26	C27	C28	C29	C30	C31	C32	C33	C26Δ 5,22	C26Δ 22	Copro stanol	Epich olesta nol	Epico pro-stanol	C27Δ 5,22	C27Δ 22	Chole sterol	Chole stanol	C28Δ 5	C28Δ 0	Brass icast erol	C28Δ 22
1	0.1	0.00	0.00	0.00	0.00	0.00	0.00	0.00	0.00	0.00	0.00	0.00	0.00	0.00	0.00	0.00	0.00	0.00	2.69	0.00	0.00	0.00
11	1.0	0.00	0.00	0.00	0.00	0.00	0.00	0.00	0.00	0.00	0.00	0.00	0.00	0.00	0.00	0.00	0.99	0.00	3.68	0.00	0.00	0.00
21	1.8	0.00	0.00	0.00	0.00	0.00	0.00	0.00	0.00	0.00	0.00	0.00	0.00	0.00	0.00	0.00	0.00	0.00	2.17	0.00	0.00	0.00
31	2.5	0.00	0.00	0.00	0.00	0.00	0.00	0.00	0.00	0.00	0.00	0.00	0.00	0.00	0.00	0.00	0.69	0.00	2.90	0.00	0.00	0.00
41	3.3	0.00	0.00	0.00	0.00	0.00	0.00	0.00	0.00	0.00	0.00	0.00	0.00	0.00	0.00	0.00	0.00	0.00	3.51	0.00	0.00	0.00
51	4.1	0.00	0.00	0.00	0.00	0.00	0.00	0.00	0.00	0.00	0.00	0.00	0.00	0.00	0.00	0.00	0.00	0.00	0.00	0.00	0.00	0.00
61	4.9	0.00	0.00	0.00	0.00	0.00	0.00	0.00	0.00	0.00	0.00	0.00	0.00	0.00	0.00	0.00	0.00	0.00	0.00	0.00	0.00	0.00
71	5.8	0.00	0.07	0.00	0.00	0.00	0.00	0.00	0.00	0.00	0.00	0.00	0.00	0.00	0.00	0.00	0.00	0.00	1.62	0.00	0.00	0.00
81	6.8	0.00	0.00	0.00	0.00	0.00	0.00	0.00	0.00	0.00	0.00	0.00	0.00	0.00	0.00	0.00	0.00	0.00	0.00	0.00	0.00	0.00
91	7.9	0.00	0.00	0.00	0.00	0.00	0.00	0.00	0.00	0.00	0.00	0.00	0.00	0.00	0.00	0.00	0.00	0.00	0.00	0.00	0.00	0.00
101	9.0	0.00	0.00	0.00	0.00	0.00	0.00	0.00	0.00	0.00	0.00	0.00	0.00	0.00	0.00	0.00	0.00	0.00	0.00	0.00	0.00	0.00
109	10.0	0.00	0.00	0.00	0.00	0.00	0.00	0.00	0.00	0.00	0.00	0.00	0.00	0.00	0.00	0.00	1.58	0.00	1.04	0.00	0.00	0.00
121	11.1	0.00	0.00	0.00	0.00	0.00	0.00	0.00	0.00	0.00	0.00	0.00	0.00	0.00	0.00	0.00	0.00	0.00	0.00	0.00	0.00	0.00
131	12.2	0.00	0.00	0.00	0.00	0.00	0.00	0.00	0.00	0.00	0.00	0.00	0.00	0.00	0.00	0.00	0.00	0.00	0.00	0.00	0.00	0.00
141	13.3	0.00	0.54	0.00	1.53	0.00	0.00	0.00	0.00	0.00	0.00	0.00	0.00	0.00	0.00	0.00	0.00	0.00	0.00	0.00	0.00	0.00
151	14.4	0.80	1.71	0.60	0.71	0.37	0.00	0.00	0.00	0.00	0.00	0.00	0.00	0.00	0.00	0.00	0.00	0.00	0.00	0.00	0.00	0.00
161	15.4	0.00	1.48	0.52	0.00	0.00	0.00	0.00	0.00	0.00	0.00	0.00	0.00	0.00	0.00	0.00	0.00	0.00	0.00	0.00	0.00	0.00
171	16.3	0.00	0.00	0.00	0.00	0.00	0.00	0.00	0.00	0.00	0.00	0.00	0.00	0.00	0.00	0.00	0.00	0.00	0.00	0.00	0.00	0.00
181	16.7	0.00	0.00	0.00	0.00	0.00	0.00	0.00	0.00	0.00	0.00	0.00	0.00	0.00	0.00	0.00	0.00	0.00	0.00	0.00	0.00	0.00
191	17.2	0.00	0.45	0.00	0.00	0.00	0.00	0.00	0.00	0.00	0.00	0.00	0.00	0.00	0.00	0.00	0.00	0.00	0.00	0.00	0.00	0.00
201	17.6	0.00	0.00	0.00	0.00	0.00	0.00	0.00	0.00	0.00	0.00	0.00	0.00	0.00	0.00	0.00	0.00	0.00	0.00	0.00	0.00	0.00
211	18.4	0.00	0.00	0.00	0.00	0.00	0.00	0.00	0.00	0.00	0.00	0.00	0.00	0.00	0.00	0.00	0.00	0.00	0.00	0.00	0.00	0.00
221	19.4	0.00	0.00	0.00	0.00	0.00	0.00	0.00	0.00	0.00	0.00	0.00	0.00	0.00	0.00	0.00	0.00	0.00	0.00	0.00	0.00	0.00
231	20.4	0.00	0.00	0.00	0.00	0.00	0.00	0.00	0.00	0.00	0.00	0.00	0.00	0.00	0.00	0.00	0.00	0.00	0.00	0.00	0.00	0.00
241	21.4	0.00	0.00	0.00	0.00	0.00	0.00	0.00	0.00	0.00	0.00	0.00	0.00	0.00	0.00	0.00	0.00	0.00	0.00	0.00	0.00	0.00
251	22.4	0.00	0.07	0.00	0.00	0.00	0.00	0.00	0.00	0.00	0.00	0.00	0.00	0.00	0.00	0.00	0.00	0.00	0.00	0.00	0.00	0.00
261	23.3	0.00	0.00	0.00	0.00	0.00	0.00	0.00	0.00	0.00	0.00	0.00	0.00	0.00	0.00	0.00	0.00	0.00	0.00	0.00	0.00	0.00
271	24.3	0.00	0.00	0.00	0.00	0.00	0.00	0.00	0.00	0.00	0.00	0.00	0.00	0.00	0.00	0.00	0.00	0.00	0.00	0.00	0.00	0.00
281	25.3	0.00	0.00	0.00	0.00	0.00	0.00	0.00	0.00	0.00	0.00	0.00	0.00	0.00	0.00	0.00	0.00	0.00	0.00	0.00	0.00	0.00
291	26.3	0.00	0.00	0.00	0.00	0.00	0.00	0.00	0.00	0.00	0.00	0.00	0.00	0.00	0.00	0.00	0.00	0.00	0.00	0.00	0.00	0.00
299	27.1	0.00	0.00	0.00	0.00	0.00	0.00	0.00	0.00	0.00	0.00	0.00	0.00	0.00	0.00	0.00	0.00	0.00	0.00	0.00	0.00	0.00

Appendix 1

		Sterols													Others							
Depth (cm)	Age cal ka BP	C28Δ 5,X	C29Δ 5,22	Stigmasterol	C29Δ 22	C29Δ 22 isom.	Sitosterol, C29Δ	C29Δ 5 isom.	Stigmastanol	Dinosterol	Dinosterol isom.	Dinostanol	Dinostanol isom.	C30Δ ...?	branched C15	branched C15	branched C16	phytodiene	branched C19	branched C17	branched C17	branched C18
1	0.1	0.00	0.00	1.53	0.00	0.00	3.34	0.00	0.00	0.00	0.00	0.00	0.00	0.00	0.00	0.00	0.00	0.00	0.00	0.11	0.09	0.00
11	1.0	0.00	0.00	1.48	0.00	0.00	5.07	0.00	0.00	0.00	0.00	0.00	0.00	0.00	0.00	0.00	0.00	0.00	0.00	0.00	0.00	0.00
21	1.8	0.00	0.00	0.79	0.00	0.00	3.87	0.00	0.00	0.00	0.00	0.00	0.00	0.00	0.00	0.00	0.00	0.00	0.00	0.00	0.00	0.00
31	2.5	0.00	0.00	1.21	0.00	0.00	4.70	0.00	0.85	0.00	0.00	0.00	0.00	0.00	0.00	0.00	0.00	0.00	0.00	0.00	0.00	0.00
41	3.3	0.00	0.00	0.67	0.00	0.00	4.60	0.00	1.61	0.00	0.00	0.00	0.00	0.00	0.00	0.00	0.00	0.00	0.00	0.00	0.00	0.00
51	4.1	0.00	0.00	0.00	0.00	0.00	0.00	0.00	0.00	0.00	0.00	0.00	0.00	0.00	0.00	0.00	0.00	0.00	0.00	0.00	0.00	0.00
61	4.9	0.00	0.00	0.00	0.00	0.00	2.65	0.00	0.00	0.00	0.00	0.00	0.00	0.00	0.00	0.00	0.00	0.00	0.00	0.00	0.00	0.00
71	5.8	0.00	0.00	0.00	0.00	0.00	0.00	0.00	0.00	0.00	0.00	0.00	0.00	0.00	0.00	0.00	0.00	0.00	0.00	0.00	0.00	0.00
81	6.8	0.00	0.00	0.00	0.00	0.00	0.00	0.00	0.00	0.00	0.00	0.00	0.00	0.00	0.00	0.00	0.00	0.00	0.00	0.00	0.00	0.00
91	7.9	0.00	0.00	0.00	0.00	0.00	0.00	0.00	0.00	0.00	0.00	0.00	0.00	0.00	0.00	0.00	0.00	0.00	0.00	0.00	0.00	0.00
101	9.0	0.00	0.00	0.00	0.00	0.00	0.00	0.00	0.00	0.00	0.00	0.00	0.00	0.00	0.00	0.00	0.00	0.00	0.00	0.00	0.00	0.00
109	10.0	0.00	0.00	0.00	0.00	0.00	1.62	0.00	0.00	0.00	0.00	0.00	0.00	0.00	0.00	0.00	1.46	0.00	0.00	0.00	0.00	0.00
121	11.1	0.00	0.00	0.00	0.00	0.00	0.00	0.00	0.00	0.00	0.00	0.00	0.00	0.00	0.00	0.00	0.00	0.00	0.00	0.00	0.00	0.00
131	12.2	0.00	0.00	0.00	0.00	0.00	0.00	0.00	0.00	0.00	0.00	0.00	0.00	0.00	0.00	0.00	0.00	0.00	0.00	0.00	0.00	0.00
141	13.3	0.00	0.00	0.00	0.00	0.00	0.00	0.00	0.00	0.00	0.00	0.00	0.00	0.00	0.00	0.00	0.00	0.00	0.00	0.00	0.00	0.00
151	14.4	0.00	0.00	0.00	0.00	0.00	0.00	0.00	0.00	0.00	0.00	0.00	0.00	0.00	0.00	0.00	0.00	0.00	0.00	0.00	0.00	0.00
161	15.4	0.00	0.00	0.00	0.00	0.00	0.00	0.00	0.00	0.00	0.00	0.00	0.00	0.00	0.00	0.00	0.00	0.00	0.00	0.00	0.00	0.00
171	16.3	0.00	0.00	0.00	0.00	0.00	0.00	0.00	0.00	0.00	0.00	0.00	0.00	0.00	0.00	0.00	0.00	0.00	0.00	0.00	0.00	0.00
181	16.7	0.00	0.00	0.00	0.00	0.00	0.00	0.00	0.00	0.00	0.00	0.00	0.00	0.00	0.00	0.00	0.00	0.00	0.00	0.00	0.00	0.00
191	17.2	0.00	0.00	0.00	0.00	0.00	1.34	0.00	0.00	0.00	0.00	0.00	0.00	0.00	0.00	0.00	0.00	0.00	0.00	0.00	0.00	0.00
201	17.6	0.00	0.00	0.00	0.00	0.00	0.00	0.00	0.00	0.00	0.00	0.00	0.00	0.00	0.00	0.00	0.00	0.00	0.00	0.00	0.00	0.00
211	18.4	0.00	0.00	0.00	0.00	0.00	0.00	0.00	0.00	0.00	0.00	0.00	0.00	0.00	0.00	0.00	0.00	0.00	0.00	0.00	0.00	0.00
221	19.4	0.00	0.00	0.00	0.00	0.00	0.00	0.00	0.00	0.00	0.00	0.00	0.00	0.00	0.00	0.00	0.00	0.00	0.00	0.00	0.00	0.00
231	20.4	0.00	0.00	0.00	0.00	0.00	0.00	0.00	0.00	0.00	0.00	0.00	0.00	0.00	0.00	0.00	0.00	0.00	0.00	0.00	0.00	0.00
241	21.4	0.00	0.00	0.00	0.00	0.00	0.00	0.00	0.00	0.00	0.00	0.00	0.00	0.00	0.00	0.00	0.00	0.00	0.00	0.00	0.00	0.00
251	22.4	0.00	0.00	0.00	0.00	0.00	0.00	0.00	0.00	0.00	0.00	0.00	0.00	0.00	0.00	0.00	0.00	0.00	0.00	0.00	0.00	0.00
261	23.3	0.00	0.00	0.00	0.00	0.00	0.00	0.00	0.00	0.00	0.00	0.00	0.00	0.00	0.00	0.00	0.00	0.00	0.00	0.00	0.00	0.00
271	24.3	0.00	0.00	0.00	0.00	0.00	0.00	0.00	0.00	0.00	0.00	0.00	0.00	0.00	0.00	0.00	0.00	0.00	0.00	0.00	0.00	0.00
281	25.3	0.00	0.00	0.00	0.00	0.00	0.00	0.00	0.00	0.00	0.00	0.00	0.00	0.00	0.00	0.00	0.00	0.00	0.00	0.00	0.00	0.00
291	26.3	0.00	0.00	0.00	0.00	0.00	0.00	0.00	0.00	0.00	0.00	0.00	0.00	0.00	0.00	0.00	0.00	0.00	0.00	0.00	0.00	0.00
299	27.1	0.00	0.00	0.00	0.00	0.00	0.00	0.00	0.00	0.00	0.00	0.00	0.00	0.00	0.00	0.00	0.00	0.00	0.00	0.00	0.00	0.00

Appendix 1

		Others																				
Depth (cm)	Age cal ka BP	branched C18	branched C19	branched C19	dimethyl hexa	9-MeO-15:0	branched C20	branched C20	branched C21	branched C21	9-MeO-17:0	dimethyl 1,18-	branched C22	dimethyl nona	branched C24	dimethyl icosa	dimethyl henic	dimethyl doco	8,14-seco hopa	8,14-seco hopa	dimethyl tricos	α-tocopherol
1	0.1	0.00	0.00	0.00	0.00	0.00	0.00	0.00	0.00	0.00	0.00	0.00	0.00	0.00	0.00	0.00	0.00	0.00	0.00	0.00	0.00	0.00
11	1.0	0.00	0.00	0.00	0.00	0.00	0.00	0.00	0.00	0.00	0.00	0.00	0.00	0.00	0.00	0.00	0.00	1.63	0.00	0.00	0.00	0.00
21	1.8	0.00	0.00	0.00	0.00	0.00	0.00	0.00	0.00	0.00	0.00	0.00	0.00	0.00	0.00	0.00	0.00	0.00	0.00	0.00	0.00	0.00
31	2.5	0.00	0.00	0.00	0.00	0.00	0.00	0.00	0.00	0.00	0.00	0.00	0.00	0.00	0.00	0.00	0.00	0.00	0.00	0.00	0.00	0.00
41	3.3	0.00	0.00	0.00	0.00	0.00	0.00	0.00	0.00	0.00	0.00	0.00	0.00	0.00	0.00	0.00	0.00	0.00	0.00	0.00	0.00	0.00
51	4.1	0.00	0.00	0.00	0.00	0.00	0.00	0.00	0.00	0.00	0.00	0.00	0.00	0.00	0.00	0.00	0.00	0.00	0.00	0.00	0.00	0.00
61	4.9	0.00	0.00	0.00	0.00	0.00	0.00	0.00	0.00	0.00	0.00	0.00	0.00	0.00	0.00	0.00	0.00	0.00	0.00	0.00	0.00	0.00
71	5.8	0.00	0.00	0.00	0.00	0.00	0.00	0.00	0.00	0.00	0.00	0.00	0.00	0.00	0.00	0.00	0.00	0.00	0.00	0.00	0.00	0.00
81	6.8	0.00	0.00	0.00	0.00	0.00	0.00	0.00	0.00	0.00	0.00	0.00	0.00	0.00	0.00	0.00	0.00	0.00	0.00	0.00	0.00	0.00
91	7.9	0.00	0.00	0.00	0.00	0.00	0.00	0.00	0.00	0.00	0.00	0.00	0.00	0.00	0.00	0.00	0.00	0.00	0.00	0.00	0.00	0.00
101	9.0	0.00	0.00	0.00	0.00	0.00	0.00	0.00	0.00	0.00	0.00	0.00	0.00	0.00	0.00	0.00	0.00	0.00	0.00	0.00	0.00	0.00
109	10.0	0.00	0.00	0.00	0.00	0.00	0.00	0.00	0.00	0.00	0.00	0.00	0.00	0.00	0.00	0.00	0.00	0.00	0.00	0.00	0.00	0.00
121	11.1	0.00	0.00	0.00	0.00	0.00	0.00	0.00	0.00	0.00	0.00	0.00	0.00	0.00	0.00	0.00	0.00	0.00	0.00	0.00	0.00	0.00
131	12.2	0.00	0.00	0.00	0.00	0.00	0.00	0.00	0.00	0.00	6.28	0.00	0.00	0.00	0.00	0.00	0.00	0.00	0.00	0.00	0.00	0.00
141	13.3	0.00	0.00	0.00	0.00	0.00	0.00	0.00	0.00	0.00	0.00	0.00	0.00	0.00	0.00	0.00	0.00	0.00	0.00	0.00	0.00	0.00
151	14.4	0.00	0.00	0.00	0.00	0.00	0.00	0.00	0.00	0.00	0.00	0.00	0.00	0.00	0.00	0.00	0.00	0.00	0.00	0.00	0.00	0.00
161	15.4	0.00	0.00	0.00	0.00	0.00	0.00	0.00	0.00	0.00	2.74	0.00	0.00	0.00	0.00	0.00	0.00	0.00	0.00	0.00	0.00	0.00
171	16.3	0.00	0.00	0.00	0.00	3.93	0.00	0.00	0.00	0.00	0.00	0.00	0.00	0.00	0.00	0.00	0.00	0.00	0.00	0.00	0.00	0.00
181	16.7	0.00	0.00	0.00	0.00	0.00	0.00	0.00	0.00	0.00	0.00	0.00	0.00	0.00	0.00	0.00	0.00	0.00	0.00	0.00	0.00	0.00
191	17.2	0.00	0.00	0.00	0.00	0.00	0.00	0.00	0.00	0.00	0.00	0.00	0.00	0.00	0.00	0.00	0.00	0.00	0.00	0.00	0.00	0.00
201	17.6	0.00	0.00	0.00	0.00	0.00	0.00	0.00	0.00	0.00	0.00	0.00	0.00	0.00	0.00	0.00	0.00	0.00	0.00	0.00	0.00	0.00
211	18.4	0.00	0.00	0.00	0.00	0.00	0.00	0.00	0.00	0.00	0.00	0.00	0.00	0.00	0.00	0.00	0.00	0.00	0.00	0.00	0.00	0.00
221	19.4	0.00	0.00	0.00	0.00	0.00	0.00	0.00	0.00	0.00	0.00	0.00	0.00	0.00	0.00	0.00	0.00	0.00	0.00	0.00	0.00	0.00
231	20.4	0.00	0.00	0.00	0.00	0.00	0.00	0.00	0.00	0.00	0.00	0.00	0.00	0.00	0.00	0.00	0.00	0.00	0.00	0.00	0.00	0.00
241	21.4	0.00	0.00	0.00	0.00	0.00	0.00	0.00	0.00	0.00	0.00	0.00	0.00	0.00	0.00	0.00	0.00	0.00	0.00	0.00	0.00	0.00
251	22.4	0.00	0.00	0.00	0.00	0.00	0.00	0.00	0.00	0.00	0.00	0.00	0.00	0.00	0.00	0.00	0.00	0.00	0.00	0.00	0.00	0.00
261	23.3	0.00	0.00	0.00	0.00	0.00	0.00	0.00	0.00	0.00	0.00	0.00	0.00	0.00	0.00	0.00	0.00	0.00	0.00	0.00	0.00	0.00
271	24.3	0.00	0.00	0.00	0.00	0.00	0.00	0.00	0.00	0.00	0.00	0.00	0.00	0.00	0.00	0.00	0.00	0.00	0.00	0.00	0.00	0.00
281	25.3	0.00	0.00	0.00	0.00	0.00	0.00	0.00	0.00	0.00	0.00	0.00	0.00	0.00	0.00	0.00	0.00	0.00	0.00	0.00	0.00	0.00
291	26.3	0.00	0.00	0.00	0.00	0.00	0.00	0.00	0.00	0.00	0.00	0.00	0.00	0.00	0.00	0.00	0.00	0.00	0.00	0.00	0.00	0.00
299	27.1	0.00	0.00	0.00	0.00	0.00	0.00	0.00	0.00	0.00	0.00	0.00	0.00	0.00	0.00	0.00	0.00	0.00	0.00	0.00	0.00	0.00

Appendix 1

		Others																				
Depth (cm)	Age cal ka BP	dimethyl tetra	C_{24} keto-ol	11-MeO-19:0	C28 triterpane	8,14-seco hopa	cholesta-3,5-	hopanoid	8,14-seco hopa	C27 hopane	cholest-4-ene-3-	onocerane III	13-MeO-21:0	C29 α,β hopa	C29 β,α hopa	unsat. C28 diol	C28 β,β hopa	C30 α,β hopa	Hop-17(21)-ene	C31 α,β S hopa	C31 α,β R hopa	β-amyrin
1	0.1	0.00	0.00	0.00	0.00	0.00	0.00	0.50	0.00	0.00	0.00	0.00	0.00	0.00	0.00	0.00	0.00	0.00	0.00	0.00	0.00	1.11
11	1.0	0.00	0.00	0.00	0.00	0.00	0.00	0.00	0.00	0.00	0.00	0.00	0.00	0.00	0.00	0.00	0.00	0.00	0.74	0.00	0.00	0.97
21	1.8	0.00	0.00	0.00	0.00	0.00	0.00	0.00	0.00	0.00	0.00	0.00	0.00	0.00	0.00	0.00	0.00	0.00	0.44	0.00	0.00	0.51
31	2.5	0.00	0.00	0.00	0.00	0.00	0.00	0.00	0.00	0.00	0.00	0.00	0.00	0.00	0.00	0.00	0.00	0.00	0.00	0.00	0.00	0.77
41	3.3	0.00	0.00	0.00	0.00	0.00	0.00	0.00	0.00	0.00	0.00	0.00	0.00	0.00	0.00	0.00	0.00	0.00	0.00	0.00	0.00	4.30
51	4.1	0.00	0.00	0.00	0.00	0.00	0.00	0.00	0.00	0.00	0.00	0.00	0.00	0.00	0.00	0.00	0.00	0.00	0.00	0.00	0.00	5.79
61	4.9	0.00	0.00	0.00	0.00	0.00	0.00	0.00	0.00	0.00	0.00	0.00	0.20	0.00	0.00	0.00	0.00	0.00	0.00	0.00	0.00	2.48
71	5.8	0.00	0.00	0.00	0.00	0.00	0.00	0.00	0.00	0.00	0.00	0.00	0.00	0.00	0.00	0.00	0.00	0.00	0.34	0.00	0.00	3.04
81	6.8	0.00	0.00	0.00	0.00	0.00	0.00	0.00	0.00	0.00	0.00	0.00	0.00	0.00	0.00	0.00	0.00	0.00	0.00	0.00	0.00	1.46
91	7.9	0.00	0.00	0.00	0.00	0.00	0.00	0.00	0.00	0.00	0.00	0.00	0.00	0.00	0.00	0.00	0.00	0.00	0.00	0.00	0.00	13.55
101	9.0	0.00	0.00	0.00	0.00	0.00	0.00	0.00	0.00	0.00	0.00	0.00	4.80	0.00	0.00	0.00	0.00	0.00	0.00	0.00	0.00	1.99
109	10.0	0.00	0.00	0.00	0.00	0.00	0.00	0.00	0.00	0.00	0.00	0.00	0.00	0.00	0.00	0.00	0.00	0.00	0.00	0.00	0.00	3.36
121	11.1	0.00	0.00	0.00	0.00	0.00	0.00	0.00	0.00	0.00	0.00	0.00	7.22	0.00	0.00	0.00	0.00	0.00	0.00	0.00	0.00	4.72
131	12.2	0.00	0.00	0.00	0.00	0.00	0.00	0.00	0.00	0.00	0.00	0.00	18.53	0.00	0.00	0.00	0.00	0.00	0.00	0.00	0.00	3.38
141	13.3	0.00	0.00	0.00	0.00	0.00	0.00	0.00	0.00	0.00	0.00	0.00	5.31	0.00	0.00	0.00	0.00	0.00	0.00	0.00	0.00	2.06
151	14.4	0.00	0.00	0.00	0.00	0.00	0.00	0.00	0.00	0.00	0.00	0.00	0.00	0.00	0.00	0.00	0.00	0.00	0.00	0.00	0.00	1.19
161	15.4	0.00	0.00	0.00	0.00	0.00	0.00	0.00	0.00	0.00	0.00	0.00	7.53	0.00	0.00	0.00	0.00	0.00	0.00	0.00	0.00	0.00
171	16.3	0.00	0.00	0.00	0.00	0.00	0.00	0.00	0.00	0.00	0.00	0.00	7.38	0.00	0.00	0.00	0.00	0.00	0.00	0.00	0.00	0.00
181	16.7	0.00	0.00	0.00	0.00	0.00	0.00	0.00	0.00	0.00	0.00	0.00	41.66	0.00	0.00	0.00	0.00	0.00	0.00	0.00	0.00	0.00
191	17.2	0.00	0.00	0.00	0.00	0.00	0.00	0.00	0.00	0.00	0.00	0.00	0.00	0.00	0.00	0.00	0.00	0.00	0.00	0.00	0.00	0.00
201	17.6	0.00	0.00	0.00	0.00	0.00	0.00	0.00	0.00	0.00	0.00	0.00	0.00	0.00	0.00	0.00	0.00	0.00	0.00	0.00	0.00	0.00
211	18.4	0.00	0.00	0.00	0.00	0.00	0.00	0.00	0.00	0.00	0.00	0.00	0.00	0.00	0.00	0.00	0.00	0.00	0.00	0.00	0.00	0.00
221	19.4	0.00	0.00	0.00	0.00	0.00	0.00	0.00	0.00	0.00	0.00	0.00	0.00	0.00	0.00	0.00	0.00	0.00	0.00	0.00	0.00	0.00
231	20.4	0.00	0.00	0.00	0.00	0.00	0.00	0.00	0.00	0.00	0.00	0.00	0.00	0.00	0.00	0.00	0.00	0.00	0.00	0.00	0.00	0.00
241	21.4	0.00	0.00	0.00	0.00	0.00	0.00	0.00	0.00	0.00	0.00	0.00	0.00	0.00	0.00	0.00	0.00	0.00	0.00	0.00	0.00	0.00
251	22.4	0.00	0.00	0.00	0.00	0.00	0.00	0.00	0.00	0.00	0.00	0.00	0.00	0.00	0.00	0.00	0.00	0.00	0.00	0.00	0.00	0.00
261	23.3	0.00	0.00	0.00	0.00	0.00	0.00	0.00	0.00	0.00	0.00	0.00	0.00	0.00	0.00	0.00	0.00	0.00	0.00	0.00	0.00	0.00
271	24.3	0.00	0.00	0.00	0.00	0.00	0.00	0.00	0.00	0.00	0.00	0.00	0.00	0.00	0.00	0.00	0.00	0.00	0.00	0.00	0.00	0.00
281	25.3	0.00	0.00	0.00	0.00	0.00	0.00	0.00	0.00	0.00	0.00	0.00	0.00	0.00	0.00	0.00	0.00	0.00	0.00	0.00	0.00	0.00
291	26.3	0.00	0.00	0.00	0.00	0.00	0.00	0.00	0.00	0.00	0.00	0.00	0.00	0.00	0.00	0.00	0.00	0.00	0.00	0.00	0.00	0.00
299	27.1	0.00	0.00	0.00	0.00	0.00	0.00	0.00	0.00	0.00	0.00	0.00	0.00	0.00	0.00	0.00	0.00	0.00	0.00	0.00	0.00	0.00

Appendix 1

		Others											
Depth (cm)	Age cal ka BP	(taraxerol)	12-OH(ω17)-	α-amyrin	friedoole	1,15(ω16) C_{30}ke	triacontane-	C_{32}keto-ol	17β(H),21β(H)ho	17β(H),21β(H)bis	ββ-hopanoic	37:3 Ketone	37:2 Ketone
1	0.1	0.00	0.00	0.39	0.00	0.00	0.00	0.00	0.00	0.00	0.00	0.00	0.00
11	1.0	0.00	0.00	1.58	0.00	0.00	0.00	0.00	4.10	0.00	0.00	0.00	0.00
21	1.8	0.00	0.00	1.04	0.25	0.00	0.00	0.00	0.00	0.00	0.00	0.00	0.00
31	2.5	0.00	0.00	0.66	0.00	0.00	0.00	0.00	0.69	0.79	0.00	0.00	0.00
41	3.3	0.00	0.00	0.56	0.00	0.00	0.00	0.00	0.00	0.00	0.00	0.00	0.00
51	4.1	0.00	0.00	0.00	0.00	0.00	0.00	0.00	0.00	0.00	0.00	0.00	0.00
61	4.9	0.00	0.00	0.00	0.00	0.00	0.00	0.00	0.00	0.00	0.00	0.00	0.00
71	5.8	0.00	0.00	0.00	0.00	0.00	0.00	0.00	0.00	0.00	0.00	0.00	0.00
81	6.8	0.00	0.00	0.00	0.00	0.00	0.00	0.00	0.00	0.00	0.00	0.00	0.00
91	7.9	0.00	0.00	0.00	0.00	0.00	0.00	0.00	0.00	0.00	0.00	0.00	0.00
101	9.0	0.00	0.00	0.00	0.00	0.00	0.00	0.00	0.00	0.00	0.00	0.00	0.00
109	10.0	0.00	0.00	0.00	0.00	0.00	0.00	0.00	0.00	0.00	0.00	0.00	0.00
121	11.1	0.00	0.00	0.00	0.00	0.00	0.00	0.00	0.00	0.00	0.00	0.00	0.00
131	12.2	0.00	0.00	0.00	0.00	0.00	0.00	0.00	0.00	0.00	0.00	0.00	0.00
141	13.3	0.00	0.00	0.00	0.00	0.00	0.00	0.00	0.00	0.00	0.00	0.00	0.00
151	14.4	0.00	0.00	0.00	0.00	0.00	0.00	0.00	0.00	0.00	0.00	0.00	0.00
161	15.4	0.00	0.00	0.00	0.00	0.00	0.00	0.00	0.00	0.00	0.00	0.00	0.00
171	16.3	0.00	0.00	0.00	0.00	0.00	0.00	0.00	0.00	0.00	0.00	0.00	0.00
181	16.7	0.00	0.00	0.00	0.00	0.00	0.00	0.00	0.00	0.00	0.00	0.00	0.00
191	17.2	0.00	0.00	0.00	0.00	0.00	0.00	0.00	0.00	0.00	0.00	0.00	0.00
201	17.6	0.00	0.00	0.00	0.00	0.00	0.00	0.00	0.00	0.00	0.00	0.00	0.00
211	18.4	0.00	0.00	0.00	0.00	0.00	0.00	0.00	0.00	0.00	0.00	0.00	0.00
221	19.4	0.00	0.00	0.00	0.00	0.00	0.00	0.00	0.00	0.00	0.00	0.00	0.00
231	20.4	0.00	0.00	0.00	0.00	0.00	0.00	0.00	0.00	0.00	0.00	0.00	0.00
241	21.4	0.00	0.00	0.00	0.00	0.00	0.00	0.00	0.00	0.00	0.00	0.00	0.00
251	22.4	0.00	0.00	0.00	0.00	0.00	0.00	0.00	0.00	0.00	0.00	0.00	0.00
261	23.3	0.00	0.00	0.00	0.00	0.00	0.00	0.00	0.00	0.00	0.00	0.00	0.00
271	24.3	0.00	0.00	0.00	0.00	0.00	0.00	0.00	0.00	0.00	0.00	0.00	0.00
281	25.3	0.00	0.00	0.00	0.00	0.00	0.00	0.00	0.00	0.00	0.00	0.00	0.00
291	26.3	0.00	0.00	0.00	0.00	0.00	0.00	0.00	0.00	0.00	0.00	0.00	0.00
299	27.1	0.00	0.00	0.00	0.00	0.00	0.00	0.00	0.00	0.00	0.00	0.00	0.00

Appendix 2

		FAMEs																				
Depth (cm)	Age cal ka BP	C14	C15	C16	C17	C18	C19	C20	C21	C22	C23	C24	C25	C26	C27	C28	C29	C30	C31	C32	C33	C34
1	0.1	0.15	0.21	9.28	0.48	2.66	0.16	2.96	0.31	1.39	0.34	2.37	0.53	2.34	0.77	5.11	1.20	6.41	0.81	2.03	0.00	0.00
11	0.7	0.00	0.47	8.15	0.14	2.95	0.08	1.88	0.43	2.66	0.71	3.59	0.85	2.78	1.35	6.28	1.93	4.85	0.00	1.57	0.00	0.00
21	1.3	0.00	0.16	10.66	0.57	6.14	0.54	4.17	0.54	1.71	0.55	1.94	0.27	0.40	0.18	0.53	0.07	0.26	0.00	0.00	0.00	0.00
31	1.8	0.28	0.95	12.77	0.93	10.88	0.48	7.45	0.30	2.54	0.46	3.04	0.37	1.50	0.24	1.40	0.22	0.93	0.10	0.41	0.04	0.10
41	2.3	0.00	0.00	5.56	1.18	17.21	0.39	12.70	0.53	3.44	0.75	2.79	0.56	1.15	0.20	1.02	0.18	0.53	0.00	0.00	0.00	0.00
51	2.5	0.99	1.10	10.68	0.56	4.37	0.28	8.12	0.26	1.71	0.31	2.00	0.30	1.54	0.17	1.31	0.15	0.77	0.06	0.23	0.00	0.00
61	2.7	0.33	0.78	16.57	1.05	8.35	0.37	13.33	0.39	2.00	0.48	2.06	0.43	1.13	0.17	1.06	0.12	0.45	0.05	0.00	0.00	0.00
71	2.9	0.21	0.34	5.53	0.39	2.85	0.32	5.16	0.32	1.34	0.82	3.37	1.39	4.56	0.84	10.78	0.98	4.59	0.00	0.47	0.00	0.29
81	3.0	0.33	0.42	2.86	0.25	1.98	0.16	3.89	0.24	1.13	0.91	3.97	2.36	5.70	0.87	7.82	0.73	4.02	0.00	0.40	0.00	0.00
91	3.3	0.20	0.25	1.99	0.15	1.69	0.15	4.07	0.28	1.15	1.15	4.72	4.57	7.94	0.96	10.44	0.49	3.48	0.00	0.38	0.00	0.00
101	3.5	0.06	0.23	2.33	0.16	1.41	0.12	4.56	0.24	1.16	1.02	4.42	3.56	8.02	0.79	10.48	0.32	3.58	0.00	0.31	0.00	0.10
111	3.7	0.00	0.13	2.91	0.17	5.35	0.11	11.09	0.32	1.68	1.43	5.05	4.69	10.19	1.28	8.16	0.78	4.18	0.00	0.36	0.00	0.00
121	3.9	0.15	0.29	2.14	0.22	1.55	0.16	2.14	0.28	0.88	1.36	4.06	4.46	6.59	1.06	8.61	0.54	4.37	0.00	0.00	0.00	0.00
131	4.1	0.14	0.31	2.34	0.18	1.83	0.18	5.59	0.20	0.95	1.23	4.60	5.32	8.83	1.44	8.11	0.59	4.86	0.00	0.33	0.00	0.00
141	4.3	0.10	0.20	2.75	0.18	2.37	0.14	7.50	0.22	0.95	1.17	5.17	6.15	10.25	1.23	7.20	0.51	3.69	0.00	0.00	0.00	0.00
151	5.2	0.00	0.08	1.96	0.07	1.55	0.08	4.17	0.21	1.33	2.07	7.68	9.09	15.36	2.08	9.12	0.00	4.63	0.00	0.56	2.35	0.00
161	6.1	0.20	0.32	2.19	0.19	1.69	0.14	5.51	0.27	1.00	1.29	5.13	6.42	10.87	1.58	8.05	0.74	4.65	0.00	0.33	0.00	0.00
171	7.0	0.18	0.30	1.65	0.16	1.09	0.10	4.58	0.18	0.87	1.28	4.79	6.33	10.58	1.82	8.14	0.76	5.67	0.00	0.57	0.00	0.00
181	8.4	0.19	0.26	1.54	0.00	0.99	0.09	4.94	0.16	0.85	1.28	4.86	6.56	11.09	2.03	8.14	0.84	4.87	0.00	0.65	0.00	0.19
191	10.2	0.13	0.23	1.75	0.25	1.10	0.15	6.73	0.18	1.06	0.89	3.85	4.53	8.93	1.96	7.59	1.39	5.35	0.94	1.13	0.12	0.25
201	12.0	0.19	0.19	1.75	0.18	0.79	0.21	2.44	0.31	1.24	1.53	5.63	5.85	11.66	2.91	9.45	2.09	5.94	1.01	1.58	0.19	0.23
211	13.0	0.09	0.15	1.33	0.23	0.70	0.21	2.56	0.37	1.76	1.71	5.69	5.45	9.97	3.52	8.29	2.66	5.61	1.62	2.48	0.26	0.48
221	13.8	0.12	0.13	1.92	0.05	0.90	0.28	2.55	0.44	1.93	1.45	5.22	3.99	8.66	2.96	7.45	2.33	4.96	1.60	2.52	0.32	0.45
231	14.7	0.14	0.06	1.30	0.10	0.55	0.17	1.89	0.68	2.59	1.82	6.14	3.63	9.20	2.64	7.86	1.81	4.61	1.10	2.24	0.33	0.51
241	15.6	0.09	0.06	1.78	0.10	0.75	0.14	1.56	0.50	2.41	1.61	5.29	2.90	8.38	2.15	8.26	1.52	4.22	0.97	2.39	0.27	0.46
251	16.5	0.25	0.11	4.86	0.20	1.25	0.20	1.37	0.65	3.57	1.97	4.91	2.75	8.78	1.51	6.14	0.88	2.28	0.81	1.36	0.24	0.24
261	17.4	0.35	0.06	3.05	0.07	1.19	0.17	1.42	0.85	4.26	2.46	10.13	2.86	9.44	1.14	5.10	0.35	1.29	0.00	0.00	0.00	0.00
271	18.3	0.20	0.08	2.13	0.10	0.71	0.12	0.74	0.45	2.34	1.44	5.85	2.45	8.72	1.74	8.02	1.24	4.71	0.84	2.56	0.24	0.44
281	19.1	0.15	0.05	2.87	0.14	1.18	0.25	1.55	1.50	4.98	2.75	8.61	2.63	9.22	1.22	6.89	0.74	2.60	0.48	1.28	0.09	0.19
291	19.9	0.00	0.08	4.78	0.00	6.76	0.00	2.60	0.39	2.49	0.83	2.87	1.28	3.55	1.65	5.37	1.76	5.84	1.58	5.07	0.29	0.61
301	20.0	0.00	0.00	5.00	0.00	9.39	0.00	5.37	0.41	2.85	0.71	2.58	1.05	2.04	0.94	3.98	0.71	2.94	0.48	2.50	0.00	0.00

Appendix 2

		OH-Fas																				
Depth (cm)	Age cal ka BP	C10	C11	C12	*i* -α-C15	*ai* -α-C15	α-C15	C14	α-C16	C15	α-C17	C16	?	α-C18	un. α-C18	C17	un. α-C19	α-C19	C18	un. α-C20	α-C20	C19
1	0.1	0.00	0.00	0.00	0.08	0.00	0.00	0.00	0.40	0.00	0.14	0.00	0.00	0.20	0.00	0.00	0.00	0.00	0.00	0.00	0.00	0.00
11	0.7	0.00	0.00	0.00	0.00	0.00	0.00	0.00	0.13	0.00	0.00	0.08	0.39	0.00	0.00	0.00	0.00	0.00	0.18	0.00	0.00	0.00
21	1.3	0.00	0.00	0.00	0.00	0.00	0.00	0.00	1.01	0.00	0.27	0.55	0.00	0.00	0.00	0.00	0.00	0.00	0.43	0.00	0.00	0.00
31	1.8	0.00	0.00	0.00	0.00	0.00	0.00	0.00	0.86	0.00	0.22	0.63	0.00	0.00	0.00	0.00	0.00	0.00	0.00	0.00	0.00	0.00
41	2.3	0.00	0.00	0.00	0.00	0.00	0.00	0.00	0.85	0.00	0.00	0.31	0.00	0.00	0.00	0.00	0.00	0.00	0.00	0.00	0.00	0.00
51	2.5	0.00	0.00	0.00	0.34	0.00	0.00	0.00	1.21	0.00	0.16	1.06	0.00	0.00	0.00	0.00	0.00	0.00	0.95	0.00	0.00	0.00
61	2.7	0.00	0.00	0.00	0.00	0.00	0.00	0.00	1.09	0.00	0.65	0.28	0.00	0.00	0.00	0.00	0.00	0.00	0.00	0.00	0.00	0.00
71	2.9	0.00	0.00	0.00	0.00	0.00	0.00	0.00	0.19	0.00	0.00	0.82	0.00	0.00	0.00	0.00	0.00	0.00	0.66	0.00	0.00	0.00
81	3.0	0.00	0.00	0.00	0.00	0.00	0.00	0.00	0.00	0.00	0.00	0.98	0.00	0.00	0.00	0.00	0.00	0.00	0.30	0.00	0.00	0.13
91	3.3	0.00	0.00	0.00	0.00	0.00	0.00	0.00	0.16	0.00	0.00	0.74	0.00	0.00	0.00	0.00	0.00	0.00	0.44	0.00	0.00	0.00
101	3.5	0.00	0.00	0.00	0.00	0.00	0.00	0.00	0.05	0.00	0.00	0.48	0.00	0.00	0.00	0.00	0.00	0.00	0.31	0.00	0.00	0.00
111	3.7	0.00	0.00	0.00	0.00	0.00	0.00	0.00	0.00	0.00	0.00	0.27	0.00	0.00	0.00	0.00	0.00	0.00	0.15	0.00	0.00	0.00
121	3.9	0.00	0.00	0.00	0.00	0.00	0.00	0.00	0.14	0.00	0.00	0.62	0.00	0.00	0.00	0.00	0.00	0.00	0.34	0.00	0.00	0.00
131	4.1	0.00	0.00	0.00	0.00	0.00	0.00	0.00	0.09	0.00	0.00	0.44	0.00	0.00	0.00	0.00	0.00	0.00	0.21	0.00	0.00	0.18
141	4.3	0.00	0.00	0.00	0.00	0.00	0.00	0.00	0.14	0.00	0.00	0.30	0.00	0.00	0.00	0.00	0.00	0.00	0.15	0.00	0.00	0.11
151	5.2	0.00	0.00	0.00	0.00	0.00	0.00	0.00	0.00	0.00	0.00	0.13	0.00	0.00	0.00	0.00	0.00	0.00	0.00	0.00	0.00	0.06
161	6.1	0.00	0.00	0.00	0.00	0.00	0.00	0.00	0.00	0.00	0.00	0.41	0.00	0.00	0.00	0.00	0.00	0.00	0.21	0.00	0.00	0.21
171	7.0	0.00	0.00	0.00	0.00	0.00	0.00	0.00	0.00	0.00	0.00	0.38	0.00	0.00	0.00	0.00	0.00	0.00	0.18	0.00	0.00	0.18
181	8.4	0.00	0.00	0.00	0.00	0.00	0.00	0.00	0.00	0.00	0.00	0.39	0.00	0.00	0.00	0.00	0.00	0.00	0.27	0.00	0.00	0.15
191	10.2	0.01	0.00	0.00	0.00	0.00	0.00	0.00	0.04	0.03	0.00	0.58	0.00	0.00	0.00	0.04	0.00	0.00	0.21	0.00	0.00	0.12
201	12.0	0.00	0.00	0.00	0.00	0.00	0.00	0.06	0.00	0.00	0.00	0.77	0.00	0.00	0.00	0.00	0.07	0.00	0.27	0.00	0.00	0.07
211	13.0	0.00	0.07	0.00	0.00	0.00	0.00	0.07	0.00	0.00	0.00	1.54	0.00	0.00	0.00	0.08	0.00	0.00	0.46	0.00	0.00	0.11
221	13.8	0.00	0.08	0.00	0.00	0.00	0.00	0.11	0.00	0.06	0.00	2.64	0.00	0.00	0.00	0.12	0.00	0.00	0.60	0.00	0.00	0.14
231	14.7	0.00	0.00	0.00	0.00	0.00	0.00	0.08	0.00	0.00	0.00	2.54	0.00	0.00	0.00	0.08	0.00	0.00	0.57	0.00	0.00	0.05
241	15.6	0.00	0.11	0.00	0.00	0.00	0.00	0.08	0.08	0.02	0.00	3.04	0.00	0.00	0.00	0.05	0.00	0.00	0.53	0.00	0.00	0.05
251	16.5	0.00	0.35	0.00	0.00	0.00	0.00	0.08	0.00	0.04	0.00	4.77	0.00	0.00	0.00	0.11	0.00	0.00	0.53	0.00	0.00	0.00
261	17.4	0.00	0.00	0.00	0.00	0.00	0.00	0.04	0.07	0.04	0.02	7.26	0.00	0.00	0.00	0.17	0.00	0.00	1.42	0.00	0.00	0.00
271	18.3	0.00	0.08	0.00	0.00	0.00	0.00	0.04	0.00	0.00	0.00	2.10	0.00	0.00	0.00	0.06	0.00	0.00	0.34	0.00	0.00	0.00
281	19.1	0.00	0.00	0.00	0.00	0.00	0.00	0.04	0.06	0.00	0.00	4.65	0.00	0.00	0.00	0.12	0.00	0.00	0.94	0.00	0.00	0.00
291	19.9	0.00	0.00	0.00	0.00	0.00	0.00	0.00	0.00	0.00	0.00	0.61	0.00	0.00	0.00	0.00	0.00	0.00	0.21	0.00	0.00	0.00
301	20.0	0.00	0.00	0.00	0.00	0.00	0.00	0.00	0.00	0.00	0.00	0.00	0.00	0.00	0.00	0.00	0.00	0.00	0.00	0.00	0.00	0.00

Appendix 2

		OH-Fas																	Branched FAs			
Depth (cm)	Age cal ka BP	α-C21	C20	α-C22	C21	α-C23	C22	α-C24	C23	α-C25	C24	α-C26	C25	C26	C27	C28	C29	C30	C14	*i*-C15:0	*a*-C15:0	*i*-C16:0
1	0.1	0.00	0.06	0.00	0.00	0.00	0.00	0.48	0.00	0.00	0.22	0.00	0.00	0.00	0.00	0.35	0.00	0.00	0.08	0.27	0.30	0.37
11	0.7	0.00	0.24	0.00	0.00	0.00	0.00	0.00	0.00	0.00	0.00	0.00	0.00	0.00	0.00	0.00	0.00	0.00	0.00	0.48	0.63	0.85
21	1.3	0.00	0.15	0.00	0.00	0.00	0.00	0.35	0.00	0.00	0.00	0.00	0.00	0.00	0.00	0.00	0.00	0.00	0.00	0.13	0.22	1.22
31	1.8	0.00	0.37	0.00	0.00	0.00	0.59	1.48	0.00	0.37	0.00	0.00	0.00	0.00	0.00	0.00	0.00	0.00	0.08	0.81	1.32	2.77
41	2.3	0.00	0.15	0.00	0.00	0.00	0.00	0.00	0.00	0.00	0.00	0.00	0.00	0.00	0.00	0.00	0.00	0.00	0.00	0.00	0.00	0.67
51	2.5	0.00	1.13	0.00	0.00	0.00	0.52	1.30	0.00	0.31	0.00	0.00	0.00	0.67	0.00	1.35	0.00	0.17	1.12	1.91	3.88	3.04
61	2.7	0.00	0.41	0.00	0.00	0.00	0.18	0.52	0.00	0.00	0.00	0.00	0.00	0.00	0.00	0.00	0.00	0.00	0.22	1.32	2.21	4.12
71	2.9	0.00	2.10	0.00	0.00	0.00	0.68	0.00	0.00	0.23	1.87	0.00	0.00	3.57	0.00	6.21	0.00	1.61	0.27	0.63	1.21	1.73
81	3.0	0.00	3.15	0.00	0.13	0.00	0.78	0.00	0.10	0.00	1.43	0.00	0.38	3.89	0.27	9.52	0.00	2.52	0.61	0.58	1.21	1.75
91	3.3	0.00	3.39	0.00	0.00	0.00	0.72	0.00	0.13	0.00	1.59	0.00	0.00	3.66	0.18	10.30	0.00	2.62	0.35	0.36	1.03	0.80
101	3.5	0.00	2.23	0.00	0.00	0.00	0.55	0.00	0.00	0.00	1.69	0.00	0.00	2.57	0.10	8.19	0.00	1.96	0.10	0.32	0.58	0.63
111	3.7	0.00	2.92	0.00	0.00	0.00	0.31	0.00	0.00	0.00	1.12	0.00	0.00	2.61	0.00	6.86	0.00	0.28	0.00	0.31	0.53	1.03
121	3.9	0.00	2.12	0.00	0.17	0.00	0.82	0.00	0.12	0.00	1.49	0.00	0.00	3.03	0.21	8.28	0.00	3.16	0.10	0.23	1.05	1.12
131	4.1	0.00	6.55	0.00	0.21	0.00	0.89	0.00	0.07	0.00	1.84	0.00	0.29	3.98	0.23	10.95	0.30	5.40	0.15	0.32	0.81	1.11
141	4.3	0.00	5.94	0.00	0.13	0.00	0.57	0.00	0.00	0.00	1.14	0.00	0.00	2.51	0.00	6.28	0.00	1.93	0.05	0.18	0.42	0.86
151	5.2	0.00	3.87	0.00	0.08	0.00	0.49	0.00	0.00	0.00	1.20	0.00	0.00	3.57	0.00	5.93	0.00	0.00	0.00	0.07	0.20	0.53
161	6.1	0.00	5.01	0.00	0.00	0.00	0.69	0.00	0.00	0.00	1.34	0.00	0.00	3.86	0.00	9.28	0.00	3.89	0.19	0.29	0.69	0.65
171	7.0	0.00	4.93	0.00	0.18	0.00	0.85	0.00	0.08	0.00	1.84	0.00	0.39	4.01	0.26	11.88	0.34	5.89	0.22	0.23	0.60	0.55
181	8.4	0.00	5.50	0.00	0.24	0.00	0.98	0.00	0.19	0.10	2.04	0.00	0.38	3.81	0.34	10.27	0.30	5.20	0.18	0.26	0.51	0.38
191	10.2	0.00	6.63	0.00	0.21	0.00	0.90	0.00	0.13	0.08	2.34	0.00	0.00	3.62	0.22	8.73	0.26	4.25	0.10	0.19	0.52	0.36
201	12.0	0.00	1.72	0.00	0.14	0.00	0.73	0.00	0.17	0.00	2.41	0.00	0.37	4.28	0.41	9.11	0.35	3.38	0.10	0.14	0.33	0.21
211	13.0	0.00	1.73	0.00	0.17	0.00	0.95	0.00	0.32	0.32	1.96	0.00	0.75	4.12	0.68	6.48	0.23	2.72	0.05	0.06	0.09	0.06
221	13.8	0.00	1.41	0.00	0.17	0.00	1.13	0.00	0.46	0.34	2.53	0.00	0.85	4.64	0.77	5.75	0.31	1.61	0.05	0.05	0.07	0.06
231	14.7	0.00	0.77	0.00	0.14	0.00	1.28	0.00	0.54	0.00	3.07	0.00	0.93	6.46	0.95	6.88	0.35	0.96	0.08	0.06	0.14	0.06
241	15.6	0.00	0.65	0.00	0.09	0.00	1.27	0.00	0.27	0.26	3.11	2.91	0.74	7.65	0.85	7.77	0.28	0.90	0.02	0.04	0.09	0.03
251	16.5	0.00	0.51	0.00	0.00	0.00	2.31	0.00	0.32	0.25	4.81	0.46	0.68	7.98	0.63	6.11	0.00	0.58	0.05	0.09	0.23	0.00
261	17.4	0.00	0.70	0.00	0.14	0.00	2.42	0.00	0.38	0.00	4.47	0.00	0.47	7.41	0.27	4.10	0.00	0.21	0.08	0.12	0.31	0.11
271	18.3	0.00	0.49	0.00	0.12	0.00	2.88	0.00	0.31	0.30	6.05	0.45	0.81	10.09	0.78	9.55	0.31	0.94	0.06	0.08	0.23	0.08
281	19.1	0.00	0.55	0.00	0.00	0.00	1.34	0.00	0.21	0.22	3.12	0.35	0.46	8.07	0.57	9.48	0.26	0.74	0.00	0.07	0.17	0.12
291	19.9	0.00	0.54	0.00	0.00	0.00	0.16	0.00	0.00	0.00	0.70	0.00	0.00	1.02	0.00	0.90	0.00	0.00	0.00	0.00	0.00	0.42
301	20.0	0.00	0.78	0.00	0.00	0.00	0.00	0.00	0.00	0.00	0.00	0.00	0.00	0.00	0.00	0.00	0.00	0.00	0.00	0.00	0.00	0.51

Appendix 2

		Branched FAs							Unsaturated FAs													
Depth (cm)	Age cal ka BP	*a*-C16:0	*i*-C17:0	*a*-C17:0	C18	C19	C20	C14:1 (cis9)	C15:1 (cis-10)	C16:2	C16:1 isomere	C16:1 (cis-9)	C16:1 isomere	C17:1 isomere	C17:1 (cis-10)	C17:1 isomere	C18:3 (cis-6)	C18:3 isomere	C18:2 (cis-9)	C18:3 (cis-9)	C18:1 (cis-	C18:2 (tr-9)
1	0.1	0.00	0.33	0.22	0.10	0.00	0.00	0.00	0.00	0.00	0.35	0.00	0.36	0.00	0.00	0.00	0.00	0.00	1.21	0.00	32.93	0.00
11	0.7	0.00	1.43	1.61	0.15	0.00	0.00	0.00	0.00	0.00	1.36	0.00	0.83	0.00	0.00	0.00	0.00	0.00	0.66	0.00	22.08	0.00
21	1.3	0.25	1.37	1.88	0.40	0.58	0.00	0.00	0.00	0.00	0.35	0.06	1.09	0.18	0.00	0.00	0.00	0.00	0.50	0.00	20.70	0.00
31	1.8	0.80	1.46	2.32	0.24	0.65	0.00	0.00	0.00	0.00	0.90	1.64	0.00	0.00	0.00	0.00	0.00	0.00	0.56	0.00	7.53	0.00
41	2.3	0.21	0.62	1.69	0.31	0.72	0.00	0.00	0.00	0.00	0.00	0.32	0.00	0.00	0.00	0.00	0.00	0.00	0.64	0.00	11.11	0.00
51	2.5	0.74	0.92	1.74	0.21	0.23	0.00	0.00	0.00	0.00	0.88	2.88	0.00	0.00	0.00	0.00	0.00	0.00	0.00	0.00	5.37	0.00
61	2.7	0.59	0.98	2.84	0.71	0.79	0.00	0.00	0.00	0.20	0.84	3.20	0.00	0.00	0.00	0.00	0.00	0.00	0.00	0.00	12.75	0.00
71	2.9	0.30	0.69	1.10	0.49	0.39	0.00	0.00	0.00	0.00	0.32	1.14	0.00	0.00	0.00	0.00	0.00	0.00	0.00	0.00	2.59	0.00
81	3.0	0.00	0.36	1.32	0.59	0.27	0.00	0.00	0.00	0.00	0.44	0.21	0.00	0.00	0.00	0.00	0.00	0.00	0.00	0.00	0.16	0.00
91	3.3	0.10	0.17	0.56	0.30	0.15	0.00	0.00	0.00	0.00	0.13	0.14	0.00	0.00	0.00	0.00	0.00	0.00	0.00	0.00	0.60	0.00
101	3.5	0.11	0.19	0.42	0.10	0.07	0.00	0.00	0.00	0.00	0.00	0.03	0.00	0.00	0.00	0.00	0.00	0.00	0.00	0.00	0.64	0.00
111	3.7	0.15	0.24	0.63	0.50	0.27	0.00	0.00	0.00	0.00	0.05	0.21	0.09	0.00	0.00	0.00	0.00	0.00	0.00	0.00	0.00	0.00
121	3.9	0.00	0.46	0.55	0.38	0.22	0.00	0.00	0.00	0.00	0.00	0.00	0.00	0.00	0.00	0.00	0.00	0.00	0.00	0.00	1.55	0.00
131	4.1	0.14	0.36	0.58	0.30	0.14	0.00	0.00	0.00	0.00	0.11	0.19	0.00	0.00	0.00	0.00	0.00	0.00	0.11	0.00	0.70	0.00
141	4.3	0.00	0.21	0.48	0.25	0.19	0.00	0.00	0.00	0.00	0.00	0.15	0.00	0.00	0.00	0.00	0.00	0.00	0.00	0.00	0.00	0.00
151	5.2	0.00	0.13	0.29	0.35	0.20	0.00	0.00	0.00	0.00	0.00	0.00	0.00	0.00	0.00	0.00	0.00	0.00	0.00	0.00	0.47	0.00
161	6.1	0.00	0.13	0.45	0.32	0.20	0.00	0.00	0.00	0.00	0.00	0.00	0.00	0.00	0.00	0.00	0.00	0.00	0.00	0.00	0.00	0.00
171	7.0	0.06	0.09	0.24	0.14	0.11	0.00	0.00	0.00	0.00	0.05	0.08	0.04	0.00	0.00	0.00	0.00	0.00	0.00	0.00	0.00	0.00
181	8.4	0.00	0.08	0.23	0.19	0.09	0.00	0.00	0.00	0.00	0.00	0.12	0.00	0.00	0.00	0.00	0.00	0.00	0.00	0.00	0.00	0.00
191	10.2	0.00	0.13	0.20	0.12	0.06	0.00	0.00	0.00	0.00	0.07	0.09	0.00	0.00	0.00	0.00	0.00	0.00	0.00	0.00	0.18	0.00
201	12.0	0.00	0.00	0.09	0.00	0.00	0.00	0.00	0.00	0.00	0.00	0.00	0.00	0.00	0.00	0.00	0.00	0.00	0.00	0.00	0.10	0.00
211	13.0	0.00	0.04	0.04	0.00	0.00	0.00	0.00	0.00	0.00	0.00	0.00	0.00	0.00	0.00	0.00	0.00	0.00	0.00	0.00	0.00	0.00
221	13.8	0.00	0.00	0.03	0.00	0.00	0.00	0.00	0.00	0.00	0.00	0.00	0.00	0.00	0.00	0.00	0.00	0.00	0.00	0.00	0.00	0.00
231	14.7	0.00	0.03	0.02	0.00	0.00	0.00	0.00	0.00	0.00	0.00	0.00	0.11	0.00	0.00	0.00	0.00	0.00	0.00	0.00	0.00	0.00
241	15.6	0.00	0.00	0.00	0.00	0.00	0.00	0.00	0.00	0.00	0.00	0.00	0.00	0.00	0.00	0.00	0.00	0.00	0.00	0.00	0.00	0.00
251	16.5	0.20	0.00	0.00	0.06	0.00	0.00	0.00	0.00	0.00	0.00	0.00	0.00	0.00	0.00	0.00	0.00	0.00	0.00	0.00	0.00	0.00
261	17.4	0.00	0.04	0.04	0.00	0.00	0.00	0.00	0.00	0.00	0.00	0.00	0.00	0.00	0.00	0.00	0.00	0.00	0.00	0.00	0.00	0.00
271	18.3	0.00	0.05	0.04	0.00	0.00	0.00	0.00	0.00	0.00	0.00	0.00	0.00	0.00	0.00	0.00	0.00	0.00	0.00	0.00	0.05	0.00
281	19.1	0.00	0.00	0.04	0.00	0.00	0.00	0.00	0.00	0.00	0.00	0.00	0.00	0.00	0.00	0.00	0.00	0.00	0.00	0.00	0.08	0.00
291	19.9	0.00	0.00	0.00	0.00	0.00	0.00	0.00	0.00	0.00	0.00	0.00	0.00	0.00	0.00	0.00	0.00	0.00	0.00	0.00	4.05	0.33
301	20.0	0.00	0.00	0.00	0.00	0.00	0.00	0.00	0.00	0.00	0.00	0.00	0.00	0.00	0.00	0.00	0.00	0.00	1.60	0.00	12.26	1.26

Appendix 2

		Unsaturated FAs																	Alcohols			
Depth (cm)	Age cal ka BP	C18:1 (tr-9)	C18:1 isomere	C18:1 isomere	C20:4 (cis-5)	C20:5 (cis-8)	C20:4 isomere	C20:3 (cis-8)	C20:2 (cis-11)	C20:3 (cis-11)	C20:1 (cis-11)	C20:1 isomere	C22:6 (cis-9)	C22:2 (cis-13)	C22:1 isomere	C22:1 (cis-13)	C24:1 isomere	C24:1 (cis-15)	C12	C13	C14	C15
1	0.1	0.59	0.00	0.00	0.00	0.00	0.00	0.00	0.00	0.00	0.00	0.00	0.00	0.00	0.00	0.94	0.00	0.00	0.00	0.00	0.00	0.00
11	0.7	0.93	0.00	0.00	0.00	0.00	0.00	0.00	0.00	0.00	0.00	0.00	0.00	0.00	0.00	3.38	0.00	0.00	0.00	0.00	0.00	0.00
21	1.3	0.96	0.00	0.00	0.00	0.00	0.00	0.00	0.00	0.00	0.54	0.00	0.00	0.00	0.00	2.48	0.00	0.00	0.00	0.00	0.00	0.00
31	1.8	1.22	0.00	0.00	0.00	0.00	0.00	0.00	0.00	0.00	0.95	0.00	0.00	0.00	0.00	6.61	0.00	0.00	0.00	0.00	0.13	0.09
41	2.3	1.17	0.00	0.00	0.00	0.00	0.00	0.00	0.00	0.00	3.03	0.00	0.00	0.00	1.18	17.22	0.00	0.00	0.00	0.00	0.00	0.00
51	2.5	1.30	0.00	0.00	0.00	0.00	0.00	0.00	0.00	0.00	0.90	0.00	0.00	0.00	0.00	4.09	0.00	0.00	0.00	0.00	0.29	0.23
61	2.7	2.75	0.00	0.00	0.00	0.00	0.00	0.00	0.00	0.00	1.02	0.00	0.00	0.00	0.00	4.31	0.00	0.00	0.00	0.00	0.10	0.00
71	2.9	0.89	0.00	0.00	0.00	0.00	0.00	0.00	0.00	0.00	0.53	0.00	0.00	0.00	0.00	3.02	0.00	0.00	0.00	0.00	0.14	0.00
81	3.0	0.58	0.23	0.00	0.00	0.00	0.00	0.00	0.00	0.00	0.00	0.00	0.00	0.00	0.00	0.67	0.00	0.00	0.00	0.00	0.22	0.00
91	3.3	0.06	0.00	0.00	0.00	0.00	0.00	0.00	0.00	0.00	0.08	0.00	0.00	0.00	0.00	0.74	0.00	0.00	0.00	0.00	0.16	0.00
101	3.5	0.00	0.00	0.00	0.00	0.00	0.00	0.00	0.00	0.00	0.00	0.00	0.00	0.00	0.00	0.57	0.00	0.00	0.00	0.00	0.18	0.00
111	3.7	0.40	0.00	0.00	0.00	0.00	0.00	0.00	0.00	0.00	0.07	0.00	0.00	0.00	0.00	0.04	0.00	0.00	0.00	0.00	0.08	0.00
121	3.9	0.00	0.00	0.00	0.00	0.00	0.00	0.00	0.00	0.00	0.00	0.00	0.00	0.00	0.00	0.54	0.00	0.00	0.00	0.00	0.29	0.06
131	4.1	0.12	0.00	0.00	0.00	0.00	0.00	0.00	0.00	0.00	0.13	0.00	0.00	0.00	0.00	0.39	0.00	0.00	0.00	0.00	0.44	0.00
141	4.3	0.76	0.00	0.00	0.00	0.00	0.00	0.00	0.00	0.00	0.00	0.00	0.00	0.00	0.00	0.59	0.00	0.00	0.00	0.00	0.29	0.00
151	5.2	0.00	0.00	0.00	0.00	0.00	0.00	0.00	0.00	0.00	0.00	0.00	0.00	0.00	0.00	0.75	0.00	0.00	0.00	0.00	0.13	0.00
161	6.1	0.97	0.00	0.00	0.00	0.00	0.00	0.00	0.00	0.00	0.17	0.00	0.00	0.00	0.00	1.33	0.00	0.00	0.00	0.00	0.56	0.00
171	7.0	0.36	0.00	0.00	0.00	0.00	0.00	0.00	0.00	0.00	0.07	0.00	0.00	0.00	0.00	0.54	0.00	0.00	0.00	0.00	0.58	0.00
181	8.4	0.32	0.06	0.00	0.00	0.00	0.00	0.00	0.00	0.00	0.00	0.00	0.00	0.00	0.00	0.32	0.00	0.00	0.00	0.00	0.62	0.00
191	10.2	0.00	0.00	0.00	0.00	0.00	0.00	0.00	0.00	0.00	0.05	0.00	0.00	0.00	0.00	0.22	0.00	0.00	0.00	0.00	0.48	0.00
201	12.0	0.04	0.00	0.00	0.00	0.00	0.00	0.00	0.00	0.00	0.00	0.00	0.00	0.00	0.00	0.07	0.00	0.00	0.00	0.00	0.36	0.00
211	13.0	0.02	0.00	0.00	0.00	0.00	0.00	0.00	0.00	0.00	0.00	0.00	0.00	0.00	0.00	0.00	0.00	0.00	0.00	0.00	0.13	0.00
221	13.8	0.00	0.00	0.00	0.00	0.00	0.00	0.00	0.00	0.00	0.00	0.00	0.00	0.00	0.00	0.00	0.00	0.00	0.00	0.00	0.08	0.00
231	14.7	0.00	0.00	0.00	0.00	0.00	0.00	0.00	0.00	0.00	0.00	0.00	0.00	0.00	0.00	0.00	0.00	0.00	0.00	0.00	0.00	0.00
241	15.6	0.00	0.00	0.00	0.00	0.00	0.00	0.00	0.00	0.00	0.00	0.00	0.00	0.00	0.00	0.00	0.00	0.00	0.00	0.00	0.02	0.00
251	16.5	0.00	0.00	0.00	0.00	0.00	0.00	0.00	0.00	0.00	0.00	0.00	0.00	0.00	0.00	0.00	0.00	0.00	0.00	0.00	0.04	0.00
261	17.4	0.00	0.00	0.00	0.00	0.00	0.00	0.00	0.00	0.00	0.25	0.00	0.00	0.00	0.00	0.00	0.00	0.00	0.00	0.00	0.00	0.00
271	18.3	0.00	0.00	0.00	0.00	0.00	0.00	0.00	0.00	0.00	0.00	0.00	0.00	0.00	0.00	0.00	0.00	0.00	0.02	0.00	0.04	0.00
281	19.1	0.07	0.00	0.00	0.00	0.00	0.00	0.00	0.00	0.00	0.00	0.00	0.00	0.00	0.00	0.00	0.00	0.00	0.00	0.00	0.00	0.00
291	19.9	0.00	0.00	0.00	0.00	0.00	0.00	0.00	0.00	0.00	0.97	0.00	0.00	0.00	0.00	8.63	0.00	0.00	0.00	0.00	0.00	0.00
301	20.0	0.00	0.00	0.00	0.30	0.00	0.00	0.00	0.00	0.00	0.00	0.00	0.00	0.00	0.00	25.17	0.00	0.00	0.00	0.00	0.00	0.00

Appendix 2

		Alcohols																				
Depth (cm)	Age cal ka BP	C16	C17	C18	C19	C20	C21	C22	C23	C24	C25	C26	C27	C28	C29	C30	C31	C32	C33	C34	C35	C36
1	0.1	0.05	0.00	0.14	0.00	0.10	0.00	0.12	0.00	0.16	0.00	0.32	0.00	3.52	0.30	1.99	0.00	1.35	0.00	0.00	0.00	0.00
11	0.7	0.07	0.00	0.14	0.00	0.35	0.00	0.27	0.00	0.55	0.07	0.86	0.00	4.05	0.59	1.19	0.00	1.26	0.00	0.00	0.00	0.00
21	1.3	0.38	0.10	0.79	0.00	0.38	0.00	0.48	0.08	0.48	0.59	0.82	0.00	2.21	0.00	0.91	0.00	0.00	0.00	0.00	0.00	0.00
31	1.8	0.33	0.00	0.44	0.00	0.00	0.00	0.50	0.25	0.53	0.00	1.36	0.00	1.78	0.00	2.13	0.00	0.82	0.00	0.00	0.00	0.00
41	2.3	0.26	0.13	0.65	0.00	0.75	0.00	0.50	0.00	0.22	0.00	0.90	0.00	0.52	0.00	0.00	0.00	0.00	0.00	0.00	0.00	0.00
51	2.5	0.65	0.11	0.61	0.00	0.70	0.11	0.96	0.30	0.83	0.71	1.67	0.54	2.29	0.00	2.64	0.00	1.07	0.00	0.19	0.00	0.00
61	2.7	0.43	0.00	0.55	0.00	0.40	0.00	0.40	0.00	0.19	0.00	0.54	0.00	0.28	0.00	0.00	0.00	0.00	0.00	0.00	0.00	0.00
71	2.9	0.63	0.13	0.56	0.00	0.63	0.00	0.83	0.23	0.62	0.47	1.03	0.00	0.90	0.00	1.14	0.00	0.47	0.00	0.00	0.00	0.00
81	3.0	0.44	0.00	0.51	0.06	0.61	0.00	0.00	0.20	1.02	0.23	1.01	0.17	0.68	0.00	0.55	0.00	0.24	0.00	0.00	0.00	0.00
91	3.3	0.49	0.00	0.60	0.00	0.66	0.09	1.12	0.20	1.06	0.40	0.00	0.00	0.54	0.00	0.00	0.00	0.16	0.00	0.00	0.00	0.00
101	3.5	0.40	0.00	0.41	0.00	0.59	0.04	1.04	0.15	0.84	0.26	0.97	0.00	0.35	0.00	0.00	0.00	0.05	0.00	0.00	0.00	0.00
111	3.7	0.43	0.00	0.56	0.00	0.68	0.00	0.80	0.14	0.50	0.19	0.42	0.05	0.19	0.00	0.00	0.00	0.00	0.00	0.00	0.00	0.00
121	3.9	1.03	0.00	0.67	0.00	0.82	0.11	0.72	0.30	1.07	0.51	0.82	0.00	0.36	0.00	0.00	0.00	0.00	0.00	0.00	0.00	0.00
131	4.1	0.00	0.00	1.36	0.05	1.34	0.08	0.81	0.22	0.69	0.34	0.56	0.00	0.22	0.00	0.00	0.00	0.15	0.00	0.00	0.00	0.00
141	4.3	0.94	0.00	1.17	0.00	1.22	0.08	0.66	0.23	0.62	0.24	0.51	0.00	0.00	0.00	0.00	0.00	0.00	0.00	0.00	0.00	0.00
151	5.2	0.53	0.00	0.58	0.00	0.73	0.04	0.72	0.26	0.84	0.32	0.40	0.00	0.13	0.00	0.00	0.00	0.00	0.00	0.00	0.00	0.00
161	6.1	1.13	0.00	0.91	0.00	1.00	0.11	0.90	0.28	0.95	0.50	0.61	0.00	0.42	0.00	0.00	0.00	0.30	0.00	0.00	0.00	0.00
171	7.0	0.99	0.00	0.64	0.05	0.84	0.10	0.78	0.30	0.90	0.43	0.67	0.19	0.37	0.00	0.00	0.00	0.34	0.00	0.00	0.00	0.00
181	8.4	1.04	0.00	0.71	0.00	0.92	0.07	0.64	0.27	0.74	0.35	0.51	0.22	0.47	0.00	0.51	0.00	0.13	0.00	0.00	0.00	0.00
191	10.2	0.84	0.00	0.89	0.06	0.98	0.07	0.65	0.18	0.71	0.32	0.74	0.20	0.96	0.22	1.50	0.00	0.36	0.00	0.00	0.00	0.00
201	12.0	0.52	0.00	0.26	0.03	0.39	0.06	0.52	0.18	0.52	0.16	0.53	0.11	0.79	0.00	0.93	0.00	0.13	0.00	0.00	0.00	0.00
211	13.0	0.23	0.00	0.21	0.03	0.27	0.05	0.38	0.11	0.47	0.18	0.53	0.11	0.81	0.00	0.69	0.00	0.29	0.00	0.00	0.00	0.00
221	13.8	0.22	0.05	0.26	0.03	0.35	0.08	0.53	0.17	0.52	0.15	0.72	0.10	0.81	0.00	0.78	0.00	0.24	0.00	0.00	0.00	0.00
231	14.7	0.13	0.03	0.15	0.00	0.31	0.12	0.74	0.18	0.78	0.16	0.88	0.22	0.92	0.00	1.12	0.00	0.45	0.00	0.00	0.00	0.00
241	15.6	0.10	0.03	0.20	0.00	0.31	0.09	0.66	0.15	0.76	0.12	0.85	0.16	0.88	0.24	0.33	0.00	0.30	0.00	0.00	0.00	0.00
251	16.5	0.24	0.04	0.27	0.00	0.28	0.06	0.64	0.00	0.46	0.07	0.66	0.00	0.75	0.00	0.00	0.00	0.30	0.00	0.00	0.00	0.00
261	17.4	0.07	0.05	0.17	0.05	0.89	0.18	1.63	0.29	1.93	0.25	1.43	0.19	0.55	0.00	0.21	0.00	0.00	0.00	0.00	0.00	0.00
271	18.3	0.12	0.03	0.00	0.02	0.19	0.06	0.63	0.12	0.81	0.10	1.00	0.19	1.34	0.29	0.83	0.00	0.50	0.00	0.10	0.00	0.00
281	19.1	0.10	0.03	0.18	0.02	0.38	0.10	0.89	0.17	1.20	0.13	1.24	0.14	0.74	0.00	0.00	0.00	0.23	0.00	0.00	0.00	0.00
291	19.9	0.34	0.00	0.64	0.00	0.40	0.00	0.46	0.16	0.66	0.24	1.12	0.27	2.49	0.00	1.62	0.00	4.03	0.00	0.00	0.00	0.00
301	20.0	0.69	0.00	1.07	0.00	1.01	0.00	0.40	0.00	0.28	0.00	0.45	0.00	0.86	0.00	0.46	0.00	1.71	0.00	0.00	0.00	0.00

Appendix 2

		n-Alkanes																			
Depth (cm)	Age cal ka BP	C16	C17	C18	C19	C20	C21	C22	C23	C24	C25	C26	C27	C28	C29	C30	C31	C32	C33	C34	C35
1	0.1	0.00	0.00	0.00	0.00	0.00	0.00	0.00	0.26	0.16	0.57	0.25	1.39	0.00	3.04	0.28	3.79	0.00	0.00	0.00	0.00
11	0.7	0.00	0.00	0.00	0.00	0.00	0.00	0.00	0.19	0.56	0.99	0.76	2.42	0.00	0.28	0.00	4.44	0.00	0.00	0.00	0.00
21	1.3	0.00	0.00	0.00	0.00	0.16	0.00	0.27	0.45	0.42	0.00	0.53	1.16	0.00	0.00	0.00	0.00	0.00	0.00	0.00	0.00
31	1.8	0.00	0.00	0.21	0.00	0.00	0.24	0.00	0.30	0.00	0.00	0.00	0.85	0.00	0.00	0.00	0.00	0.00	0.00	0.00	0.00
41	2.3	0.00	0.00	0.00	0.00	0.17	0.00	0.00	0.34	0.00	0.00	0.00	0.69	0.00	0.00	0.00	0.00	0.00	0.00	0.00	0.00
51	2.5	0.00	0.00	0.26	0.00	0.00	0.42	0.00	0.00	0.00	0.00	0.00	0.00	0.00	0.00	0.00	1.41	0.00	0.00	0.00	0.00
61	2.7	0.00	0.00	0.15	0.00	0.35	0.41	0.00	0.18	0.00	0.00	0.00	0.00	0.00	0.00	0.00	0.00	0.00	0.00	0.00	0.00
71	2.9	0.00	0.00	0.00	0.00	0.00	0.00	0.00	0.11	0.00	0.00	0.00	0.00	0.00	0.00	0.00	0.59	0.00	0.00	0.00	0.00
81	3.0	0.00	0.06	0.00	0.12	0.21	0.19	0.15	0.13	0.14	0.00	0.00	0.00	0.00	0.00	0.00	0.28	0.00	0.00	0.00	0.00
91	3.3	0.00	0.00	0.00	0.00	0.04	0.13	0.00	0.12	0.30	0.00	0.00	0.00	0.00	0.00	0.00	0.24	0.00	0.00	0.00	0.00
101	3.5	0.00	0.00	0.00	0.02	0.00	0.12	0.00	0.14	0.32	0.00	0.00	0.00	0.00	0.00	0.00	0.00	0.00	0.00	0.00	0.00
111	3.7	0.00	0.00	0.00	0.04	0.06	0.00	0.00	0.17	0.68	0.29	0.08	0.06	0.00	0.00	0.00	0.00	0.00	0.00	0.00	0.00
121	3.9	0.00	0.00	0.00	0.00	0.00	0.18	0.20	0.16	0.43	0.00	0.00	0.00	0.00	0.00	0.00	0.00	0.00	0.00	0.00	0.00
131	4.1	0.00	0.00	0.00	0.00	0.06	0.13	0.00	0.16	0.42	0.00	0.00	0.00	0.00	0.00	0.00	0.00	0.00	0.00	0.00	0.00
141	4.3	0.00	0.00	0.04	0.00	0.00	0.10	0.17	0.23	0.76	0.00	0.11	0.00	0.00	0.00	0.00	0.00	0.00	0.00	0.00	0.00
151	5.2	0.00	0.00	0.04	0.00	0.00	0.12	0.19	0.34	1.18	0.00	0.20	0.00	0.00	0.00	0.00	0.00	0.00	0.00	0.00	0.00
161	6.1	0.00	0.00	0.10	0.11	0.09	0.12	0.14	0.28	0.61	0.00	0.18	0.00	0.00	0.00	0.00	0.00	0.00	0.00	0.00	0.00
171	7.0	0.00	0.00	0.03	0.00	0.00	0.09	0.12	0.23	0.51	0.41	0.16	0.07	0.00	0.00	0.00	0.00	0.00	0.00	0.00	0.00
181	8.4	0.00	0.04	0.07	0.00	0.00	0.07	0.10	0.17	0.42	0.00	0.15	0.12	0.00	0.00	0.00	0.00	0.00	0.00	0.00	0.00
191	10.2	0.00	0.00	0.00	0.00	0.00	0.00	0.00	0.18	0.24	0.25	0.00	0.15	0.00	0.00	0.00	0.77	0.00	0.00	0.00	0.00
201	12.0	0.00	0.00	0.00	0.03	0.04	0.08	0.11	0.44	0.35	0.00	0.17	0.26	0.00	0.00	0.00	0.72	0.00	0.00	0.00	0.00
211	13.0	0.00	0.00	0.00	0.05	0.07	0.08	0.11	0.00	0.19	0.20	0.12	0.15	0.00	0.00	0.00	0.71	0.00	0.00	0.00	0.00
221	13.8	0.00	0.00	0.00	0.00	0.04	0.07	0.09	0.00	0.10	0.14	0.00	0.09	0.20	0.00	0.00	0.57	0.00	0.00	0.00	0.00
231	14.7	0.00	0.00	0.00	0.06	0.13	0.19	0.00	0.00	0.13	0.00	0.07	0.11	0.38	0.00	0.00	0.67	0.00	0.00	0.00	0.00
241	15.6	0.00	0.00	0.00	0.00	0.00	0.05	0.05	0.18	0.04	0.00	0.00	0.14	0.24	0.00	0.09	0.25	0.00	0.00	0.00	0.00
251	16.5	0.00	0.00	0.00	0.03	0.05	0.10	0.07	0.67	0.00	0.00	0.00	0.00	0.00	0.00	0.00	0.24	0.00	0.00	0.00	0.00
261	17.4	0.00	0.00	0.00	0.08	0.14	0.28	0.20	0.26	0.08	0.10	0.00	0.12	0.00	0.14	0.00	0.00	0.00	0.00	0.00	0.00
271	18.3	0.00	0.00	0.00	0.00	0.00	0.05	0.00	0.09	0.00	0.00	0.00	0.06	0.25	0.00	0.00	0.52	0.00	0.00	0.00	0.00
281	19.1	0.00	0.00	0.00	0.00	0.07	0.13	0.11	0.28	0.00	0.07	0.00	0.00	0.28	0.00	0.00	0.45	0.00	0.00	0.00	0.00
291	19.9	0.00	0.00	0.00	0.00	0.00	0.16	0.00	0.00	0.46	0.00	0.59	0.88	2.28	0.00	0.00	3.27	0.00	1.49	0.00	0.00
301	20.0	0.00	0.00	0.00	0.00	1.07	0.33	0.00	0.00	0.54	0.00	0.00	0.67	0.00	0.00	0.00	1.86	0.00	0.00	0.00	0.00

Appendix 2

		Methyl Ketones															Sterols					
Depth (cm)	Age cal ka BP	C19	C20	C21	C22	C23	C24	C25	C26	C27	C28	C29	C30	C31	C32	C33	C26Δ 5,22	C26Δ 22	Copro stanol	Epich olesta nol	Epico pro-stanol	C27Δ 5,22
1	0.1	0.00	0.00	0.00	0.00	0.00	0.00	0.00	0.00	0.00	0.00	0.00	0.00	0.00	0.00	0.00	0.00	0.00	0.00	0.00	0.00	0.00
11	0.7	0.00	0.00	0.00	0.00	0.33	0.17	0.24	0.00	0.84	0.71	0.00	0.51	1.65	0.00	0.00	0.00	0.00	0.00	0.00	0.00	0.00
21	1.3	0.00	0.00	0.00	0.00	0.00	0.43	0.00	0.00	0.00	0.00	0.00	0.00	0.00	0.00	0.00	0.00	0.00	0.00	0.00	0.00	0.00
31	1.8	0.00	0.00	0.00	0.00	0.00	0.11	0.59	0.00	0.00	0.00	0.00	0.00	0.00	0.00	0.00	0.00	0.00	0.00	0.00	0.00	0.00
41	2.3	0.00	0.00	0.00	0.00	0.00	0.00	0.44	0.00	0.00	0.00	0.00	0.00	0.00	0.00	0.00	0.00	0.00	0.00	0.00	0.00	0.00
51	2.5	0.00	0.00	0.00	0.00	0.24	0.14	0.49	0.00	0.00	0.00	0.00	0.00	0.00	0.00	0.00	0.00	0.00	0.00	0.00	0.00	0.00
61	2.7	0.00	0.00	0.00	0.00	0.00	0.00	0.41	0.00	0.00	0.00	0.00	0.00	0.00	0.00	0.00	0.00	0.00	0.00	0.00	0.00	0.00
71	2.9	0.00	0.00	0.00	0.00	0.20	0.00	0.44	0.00	0.00	0.00	0.00	0.00	0.00	0.00	0.00	0.00	0.00	0.00	0.00	0.00	0.00
81	3.0	0.00	0.00	0.00	0.00	0.10	0.14	0.28	0.00	0.39	0.00	0.00	0.00	0.00	0.00	0.00	0.00	0.00	0.00	0.00	0.00	0.00
91	3.3	0.00	0.00	0.00	0.00	0.16	0.12	0.36	0.00	0.00	0.00	0.00	0.00	0.00	0.00	0.00	0.00	0.00	0.00	0.00	0.00	0.00
101	3.5	0.00	0.00	0.00	0.00	0.14	0.10	0.39	0.00	0.81	0.00	0.00	0.00	0.00	0.00	0.00	0.00	0.00	0.00	0.00	0.00	0.00
111	3.7	0.00	0.00	0.00	0.00	0.16	0.11	0.41	0.00	0.72	0.00	0.23	0.00	0.00	0.00	0.00	0.00	0.00	0.00	0.00	0.00	0.00
121	3.9	0.00	0.00	0.00	0.00	0.20	0.23	0.57	0.00	1.40	0.00	0.23	0.00	0.00	0.00	0.00	0.00	0.00	0.00	0.00	0.00	0.00
131	4.1	0.00	0.00	0.00	0.00	0.13	0.16	0.40	0.00	1.09	0.27	0.25	0.00	0.00	0.00	0.00	0.00	0.00	0.00	0.00	0.00	0.00
141	4.3	0.00	0.00	0.00	0.00	0.12	0.17	0.56	0.00	1.71	0.20	0.37	0.00	0.00	0.00	0.00	0.00	0.00	0.00	0.00	0.00	0.00
151	5.2	0.00	0.00	0.00	0.00	0.08	0.25	0.69	0.00	2.01	0.40	0.45	0.00	0.00	0.00	0.00	0.00	0.00	0.00	0.00	0.00	0.00
161	6.1	0.00	0.00	0.00	0.00	0.23	0.18	0.64	0.00	2.30	0.46	0.60	0.00	0.00	0.00	0.00	0.00	0.00	0.00	0.00	0.00	0.00
171	7.0	0.00	0.00	0.00	0.07	0.13	0.21	0.54	0.00	1.91	0.41	0.56	0.00	0.00	0.00	0.00	0.00	0.00	0.00	0.00	0.00	0.00
181	8.4	0.00	0.00	0.00	0.00	0.11	0.19	0.45	0.00	1.83	0.43	0.59	0.00	0.00	0.00	0.00	0.00	0.00	0.00	0.00	0.00	0.00
191	10.2	0.00	0.00	0.00	0.00	0.08	0.12	0.34	0.00	1.03	0.27	0.00	0.00	0.00	0.08	0.00	0.00	0.00	0.00	0.00	0.00	0.00
201	12.0	0.00	0.00	0.00	0.00	0.12	0.15	0.40	0.00	1.35	0.43	0.00	0.10	0.00	0.00	0.00	0.00	0.00	0.00	0.00	0.00	0.00
211	13.0	0.00	0.00	0.00	0.02	0.17	0.15	0.39	0.00	0.91	0.34	0.00	0.13	0.00	0.00	0.00	0.00	0.00	0.00	0.00	0.00	0.00
221	13.8	0.00	0.00	0.00	0.00	0.17	0.11	0.34	0.00	0.42	0.27	0.00	0.09	0.00	0.00	0.00	0.00	0.00	0.00	0.00	0.00	0.00
231	14.7	0.00	0.00	0.00	0.00	0.87	0.16	0.78	0.00	0.00	0.00	0.00	0.00	0.00	0.00	0.00	0.00	0.00	0.00	0.00	0.00	0.00
241	15.6	0.00	0.00	0.00	0.00	0.25	0.07	0.38	0.14	0.27	0.00	0.06	0.00	0.00	0.00	0.40	0.00	0.00	0.00	0.00	0.00	0.00
251	16.5	0.00	0.00	0.00	0.00	0.55	0.00	0.51	0.00	0.36	0.00	0.00	0.00	0.00	0.00	0.00	0.00	0.00	0.00	0.00	0.00	0.00
261	17.4	0.07	0.00	0.00	0.00	0.00	0.15	1.91	0.09	0.21	0.00	0.00	0.00	0.00	0.00	0.00	0.00	0.00	0.00	0.00	0.00	0.00
271	18.3	0.00	0.00	0.00	0.00	0.29	0.08	0.37	0.00	0.18	0.00	0.00	0.00	0.00	0.00	0.24	0.00	0.00	0.00	0.00	0.00	0.00
281	19.1	0.00	0.00	0.00	0.10	0.77	0.16	1.38	0.00	0.38	0.12	0.00	0.00	0.00	0.00	0.00	0.00	0.00	0.00	0.00	0.00	0.00
291	19.9	0.00	0.00	0.00	0.00	0.00	0.00	0.45	0.00	0.98	1.15	0.00	0.54	0.00	0.25	0.51	0.00	0.00	0.00	0.00	0.00	0.00
301	20.0	0.00	0.00	0.00	0.00	0.00	0.00	0.38	0.00	1.41	0.60	0.00	0.39	0.66	0.00	0.00	0.00	0.00	0.00	0.00	0.00	0.00

Appendix 2

		Sterols																				
Depth (cm)	Age cal ka BP	C27Δ 22	Cholesterol	Cholestanol	C28Δ 5	C28Δ 0	Brassicasterol	C28Δ 22	C28Δ 5,X	C29Δ 5,22	Stigmasterol	C29Δ 22	C29Δ 22 isom.	Sitosterol, C29Δ	C29Δ 5 isom.	Stigmastanol	Dinosterol	Dinosterol isom.	Dinostanol	Dinostanol isom.	C30Δ	branched C15
1	0.1	0.00	0.00	0.00	0.00	0.00	0.00	0.00	0.00	0.00	0.00	0.00	0.00	2.73	0.00	0.00	0.00	0.00	0.00	0.00	0.00	0.00
11	0.7	0.00	0.00	0.00	0.00	0.00	0.00	0.00	0.00	0.00	0.45	0.00	0.00	0.00	0.00	0.00	0.00	0.00	0.00	0.00	0.00	0.00
21	1.3	0.00	0.00	0.00	0.63	0.00	0.00	0.00	0.00	0.00	0.00	0.00	0.00	0.00	0.00	0.00	0.00	0.00	0.00	0.00	0.00	0.00
31	1.8	0.00	0.00	0.00	0.00	0.00	0.00	0.00	0.00	0.00	0.00	0.00	0.00	0.00	0.00	0.00	0.00	0.00	0.00	0.00	0.00	0.00
41	2.3	0.00	0.00	0.00	0.00	0.00	0.00	0.00	0.00	0.00	0.00	0.00	0.00	0.00	0.00	0.00	0.00	0.00	0.00	0.00	0.00	0.00
51	2.5	0.00	0.00	0.00	0.00	0.00	0.00	0.00	0.00	0.00	0.00	0.00	0.00	1.63	0.00	0.00	0.00	0.00	0.00	0.00	0.00	0.00
61	2.7	0.00	0.00	0.00	0.00	0.00	0.00	0.00	0.00	0.00	0.00	0.00	0.00	0.00	0.00	0.00	0.00	0.00	0.00	0.00	0.00	0.00
71	2.9	0.00	0.00	0.00	0.00	0.00	0.00	0.00	0.00	0.00	0.00	0.00	0.00	1.32	0.00	0.00	0.00	0.00	0.00	0.00	0.00	0.00
81	3.0	0.00	0.00	0.00	0.00	0.00	0.00	0.00	0.00	0.00	0.00	0.00	0.00	0.00	0.00	0.00	0.00	0.00	0.00	0.00	0.00	0.00
91	3.3	0.00	0.00	0.00	0.00	0.00	0.00	0.00	0.00	0.00	0.00	0.00	0.00	0.00	0.00	0.00	0.00	0.00	0.00	0.00	0.00	0.00
101	3.5	0.00	0.00	0.00	0.00	0.00	0.00	0.00	0.00	0.00	0.00	0.00	0.00	0.00	0.00	0.00	0.00	0.00	0.00	0.00	0.00	0.00
111	3.7	0.00	0.00	0.00	0.00	0.00	0.00	0.00	0.00	0.00	0.00	0.00	0.00	0.37	0.00	0.00	0.00	0.00	0.00	0.00	0.00	0.00
121	3.9	0.00	0.00	0.00	0.00	0.00	0.00	0.00	0.00	0.00	0.00	0.00	0.00	0.00	0.00	0.00	0.00	0.00	0.00	0.00	0.00	0.00
131	4.1	0.00	0.00	0.00	0.00	0.00	0.00	0.00	0.00	0.00	0.00	0.00	0.00	0.21	0.00	0.00	0.00	0.00	0.00	0.00	0.00	0.00
141	4.3	0.00	0.00	0.00	0.00	0.00	0.00	0.00	0.00	0.00	0.00	0.00	0.00	0.00	0.00	0.00	0.00	0.00	0.00	0.00	0.00	0.00
151	5.2	0.00	0.00	0.00	0.00	0.00	0.00	0.00	0.00	0.00	0.00	0.00	0.00	0.63	0.00	0.00	0.00	0.00	0.00	0.00	0.00	0.00
161	6.1	0.00	0.00	0.00	0.00	0.00	0.00	0.00	0.00	0.00	0.00	0.00	0.00	0.00	0.00	0.00	0.00	0.00	0.00	0.00	0.00	0.00
171	7.0	0.00	0.00	0.00	0.00	0.00	0.00	0.00	0.00	0.00	0.00	0.00	0.00	0.48	0.00	0.00	0.00	0.00	0.00	0.00	0.00	0.00
181	8.4	0.00	0.00	0.00	0.00	0.00	0.00	0.00	0.00	0.00	0.00	0.00	0.00	0.00	0.00	0.00	0.00	0.00	0.00	0.00	0.00	0.00
191	10.2	0.00	0.00	0.00	0.00	0.00	0.00	0.00	0.00	0.00	0.00	0.00	0.00	0.00	0.00	0.00	0.00	0.00	0.00	0.00	0.00	0.00
201	12.0	0.00	0.00	0.00	0.00	0.00	0.00	0.00	0.00	0.00	0.00	0.00	0.00	0.00	0.00	0.00	0.00	0.00	0.00	0.00	0.00	0.00
211	13.0	0.00	0.00	0.00	0.00	0.00	0.00	0.00	0.00	0.00	0.00	0.00	0.00	0.00	0.00	0.00	0.00	0.00	0.00	0.00	0.00	0.00
221	13.8	0.00	0.00	0.00	0.00	0.00	0.00	0.00	0.00	0.00	0.00	0.00	0.00	0.00	0.00	0.00	0.00	0.00	0.00	0.00	0.00	0.00
231	14.7	0.00	0.00	0.00	0.00	0.00	0.00	0.00	0.00	0.00	0.00	0.00	0.00	0.00	0.00	0.00	0.00	0.00	0.00	0.00	0.00	0.00
241	15.6	0.00	0.00	0.00	0.00	0.00	0.00	0.00	0.00	0.00	0.00	0.00	0.00	0.00	0.00	0.00	0.00	0.00	0.00	0.00	0.00	0.00
251	16.5	0.00	0.00	0.00	0.00	0.00	0.00	0.00	0.00	0.00	0.00	0.00	0.00	0.00	0.00	0.00	0.00	0.00	0.00	0.00	0.00	0.00
261	17.4	0.00	0.00	0.00	0.00	0.00	0.00	0.00	0.00	0.00	0.00	0.00	0.00	1.43	0.00	0.76	0.00	0.00	0.00	0.00	0.00	0.00
271	18.3	0.00	0.00	0.00	0.00	0.00	0.00	0.00	0.00	0.00	0.00	0.00	0.00	0.00	0.00	0.00	0.00	0.00	0.00	0.00	0.00	0.00
281	19.1	0.00	0.00	0.00	0.00	0.00	0.00	0.00	0.00	0.00	0.00	0.00	0.00	0.00	0.00	0.00	0.00	0.00	0.00	0.00	0.00	0.00
291	19.9	0.00	0.00	0.00	0.00	0.00	0.00	0.00	0.00	0.00	0.00	0.00	0.00	0.00	0.00	0.00	0.00	0.00	0.00	0.00	0.00	0.00
301	20.0	0.00	0.00	0.00	0.00	0.00	0.00	0.00	0.00	0.00	0.00	0.00	0.00	0.00	0.00	0.00	0.00	0.00	0.00	0.00	0.00	0.00

Appendix 2

		Others																				
Depth (cm)	Age cal ka BP	branched C15	branched C16	phytodiene	branched C19	branched C17	branched C17	branched C18	branched C18	branched C19	branched C19	dimethyl hexa	9-MeO-15:0	branched C20	branched C20	branched C21	branched C21	9-MeO-17:0	dimethyl 1,18-	branched C22	dimethyl nona	branched C24
1	0.1	0.00	0.00	0.00	0.00	0.00	0.00	0.00	0.00	0.00	0.00	0.00	0.00	0.00	0.00	0.00	0.00	0.00	0.00	0.00	0.00	0.00
11	0.7	0.00	0.00	0.00	0.00	0.00	0.00	0.00	0.00	0.00	0.00	0.00	0.00	0.00	0.00	0.00	0.00	0.00	0.00	0.00	0.00	0.00
21	1.3	0.00	0.00	0.00	0.00	0.00	0.00	0.00	0.00	0.00	0.00	0.00	0.00	0.00	0.00	0.00	0.00	0.00	0.00	0.00	0.00	0.00
31	1.8	0.00	0.00	0.00	0.00	0.00	0.00	0.00	0.00	0.00	0.00	0.00	0.00	0.00	0.00	0.00	0.00	0.00	0.00	0.00	0.00	0.00
41	2.3	0.00	0.00	0.00	0.00	0.00	0.00	0.00	0.00	0.00	0.00	0.00	0.00	0.00	0.00	0.00	0.00	0.00	0.00	0.00	0.00	0.00
51	2.5	0.00	0.00	0.00	0.00	0.00	0.00	0.00	0.00	0.00	0.00	0.00	0.00	0.00	0.00	0.00	0.00	0.00	0.00	0.00	0.00	0.00
61	2.7	0.00	0.00	0.00	0.00	0.00	0.00	0.00	0.00	0.00	0.00	0.00	0.00	0.00	0.00	0.00	0.00	0.00	0.00	0.00	0.00	0.00
71	2.9	0.00	0.00	0.00	0.00	0.00	0.00	0.00	0.00	0.00	0.00	0.00	0.00	0.00	0.00	0.00	0.00	0.00	0.00	0.00	0.00	0.00
81	3.0	0.00	0.00	0.00	0.00	0.00	0.00	0.00	0.00	0.00	0.00	0.00	0.00	0.00	0.00	0.00	0.00	0.00	0.00	0.00	0.00	0.00
91	3.3	0.00	0.00	0.00	0.00	0.00	0.00	0.00	0.00	0.00	0.00	0.00	0.00	0.00	0.00	0.00	0.00	0.00	0.00	0.00	0.00	0.00
101	3.5	0.00	0.00	0.00	0.00	0.00	0.00	0.00	0.00	0.00	0.00	0.00	0.00	0.00	0.00	0.00	0.00	0.00	0.00	0.00	0.00	0.00
111	3.7	0.00	0.00	0.00	0.00	0.00	0.00	0.00	0.00	0.00	0.00	0.00	0.00	0.00	0.00	0.00	0.00	0.00	0.00	0.00	0.00	0.00
121	3.9	0.00	0.00	0.00	0.00	0.00	0.00	0.00	0.00	0.00	0.00	0.00	0.00	0.00	0.00	0.00	0.00	0.00	0.00	0.00	0.00	0.00
131	4.1	0.00	0.00	0.00	0.00	0.00	0.00	0.00	0.00	0.00	0.00	0.00	0.00	0.00	0.00	0.00	0.00	0.00	0.00	0.00	0.00	0.00
141	4.3	0.00	0.00	0.00	0.00	0.00	0.00	0.00	0.00	0.00	0.00	0.00	0.00	0.00	0.00	0.00	0.00	0.00	0.00	0.00	0.00	0.00
151	5.2	0.00	0.00	0.00	0.00	0.00	0.00	0.00	0.00	0.00	0.00	0.00	0.00	0.00	0.00	0.00	0.00	0.00	0.00	0.00	0.00	0.00
161	6.1	0.00	0.00	0.00	0.00	0.00	0.00	0.00	0.00	0.00	0.00	0.00	0.00	0.00	0.00	0.00	0.00	0.00	0.00	0.00	0.00	0.00
171	7.0	0.00	0.00	0.00	0.00	0.00	0.00	0.00	0.00	0.00	0.00	0.00	0.00	0.00	0.00	0.00	0.00	0.00	0.00	0.00	0.00	0.00
181	8.4	0.00	0.00	0.00	0.00	0.00	0.00	0.00	0.00	0.00	0.00	0.00	0.00	0.00	0.00	0.00	0.00	0.00	0.00	0.00	0.00	0.00
191	10.2	0.00	0.00	0.00	0.00	0.00	0.00	0.00	0.00	0.00	0.00	0.00	0.00	0.00	0.00	0.00	0.00	0.00	0.00	0.00	0.00	0.00
201	12.0	0.00	0.00	0.00	0.00	0.00	0.00	0.00	0.00	0.00	0.00	0.00	0.00	0.00	0.00	0.00	0.00	0.00	0.00	0.00	0.00	0.00
211	13.0	0.00	0.00	0.00	0.00	0.00	0.00	0.00	0.00	0.00	0.00	0.01	0.00	0.00	0.00	0.00	0.00	0.00	0.00	0.00	0.00	0.00
221	13.8	0.00	0.00	0.00	0.00	0.00	0.00	0.00	0.00	0.00	0.00	0.00	0.00	0.00	0.00	0.00	0.00	0.00	0.00	0.00	0.00	0.00
231	14.7	0.00	0.00	0.00	0.00	0.00	0.00	0.00	0.00	0.00	0.00	0.00	0.00	0.00	0.00	0.00	0.00	0.00	0.00	0.00	0.00	0.00
241	15.6	0.00	0.00	0.00	0.00	0.00	0.00	0.00	0.00	0.00	0.00	0.25	0.00	0.00	0.00	0.00	0.00	0.00	0.10	0.00	0.00	0.00
251	16.5	0.00	0.00	0.00	0.00	0.00	0.00	0.00	0.00	0.00	0.00	0.00	0.00	0.00	0.00	0.00	0.00	0.00	0.00	0.00	0.00	0.00
261	17.4	0.00	0.00	0.00	0.00	0.00	0.00	0.00	0.00	0.00	0.00	0.00	0.00	0.00	0.00	0.00	0.00	0.00	0.00	0.00	0.00	0.00
271	18.3	0.00	0.00	0.00	0.00	0.00	0.00	0.00	0.00	0.00	0.00	0.00	0.00	0.00	0.00	0.00	0.00	0.00	0.00	0.00	0.00	0.00
281	19.1	0.00	0.00	0.00	0.00	0.00	0.00	0.00	0.00	0.00	0.00	0.00	0.00	0.00	0.00	0.00	0.00	0.00	0.00	0.00	0.00	0.00
291	19.9	0.00	0.00	0.00	0.00	0.00	0.00	0.00	0.00	0.00	0.00	0.00	0.00	0.00	0.00	0.00	0.00	0.00	0.00	0.00	0.00	0.00
301	20.0	0.00	0.00	0.00	0.00	0.00	0.00	0.00	0.00	0.00	0.00	0.00	0.00	0.00	0.00	0.00	0.00	0.00	0.00	0.00	0.00	0.00

Appendix 2

		Others																			
Depth (cm)	Age cal ka BP	dimethyl icosa	dimethyl henic	dimethyl doco	8,14-seco hopa	8,14-seco hopa	dimethyl tricos	α-tocopherol	dimethyl tetra	dimethyl tetra	C_{24} keto-ol	11-MeO-19:0	C28 triterpane	8,14-seco hopa	cholesta-3,5-	hopanoid	8,14-seco hopa	C27 hopane	cholest-4-ene-3-	onocerane III	13-MeO-21:0	C29 α,β hopa
1	0.1	0.00	0.00	0.00	0.00	0.00	0.00	0.00	0.00	0.00	0.00	0.00	0.00	0.00	0.00	0.00	0.00	0.00	0.00	0.00	0.00	0.00
11	0.7	0.00	0.00	0.00	0.00	0.00	0.00	0.00	0.00	0.00	0.00	0.00	0.00	0.00	0.00	0.00	0.00	0.00	0.00	0.00	0.00	0.00
21	1.3	0.00	0.00	0.00	0.00	0.00	0.00	0.00	0.00	0.00	0.00	0.00	0.00	0.00	0.00	0.00	0.00	0.00	0.00	0.00	0.00	0.00
31	1.8	0.00	0.00	0.00	0.00	0.00	0.00	0.00	0.00	0.00	0.00	0.00	0.00	0.00	0.00	0.00	0.00	0.00	0.00	0.00	0.00	0.00
41	2.3	0.00	0.00	0.00	0.00	0.00	0.00	0.00	0.00	0.00	0.00	0.00	0.00	0.00	0.00	0.00	0.00	0.00	0.00	0.00	0.00	0.00
51	2.5	0.00	0.00	0.00	0.00	0.00	0.00	0.00	0.00	0.00	0.00	0.00	0.00	0.00	0.00	0.00	0.00	0.00	0.00	0.00	0.00	0.00
61	2.7	0.00	0.00	0.00	0.00	0.00	0.00	0.00	0.00	0.00	0.00	0.00	0.00	0.00	0.00	0.00	0.00	0.00	0.00	0.00	0.00	0.00
71	2.9	0.00	0.00	0.00	0.00	0.00	0.00	0.00	0.00	0.00	0.00	0.00	0.00	0.00	0.00	2.70	0.00	0.00	0.00	0.00	0.00	0.00
81	3.0	0.00	0.00	0.00	0.00	0.00	0.00	0.00	0.00	0.00	0.00	0.00	0.00	0.00	0.00	0.00	0.00	0.00	0.00	0.00	0.00	0.00
91	3.3	0.00	0.00	0.00	0.00	0.00	0.00	0.00	0.00	0.00	0.00	0.00	0.00	0.00	0.00	0.94	0.00	0.00	0.00	0.00	0.00	0.00
101	3.5	0.00	0.00	0.00	0.00	0.00	0.00	0.00	0.00	0.00	0.00	0.00	0.00	0.00	0.00	1.20	0.00	0.00	0.00	0.00	0.00	0.00
111	3.7	0.00	0.00	0.00	0.00	0.00	0.00	0.00	0.00	0.00	0.00	0.00	0.00	0.00	0.00	0.43	0.00	0.00	0.00	0.00	0.00	0.00
121	3.9	0.00	0.00	0.00	0.00	0.00	0.00	0.00	0.00	0.00	0.00	0.00	0.00	0.00	0.00	1.15	0.00	0.00	0.00	0.00	0.00	0.00
131	4.1	0.00	0.00	0.00	0.00	0.00	0.00	0.00	0.00	0.00	0.00	0.00	0.00	0.00	0.00	0.95	0.00	0.00	0.00	0.00	0.00	0.00
141	4.3	0.00	0.00	0.00	0.00	0.00	0.00	0.00	0.00	0.00	0.00	0.00	0.00	0.00	0.00	0.39	0.00	0.00	0.00	0.00	0.00	0.00
151	5.2	0.00	0.00	0.00	0.00	0.00	0.00	0.00	0.00	0.00	0.00	0.00	0.00	0.00	0.00	0.41	0.00	0.00	0.00	0.00	0.00	0.00
161	6.1	0.00	0.00	0.00	0.00	0.00	0.00	0.00	0.00	0.00	0.00	0.00	0.00	0.00	0.00	0.00	0.00	0.00	0.00	0.00	0.00	0.00
171	7.0	0.00	0.00	0.00	0.00	0.00	0.00	0.00	0.00	0.00	0.00	0.00	0.00	0.00	0.00	0.00	0.00	0.00	0.00	0.00	0.00	0.00
181	8.4	0.09	0.00	0.00	0.00	0.00	0.00	0.00	0.00	0.00	0.00	0.00	0.00	0.00	0.00	0.00	0.00	0.00	0.00	0.00	0.00	0.00
191	10.2	0.10	0.00	0.00	0.00	0.00	0.00	0.00	0.00	0.00	0.00	0.00	0.00	0.00	0.00	1.27	0.00	0.00	0.00	0.00	0.00	0.00
201	12.0	0.00	0.00	0.00	0.00	0.00	0.00	0.00	0.00	0.00	0.00	0.00	0.00	0.00	0.00	0.00	0.00	0.00	0.00	0.00	0.00	0.00
211	13.0	0.00	0.00	0.24	0.00	0.00	0.24	0.00	1.03	0.62	0.00	0.00	0.00	0.00	0.00	0.00	0.00	0.00	0.00	0.00	0.00	0.00
221	13.8	0.17	0.14	0.41	0.00	0.00	0.62	0.00	1.43	1.02	0.00	0.00	0.00	0.00	0.00	0.00	0.00	0.00	0.00	0.00	0.00	0.00
231	14.7	0.00	0.00	0.28	0.00	0.00	0.37	0.00	1.08	0.91	0.00	0.00	0.00	0.00	0.00	0.00	0.00	0.00	0.00	0.00	0.00	0.00
241	15.6	0.08	0.07	0.31	0.00	0.00	0.39	0.00	1.16	1.02	0.00	0.00	0.00	0.00	0.00	0.00	0.00	0.00	0.00	0.00	0.00	0.00
251	16.5	0.00	0.00	0.54	0.00	0.00	0.00	0.00	1.81	1.23	0.00	0.00	0.00	0.00	0.00	0.00	0.00	0.00	0.00	0.00	0.00	0.00
261	17.4	0.00	0.00	0.22	0.00	0.00	0.00	0.00	0.55	0.00	0.00	0.00	0.00	0.00	0.00	0.00	0.00	0.00	0.00	0.00	0.00	0.00
271	18.3	0.06	0.07	0.31	0.00	0.00	0.26	0.00	1.00	0.57	0.00	0.00	0.00	0.00	0.00	0.00	0.00	0.00	0.00	0.00	0.00	0.00
281	19.1	0.00	0.00	0.17	0.00	0.00	0.15	0.00	0.43	0.34	0.00	0.00	0.00	0.00	0.00	0.00	0.00	0.00	0.00	0.00	0.00	0.00
291	19.9	0.00	0.00	0.00	0.00	0.00	0.00	0.00	0.00	0.00	0.00	0.00	0.00	0.00	0.00	0.00	0.00	0.00	0.00	0.00	0.00	0.00
301	20.0	0.00	0.00	0.00	0.00	0.00	0.00	0.00	0.00	0.00	0.00	0.00	0.00	0.00	0.00	0.00	0.00	0.00	0.00	0.00	0.00	0.00

Appendix 2

		Others																				
Depth (cm)	Age cal ka BP	C28 β,β hopa	C30 α,β hopa	C31 α,β R hopa	β-amyrin	dimethyl tetra	(taraxerol)	12-OH(ω17)-	α-amyrin	dimethyl tetra	onocerane IV	dimethyl tetra	friedoole	1,15(ω16) C_{30}ke	triacontane-	dimethyl tetra	dimethyl tetra	dimethyl tetra	C_{32}keto-ol	17β(H),21β(H)bis	ββ-hopanoic	dimethyl tetra
1	0.1	0.00	0.00	0.00	0.00	0.00	0.00	0.00	0.00	0.00	0.00	0.00	0.00	0.00	0.00	0.00	0.00	0.00	0.00	0.00	0.00	0.00
11	0.7	0.00	0.00	0.00	0.00	0.00	0.00	0.00	0.00	0.00	0.00	0.00	0.00	0.00	0.00	0.00	0.00	0.00	0.00	0.00	0.00	0.00
21	1.3	0.00	0.00	0.00	7.15	0.00	0.00	0.00	8.89	0.00	5.20	0.00	0.00	0.00	0.00	0.00	0.00	0.00	0.00	0.99	2.17	0.00
31	1.8	0.00	0.00	0.00	1.55	0.00	0.00	0.00	6.45	0.00	0.00	0.00	0.00	0.00	0.00	0.00	0.00	0.00	0.00	0.00	1.56	0.00
41	2.3	0.00	0.00	0.00	2.05	0.00	0.00	0.00	0.00	0.00	0.00	0.00	3.99	0.00	0.00	0.00	0.00	0.00	0.00	0.00	0.00	0.00
51	2.5	0.00	0.00	0.00	1.85	0.00	0.00	0.00	5.28	0.00	0.00	0.00	0.00	0.00	0.00	0.00	0.00	0.00	0.00	0.00	1.09	0.00
61	2.7	0.00	0.00	0.00	2.69	0.00	0.00	0.00	1.82	0.00	0.00	0.00	0.00	0.00	0.00	0.00	0.00	0.00	0.00	0.00	0.00	0.00
71	2.9	0.88	0.00	0.00	2.70	0.00	0.00	0.00	4.89	0.00	0.00	0.00	0.00	0.00	0.00	0.00	0.00	0.00	0.00	0.00	0.60	0.00
81	3.0	0.48	0.00	0.00	2.90	0.00	0.00	0.00	5.35	0.00	0.00	12.24	0.00	0.00	0.00	0.00	0.00	0.00	0.00	0.00	0.29	0.00
91	3.3	0.00	0.00	0.00	4.48	0.00	0.00	0.00	4.76	0.00	8.83	0.00	0.00	0.00	0.00	0.00	0.00	0.00	0.00	0.00	0.49	0.00
101	3.5	0.00	0.00	0.00	9.08	0.00	0.00	0.00	2.57	0.00	14.62	0.00	0.00	0.00	0.00	0.00	0.00	0.00	0.00	0.00	0.42	0.00
111	3.7	0.00	0.04	0.00	13.15	0.00	0.45	0.00	1.64	0.00	0.00	0.00	0.00	0.00	0.00	0.00	0.00	0.00	0.00	0.00	0.00	0.00
121	3.9	0.00	0.00	0.00	5.11	0.00	0.00	0.00	1.75	0.00	16.04	0.00	0.00	0.00	0.00	0.00	0.00	0.00	0.00	0.00	0.00	0.00
131	4.1	0.00	0.00	0.00	4.73	0.00	0.00	0.00	0.46	0.00	0.00	0.00	0.00	0.00	0.00	0.00	0.00	0.00	0.00	0.00	0.00	0.00
141	4.3	0.00	0.00	0.00	4.79	0.00	0.00	0.00	0.58	0.00	10.63	0.00	0.00	0.00	0.00	0.00	0.00	0.00	0.00	0.00	0.00	0.00
151	5.2	0.00	0.00	0.00	5.85	0.00	1.05	0.00	0.70	0.00	0.00	0.00	0.00	0.00	0.00	0.00	0.00	0.00	0.00	0.00	0.00	0.00
161	6.1	0.00	0.00	0.00	4.37	0.00	0.00	0.00	1.02	0.00	0.00	0.00	0.00	0.00	0.00	0.00	0.00	0.00	0.00	0.00	0.00	0.00
171	7.0	0.00	0.00	0.00	2.22	0.00	0.00	0.00	0.86	0.00	0.00	0.00	0.00	0.00	0.00	0.00	0.00	0.00	0.00	0.00	0.00	0.00
181	8.4	0.00	0.00	0.00	4.37	0.00	0.00	0.00	1.20	0.00	0.00	0.00	0.00	0.00	0.00	0.00	0.00	0.00	0.00	0.00	0.00	0.00
191	10.2	0.00	0.00	0.00	3.82	0.00	0.00	0.00	2.96	0.00	0.00	0.00	0.00	0.00	0.00	0.00	0.00	0.00	0.00	0.00	0.00	0.00
201	12.0	0.00	0.00	0.00	0.69	0.00	0.00	0.00	4.40	0.00	3.88	0.00	0.00	0.00	0.00	0.00	0.00	0.00	0.00	0.00	0.00	0.00
211	13.0	0.00	0.00	0.00	0.38	1.29	0.00	0.00	5.79	0.72	0.00	1.33	0.00	0.00	0.00	0.57	0.64	0.40	0.00	0.00	0.00	0.23
221	13.8	0.00	0.00	0.00	0.00	1.96	0.00	0.00	6.13	1.27	0.00	2.26	0.00	0.00	0.00	0.87	0.98	0.45	0.00	0.00	0.00	0.31
231	14.7	0.00	0.00	0.00	0.38	2.49	0.00	0.00	4.29	1.24	0.00	2.09	0.00	0.00	0.00	0.48	0.68	0.32	0.00	0.00	0.00	0.13
241	15.6	0.00	0.06	0.00	0.00	2.49	0.00	0.00	3.50	1.29	0.00	2.84	0.00	0.00	0.00	0.50	0.72	0.32	0.00	0.00	0.25	0.14
251	16.5	0.00	0.00	0.00	0.00	3.02	0.00	0.00	6.32	1.29	0.00	2.70	0.00	0.00	0.00	0.49	0.70	0.00	0.00	0.00	0.05	0.00
261	17.4	0.00	0.00	0.00	0.28	0.68	0.00	0.00	8.68	0.00	0.00	0.34	0.00	0.00	0.00	0.00	0.00	0.00	0.00	0.56	0.00	0.00
271	18.3	0.00	0.00	0.00	0.00	1.73	0.00	0.00	2.56	0.67	0.00	1.76	0.00	0.00	0.00	0.21	0.42	0.09	0.00	0.00	0.31	0.10
281	19.1	0.00	0.00	0.00	0.00	0.99	0.00	0.00	4.70	0.55	0.00	1.02	0.00	0.00	0.00	0.16	0.26	0.00	0.00	0.00	0.31	0.00
291	19.9	0.00	0.00	0.00	0.00	0.00	0.00	0.00	7.64	0.00	0.00	0.00	0.00	0.00	0.00	0.00	0.00	0.00	0.00	0.00	0.61	0.00
301	20.0	0.00	0.00	0.00	0.00	0.00	0.00	0.00	2.35	0.00	0.00	0.00	0.00	0.00	0.00	0.00	0.00	0.00	0.00	0.00	0.00	0.00

Appendix 3

		Isoprenoidal GDGTs						Branched GDGTS														
Depth (cm)	Age cal ka BP	GDGT-0	GDGT-1	GDGT-2	GDGT-3	Cren.	Cren. Iso	I a	I b	I c	II a	II a'	II b	II b'	II c	II c'	III a	III a'	III b	III b'	III c	III c'
1	0.1	16.08	8.00	2.91	1.54	11.05	1.88	7.40	9.59	1.64	5.57	8.37	5.64	7.92	0.43	1.41	2.82	4.89	0.45	1.78	0.14	0.47
11	0.7	16.39	9.62	3.48	1.64	12.12	1.63	6.76	8.95	2.07	4.24	7.22	5.97	7.54	0.51	1.65	2.69	4.55	0.52	1.82	0.15	0.48
21	1.3	8.30	2.88	1.49	1.16	10.30	0.72	7.95	16.40	4.24	4.84	7.85	6.79	12.42	0.90	2.23	2.64	4.68	0.59	2.68	0.18	0.75
31	1.8	12.60	5.35	2.21	1.04	7.97	1.25	8.23	11.95	3.34	6.11	7.41	9.46	8.59	0.99	1.95	2.89	4.91	0.89	2.06	0.25	0.54
41	2.3	15.43	6.62	2.27	1.15	7.91	1.31	8.46	10.97	3.09	7.71	7.30	8.22	6.88	1.24	1.15	3.09	4.52	0.93	1.21	0.23	0.31
51	2.5	21.72	8.71	2.34	0.80	6.46	0.95	8.12	9.82	3.11	8.69	5.10	8.07	4.35	1.13	1.03	4.03	3.41	0.90	0.84	0.20	0.24
61	2.7	18.02	2.33	1.13	0.62	4.41	0.55	18.24	11.43	3.61	13.57	5.53	6.44	3.75	1.11	0.67	3.79	3.20	0.61	0.64	0.17	0.19
71	2.9	7.67	0.92	0.87	0.48	2.86	0.34	30.00	13.27	4.78	18.76	5.25	4.77	2.78	1.10	0.71	2.88	1.79	0.30	0.32	0.09	0.05
81	3.0	3.40	0.86	1.10	0.37	3.23	0.25	41.52	14.15	4.57	15.93	4.50	3.92	2.04	0.65	0.50	1.69	0.95	0.17	0.21	0.00	0.00
91	3.3	4.61	0.77	0.94	0.23	2.47	0.17	37.36	11.68	2.57	19.81	7.15	3.23	2.46	0.45	0.43	3.47	1.76	0.19	0.21	0.00	0.00
101	3.5	5.23	0.81	0.89	0.28	2.67	0.18	27.34	15.64	4.75	15.48	7.81	7.60	3.89	1.17	0.63	2.92	2.02	0.31	0.37	0.00	0.00
111	3.7	6.75	3.52	12.23	4.12	25.81	2.11	19.25	5.66	1.65	8.74	3.59	1.80	1.02	0.21	0.21	1.45	1.52	0.10	0.12	0.09	0.05
111	3.7	6.82	3.68	12.17	4.04	25.97	2.15	19.40	5.73	1.58	8.61	3.54	1.74	0.99	0.23	0.23	1.34	1.41	0.09	0.13	0.09	0.06
121	3.9	6.74	0.96	1.20	0.26	2.01	0.16	32.78	10.99	2.80	20.61	7.51	4.23	2.08	0.55	0.30	3.46	2.71	0.21	0.22	0.10	0.12
131	4.1	6.14	0.88	1.10	0.27	2.74	0.30	30.81	13.98	4.12	16.11	8.37	4.38	2.76	0.97	0.65	2.87	2.50	0.28	0.38	0.24	0.14
141	4.3	7.41	1.39	1.94	0.37	3.41	0.29	28.07	11.20	3.06	20.37	6.54	5.74	2.22	1.04	0.40	3.26	2.62	0.26	0.24	0.11	0.05
151	5.2	8.50	0.87	0.71	0.19	1.12	0.09	27.49	11.70	3.54	21.02	6.13	6.69	2.73	1.43	0.50	4.09	2.03	0.39	0.52	0.14	0.11
161	6.1	9.40	1.83	4.09	1.07	7.25	0.58	22.63	10.96	3.17	16.84	6.10	6.33	1.77	1.24	0.34	3.60	1.98	0.37	0.29	0.08	0.07
171	7.0	9.48	1.24	2.01	0.50	3.73	0.30	22.67	12.69	4.16	18.30	5.91	8.59	1.91	1.73	0.46	3.63	1.76	0.42	0.30	0.12	0.08
181	8.4	7.33	1.25	2.29	0.51	3.49	0.33	27.80	12.33	3.44	18.56	6.80	5.52	2.45	1.10	0.41	3.41	2.29	0.35	0.32	0.00	0.00
191	10.2	9.95	1.07	2.00	0.39	3.52	0.33	23.28	13.54	3.89	18.15	5.97	6.98	2.28	1.67	0.48	3.31	2.27	0.45	0.31	0.11	0.07
201	12.0	10.91	0.64	0.64	0.10	0.68	0.15	21.36	14.99	3.93	15.68	7.39	9.11	3.43	1.60	0.52	4.74	2.93	0.62	0.33	0.16	0.11
211	13.0	1.97	0.09	0.07	0.03	0.08	0.02	28.31	18.21	5.36	17.43	6.05	9.28	3.92	2.94	0.95	2.55	1.61	0.56	0.25	0.21	0.11
221	13.8	2.09	0.10	0.08	0.02	0.06	0.02	36.30	16.31	4.25	16.13	5.32	8.38	2.80	1.88	0.78	2.49	1.67	0.68	0.36	0.20	0.08
231	14.7	3.05	0.14	0.14	0.02	0.09	0.02	26.17	19.21	6.34	15.26	7.71	7.86	3.51	2.93	0.88	3.46	2.13	0.51	0.20	0.21	0.14
241	15.6	9.39	1.27	0.93	0.10	0.42	0.05	29.23	15.62	4.26	14.77	5.64	6.34	2.87	1.82	0.82	3.54	2.22	0.35	0.35	0.00	0.00
251	16.5	10.97	1.18	0.90	0.12	1.14	0.10	26.82	16.34	3.48	16.17	6.26	5.83	2.67	0.75	0.56	3.90	2.28	0.27	0.27	0.00	0.00
261	17.4	9.16	0.76	0.47	0.07	0.40	0.03	29.64	17.30	3.99	15.13	6.49	5.73	3.08	0.72	0.74	3.64	2.17	0.22	0.28	0.00	0.00
271	18.3	5.01	0.38	0.27	0.06	0.57	0.06	30.06	20.20	4.28	15.31	6.56	6.64	2.94	0.88	0.62	3.57	2.09	0.26	0.25	0.00	0.00
281	19.1	21.53	2.45	1.83	0.19	0.54	0.04	19.69	11.59	2.86	16.00	6.11	5.20	3.13	0.49	0.56	4.54	2.47	0.25	0.37	0.08	0.08
291	19.9	12.76	3.26	2.56	1.12	5.66	0.39	16.43	11.89	7.30	6.57	4.55	11.17	3.86	2.95	2.05	1.65	2.87	0.66	1.38	0.51	0.40
301	20.0	18.53	6.11	3.83	1.33	2.62	0.28	13.25	9.23	6.84	6.84	5.30	9.68	3.36	2.70	1.67	2.09	3.33	0.84	1.01	0.68	0.49

References

Ahlgren, G., Gustafsson, I.B. and Boberg, M., 1992. Fatty acid content and chemical composition of freshwater microalgae. Journal of phycology, 28(1), pp.37-50.

Amblès, A., Jambu, P., Parlanti, E., Joffre, J. and Riffe, C., 1994. Incorporation of natural monoacids from plant residues into an hydromorphic forest podzol. European Journal of Soil Science, 45(2), pp.175-182.

Amezcua-Torres, N., 2003. Análisis de la Cuenca Lacustre del Potosí y sus peligros geológicos asociados a la materia orgánica sedimentaria, Nuevo León, Méx (Master's dissertation, Universidad Autónoma de Nuevo León).

Anderson, D.E., 1998. A reconstruction of Holocene climatic changes from peat bogs in north-west Scotland. Boreas, 27(3), pp.208-224.

Anderson, T.F. and Arthur, M.A., 1983. Stable isotopes of oxygen and carbon and their application to sedimentological and palaeoenvironmental problems. Stable Isotopes in Sedimentary Geochemistry, Society of Economic Palaeontologists and Mineralogists Short course, 10, p. 111-151.

Andrews, J.E., Riding, R. and Dennis, P.F., 1997. The stable isotope record of environmental and climatic signals in modern terrestrial microbial carbonates from Europe. Palaeogeography, Palaeoclimatology, Palaeoecology, 129(1-2), pp.171-189.

Arts, M.T., Ackman, R.G. and Holub, B.J., 2001. "Essential fatty acids" in aquatic ecosystems: a crucial link between diet and human health and evolution. Canadian Journal of Fisheries and Aquatic Sciences, 58(1), pp.122-137.

Asmerom, Y., Polyak, V.J. and Burns, S.J., 2010. Variable winter moisture in the southwestern United States linked to rapid glacial climate shifts. Nature Geoscience, 3(2), pp.114-117.

Baas, M., Pancost, R., van Geel, B. and Damsté, J.S.S., 2000. A comparative study of lipids in Sphagnum species. Organic Geochemistry, 31(6), pp.535-541.

Badan-Dangon, A., Dorman, C.E., Merrifield, M.A. and Winant, C.D., 1991. The lower atmosphere over the Gulf of California. Journal of Geophysical Research: Oceans, 96(19), pp.16877-16896.

Báez, S., Collins, S.L., Pockman, W.T., Johnson, J.E. and Small, E.E., 2013. Effects of experimental rainfall manipulations on Chihuahuan Desert grassland and shrubland plant communities. Oecologia, 172(4), pp.1117-1127.

Baker, E.A., and Martin, J.T., 1963. Cutin of plant cuticles. Nature, 199(4900), pp.1268-1270.

Barbour, M.G., 1988. Californian upland forests and woodlands. Cambridge University Press, Cambridge.

Barnathan, G., Bourgougnon, N. and Kornprobst, J.M., 1998. Methoxy fatty acids isolated from the red alga, Schzymenia dubyi. Phytochemistry, 47(5), pp.761-765.

Barron, J.A., Bukry, D. and Bischoff, J.L., 2004. High resolution paleoceanography of the Guaymas Basin, Gulf of California, during the past 15 000 years. Marine Micropaleontology, 50(3), pp.185-207.

Barron, J.A., Bukry, D. and Dean, W.E., 2005. Paleoceanographic history of the Guaymas Basin, Gulf of California, during the past 15,000 years based on diatoms, silicoflagellates, and biogenic sediments. Marine Micropaleontology, 56(3-4), pp.81-102.

Barron, J.A., Metcalfe, S.E. and Addison, J.A., 2012. Response of the North American monsoon to regional changes in ocean surface temperature. Paleoceanography, 27(3).

Bartlein, P.J., Anderson, K.H., Anderson, P.M., Edwards, M.E., Mock, C.J., Thompson, R.S., Webb, R.S., Webb, T., Whitlock, C., 1998. Paleoclimate simulations for North America over the past 21,000 years: features of the simulated climate and comparisons with paleoenvironmental data. Quaternary Science Reviews, 17 (6-7), pp.549-585.

Bechtel, A., Smittenberg, R.H., Bernasconi, S.M. and Schubert, C.J., 2010. Distribution of branched and isoprenoid tetraether lipids in an oligotrophic and a eutrophic Swiss lake: insights into sources and GDGT-based proxies. Organic Geochemistry, 41(8), pp.822-832.

Benson, L., Lund, S., Negrini, R., Linsley, B. and Zic, M., 2003. Response of north American Great basin lakes to Dansgaard-Oeschger oscillations. Quaternary Science Reviews, 22(21-22), pp.2239-2251.

Berke, M.A., Johnson, T.C., Werne, J.P., Schouten, S. and Sinninghe Damsté, J.S., 2009, December. Holocene TEX86 temperature reconstructions from Lake Turkana, East Africa. In AGU Fall Meeting Abstracts.

Betancourt, J.L., Van Devender, T.R. and Martin, P.S. eds., 1990. Packrat middens: the last 40,000 years of biotic change. University of Arizona Press.

Beuning, K.R., Talbot, M.R. and Kelts, K., 1997. A revised 30,000-year paleoclimatic and paleohydrologic history of Lake Albert, East Africa. Palaeogeography, Palaeoclimatology, Palaeoecology, 136(1-4), pp.259-279.

Bhattacharya, T., Tierney, J.E. and DiNezio, P., 2017. Glacial reduction of the North American Monsoon via surface cooling and atmospheric ventilation. Geophysical Research Letters, 44, pp.5113-5122.

Bidigare, R.R., Fluegge, A., Freeman, K.H., Hanson, K.L., Hayes, J.M., Hollander, D., Jasper, J.P., King, L.L., Laws, E.A., Milder, J. and Millero, F.J., 1997. Consistent fractionation of 13C in nature and in the laboratory: Growth-rate effects in some haptophyte algae. Global Biogeochemical Cycles, 11(2), pp.279-292.

Blaga, C.I., Reichart, G.J., Heiri, O. and Damsté, J.S.S., 2009. Tetraether membrane lipid distributions in water-column particulate matter and sediments: a study of 47 European lakes along a north–south transect. Journal of Paleolimnology, 41(3), pp.523-540.

Blair, N., Leu, A., Muñoz, E., Olsen, J., Kwong, E. and Des Marais, D., 1985. Carbon isotopic fractionation in heterotrophic microbial metabolism. Applied and Environmental Microbiology, 50(4), pp.996-1001.

Bliedtner, M., Schäfer, I.K., Zech, R. and Suchodoletz, H.V., 2018. Leaf wax n-alkanes in modern plants and topsoils from eastern Georgia (Caucasus)–implications for reconstructing regional paleovegetation. Biogeosciences, 15(12), pp.3927-3936.

Bliedtner, M., Schäfer, I.K., Zech, R., and von Suchodoletz, H., 2017. Leaf wax n-alkanes in modern plants and topsoils from eastern Georgia (Caucasus) – implications for reconstructing regional paleovegetation, Biogeosciences Discussions, doi:10.5194/bg-2017-277.

Bobbie, R.J. and White, D.C., 1980. Characterization of benthic microbial community structure by high-resolution gas chromatography of fatty acid methyl esters. Applied and Environmental Microbiology, 39(6), pp.1212-1222.

Bond, G., Broecker, W., Johnsen, S., McManus, J., Labeyrie, L., Jouzel, J. and Bonani, G., 1993. Correlations between climate records from North Atlantic sediments and Greenland ice. Nature, 365(6442), p.143.

Bond, G.C., Lotti, R., 1995. Icebergs discharges into the north Atlantic on millennial time scales during the last glaciations. Science, 267(1), pp.05-10.

Bowen, D.Q., 2009. Pleistocene Climates. Encyclopaedia of paleoclimatology and ancient environments. Springer New York, pp.798-803.

Bradley, R.S., 1999. Paleoclimatology: reconstructing climates of the Quaternary (Vol. 68). Elsevier.

Bray, E.E. and Evans, E.D., 1961. Distribution of n-paraffins as a clue to recognition of source beds. Geochimica et Cosmochimica Acta, 22(1), pp.2-15.

Brooks, P.W., Eglinton, G., Gaskell, S.J., McHugh, D.J., Maxwell, J.R. and Philp, R.P., 1976. Lipids of recent sediments, Part I: straight-chain hydrocarbons and carboxylic acids of some temperate lacustrine and sub-tropical lagoonal/tidal flat sediments. Chemical Geology, 18(1), pp.21-38.

Buck, B.J. and Monger, H.C., 1999. Stable isotopes and soil-geomorphology as indicators of Holocene climate change, northern Chihuahuan Desert. Journal of Arid Environments, 43(4), pp.357-373.

Bush, R.T. and McInerney, F.A., 2013. Leaf wax n-alkane distributions in and across modern plants: implications for paleoecology and chemotaxonomy. Geochimica et Cosmochimica Acta, 117, pp.161-179.

Caballero, M., Ortega, B., Valadez, F., Metcalfe, S., Macias, J.L. and Sugiura, Y., 2002. Sta. Cruz Atizapan: a 22-ka lake level record and climatic implications for the late Holocene human occupation in the Upper Lerma Basin, Central Mexico. Palaeogeography, Palaeoclimatology, Palaeoecology, 186(3-4), pp.217-235.

Caballero, M., Peinalba, M.C., Martínez, M., Ortega-Guerrerol, B. and Vázquez, L., 2005. A Holocene record from a former coastal lagoon in Bahía Kino, Gulf of California, Mexico. The Holocene, 15(8), pp.1236-1244.

Calvert, S.E., 2004. Beware intercepts: interpreting compositional ratios in multi-component sediments and sedimentary rocks. Organic Geochemistry, 35(8), pp.981-987.

Carleton, A.M., Carpenter, D.A. and Weser, P.J., 1990. Mechanisms of interannual variability of the southwest United States summer rainfall maximum. Journal of Climate, 3(9), pp.999-1015.

Castañeda, I.S. and Schouten, S., 2011. A review of molecular organic proxies for examining modern and ancient lacustrine environments. Quaternary Science Reviews, 30(21-22), pp.2851-2891.

Castañeda, I.S., Werne, J.P., Johnson, T.C. and Powers, L.A., 2011. Organic geochemical records from Lake Malawi (East Africa) of the last 700 years, part II: Biomarker evidence for recent changes in primary productivity. Palaeogeography, Palaeoclimatology, Palaeoecology, 303(1-4), pp.140-154.

Chávez-Lara, C.M., Holtvoeth, J., Roy, P.D. and Pancost, R.D., 2018. A 27cal ka biomarker-based record of ecosystem changes from lacustrine sediments of the Chihuahua Desert of Mexico. Quaternary Science Reviews, 191, pp.132-143.

Chávez-Lara, C.M., Roy, P.D., Pérez, L., Sankar, G.M. and Lemus-Neri, V.H.L., 2015. Ostracode and C/N based paleoecological record from Santiaguillo basin of subtropical Mexico over last 27 cal kyr BP. Revista Mexicana de Ciencias Geológicas, 32(1), pp.1-10.

Cheshire, H., Thurow, J., Nederbragt, A., 2005. Late Quaternary climatic change record from two long sediment cores from Guaymas Basin, Gulf of California. Journal of Quaternary Science, 20, pp.457-469.

Clark, P.U. and Mix, A.C., 2002. Ice sheets and sea level of the Last Glacial Maximum. Quaternary Science Reviews, 21(1-3), pp.1-7.

Cockerton, H.E., Street-Perrott, F.A., Barker, P.A., Leng, M.J., Sloane, H.J. and Ficken, K.J., 2015. Orbital forcing of glacial/interglacial variations in chemical weathering and silicon cycling within the upper White Nile basin, East Africa: Stable-isotope and biomarker evidence from Lakes Victoria and Edward. Quaternary science reviews, 130, pp.57-71.

Cohen, A.S., 2003. Paleolimnology: The history and evolution of lake systems. Oxford University Press, New York.

Cohen, Z. and Vonshak, A., 1991. Fatty acid composition of Spirulina and Spirulina-like cyanobacteria in relation to their chemotaxonomy. Phytochemistry, 30(1), pp.205-206.

COHMAP members, 1988. Climatic change of the past 18,000 years: Observations and model simulations. Science, 241, pp.1043-1052.

Coletta, P., Pentecost, A. and Spiro, B., 2001. Stable isotopes in charophyte incrustations: relationships with climate and water chemistry. Palaeogeography, Palaeoclimatology, Palaeoecology, 173(1-2), pp.9-19.

Conroy, J.L., Overpeck, J.T., Cole, J.E., Shanahan, T.M. and Steinitz-Kannan, M., 2008. Holocene changes in eastern tropical Pacific climate inferred from a Galápagos lake sediment record. Quaternary Science Reviews, 27(11), pp.1166-1180.

Conroy, Jessica L., Jonathan T. Overpeck, Julia E. Cole, Timothy M. Shanahan, and Miriam Steinitz-Kannan. "Holocene changes in eastern tropical Pacific climate inferred from a Galápagos lake sediment record." Quaternary Science Reviews 27, no. 11-12 (2008): 1166-1180.

Craig, H., 1965. The measurement of oxygen isotope paleotemperatures. Stable isotopes in oceanographic studies and paleotemperatures: Consiglio Nazionale delle Richerche, pp.161-182.

Cranwell, P.A., 1982. Lipids of aquatic sediments and sedimenting particulates. Progress in lipid research, 21(4), pp.271-308.

Cranwell, P.A., 1984. Lipid geochemistry of sediments from Upton Broad, a small productive lake. Organic Geochemistry, 7(1), pp.25-37.

Cranwell, P.A., Eglinton, G. and Robinson, N., 1987. Lipids of aquatic organisms as potential contributors to lacustrine sediments—II. Organic Geochemistry, 11(6), pp.513-527.

Cui, J., Huang, J. and Xie, S., 2008. Characterstics of seasonal variations of leaf n-alkanes and n-alkenes in modern higher plants in Qingjiang, Hubei Province, China. Chinese Science Bulletin, 53(17), pp.2659-2664.

Damsté, J.S.S., 2016. Spatial heterogeneity of sources of branched tetraethers in shelf systems: The geochemistry of tetraethers in the Berau River delta (Kalimantan, Indonesia). Geochimica et Cosmochimica Acta, 186, pp.13-31.

Damsté, J.S.S., Hopmans, E.C., Pancost, R.D., Schouten, S. and Geenevasen, J.A., 2000. Newly discovered non-isoprenoid glycerol dialkyl glycerol tetraether lipids in sediments. Chemical Communications, (17), pp.1683-1684.

Damsté, J.S.S., Ossebaar, J., Abbas, B., Schouten, S. and Verschuren, D., 2009. Fluxes and distribution of tetraether lipids in an equatorial African lake: constraints on the application of the TEX86 palaeothermometer and BIT index in lacustrine settings. Geochimica et Cosmochimica Acta, 73(14), pp.4232-4249.

Dansgaard, W., Johnsen, S.J., Clausen, H.B., Dahl-Jensen, D., Gundenstrup, N.S., Hammer, C.U., Hvidberg, C.S., Steffensen, J.P., Sveinbjörnsdottir, A.E., Jouzel, J., Bond, G., 1993. Evidence for general instability of past climate from a 250-kyr ice-core record. Nature, 364, pp.218-220.

Dastillung, M. and Corbet, B., 1978. La géochimie organique des sédiments marins profonds. I. Hydrocarbures saturés et insatures des sédiments. Géochimie organique des sédiments marins profonds, Orgon II, Atlantique. NE Brésil. CNRS, Paris, pp.293-323.

Dean, W.E., 1999. The carbon cycle and biogeochemical dynamics in lake sediments. Journal of paleolimnology, 21(4), pp.375-393.

Debyser, Y., Pelet, R. and Dastillung, M., 1975. Géochimie organique des sédiments marins récents: Mer Noire, Baltique, Atlantique (Mauritanie). Campos R, Goni J (eds) Advances in organic geochemistry, pp.289-320.

Deevey, E.S. and Flint, R.F., 1957. Postglacial hypsithermal interval. Science, 125(3240), pp.182-184.

Denton, G.H. and Porter, S.C., 1970. Neoglaciation. Scientific American, 222(6), pp.100-111.

Denton, G.H., Anderson, R.F., Toggweiler, J.R., Edwards, R.L., Schaefer, J.M. and Putnam, A.E., 2010. The last glacial termination. Science, 328(5986), pp.1652-1656.

Desvilettes, C.H., Bourdier, G., Amblard, C.H. and Barth, B., 1997. Use of fatty acids for the assessment of zooplankton grazing on bacteria, protozoans and microalgae. Freshwater Biology, 38(3), pp.629-637.

Dong, H., Zhang, G., Jiang, H., Yu, B., Chapman, L.R., Lucas, C.R. and Fields, M.W., 2006. Microbial diversity in sediments of saline Qinghai Lake, China: linking geochemical controls to microbial ecology. Microbial Ecology, 51(1), pp.65-82.

Douglas, M.W., Maddox, R.A., Howard, K. and Reyes, S., 1993. The Mexican Monsoon. Journal of Climate, 6(8), pp.1665-1677.

Durán-Zuazo, V.H., Rodríguez-Pleguezuelo, C.R., 2008. Soil-erosion and runoff prevention by plant covers. A review. Agronomy for Sustainable Development, 28, pp.65-86.

Eglinton, G. and Hamilton, R.J., 1967. Leaf epicuticular waxes. Science, 156(3780), pp.1322-1335.

Eglinton, G., Hunneman, D.H. and Douraghi-Zadeh, K., 1968. Gas chromatographic—mass spectrometric studies of long chain hydroxy acids—II: The hydroxy acids and fatty acids of a 5000-year-old lacustrine sediment. Tetrahedron, 24(18), pp.5929-5941.

Eguiluz, S., Aranda-García, M. and Marrett, R., 2000. Tectónica de la Sierra Madre Oriental, México. Boletín de la Sociedad Geológica Mexicana, 53(1), pp.1-26.

Ehleringer, J.R., 1991. 13C/12C fractionation and its utility in terrestrial plant studies. Carbon isotope techniques, 1, p.187.

Ehleringer, J.R., Phillips, S.L., Schuster, W.S. and Sandquist, D.R., 1991. Differential utilization of summer rains by desert plants. Oecologia, 88(3), pp.430-434.

Englehart, P.J. and Douglas, A.V., 2001. The role of eastern North Pacific tropical storms in the rainfall climatology of western Mexico. International Journal of Climatology, 21(11), pp.1357-1370.

Enzel, Y., Wells, S.G., Lancaster, N., 2003. Late Pleistocene lakes along the Mojave river, southwest California. In: Enzel, Y., Wells, S.G., Lancaster, N. (Eds.), Paleoenvironments and paleohydrology of the Mojave and southern Great Basin deserts. Geological Society of America Special Paper, 368, pp.61-77.

Espinosa, D., Llorente, J. and Morrone, J.J., 2006. Historical biogeographical patterns of the species of Bursera (Burseraceae) and their taxonomic implications. Journal of Biogeography, 33(11), pp.1945-1958.

Eugster, H.P. and Hardie, L.A., 1978. Saline lakes. In Lakes (pp. 237-293). Springer, New York, NY.

Ficken, K.J., Wooller, M.J., Swain, D.L., Street-Perrott, F.A. and Eglinton, G., 2002. Reconstruction of a subalpine grass-dominated ecosystem, Lake Rutundu, Mount Kenya: a novel multi-proxy approach. Palaeogeography, Palaeoclimatology, Palaeoecology, 177(1), pp.137-149.

Fideicomiso para el Desarrollo del Sur del Estado de Nuevo León (FIDESUR), 2018. Agricultura en Invernadero y Agroparques Hortícolas. http://www.agronuevoleon.gob.mx/oeidrus/invernaderos.pdf

Flower, B.P., Hastings, D.W., Hill, H.W. and Quinn, T.M., 2004. Phasing of deglacial warming and Laurentide Ice Sheet meltwater in the Gulf of Mexico. Geology, 32(7), pp.597-600.

Freudenthal, T., Wagner, T., Wenzhöfer, F., Zabel, M. and Wefer, G., 2001. Early diagenesis of organic matter from sediments of the eastern subtropical Atlantic: evidence from stable nitrogen and carbon isotopes. Geochimica et Cosmochimica Acta, 65(11), pp.1795-1808.

Fuhrmann, A., Mingram, J., Lücke, A., Lu, H., Horsfield, B., Liu, J., Negendank, J.F., Schleser, G.H. and Wilkes, H., 2003. Variations in organic matter composition in sediments from Lake Huguang Maar (Huguangyan), south China during the last 68 ka:

implications for environmental and climatic change. Organic Geochemistry, 34(11), pp.1497-1515.

Fukushima, K., Kondo, H. and Sakata, S., 1992. Geochemistry of hydroxy acids in sediments-I. Some freshwater and brackish water lakes in Japan. Organic Geochemistry, 18(6), pp.913-922.

Gifford, R.M. and Howden, M., 2001. Vegetation thickening in an ecological perspective: significance to national greenhouse gas inventories. Environmental Science & Policy, 4(2-3), pp.59-72.

Goad L.J. and Goodwin T.W., 1972. The biosynthesis of plant sterols. Progress in Phytochemistry, 3, pp.113-198.

Goossens, H., Düren, R.R., De Leeuw, J.W. and Schenck, P.A., 1989. Lipids and their mode of occurrence in bacteria and sediments-II. Lipids in the sediment of a stratified, freshwater lake. Organic Geochemistry, 14(1), pp.27-41.

Gornitz, V. ed., 2008. Encyclopedia of paleoclimatology and ancient environments. Springer Science & Business Media.

Greenland, N., 2004. Ice Core Project members. High-resolution record of Northern Hemisphere climate extending into the last interglacial period. Nature, 431, pp.147-151.

Grimalt, J. and Albaigés, J., 1987. Sources and occurrence of C12-C22 n-alkane distributions with even carbon-number preference in sedimentary environments. Geochimica et Cosmochimica Acta, 51(6), pp.1379-1384.

Grimalt, J., Albaigés, J., Alexander, G. and Hazai, I., 1986. Predominance of even carbon-numbered n-alkanes in coal seam samples of Nograd Basin (Hungary). Naturwissenschaften, 73(12), pp.729-731.

Grogan, D.W. and Cronan, J.E., 1997. Cyclopropane ring formation in membrane lipids of bacteria. Microbiology and Molecular Biology Reviews, 61(4), pp.429-441.

Grossman, E.L. and Ku, T.L., 1986. Oxygen and carbon isotope fractionation in biogenic aragonite: temperature effects. Chemical Geology: Isotope Geoscience Section, 59, pp.59-74.

Hafsten, U., 1961. Pleistocene development of vegetation and climate in the southern High Plains as evidenced by pollen analysis. Paleoecology of the Llano Estacado. Santa Fe: Museum of New Mexico Press, Fort Burgwin Research Centre Publication, 1, pp.59-91.

Hairston, N.G. and Walton, W.E., 1986. Rapid evolution of a life history trait. Proceedings of the National Academy of Sciences, 83(13), pp.4831-4833.

Han, J. and Calvin, M., 1969. Hydrocarbon distribution of algae and bacteria, and microbiological activity in sediments. Proceedings of the National Academy of Sciences, 64(2), pp.436-443.

Han, J., McCarthy, E.D., Van Hoeven, W., Calvin, M. and Bradley, W.H., 1968. Organic geochemical studies, II. A preliminary report on the distribution of aliphatic hydrocarbons in algae, in bacteria, and in a recent lake sediment. Proceedings of the National Academy of Sciences, 59(1), pp.29-33.

Hardie, L.A., Smoot, J.P., Eugster, H.P., Matter, A. and Tucker, M.E., 1978. Saline lakes and their deposits: a sedimentological approach. Modern and ancient lake sediments, 2, pp.7-41.

Harrison, S.P.A., Kutzbach, J.E., Liu, Z., Bartlein, P.J., Otto-Bliesner, B., Muhs, D., Prentice, I.C. and Thompson, R.S., 2003. Mid-Holocene climates of the Americas: a dynamical response to changed seasonality. Climate Dynamics, 20(7-8), pp.663-688.

Heinrich, H., 1988. Origin and consequences of cyclic ice rafting in the northeast Atlantic Ocean during the past 130,000 years. Quaternary Research, 29, pp.142-152.

Hernández-Vázquez, L., Palazon, J. and Navarro-Ocaña, A., 2012. The pentacyclic triterpenes α-, β-amyrins: a review of sources and biological activities. Phytochemicals-A Global Perspective of Their Role in Nutrition and Health, 23, pp.487-502.

Heusser, L., 1998. Direct correlation of millennial-scale changes in western North America vegetation and climate with changes in the California current system over the past ~60kyr. Paleoceanography, 13(3), pp.252-262.

Higgins, R.W., Yao, Y. and Wang, X.L., 1997. Influence of the North American monsoon system on the US summer precipitation regime. Journal of Climate, 10(10), pp.2600-2622.

Hobbie, E. and Werner, R.A., 2004. Intramolecular, compound-specific, and bulk carbon isotope patterns in C3 and C4 plants: a review and synthesis. New Phytologist, 161(2), pp.371-385.

Hollander, D.J. and McKenzie, J.A., 1991. CO2 control on carbon-isotope fractionation during aqueous photosynthesis: A paleo-pCO2 barometer. Geology, 19(9), pp.929-932.

Holmgren, C.A., Betancourt, J.L. and Rylander, K.A., 2006. A 36,000-yr vegetation history from the Peloncillo Mountains, southeastern Arizona, USA. Palaeogeography, Palaeoclimatology, Palaeoecology, 240(3-4), pp.405-422.

Holmgren, C.A., Norris, J. and Betancourt, J.L., 2007. Inferences about winter temperatures and summer rains from the late Quaternary record of C4 perennial grasses and C3 desert shrubs in the northern Chihuahuan Desert. Journal of Quaternary Science, 22(2), pp.141-161.

Holmgren, C.A., Penalba, M.C., Rylander, K.A. and Betancourt, J.L., 2003. A 16,000 14 C yr BP packrat midden series from the USA–Mexico Borderlands. Quaternary Research, 60(3), pp.319-329.

Holmgren, C.A., Peñalba, M.C., Rylander, K.A., Betancourt, J.L., 2003. A 16,000 ^{14}C yr BP packrat midden series from the USA-Mexico Borderlands. Quaternary Research, 60, pp.319-329.

Holtvoeth, J., Rushworth, D., Copsey, H., Imeri, A., Cara, M., Vogel, H., Wagner, T. and Wolff, G.A., 2016. Improved end-member characterisation of modern organic matter pools in the Ohrid Basin (Albania, Macedonia) and evaluation of new palaeoenvironmental proxies. Biogeosciences, 13(3), pp.795-816.

Holtvoeth, J., Vogel, H., Wagner, B. and Wolff, G.A., 2010. Lipid biomarkers in Holocene and glacial sediments from ancient Lake Ohrid (Macedonia, Albania). Biogeosciences, 7(11), pp.3473-3489.

Hopmans, E.C., Weijers, J.W., Schefuß, E., Herfort, L., Damsté, J.S.S. and Schouten, S., 2004. A novel proxy for terrestrial organic matter in sediments based on branched and isoprenoid tetraether lipids. Earth and Planetary Science Letters, 224(1-2), pp.107-116.

Horel, J.D. and Wallace, J.M., 1981. Planetary-scale atmospheric phenomena associated with the Southern Oscillation. Monthly Weather Review, 109(4), pp.813-829.

Ibarra, D.E., Egger, A.E., Weaver, K.L., Harris, C.R. and Maher, K., 2014. Rise and fall of late Pleistocene pluvial lakes in response to reduced evaporation and precipitation: Evidence from Lake Surprise, California. Bulletin, 126(11-12), pp.1387-1415.

INEGI, 2015. Guía para la interpretación de cartografía Uso del suelo y vegetación Escala 1:250 000 Serie V. http://www.inegi.org.mx/

Jáuregui, E., 2003. Climatology of landfalling hurricanes and tropical storms in Mexico. Atmósfera, 16(4), pp.193-204.

Justino, F., Stordal, F., Vizy, E.K., Cook, K.H. and Pereira, M.P., 2016. Greenhouse gas induced changes in the seasonal cycle of the Amazon Basin in coupled climate-vegetation regional model. Climate, 4(1), p.3.

Kattner, G., Gercken, G. and Hammer, K.D., 1983. Development of lipids during a spring plankton bloom in the northern North Sea: II. Dissolved lipids and fatty acids. Marine chemistry, 14(2), pp.163-173.

Katz, B. J., 1990. Controls on distribution of lacustrine source rocks through time and space. Lacustrine Basin Exploration: Case Studies and Modern Analogues, 50, pp.61-76.

Kerger, B.D., Nichols, P.D., Antworth, C.P., Sand, W., Bock, E., Cox, J.C., Langworthy, T.A. and White, D.C., 1986. Signature fatty acids in the polar lipids of acid-producing Thiobacillus spp.: methoxy, cyclopropyl, alpha-hydroxy-cyclopropyl and branched and normal monoenoic fatty acids. FEMS Microbiology Ecology, 2(2), pp.67-77.

Kim, S.T. and O'Neil, J.R., 1997. Equilibrium and nonequilibrium oxygen isotope effects in synthetic carbonates. Geochimica et cosmochimica acta, 61(16), pp.3461-3475.

Kirby, M.E., Lund, S.P., Bird, B.W., 2006. Mid-Wisconsin sediment record from Baldwin Lake reveals hemispheric climate dynamics (Southern CA, USA). Palaeogeography, Palaeoclimatology, Palaeoecology, 241, pp.267-283.

Kirby, M.E., Zimmerman, S.R., Patterson, W.P. and Rivera, J.J., 2012. A 9170-year record of decadal-to-multi-centennial scale pluvial episodes from the coastal Southwest United States: a role for atmospheric rivers? Quaternary Science Reviews, 46, pp.57-65.

Kluge, M. and Ting, I.P., 1978. Crassulacean acid metabolism, Springer-Verlag: Berlin.

Kolattukudy, P., 1984. Biochemistry and function of cutin and suberin. Canadian Journal of Botany, 62(12), pp.2918-2933.

Kolattukudy, P., 1981. Structure, biosynthesis, and biodegradation of cutin and suberin. Annual Review of Plant Physiology, 32(1), pp.539-567.

Kunst, L. and Samuels, A.L., 2003. Biosynthesis and secretion of plant cuticular wax. Progress in lipid research, 42(1), pp.51-80.

Lachniet, M.S., Asmerom, Y., Bernal, J.P., Polyak, V.J. and Vazquez-Selem, L., 2013. Orbital pacing and ocean circulation-induced collapses of the Mesoamerican monsoon over the past 22,000 y. Proceedings of the National Academy of Sciences, 110(23), pp.9255-9260.

Larson, J., Zhou, Y. and Higgins, R.W., 2005. Characteristics of landfalling tropical cyclones in the United States and Mexico: Climatology and interannual variability. Journal of Climate, 18(8), pp.1247-1262.

Lee, S. and Fuhrman, J.A., 1987. Relationships between biovolume and biomass of naturally derived marine bacterioplankton. Applied and environmental microbiology, 53(6), pp.1298-1303.

Lehmeier, C.A., Ballantyne IV, F., Min, K. and Billings, S.A., 2016. Temperature-mediated changes in microbial carbon use efficiency and 13C discrimination. Biogeosciences, 13, pp.3319-3329.

Leng, M.J. and Henderson, A.C., 2013. Recent advances in isotopes as palaeolimnological proxies. Journal of Paleolimnology, 49(3), pp.481-496.

Leng, M.J. and Marshall, J.D., 2004. Palaeoclimate interpretation of stable isotope data from lake sediment archives. Quaternary Science Reviews, 23(7-8), pp.811-831.

Li Y, Zhu X, Tian J. 1991. Effectiveness of plant roots in increase the anti-scourability of soil on the Loess Plateau. Chinese Science Bulletin, 3, pp.2077-2082.

Livingstone, D.M. and Lotter, A.F., 1998. The relationship between air and water temperatures in lakes of the Swiss Plateau: a case study with pal\sgmaelig; olimnological implications. Journal of Paleolimnology, 19(2), pp.181-198.

Lora, J.M., 2018. Components and Mechanisms of Hydrologic Cycle Changes over North America at the Last Glacial Maximum. Journal of Climate, 31(17), pp.7035-7051.

Lora, J.M., Mitchell, J.L., Risi, C. and Tripati, A.E., 2017. North Pacific atmospheric rivers and their influence on western North America at the Last Glacial Maximum. Geophysical Research Letters, 44(2), pp.1051-1059.

Lozano-García, M.S. and Ortega-Guerrero, B., 1998. Late Quaternary environmental changes of the central part of the Basin of Mexico; correlation between Texcoco and Chalco basins. Review of Palaeobotany and Palynology, 99(2), pp.77-93.

Lozano-García, M.S., Ortega-Guerrero, B. and Sosa-Nájera, S., 2002. Mid-to late-Wisconsin pollen record of San Felipe basin, Baja California. Quaternary Research, 58(1), pp.84-92.

Lozano-García, M.S., Ortega-Guerrero, B., Caballero-Miranda, M. and Urrutia-Fucugauchi, J., 1993. Late Pleistocene and Holocene paleoenvironments of Chalco lake, central Mexico. Quaternary Research, 40(3), pp.332-342.

Lyle, M., Heusser, L., Ravelo, C., Yamamoto, M., Barron, J., Diffenbaugh, N.S., Herbert, T. and Andreasen, D., 2012. Out of the tropics: the Pacific, Great Basin Lakes, and Late Pleistocene water cycle in the western United States. Science, 337(6102), pp.1629-1633.

Maffei, M., 1996. Chemotaxonomic significance of leaf wax alkanes in the Gramineae. Biochemical systematics and ecology, 24(1), pp.53-64.

Magaña, V.O., Vázquez, J.L., Pérez, J.L. and Pérez, J.B., 2003. Impact of El Niño on precipitation in Mexico. Geofísica internacional, 42(3), pp.313-330.

Maslin, M.A., and Shackleton, N.J., 1995. Surface water temperatures, salinity, and density changes in the northeast Atlantic during the last 45,000 years: Heinrich events, deep water formation, and climatic rebounds. Paleoceanography, 10, pp.527-544.

Matsuda, H. and Koyama, T., 1977. Early diagenesis of fatty acids in lacustrine sediments-I. Identification and distribution of fatty acids in recent sediment from a freshwater lake. Geochimica et Cosmochimica Acta, 41(6), pp.777-783.

Mayewski, P.A., Rohling, E.E., Stager, J.C., Karlen, W., Maasch, K.A., Meeker, L.D., Meyerson, E.A., Gasse, F., Van Kreveld, S., Holmgren, K. and Lee-Thorp, J., 2004. 2004: Holocene climate variability. Quaternary Research 62, 243-55.

McAuliffe, J.R. and Van Devender, T.R., 1998. A 22,000-year record of vegetation change in the north-central Sonoran Desert. Palaeogeography, Palaeoclimatology, Palaeoecology, 141(3-4), pp.253-275.

McClaran, M.P. and Van Devender, T.R. eds., 1997. The desert grassland. University of Arizona Press, pp.68-99.

McClymont, E.L., Ganeshram, R.S., Pichevin, L.E., Talbot, H.M., Dongen, B.E., Thunell, R.C., Haywood, A.M., Singarayer, J.S. and Valdes, P.J., 2012. Sea-surface temperature records of Termination 1 in the Gulf of California: Challenges for seasonal and interannual analogues of tropical Pacific climate change. Paleoceanography, 27(2).

Méndez, M. and Magaña, V., 2010. Regional aspects of prolonged meteorological droughts over Mexico and Central America. Journal of Climate, 23(5), pp.1175-1188.

Menking, K.M. and Anderson, R.Y., 2003. Contributions of La Niña and El Niño to middle Holocene drought and late Holocene moisture in the American Southwest. Geology, 31(11), pp.937-940.

Metcalfe, S.E., Barron, J.A. and Davies, S.J., 2015. The Holocene history of the North American Monsoon: 'known knowns' and 'known unknowns' in understanding its spatial and temporal complexity. Quaternary Science Reviews, 120, pp.1-27.

Metcalfe, S.E., Bimpson, A., Courtice, A.J., O'Hara, S.L. and Taylor, D.M., 1997. Climate change at the monsoon/westerly boundary in northern Mexico. Journal of Paleolimnology, 17(2), pp.155-171.

Metcalfe, S.E., O'Hara, S.L., Caballero, M. and Davies, S.J., 2000. Records of Late Pleistocene–Holocene climatic change in Mexico – a review. Quaternary Science Reviews, 19(7), pp.699-721.

Metcalfe, S.E., Say, A., Black, S., McCulloch, R., O´Hara, S., 2002. Wet conditions during the Last Glaciation in the Chihuahuan Desert, Alta Babicora Basin, Mexico. Quaternary Research, 57, pp.91-101.

Metcalfe, S.E., Street-Perrott, F.A., Perrott, R.A. and Harkness, D.D., 1991. Palaeolimnology of the Upper Lerma Basin, Central Mexico: a record of climatic change and anthropogenic disturbance since 11 600 yr BP. Journal of Paleolimnology, 5(3), pp.197-218.

Meyer, E.R., 1973. Late-Quarternary Paleoecology of the Cuatro Cienegas Basin, Coahuila, Mexico. Ecology, 54(5), pp.982-995.

Meyers, P.A. and Benson, L.V., 1988. Sedimentary biomarker and isotopic indicators of the paleoclimatic history of the Walker Lake basin, western Nevada. Organic Geochemistry, 13, pp.807-813.

Meyers, P.A. and Ishiwatari, R., 1993. Lacustrine organic geochemistry - an overview of indicators of organic matter sources and diagenesis in lake sediments. Organic geochemistry, 20(7), pp.867-900.

Meyers, P.A., 2003. Applications of organic geochemistry to paleolimnological reconstructions: a summary of examples from the Laurentian Great Lakes. Organic geochemistry, 34(2), pp.261-289.

Meyers, P.A., Leenheer, M.J., Eaoie, B.J. and Maule, S.J., 1984. Organic geochemistry of suspended and settling particulate matter in Lake Michigan. Geochimica et Cosmochimica Acta, 48(3), pp.443-452.

Milankovitch, M., 1941. Kanon der Erdbestrahlung und Seine Andwendung auf das Eiszeitenproblem. Royal Serbian Academy, Special Publication, 132.

Molina, I., Bonaventure, G., Ohlrogge, J. and Pollard, M., 2006. The lipid polyester composition of Arabidopsis thaliana and Brassica napus seeds. Phytochemistry, 67(23), pp.2597-2610.

Moy, C.M., Seltzer, G.O., Rodbell, D.T. and Anderson, D.M., 2002. Variability of El Niño/Southern Oscillation activity at millennial timescales during the Holocene epoch. Nature, 420(6912), pp.162-165.

Nagata, T., 1986. Carbon and nitrogen content of natural planktonic bacteria. Applied and environmental microbiology, 52(1), pp.28-32.

Nalborczyk, E., LaCroix, L.J. and Hill, R.D., 1975. Environmental influences on light and dark CO_2 fixation by Kalanchoe daigremontiana. Canadian Journal of Botany, 53(11), pp.1132-1138.

Negrini, R.M., 2002. Pluvial lake sizes in the northwestern Great Basin throughout the Quaternary period. In: Hershler, R., Madsen, D.B., Currey, D.R. (Eds.), Great Basin Aquatics Systems History. Smithsonian Contribution to the Earth Sciences. Smithsonian Press, Washington DC, pp.11-52.

Nichols, G., 2009. Sedimentology and stratigraphy. John Wiley & Sons, 419, pp.151-162.

Nichols, J.E. and Huang, Y., 2007. C 23–C 31 n-alkan-2-ones are biomarkers for the genus Sphagnum in freshwater peatlands. Organic Geochemistry, 38(11), pp.1972-1976.

Nieto-Samaniego, Á.F., Barajas-Gea, C.I., Gómez-González, J.M., Rojas, A., Alaniz-Álvarez, S.A. and Xu, S., 2012. Geología, evolución estructural (Eoceno al actual) y eventos sísmicos del Graben de Santiaguillo, Durango, México. Revista mexicana de ciencias geológicas, 29(1), pp.115-130.

Nott, C.J., Xie, S., Avsejs, L.A., Maddy, D., Chambers, F.M. and Evershed, R.P., 2000. n-Alkane distributions in ombrotrophic mires as indicators of vegetation change related to climatic variation. Organic Geochemistry, 31(2), pp.231-235.

O'Leary, M.H., 1981. Carbon isotope fractionation in plants. Phytochemistry, 20(4), pp.553-567.

O'Leary, M.H., 1988. Carbon isotopes in photosynthesis. Bioscience, 38(5), pp.328-336.

Oliver, J.E., 2005. Encyclopedia of World Climatology. National Oceanic and Atmospheric Administration. ISBN 978-1-4020-3264-6.

Orgambide, G.G., Reusch, R.N. and Dazzo, F.B., 1993. Methoxylated fatty acids reported in Rhizobium isolates arise from chemical alterations of common fatty acids upon acid-catalyzed transesterification procedures. Journal of bacteriology, 175(15), pp.4922-4926.

Ortega-Ramirez, J., Valiente Banuet, A., Urrutia Fucugauchi, J., Mortera Gutierrez, C., Alvarado Valdez, G., 1998. Paleoclimatic changes during the Late Pleistocene-Holocene in Laguna Babicora, near Chihuahua Desert, Mexico. Canadian Journal of Earth Sciences, 35, pp.1168-1179.

Ortega-Rosas, C.I., Guiot, J., Penalba, M.C. and Ortiz-Acosta, M.E., 2008. Biomization and quantitative climate reconstruction techniques in northwestern Mexico—With an application to four Holocene pollen sequences. Global and Planetary Change, 61(3-4), pp.242-266.

Ortega-Rosas, C.I., Peñalba, M.C. and Guiot, J., 2016. The Lateglacial interstadial at the southeastern limit of the Sonoran Desert, Mexico: vegetation and climate reconstruction based on pollen sequences from Ciénega San Marcial and comparison with the subrecent record. Boreas, 45(4), pp.773-789.

Osmond, C.B., Bender, M.M. and Burris, R.H., 1976. Pathways of CO_2 fixation in the CAM plant Kalanchoë daigremontiana. III. Correlation with $\delta^{13}C$ value during growth and water stress. Functional Plant Biology, 3(6), pp.787-799.

Oster, J.L., Ibarra, D.E., Winnick, M.J. and Maher, K., 2015. Steering of westerly storms over western North America at the Last Glacial Maximum. Nature Geoscience, 8(3), p.201.

Palacios-Fest, M.R., Carreño, A.L., Ortega-Ramírez, J.R. and Alvarado-Valdéz, G., 2002. A paleoenvironmental reconstruction of Laguna Babícora, Chihuahua, Mexico based on ostracode paleoecology and trace element shell chemistry. Journal of Paleolimnology, 27(2), pp.185-206.

Parker, S.S., Hawes, J.T., Colucci, S.J. and Hayden, B.P., 1989. Climatology of 500 mb cyclones and anticyclones, 1950–85. Monthly weather review, 117(3), pp.558-571.

Pearson, A., Pi, Y., Zhao, W., Li, W., Li, Y., Inskeep, W., Perevalova, A., Romanek, C., Li, S. and Zhang, C.L., 2008. Factors controlling the distribution of archaeal tetraethers in terrestrial hot springs. Applied and Environmental Microbiology, 74(11), pp.3523-3532.

Pearson, E.J., Farrimond, P. and Juggins, S., 2007. Lipid geochemistry of lake sediments from semi-arid Spain: relationships with source inputs and environmental factors. Organic Geochemistry, 38(7), pp.1169-1195.

Pérez-Cruz, L., 2006. Climate and ocean variability during the middle and late Holocene recorded in laminated sediments from Alfonso Basin, Gulf of California, Mexico. Quaternary Research, 65(3), pp.401-410.

Perry, G.J., Volkman, J.K., Johns, R.B. and Bavor, H.J., 1979. Fatty acids of bacterial origin in contemporary marine sediments. Geochimica et Cosmochimica Acta, 43(11), pp.1715-1725.

Peterse, F., van der Meer, J., Schouten, S., Weijers, J.W., Fierer, N., Jackson, R.B., Kim, J.H. and Damsté, J.S.S., 2012. Revised calibration of the MBT–CBT paleotemperature proxy based on branched tetraether membrane lipids in surface soils. Geochimica et Cosmochimica Acta, 96, pp.215-229.

Pillay, D. and Perissinotto, R., 2009. Community structure of epibenthic meiofauna in the St. Lucia Estuarine Lake (South Africa) during a drought phase. Estuarine, Coastal and Shelf Science, 81(1), pp.94-104.

Poger, D. and Mark, A.E., 2015. A ring to rule them all: the effect of cyclopropane Fatty acids on the fluidity of lipid bilayers. The journal of physical chemistry B, 119(17), pp.5487-5495.

Polyak, V.J., Rasmussen, J.B.T., Asmerom, Y., 2004. Prolonged wet period in the southwestern United States through the Younger Dryas. Geology, 32(1), pp.5-8.

Porter, D.M., 1974. The Burseraceae in North America north of Mexico. Madrono, 22(5), pp.273-276.

Powell, P.W., 1945. The Chichimecas: scourge of the silver frontier in sixteenth-century Mexico. The Hispanic American Historical Review, 25(3), pp.315-338.

Powers, L.A, Werne, J.P., Vanderwoude, A.J., Damsté, J.S.S., Hopmans, E.C. and Schouten, S., 2010. Applicability and calibration of the TEX86 paleothermometer in lakes. Organic Geochemistry, 41(4), pp.404-413.

Powers, L.A., Johnson, T.C., Werne, J.P., Castaneda, I.S., Hopmans, E.C., Sinninghe Damsté, J.S. and Schouten, S., 2005. Large temperature variability in the southern African tropics since the Last Glacial Maximum. Geophysical Research Letters, 32(8).

Powers, L.A., Werne, J.P., Johnson, T.C., Hopmans, E.C., Damsté, J.S.S. and Schouten, S., 2004. Crenarchaeotal membrane lipids in lake sediments: a new paleotemperature proxy for continental paleoclimate reconstruction? Geology, 32(7), pp.613-616.

Quiroz-Jiménez, J.D., Roy, P.D., Beramendi-Orosco, L.E., Lozano-García, S. and Vázquez-Selem, L., 2018. Orbital-scale droughts in central-northern Mexico during the late Quaternary and comparison with other subtropical and tropical records. Geological Journal, 53(1), pp.230-242.

Quiroz-Jimenez, J.D., Roy, P.D., Lozano-Santacruz, R. and Giron-García, P., 2017. Hydrological responses of the Chihuahua Desert of Mexico to possible Heinrich Stadials. Journal of South American Earth Sciences, 73, pp.1-9.

Rach, O., Brauer, A., Wilkes, H. and Sachse, D., 2014. Delayed hydrological response to Greenland cooling at the onset of the Younger Dryas in western Europe. Nature Geoscience, 7(2), p.109.

Ramirez, M.E., Nuñez, J.D., Ocampo, E.H., Matula, C.V., Suzuki, M., Hashimoto, T. and Cledón, M., 2012. Schizymenia dubyi (Rhodophyta, Schizymeniaceae), a new introduced species in Argentina. New Zealand Journal of Botany, 50(1), pp.51-58.

Reimer, P.J., Bard, E., Bayliss, A., Beck, J.W., Blackwell, P.G., Ramsey, C.B., Buck, C.E., Cheng, H., Edwards, R.L., Friedrich, M. and Grootes, P.M., 2013. IntCal13 and Marine13 radiocarbon age calibration curves 0–50,000 years cal BP. Radiocarbon, 55(4), pp.1869-1887.

Reubens, B., Poesen, J., Danjon, F., Geudens, G. and Muys, B., 2007. The role of fine and coarse roots in shallow slope stability and soil erosion control with a focus on root system architecture: a review. Trees, 21(4), pp.385-402.

Reyes, S. and Mejía-Trejo, A., 1991. Tropical perturbations in the Eastern Pacific and the Precipitation field over North-Western Mexico in relation to the ENSO phenomenon. International Journal of Climatology, 11(5), pp.515-528.

Reyes, S., Douglas, M.W. and Maddox, R.A., 1994. El monzón del suroeste de Norteamérica (TRAVASON/SWAMP). Atmósfera, 7(2), pp.117-137.

Řezanka, T. and Sigler, K., 2009. Odd-numbered very-long-chain fatty acids from the microbial, animal and plant kingdoms. Progress in lipid research, 48(3), pp.206-238.

Rhode, D., 2002. Early Holocene juniper woodland and chaparral taxa in the central Baja California peninsula, Mexico. Quaternary Research, 57(1), pp.102-108.

Rieley, G., 1994. Derivatization of organic compounds prior to gas chromatographic–combustion–isotope ratio mass spectrometric analysis: identification of isotope fractionation processes. Analyst, 119(5), pp.915-919.

Rodgers, E.B., Adler, R.F. and Pierce, H.F., 2000. Contribution of tropical cyclones to the North Pacific climatological rainfall as observed from satellites. Journal of Applied Meteorology, 39(10), pp.1658-1678.

Rommerskirchen, F., Plader, A., Eglinton, G., Chikaraishi, Y. and Rullkötter, J., 2006. Chemotaxonomic significance of distribution and stable carbon isotopic composition of long-chain alkanes and alkan-1-ols in C4 grass waxes. Organic Geochemistry, 37(10), pp.1303-1332.

Ronkainen, T., McClymont, E.L., Väliranta, M. and Tuittila, E.S., 2013. The n-alkane and sterol composition of living fen plants as a potential tool for palaeoecological studies. Organic geochemistry, 59, pp.1-9.

Ropelewski, C.F. and Halpert, M.S., 1987. Global and regional scale precipitation patterns associated with the El Niño/Southern Oscillation. Monthly weather review, 115(8), pp.1606-1626.

Roy, P.D., Caballero, M., Lozano, R., Ortega, B., Lozano, S., Pi, T., Israde, I., Morton, O., 2010. Geochemical record of Late Quaternary paleoclimate from lacustrine sediments

of paleolake San Felipe, western Sonora Desert, Mexico. Journal of South American Earth Sciences, 29, pp.586-596.

Roy, P.D., Caballero, M., Lozano, S., Morton, O., Lozano, R., Jonathan, M.P., Sánchez, J.L. and Macías, M.C., 2012. Provenance of sediments deposited at paleolake San Felipe, western Sonora Desert: Implications to regimes of summer and winter precipitation during last 50 cal kyr BP. Journal of Arid Environments, 81, pp.47-58.

Roy, P.D., Chávez-Lara, C.M., Beramendi-Orosco, L.E., Sánchez-Zavala, J.L., Muthu-Sankar, G., Lozano-Santacruz, R., Quiroz-Jimenez, J.D. and López-Balbiaux, N., 2015. Paleohydrology of the Santiaguillo Basin (Mexico) since late last glacial and climate variation in southern part of western subtropical North America. Quaternary Research, 84(3), pp.335-347.

Roy, P.D., Quiroz-Jiménez, J.D., Chávez-Lara, C.M., Sánchez-Zavala, J.L., Pérez-Cruz, L.L. and Sankar, G.M., 2014. Humid Pleistocene− Holocene transition and early Holocene in sub-tropical northern Mexico and possible Gulf of California forcing. Boreas, 43(3), pp.577-587.

Roy, P.D., Quiroz-Jimenez, J.D., Pérez-Cruz, L.L., Lozano-García, S., Metcalfe, S.E., Lozano-Santacruz, R., López-Balbiaux, N., Sánchez-Zavala, J.L. and Romero, F.M., 2013. Late Quaternary paleohydrological conditions in the drylands of northern Mexico: a summer precipitation proxy record of the last 80 cal ka BP. Quaternary Science Reviews, 78, pp.342-354.

Roy, P.D., Rivero-Navarrete, A., Sánchez-Zavala, J.L. and López-Balbiaux, N., 2014. Subsurface fire and subsidence at Valle del Potosí (Nuevo León, Mexico): preliminary observations. Boletín de la Sociedad Geológica Mexicana, 66(3), pp.553-557.

Roy, P.D., Rivero-Navarrete, A., Sánchez-Zavala, J.L., Beramendi-Orosco, L.E., Muthu-Sankar, G. and Lozano-Santacruz, R., 2016. Atlantic Ocean modulated hydroclimate of the subtropical northeastern Mexico since the last glacial maximum and comparison with the southern US. Earth and Planetary Science Letters, 434, pp.141-150.

Samuels, L., Kunst, L. and Jetter, R., 2008. Sealing plant surfaces: cuticular wax formation by epidermal cells. Annual review of plant biology, 59, pp.683-707.

Schindler, D.E., Carpenter, S.R., Cole, J.J., Kitchell, J.F. and Pace, M.L., 1997. Influence of food web structure on carbon exchange between lakes and the atmosphere. Science, 277(5323), pp.248-251.

Schmidt Jr, R.H., 1979. A climatic delineation of the'real'Chihuahuan Desert [Mexico]. Journal of Arid Environments, 2, pp.243-250.

Schouten, S., Hopmans, E.C. and Sinninghe Damsté, J.S., 2013. The organic geochemistry of glycerol dialkyl glycerol tetraether lipids: a review. Organic geochemistry, 54, pp.19-61.

Schouten, S., Hopmans, E.C., Schefuß, E. and Sinninghe Damsté, J.S., 2002. Distributional variations in marine crenarchaeotal membrane lipids: a new tool for reconstructing

ancient sea water temperatures? Earth and Planetary Science Letters, 204(1-2), pp.265-274.

Schwark, L., Zink, K. and Lechterbeck, J., 2002. Reconstruction of postglacial to early Holocene vegetation history in terrestrial Central Europe via cuticular lipid biomarkers and pollen records from lake sediments. Geology, 30(5), pp.463-466.

Sears, P.B. and Clisby, K.H., 1956. San Agustin Planes-Pleistocene climatic changes. Science, 124, pp.537-539.

Secretará de Agricultura, Ganadería, desarrollo Rural, Pesca y Alimentación (SAGARPA), Gobierno de México. http://www.sagarpa.gob.mx/

Secretaría de Gobernación (SEGOB), 1988. Centro Nacional de Estudios Municipales, Gobierno del Estado de Nuevo León, "Los Municipios de Nuevo León". Enciclopedia de los Municipios de México. Monterrey, N.L. http://siglo.inafed.gob.mx/enciclopedia/EMM19nuevoleon/municipios/19017a.html

Servicio Geológico Mexicano, 2000. Carta Geológico-Minera Concepción del Oro, G14-10, Zacatecas, Nuevo León, Coahuila y San Luis Potosí, escala 1:250000.

Servicio Meteorológico Nacional (SMN), México. Estación 10137 Guatimape (DGE) (24°48'25" N., 104°55'19" W., 1,974.0 msnm). Normales Climatológicas 1981-2010. <http://smn.cna.gob.mx/tools/RESOURCES/Normales8110/NORMAL10137.TXT>, August, 2017.

Servicio Meteorológico Nacional (SMN), México. Estación 19020 El Potosi (Nuevo Leon) (24°50'36" N., 100°19'15" W., 1,890.0 msnm). Normales Climatológicas 1981-2010. <http://smn.cna.gob.mx/tools/RESOURCES/Normales8110/NORMAL10137.TXT>

Servicio Meteorológico Nacional-Comisión Nacional del Agua (SMN-CONAGUA), México. http://smn.cna.gob.mx

Simon, A. and Collison, A.J., 2002. Quantifying the mechanical and hydrologic effects of riparian vegetation on streambank stability. Earth Surface Processes and Landforms, 27(5), pp.527-546.

Singh, S.C., Sinha, R.P. and Hader, D.P., 2002. Role of lipids and fatty acids in stress tolerance in cyanobacteria. Acta protozoologica, 41(4), pp.297-308.

Sinninghe Damsté, J.S., Hopmans, E.C., Pancost, R.D., Schouten, S. and Geenevasen, J.A., 2000. Newly discovered non-isoprenoid glycerol dialkyl glycerol tetraether lipids in sediments. Chemical Communications, (17), pp.1683-1684.

Sinninghe Damsté, J.S., Ossebaar, J., Abbas, B., Schouten, S. and Verschuren, D., 2009. Fluxes and distribution of tetraether lipids in an equatorial African lake: constraints on the application of the TEX86 palaeothermometer and BIT index in lacustrine settings. Geochimica et Cosmochimica Acta, 73(14), pp.4232-4249.

Smith, A.E. and Morris, I., 1980. Synthesis of lipid during photosynthesis by phytoplankton of the Southern Ocean. Science, 207(4427), pp.197-199.

Smith, R.W., Bianchi, T.S. and Li, X., 2012. A re-evaluation of the use of branched GDGTs as terrestrial biomarkers: Implications for the BIT Index. Geochimica et Cosmochimica Acta, 80, pp.14-29.

Solomon, S., Qin, D., Manning, M., Chen, Z., Marquis, M., Averyt, K.B., Tignor, M. and Miller, H.L., 2007. Contribution of working group I to the fourth assessment report of the intergovernmental panel on climate change, 2007.

Soper, F.M., McCalley, C.K., Sparks, K. and Sparks, J.P., 2017. Soil carbon dioxide emissions from the Mojave Desert: isotopic evidence for a carbonate source. Geophysical Research Letters, 44(1), pp.245-251.

Stahle, D.W., Burnette, D.J., Díaz, J.V., Heim, R.R., Fye, F.K., Paredes, J.C., Soto, R.A. and Cleaveland, M.K., 2012. Pacific and Atlantic influences on Mesoamerican climate over the past millennium. Climate Dynamics, 39(6), pp.1431-1446.

Stensrud, D.J., Gall, R.L., Mullen, S.L. and Howard, K.W., 1995. Model climatology of the Mexican monsoon. Journal of Climate, 8(7), pp.1775-1794.

Theissen, K.M., Zinniker, D.A., Moldowan, J.M., Dunbar, R.B. and Rowe, H.D., 2005. Pronounced occurrence of long-chain alkenones and dinosterol in a 25,000-year lipid molecular fossil record from Lake Titicaca, South America. Geochimica et Cosmochimica Acta, 69(3), pp.623-636.

Throop, H.L., Reichmann, L.G., Sala, O.E. and Archer, S.R., 2012. Response of dominant grass and shrub species to water manipulation: an ecophysiological basis for shrub invasion in a Chihuahuan Desert grassland. Oecologia, 169(2), pp.373-383.

Tierney, J.E. and Russell, J.M., 2009. Distributions of branched GDGTs in a tropical lake system: implications for lacustrine application of the MBT/CBT paleoproxy. Organic Geochemistry, 40(9), pp.1032-1036.

Tierney, J.E., Russell, J.M., Eggermont, H., Hopmans, E.C., Verschuren, D. and Damsté, J.S., 2010. Environmental controls on branched tetraether lipid distributions in tropical East African lake sediments. Geochimica et Cosmochimica Acta, 74(17), pp.4902-4918.

Tierney, J.E., Russell, J.M., Huang, Y., Damsté, J.S.S., Hopmans, E.C. and Cohen, A.S., 2008. Northern hemisphere controls on tropical southeast African climate during the past 60,000 years. Science, 322(5899), pp.252-255.

Trommer, G., Siccha, M., van der Meer, M.T., Schouten, S., Damsté, J.S.S., Schulz, H., Hemleben, C. and Kucera, M., 2009. Distribution of Crenarchaeota tetraether membrane lipids in surface sediments from the Red Sea. Organic Geochemistry, 40(6), pp.724-731.

United Nations Framework Convention on Climate Change, 2015. Adoption of the Paris Agreement. Report No. FCCC/CP/2015/L.9/Rev.1, http://unfccc.int/resource/docs/2015/cop21/eng/l09r01.pdf

Van Bree, L.G., Rijpstra, W.I.C., Al-Dhabi, N.A., Verschuren, D., Damsté, J.S. and de Leeuw, J.W., 2016. Des-A-lupane in an East African lake sedimentary record as a new proxy for the stable carbon isotopic composition of C3 plants. Organic Geochemistry, 101, pp.132-139.

Van Bree, L.G.J., Peterse, F., van der Meer, M.T.J., Middelburg, J.J., Negash, A.M.D., De Crop, W., Cocquyt, C., Wieringa, J.J., Verschuren, D. and Damsté, J.S., 2018. Seasonal variability in the abundance and stable carbon-isotopic composition of lipid biomarkers in suspended particulate matter from a stratified equatorial lake (Lake Chala, Kenya/Tanzania): Implications for the sedimentary record. Quaternary Science Reviews, 192, pp.208-224.

Van den Bos, V., Engels, S., Bohncke, S.J.P., Cerli, C., Jansen, B., Kalbitz, K., Peterse, F., Renssen, H. and Sachse, D., 2018. Late Holocene changes in vegetation and atmospheric circulation at Lake Uddelermeer (The Netherlands) reconstructed using lipid biomarkers and compound-specific δD analysis. Journal of Quaternary Science, 33(1), pp.100-111.

Van Devender, T.R. and Burgess, T.L., 1985. Late Pleistocene woodlands in the Bolson de Mapimi: A refugium for the Chihuahuan Desert Biota? Quaternary Research, 24(3), pp.346-353.

Van Devender, T.R., 1987. Holocene vegetation and climate in the Puerto Blanco Mountains, southwestern Arizona. Quaternary Research, 27, pp.51–72.

Van Devender, T.R., 1990. Late quaternary vegetation and climate of the Chihuahuan Desert, United States and Mexico (pp. 104-133). Tucson, AZ: University of Arizona Press.

Van Devender, T.R., 1997. August. 21,000 years of vegetation change in the northern Vizcaino, Baja California. In Second Annual Botanical Symposium, pp.14-16.

Van Devender, T.R., and Worthington, R.D., 1977. The herpetofauna of Howell's Ridge Cave and the paleoecology of the northwestern Chihuahuan Desert. In Transactions of the Symposium on the Biological Resources of the Chihuahuan Desert Region, United States and Mexico: National Park Service Transactions and Proceedings, 3, pp.85-106.

Vázquez, G., Roy, P.D., Solis, B., Blanco, E. and Lozano-Santacruz, R., 2017. Holocene paleohydrology of the Etzatlán-Magdalena basin in western-central Mexico and evaluation of main atmospheric forcings. Palaeogeography, Palaeoclimatology, Palaeoecology, 487, pp.149-157.

Vidal, L., Labeyrie, L., Cortijo, E., Arnold, M., Duplessy, J. C., Michel, E., Becqué, S., van Weering, T.C. E., 1997. Evidence for changes in the North Atlantic deep water linked to meltwater surges during the Heinrich events. Earth and Planetary Science Letters, 146, pp.13-27.

Volkman, J.K., 1986. A review of sterol markers for marine and terrigenous organic matter. Organic Geochemistry, 9(2), pp.83-99.

Volkman, J.K., 2003. Sterols in microorganisms. Applied microbiology and Biotechnology, 60(5), pp.495-506.

Volkman, J.K., 2005. Sterols and other triterpenoids: source specificity and evolution of biosynthetic pathways. Organic geochemistry, 36(2), pp.139-159.

Von Post, L., 1946. The prospect for pollen analysis in the study oe the earth's climatic history. New Phytologist, 45(2), pp.193-193.

Wagner, J.D., Cole, J.E., Beck, J.W., Patchett, P.J., Henderson, G.M. and Barnett, H.R., 2010. Moisture variability in the southwestern United States linked to abrupt glacial climate change. Nature Geoscience, 3(2), p.110.

Walker, M.J., Berkelhammer, M., Björck, S., Cwynar, L.C., Fisher, D.A., Long, A.J., Lowe, J.J., Newnham, R.M., Rasmussen, S.O. and Weiss, H., 2012. Formal subdivision of the Holocene Series/Epoch: a Discussion Paper by a Working Group of INTIMATE (Integration of ice-core, marine and terrestrial records) and the Subcommission on Quaternary Stratigraphy (International Commission on Stratigraphy). Journal of Quaternary Science, 27(7), pp.649-659.

Wang, C., Enfield, D.B., Lee, S.K. and Landsea, C.W., 2006. Influences of the Atlantic warm pool on Western Hemisphere summer rainfall and Atlantic hurricanes. Journal of Climate, 19(12), pp.3011-3028.

Wang, C., Liu, H., Lee, S.K. and Atlas, R., 2011. Impact of the Atlantic warm pool on United States landfalling hurricanes. Geophysical Research Letters, 38(19).

Waters, M.R., 1989. Late Quaternary lacustrine history and paleoclimatic significance of pluvial Lake Cochise, southeastern Arizona. Quaternary Research, 32(1), pp.1-11.

Weijers, J.W., Schouten, S., Spaargaren, O.C. and Damsté, J.S.S., 2006. Occurrence and distribution of tetraether membrane lipids in soils: Implications for the use of the TEX86 proxy and the BIT index. Organic Geochemistry, 37(12), pp.1680-1693.

Weijers, J.W., Schouten, S., van den Donker, J.C., Hopmans, E.C. and Damsté, J.S.S., 2007. Environmental controls on bacterial tetraether membrane lipid distribution in soils. Geochimica et Cosmochimica Acta, 71(3), pp.703-713.

Wells, P.V., 1966. Late Pleistocene vegetation and degree of pluvial climatic change in the Chihuahuan Desert. Science, 153(3739), pp.970-975.

Wood, A.P. and Kelly, D.P., 1991. Isolation and characterisation of Thiobacillus halophilus sp. nov., a sulphur-oxidising autotrophic eubacterium from a Western Australian hypersaline lake. Archives of microbiology, 156(4), pp.277-280.

Xie, S., Pancost, R.D., Chen, L., Evershed, R.P., Yang, H., Zhang, K., Huang, J. and Xu, Y., 2012. Microbial lipid records of highly alkaline deposits and enhanced aridity

associated with significant uplift of the Tibetan Plateau in the Late Miocene. Geology, 40(4), pp.291-294.

Xiong, Y., Wu, F., Fang, J., Wang, L., Li, Y. and Liao, H., 2010. Organic geochemical record of environmental changes in Lake Dianchi, China. Journal of Paleolimnology, 44(1), pp.217-231.

Yano, I., Furukawa, Y. and Kusunose, M., 1971. Fatty-Acid Composition of Arthrobacter simplex Grown on Hydrocarbons. The FEBS Journal, 23(2), pp.220-228.

Yongdong, Z., Yaling, S., Zhengwen, L., Xiangchao, C., Jinlei, Y., Xiaodan, D. and Miao, J., 2015. Sediment lipid biomarkers record increased eutrophication in Lake Fuxian (China) during the past 150 years. Journal of Great Lakes Research, 41(1), pp.30-40.

Zhang, Y., Su, Y., Liu, Z., Sun, K., Kong, L., Yu, J. and Jin, M., 2018. Sedimentary lipid biomarker record of human-induced environmental change during the past century in Lake Changdang, Lake Taihu basin, Eastern China. Science of The Total Environment, 613, pp.907-918.

Zhou, Z.C. and Shangguan, Z.P., 2005. Soil anti-scouribility enhanced by plant roots. Journal of Integrative Plant Biology, 47(6), pp.676-682.

Zic, M., Negrini, R., Wigand, P., 2002. Evidence of synchronous climate change across the Northern Hemisphere between the North Atlantic and northwestern Great Basin, United States. Geology, 30(7), pp.635-638.

Ziegler, M., Nürnberg, D., Karas, C., Tiedemann, R. and Lourens, L.J., 2008. Persistent summer expansion of the Atlantic Warm Pool during glacial abrupt cold events. Nature Geoscience, 1(9), p.601.

Zink, K.G., Vandergoes, M.J., Mangelsdorf, K., Dieffenbacher-Krall, A.C. and Schwark, L., 2010. Application of bacterial glycerol dialkyl glycerol tetraethers (GDGTs) to develop modern and past temperature estimates from New Zealand lakes. Organic Geochemistry, 41(9), pp.1060-1066.